Investigating metabolic dependencies of acute myeloid leukaemia and state-of-the-art metabolomics development by NMR spectroscopy

---

Dissertation

To obtain the two academic degrees

doctor philosophiae naturalis (Dr. phil. nat.)

doctor of philosophy (PhD)

Submitted to

Johann Wolfgang Goethe-University

Frankfurt am Main, Germany

Faculty of Chemistry, Biochemistry and Pharmacy

&

The University of Birmingham

Birmingham, United Kingdom

College of Medical and Dental Sciences

Presented by

Islam Alshamleh

Born in Bahrain

Frankfurt am Main

2021

(D30)

UNIVERSITY OF
BIRMINGHAM

University of Birmingham Research Archive

e-theses repository

This unpublished thesis/dissertation is copyright of the author and/or third parties. The intellectual property rights of the author or third parties in respect of this work are as defined by The Copyright Designs and Patents Act 1988 or as modified by any successor legislation.

Any use made of information contained in this thesis/dissertation must be in accordance with that legislation and must be properly acknowledged. Further distribution or reproduction in any format is prohibited without the permission of the copyright holder.

Accepted dissertation by the Faculty of Chemistry, Biochemistry and Pharmacy, Johann Wolfgang Goethe-University

Dean: Prof. Dr. Clemens Glaubitz

Assessors: Prof. Dr. Harald Schwalbe
Prof. Dr. med. Hubert Serve

Disputation date:

To *Zuhair Shamleh*
(1945-2019)

This PhD thesis was carried out under the supervision and advice of Prof. Dr. Harald Schwalbe.

Its palliation is a daily task, its cure a fervent hope.
-William Castle,

describing leukaemia in 1950

Etymologically, patient means sufferer. It is not suffering as such that is most deeply feared but suffering that degrades.

- Susan Sontag, *Illness as Metaphor*

Table of Contents

Summary **15**
Zusammenfassung (Summary in German) **21**
Table of figures **28**
List of abbreviation **30**
Chapter I **34**
General introduction **34**
1.1. Altered metabolism in acute myeloid leukaemia 35
1.1.1. Acute myeloid leukaemia 35
1.1.2. Fms-Like Tyrosine Kinase III 37
1.1.3. Cancer and metabolism 43
1.1.4. Mitochondrial metabolism or glycolysis? 49
1.1.5. FLT3-ITD and metabolism 52
1.1.6. Motivation and project aims (A) 54
1.2. Amino acid metabolism and cancer 55
1.2.1. General amino acid dependencies in AML 55
1.2.2. Methionine metabolism 56
1.2.3. Motivation and project aims (B) 58
1.3. Nuclear magnetic resonance (NMR) spectroscopy for metabolomics studies 59
1.3.1. Theoretical principle of NMR 60
1.3.2. NMR metabolomics and biological applications 61
1.3.3. NMR of live-cells 65
1.3.4. Motivation and project aims (C) 66
Chapter II **68**
Materials and methods **68**
2.1. Cellular assays and *in vivo* experiments section 69
2.1.1. Cell culture and maintenance 69
2.1.2. Hypoxic cell culture 70
2.1.3. Inhibitors, reagents and chemicals 70
2.1.4. Seahorse measurement 70
2.2. Gene editing section 72
2.2.1. Generation of gRNA-expressing vectors 72
2.2.2. Transformation 72
2.2.3. Mini-preparation 72
2.2.4. Midi-preparation 73
2.2.5. Lentivirus production in Hek293T cells 73

2.2.6. shRNA PDP1 knockdown transduction 74
2.2.7. PDP1 knockout 75
2.2.8. siRNA PDP1 KD 75
2.2.9. PDP1 overexpression 76
2.2.10. Generation of Rho Zero cells 76
2.3. Flow cytometry section 77
2.3.1. Fluorescence-activated cell sorting (FACS) 77
2.3.2. Gating strategy 77
2.4. Proliferation and viability assays 78
2.4.1. Cellular ATP assays 78
2.4.2. Competition growth assay 79
2.4.3. Cumulative growth assay 79
2.4.4. Apoptosis assay 79
2.4.5. Dead-cell staining (eFlour) 79
2.4.6. Cell cycle assay 79
2.4.7. Synergy assays 80
2.4.8. Glucose consumption assay 80
2.5. *In vivo* experiments 80
2.5.1. Xenotransplantation mouse experiments 80
2.5.2. Ethical and regulatory information 81
2.6. Protein and RNA section 81
2.6.1. Western blotting 81
2.6.2. RNA extraction and reverse transcription 82
2.6.3. qPCR measurement 83
2.7. Metabolomics and NMR section 84
2.7.1. Metabolites extraction and sample preparation 84
2.7.2. Tracer-based assay 85
2.7.3. Real-time NMR cell culture and sample preparation 85
2.7.4. NMR data acquisition 85
2.7.5. Real-time NMR experimental setup and measurement 87
2.7.6. NMR Data analysis 89
2.8. Statistical analysis 89
Chapter III 90
3.1. Results 91
3.1.1. FLT3-ITD-positive AML cells exhibit dominant mitochondrial metabolism 91
3.1.2. FLT3-ITD cells are highly sensitive to OXPHOS perturbations 95
3.1.3. FLT3-ITD cells express high PDP1 levels 95
3.1.4. PDP1 is a targetable vulnerability in FLT3-ITD-positive AML 97

3.1.5. High PDP1 levels boost energy levels 102
3.1.6. PDP1 provides cellular flexibility for metabolic switch under oscillating oxygen conditions 103
3.1.7. PDP1 acts as a survival mechanism to overcome FLT3-inhibition and mediates drug resistance 106
3.2. Discussion 112
3.2.1. FLT3-ITD and the OXPHOS phenotype 112
3.2.2. Metabolic consequences of FLT3-ITD/ PDP1 signalling axis 114
3.2.3. PDP1 targetability and clinical relevance 115
3.2.4. PDP1 roles in therapeutic responses and metabolic flexibility 117
Chapter IV 120
Methionine metabolism in AML 120
4.1. Results 121
4.1.1. Methionine dependence in AML 121
4.1.2. Methionine utilization and DNA methylation 124
4.1.3. Methionine recycling 127
4.2. Discussion 131
Chapter V 134
Real-time NMR for studying metabolism 134
5.1. Results 135
5.1.1. Optimisation towards a cell-friendly approach 135
5.1.2. Application on sensitive cellular entities 139
5.1.3. Incorporation of tracer-based assays 139
5.2. Discussion 142
5.2.1. Bridging closer to physiological conditions: 143
5.2.2. Technicalities, applications and limitations: 144
Concluding remarks 147
References 149
Appendices 166
Declaration for collaboration work 181
Acknowledgment 183
Curriculum vitae 185

Summary

The scope of this doctoral thesis is focused on identifying metabolic vulnerabilities and therapeutic targets in acute myeloid leukaemia (AML). In the course of this PhD, three main projects were carried out next to seven other collaboration projects on metabolomics profiling in health and disease. In addition, a scientific review covering current literature on metabolic reprogramming in AML was written. The first project studied the unique mitochondrial metabolism in AML caused by internal tandem duplication mutations (ITDs) of fms-like tyrosine kinase III (FLT3). This led to the identification of an essential protein (PDP1) which was validated as a putative targetable vulnerability in AML. The second part investigated amino acid dependencies in AML with a special focus on methionine. The cellular utilisation of methionine in AML was studied, as well as the molecular aspects of the dependence on exogenous methionine. Lastly, the third part addresses advancing NMR as a technology platform for metabolomics analysis by developing a real-time metabolism-imaging approach to profile metabolism of living cells.

Project one: PDP1 is a key metabolic gatekeeper and modulator of drug resistance in FLT3-ITD-positive acute myeloid leukaemia

AML is a malignant disorder of the haematopoietic system. It is mainly caused by genetic alterations in genes regulating cell cycle and differentiation. FLT3 plays a prominent role in cell proliferation and differentiation. FLT3 mutations are present in 20-30% of AML patients and are associated with poor prognosis. These mutations mostly occur as internal tandem duplications (ITDs) in the FLT3 receptor's juxtamembrane domain. FLT3 inhibitors have shown some efficacy in patients with relapsed or refractory AML. Nevertheless, overall patient outcomes are still relatively poor and thus, further therapeutic developments are needed. This thesis sought to address the clinical need for new therapeutic targets by better understanding the cellular processes in AML.

Considering the high proliferation rates in AML, higher metabolic reactivities are required to cope with the high energy needs of the cells. In fact, metabolic reprograming is an essential survival strategy in leukaemia cells. This metabolic phenotype contributes to the aggressiveness and drug sensitivity in AML. Most cancers are believed to be dependent on a special form of glucose metabolism termed as the 'Warburg effect'. To the contrary of healthy cells, Warburg metabolism allows cancer cells to metabolise glucose-derived pyruvate to produce lactate regardless to oxygen levels. Thus, glycolysis was evaluated as a therapeutic target in AML.

Nonetheless, since metabolic rewiring is induced by specific genetic and epigenetic modulations, different oncogenes can lead to different metabolic dependencies. In agreement with recent literature, the current thesis suggests higher efficacy in targeting mitochondrial metabolism in AML with FLT3-ITD background. Several cellular models were used to characterise the metabolic phenotype of FLT3-ITD-positive AML cells, which all suggested higher mitochondrial tricarboxylic acid (TCA) cycle and OXPHOS activity in comparison to FLT3-WT AML cells. Mechanistically, ^{13}C-glucose tracer-based assay also demonstrated higher shuffling of glucose into the TCA cycle under FLT3-ITD kinase activity. Functionally, this mitochondrial dependence was exploited by mitochondrial targeting using a variety of mitochondrial inhibitors. Here, FLT3-ITD cell lines were significantly more sensitive to different mitochondrial inhibitors such as venetoclax and rotenone. This sensitivity was similarly observed in FLT3-ITD-positive bone marrow-derived primary patient AML blasts. In addition, mitochondrial inhibitors synergised with FLT3-inhibition by AC220, suggesting a combinatorial effect that has potential clinical relevance in the patients.

To investigate the molecular mechanism behind this mitochondrial reliance, the activity of the different proteins involved at the interface between glycolysis and the TCA cycle was evaluated (mainly proteins within the pyruvate dehydrogenase complex (PDC)). Interestingly, unlike FLT3-WT cells, FLT3-ITD cells showed higher pyruvate dehydrogenase phosphatase 1 (PDP1) levels, (the phosphatase that promotes pyruvate incorporation into the TCA cycle), which explains the observed OXPHOS phenotype (Figure S1). These findings were confirmed by a proteomic analysis of 177 newly diagnosed AML patients' cohort, where higher PDP1 protein levels were detected in primary AML blasts with FLT3-ITD mutations (in collaboration with Prof. Thomas Oellerich, Goethe University Hospital Frankfurt, Germany).

These findings suggest that PDP1 is the essential player in promoting the OXPHOS phenotype in FLT3-ITD cells and thus, it was evaluated as a targetable vulnerability. PDP1 knockdown resulted in a severe proliferation disadvantage in FLT3-ITD cells but not FLT3-WT cells. This effect was also observed in FLT3-ITD-positive bone marrow-derived primary AML blasts. Moreover, PDP1 abrogation had a detrimental impact on leukaemia progression *in vivo*. PDP1 knockdown in a Molm13-based xenotransplantation mouse model prolonged the overall survival and more interestingly, 37% of the mice in this group did not succumb to leukaemia. Furthermore, evaluation of published genomic datasets revealed that patients with higher PDP1 gene expression levels have poorer overall survival.

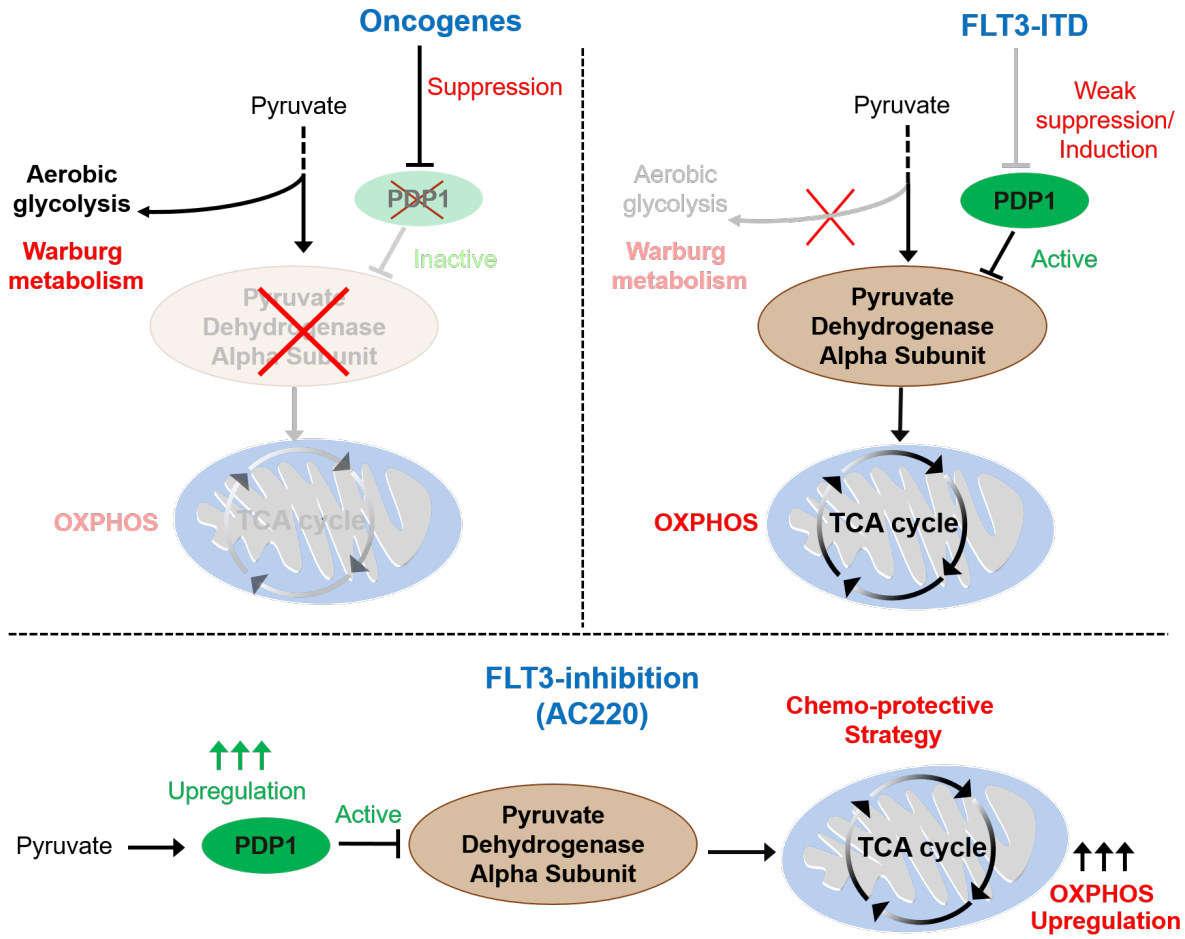


Figure S1: Proposed model of metabolic regulation in FLT3-ITD cells. PDP1 as a gatekeeper in FLT3-ITD AML OXPHOS metabolism and drug response.

As of the cellular functions of PDP1, three main advantages of high PDP1 levels in FLT3-ITD cells were identified. First, its classical role in generating energy by mitochondrial metabolism. This role was shown by PDP1 overexpression experiment, where higher PDP1 levels boosted the intracellular ATP pool. Second, PDP1 exerted essential functions under hypoxic environment. Here, PDP1 knockdown impaired cellular proliferation in spite of the low oxygen levels which do not favour mitochondrial metabolism. Furthermore, unlike FLT3-WT, FLT3-ITD cells retain a conserved mitochondrial respiration capacity after adaption to hypoxia (1% O_2 as physiologically encountered in the bone marrow). This ability was shown to be mediated by PDP1, as PDP1 knockdown impaired their capacity to restore mitochondrial activity and rapidly enter the cell cycle upon reoxygenation. Third, a dual role of PDP1 in responses to FLT3-inhibitors (sensitisation/ resistance) was described. Mechanistically, upon FLT3-inhibition, cells upregulate their PDP1 in order to sustain the metabolic integrity of the cells by shifting them towards chemo-protective mitochondrial metabolism. When provided with its substrate, pyruvate, PDP1 activity could partially, but significantly, rescue the effects of

AC220. PDP1 was confirmed to be the key driver of this rescue. The role of PDP1 in resistance to AC220 was further elucidated by a PDP1 overexpression experiment where higher PDP1 levels correlated with lower sensitivity to FLT3-inhibition. Vice versa, PDP1 suppression sensitised the cells to FLT3-inhibition and primed them to apoptosis induced by low doses of the FLT3-inhibitor AC220. This was shown on primary AML blasts from an AC220-resistant patient. Strikingly, PDP1 knockdown in these patients' cells sensitized them to AC220 treatment. These findings suggest a chemo-protective nature of mitochondrial metabolism against cytotoxic agents and a pivotal role of PDP1 in therapeutic outcomes (Figure S1).

In summary, PDP1 was identified as a new metabolic vulnerability in FLT3-ITD-positive AML and its role in therapeutic responses was elucidated. Further research is needed to study the role of PDP1 in disease relapse and evolution of drug resistance.

Project two: Methionine metabolism in AML

Beyond the specific FLT3-ITD OXPHOS essentiality, this thesis presents in a separate project the general amino acid dependencies in AML. Only a few amino acids have been studied so far for their importance in AML while many others are yet to be explored. Therefore, an individual amino acid dropout assay was performed and revealed methionine as a crucial dependency in AML. *In vivo* studies with methionine restriction diets showed detrimental effect on leukaemia progression, which poses methionine as a targetable vulnerability in AML. Importantly, methionine depletion affected AML cells significantly more than healthy hematopoietic stem cells.

To gain mechanistic insights into the role of methionine in AML, NMR tracer-based assays with ^{13}C methionine were performed with an untargeted metabolomics approach. Interestingly, the bulk of methionine in the AML cells was utilized for transmethylation reactions. Unlike healthy donor stem cells, no label incorporation in other methionine metabolism pathways was detected, including the redox control intermediates

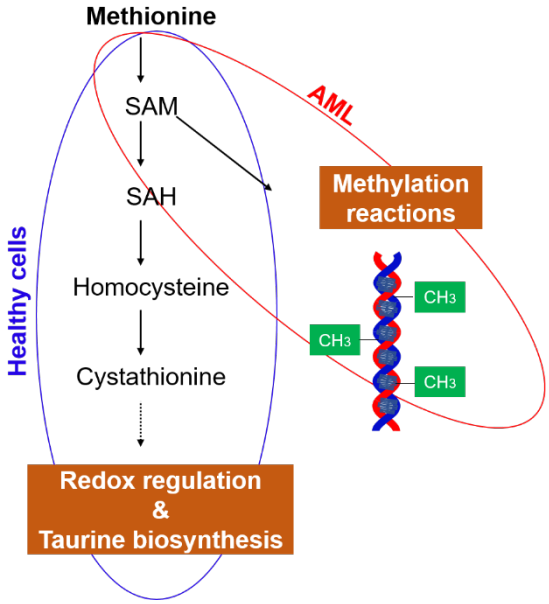


Figure S2: AML cells utilise methionine for methylation reactions. Tracer-based assay using NMR revealed different utilisations of methionine in AML compared to healthy cells.

cysteine and glutathione (Figure S2). Abrogating methionine metabolism altered histone modification and blocked transcription.

Furthermore, this chapter investigated the molecular driver of the unique reliance on exogenous methionine, specifically the ability of AML cells to regenerate methionine from homocysteine. Using NMR spectroscopy, it was demonstrated that AML cells have low methionine recycling capacity from homocysteine. Nevertheless, further research is needed in order to understand the mechanistical differences in methionine recycling in AML compared to healthy $CD34^+$ cells.

Project three: Real-time NMR for studying metabolism

The third section of this thesis addresses the application and development of NMR spectroscopy as a high throughput method for metabolomics studies. Traditional metabolomics approaches employ metabolite extraction protocols that are cell-destructive, require high cell numbers and only provide a snapshot of metabolism. Recent NMR approaches, mainly in-cell NMR, are being widely utilised for studying macromolecules dynamics intracellularly non-invasively. This thesis delivers a parallel and fully automated approach that allows monitoring cellular metabolism in a real-time manner with less than a tenth of the commonly needed cell numbers. This method is conceptualised on measuring the influx/efflux of extracellular metabolites over a time course without cell destruction (Figure S3). Uniquely, this approach was supplemented with a cell-friendly matrix, methylcellulose, which outperforms all other described alternatives. This matrix was demonstrated to have no impact on cellular viability. The studied cells exerted full capacity to normally respond to external stimuli and interferences in signalling pathways. Moreover, this setup maintains physiological oxygen and pH levels.

For the first time, this new approach was successfully utilised to study the exceptionally sensitive primary mononuclear cells isolated from AML patients' bone marrow. These cells demonstrated a fully active and ordinary metabolic behaviour in the developed experimental settings. This approach was further enabled with the possibility to carry out tracer-based assays. These assays were performed using pseudo-2D double-filter experiments with short measurement time (~7 minutes) to preserve the real-time nature of this method. With the capacity to profile over 15 samples simultaneously, this thesis delivers here a state-of-the-art high-throughput metabolomics platform that can be robustly implemented in personalised

medicine and diagnostics. Further development in assessing levels of mitochondrial and TCA cycle metabolites will significantly enhance the relevance and applicability of this method.

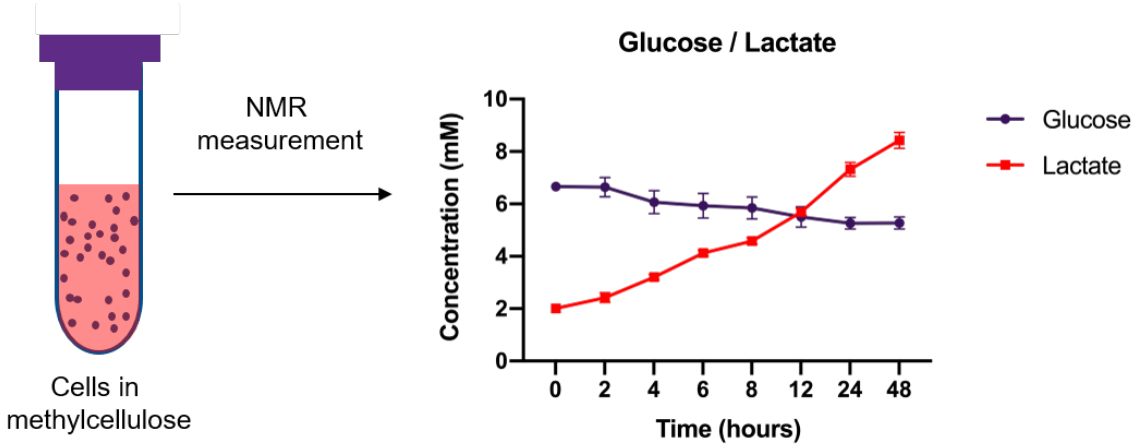


Figure S3: Real-time NMR for studying cellular metabolism. Development of a cell-friendly approach for studying metabolism of live cells.

Zusammenfassung (Summary in German)

Im Rahmen der vorliegenden Doktorarbeit sollten metabolische Vulnerabilitäten der akuten myeloischen Leukämie (AML) charakterisiert und damit einhergehend neue therapeutische Ansatzpunkte bei deren Behandlung identifiziert werden. Im Verlauf dieser Arbeit wurden, neben sieben weiteren Kollaborationsprojekten, drei Hauptprojekte bearbeitet, die sich hauptsächlich mit der Erstellung metabolischer Profile von Leukämiezellen beschäftigen. Darüber hinaus wurde ein wissenschaftlicher Review-Artikel zur aktuellen Literatur über die metabolische Plastizität der AML verfasst. Die drei Hauptprojekte der Doktorarbeit umfassten folgende Punkte: In Projekt 1 wurde der mitochondriale Metabolismus der FLT3-ITD (interne Tandemduplikationsmutation der Rezeptor-Tyrosinkinase FLT3) positiven AML untersucht. Dabei wurde ein essentielles Protein (PDP1) als potentielle Vulnerabilität mit vielversprechendem therapeutischem Potential identifiziert. In Projekt 2 wurde die Aminosäureabhängigkeit der AML untersucht, wobei ein besonderer Fokus auf Methionin gelegt wurde und dessen zelluläre Verwendung sowie die molekularen Aspekte der exogenen Methioninabhängigkeit erforscht wurden. Projekt 3 befasste sich mit Technologieentwicklung zu Anwendung der NMR Spektroskopie als Plattform für Metabolomik. Hier wurde eine Echtzeitmethode zur Erstellung metabolomischer Profile lebender Zellen entwickelt.

Projekt 1: Metabolische Abhängigkeit der FLT3-ITD positiven akuten myeloischen Leukämie

AML ist eine bösartige Erkrankung des blutbildenden Systems, verursacht durch eine Vielzahl unterschiedlicher genetischer Veränderungen der hämatopoetischen Stamm- und Vorläuferzellen. Diese Krankheit ist charakterisiert durch die unkontrollierte klonale Expansion undifferenzierter myeloischer Blasten, was zu einer Beeinträchtigung der normalen Hämatopoese und letztendlich zum Versagen des Knochenmarks führt. Eine wesentliche Rolle bei der Zellproliferation und Zelldifferenzierung des hämatopoetischen Systems spielt die Rezeptor-Tyrosinkinase FLT3. FLT3-Mutationen können daher auch in 20-30% Prozent der AML-Patienten festgestellt werden, was mit einer ungünstigen Prognose der Krankheit in Verbindung steht. Diese Mutationen liegen meistens als Interne Tandemduplikation in der Juxtamembran-Domäne (ITD; am häufigsten) vor. FLT3 Inhibitoren haben bereits Wirksamkeit bei rezidivierender und bei refraktärer AML gezeigt, jedoch mit insgesamt mäßigem therapeutischem Erfolg, sodass weitere Entwicklungen notwendig sind. Diese Arbeit trägt zum Verständnis der zellulären Prozesse der AML bei, als Grundlage für klinisch notwendige, neue therapeutische Ansätze.

Aufgrund der hohen Proliferationsrate der AML, ist eine hohe metabolische Aktivität notwendig, um den hohen Energie- und Materialbedarf der Zellen zu decken. Daher ist die metabolische Re-Programmierung eine essentielle Überlebensstrategie von Leukämiezellen. Die Ausbildung dieses metabolischen Phänotyps ist einer der Gründe für die Aggressivität der AML aber auch für die Sensitivität gegenüber Arzneistoffen. Nach heutigem Stand der Forschung sind die meisten Krebskrankheiten von einer speziellen Form des Glucose-Metabolismus abhängig, der als Warburg-Effekt bekannt ist. Im Gegensatz zu gesunden Zellen ermöglicht es der Warburg-Metabolismus den Krebszellen, Pyruvat aus Glucose zu Laktat unabhängig vom Sauerstoffgehalt umzusetzen. Daher wurde in der AML Therapie die Wirksamkeit von Glycolysehemmern getestet.

Da die metabolische Re-Programmierung der Zellen durch spezifische genetische Mutationen induziert wird, führen verschiedene Onkogene zu unterschiedlichen metabolischen Abhängigkeiten. In Einklang mit jüngster Fachliteratur, legt die vorliegende Arbeit nahe, dass bei FLT3-ITD positiver AML eine höhere therapeutische Wirkung durch Beeinflussung des mitochondrialen Metabolismus erzielt werden kann. Mehrere zelluläre Modelle wurden verwendet, um den metabolischen Phänotyp von FLT3-ITD-positiven AML Zellen zu charakterisieren, die alle auf höhere mitochondrialeCitrat-(TCA)-Zyklus und OXPHOS Aktivität in FLT3-ITD gegenüber FLT3-WT AML Zellen hindeuteten. Darüber hinaus konnte durch ^{13}C-Glucose-Tracer basierte Assays gezeigt werden, dass bei FLT3-ITD Aktivität ein erhöhtes Einschleusen von Glucose in den TCA-Zyklus stattfindet. Funktional konnte diese mitochondriale Abhängigkeit als pharmazeutische Zielstruktur ausgenutzt werden. So erwiesen sich FLT3-ITD Zelllinien als bedeutend sensitiver gegenüber einer Auswahl mitochondrialer Inhibitoren darunter Venetoclax und Rotenon. Diese Sensitivität wurde ebenso an FLT3-ITD positiven Blasten aus dem Knochenmark von Patienten mit primärer AML beobachtet. Darüber hinaus gab es Synergie-Effekte zwischen mitochondrialen Inhibitoren und FLT3 Inhibition durch AC220, was eine klinische Relevanz dieses kombinatorischen Effekts in Patienten suggeriert.

Um den molekularen Mechanismus hinter dieser mitochondrialen Abhängigkeit zu untersuchen, wurde die Aktivität unterschiedlicher Proteine an der Schnittstelle zwischen Glykolyse und TCA-Zyklus untersucht (hauptsächlich Proteine innerhalb des Pyruvat-Dehydrogenase-Komplexes, PDC). Interessanterweise , ungleich zu FLT3-WT Zellen, zeigten FLT3-ITD Zellen geringere PDHK1 Aktivität und erhöhte Expression von Pyruvat-Dehydrogenase-Phosphatase 1 (PDP1) (die Phosphatase, die einen höhere Pyruvat Aufnahme in den TCA Zyklus fördert), welches den beobachteten OXPHOS Phenotyp erklärt (Abbildung Z1). Diese Ergebnisse wurden bestätigt durch eine Analyse eines Proteom

Datensatzes primärer AML Blasten einer Patientenkohorte, welche eine signifikante Korrelation der PDP1 Expression mit dem Auftreten von FLT3-ITD Mutationen zeigte (durchgeführt von der Prof. Thomas Oellerich-Gruppe, Goethe-Universitätsklinikum Frankfurt, Deutschland).

Diese Erkenntnisse suggerieren, dass PDP1 als essentieller Akteur den OXPHOS Phänotyp in FLT3-ITD Zellen hervorruft, und deuten somit auf PDP1 als Vulnerabilität und potentielles pharmazeutisches Target für die Behandlung der AML. Der Knockdown von PDP1 mittels RNA Interferenz resultierte dementsprechend in einer starken Reduktion der Zellproliferation in FLT3-ITD, nicht aber in FLT3-WT Zellen. Ein ähnlicher Effekt wurde auch in FLT3-ITD positiven primären AML Blasten aus Knochenmark beobachtet. Darüber hinaus konnte mit *in vivo* Experimenten gezeigt werden, dass die Reduktion der PDP1 Expression einen verlangsamenden Effekt auf die Progression der Leukämie hat. So verlängerte ein PDP1-Knockdown im Molm13-basierten Xenotransplantations-Modell in NSG Mäusen insgesamt das Überleben und 37% der Mäuse in dieser Gruppe erlagen nicht der Leukämie. Zusätzlich zeigte die Evaluierung von publizierten genomischen Daten, dass Patienten mit höherer PDP1 Genexpression eine höhere Mortalität aufweisen.

Was die zellulären Funktionen von PDP1 betrifft, wurden drei Hauptvorteile einer erhöhten PDP1 Expression in FLT3-ITD Zellen identifiziert. Erstens seine klassische Rolle bei der Energiegewinnung durch den mitochondrialen Metabolismus. Es wurde durch PDP1 Überexpression gezeigt, dass höhere PDP1-Spiegel den intrazellulären ATP Pool steigerten. Zweitens übte PDP1 wesentliche Funktionen unter hypoxischer Umgebung aus. Hier beeinträchtigte der Knockdown von PDP1 die zelluläre Proliferation trotz der niedrigen Sauerstoffwerte, die den mitochondrialen Stoffwechsel unter Hypoxie nicht begünstigen. Darüber hinaus behalten FLT3-ITD Zellen im Gegensatz zu FLT3 WT Zellen eine konservierte mitochondriale Atmungskapazität nach Adaptation an Hypoxie (1% O_2, wie sie physiologisch im Knochenmark vorkommt). Es konnte gezeigt werden, dass diese Fähigkeit durch PDP1 vermittelt wird, da der Knockdown von PDP1 die Fähigkeit zur Wiederherstellung der mitochondrialen Aktivität und zum schnellen Eintritt in den Zellzyklus nach Reoxygenierung beeinträchtigte. Drittens wurde eine duale Rolle von PDP1 bei Reaktionen auf FLT3-Inhibitoren beschrieben. Mechanistisch gesehen regulieren die Zellen bei FLT3-Inhibition ihre PDP1 Expression hoch indem sie auf den chemo-protektiven mitochondrialen Stoffwechsel umgestellt werden, um die metabolische Integrität der Zellen zu wahren. Mit zur Verfügung gestelltem Substrat Pyruvat konnte diese erhöhte PDP1 Aktivität teilweise, aber signifikant, die Effekte von AC220 ausgleichen. Durch ^{13}C-Labelling-Experimente unter AC220 Behandlung konnte bestätigt werden, dass PDP1 der Schlüsselfaktor dieser Umgehung des

Phänotyps ist, da Pyruvat durch diese PDP1 Aktivität vermehrt in den TCA-Zyklus eingeschleust wurde. Die Rolle von PDP1 bei der Resistenz gegenüber AC220 wurde durch PDP1 Überexpressionsexperimente weiter aufgeklärt, indem gezeigt wurde, dass höhere PDP1-Spiegel mit geringerer Sensitivität gegenüber FLT3-Inhibitoren korrelierten. Umgekehrt sensibilisierte die PDP1 Suppression die Zellen für die FLT3 Inhibition und bereitete sie auf die durch niedrige Dosen des FLT3 Inhibitors AC220 induzierte Apoptose vor. Dies wurde anhand primärer AML Blasten eines AC220 resistenten Patienten gezeigt: Ein PDP1-Knockdown in den Zellen dieses Patienten sensibilisierte sie für AC220 Behandlung. Diese Befunde deuten auf einen chemoprotektiven Charakter des mitochondrialen Metabolismus gegenüber zytotoxischen Wirkstoffen und eine zentrale Rolle von PDP1 für den Therapieerfolge hin (Abbildung Z1).

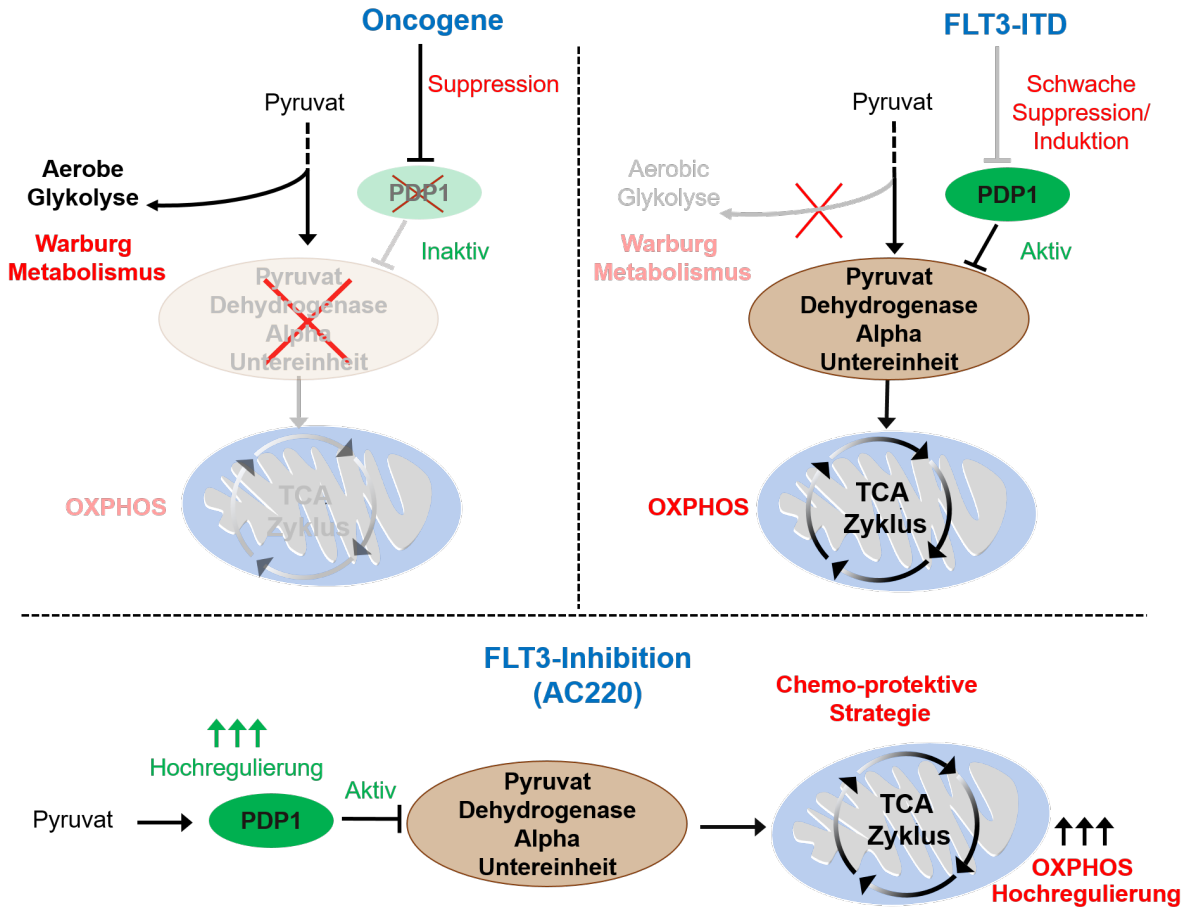


Abbildung Z1: Vorgeschlagenes Modell der metabolischen Regulation in FLT3-ITD-Zellen. PDP1 als Gatekeeper im FLT3-ITD-Zellmetabolismus und bei Arzneimittelreaktionen.

Zusammenfassend wurde PDP1 als eine neue metabolische Vulnerabilität bei FLT3-ITD AML identifiziert und ihre Rolle bei therapeutischen Reaktionen wurde aufgeklärt. Es sind weitere

Forschungsarbeiten erforderlich, um die Rolle von PDP1 beim Rezidiv der Krankheit und bei der Entwicklung von Arzneimittelresistenzen zu untersuchen.

Projekt 2: Methioninmetabolismus in der AML

Neben der spezifischen FLT3-ITD OXPHOS Essentialität präsentiert diese Arbeit in einem separaten Projekt die allgemeine Aminosäureabhängigkeit bei der AML. Nur wenige Aminosäuren sind bisher hinsichtlich ihrer Wichtigkeit in der AML untersucht worden, während viele bisher nicht untersucht wurden. Daher wurde zunächst ein individueller Aminosäure-Dropout Assay durchgeführt, der Methionin als signifikante Anhängigkeit in der AML zeigte. *In vivo* Studien unter Methionin-Restriktions-Diät zeigten eine nachteilige Wirkung auf die Progression der Leukämie, welche Methionin als eine angreifbare Vulnerabilität in AML aufgezeigt (durchgeführt von der Prof. JJ Schuringa-Gruppe, Universität Groningen, Niederlande). Wichtig ist, dass Methioninentzug nur AML Zellen, nicht aber gesunde hämatopoetische Stammzellen beeinflusste.

Um mechanistische Erkenntnisse über die Rolle von Methionin in AML Zellen zu gewinnen, wurden NMR Tracer-basierte Assays mit ^{13}C-Methionin mit einem ungezielten Metabolomik-Ansatz durchgeführt. Interessanterweise wurde der Großteil des Methionins in den AML Zellen zur Transmethylierungsreaktionen verwendet. Im Gegensatz zu gesunden Stammzellen wurden keine ^{13}C-Label in anderen Methioninstoffwechselwegen gefunden, einschließlich der Redox-Kontrollzwischenprodukte Cystein und Glutathion (Abbildung Z2). Die Aufhebung des Methioninstoffwechsels veränderte die Histonmodifikation und blockierte die Transkription.

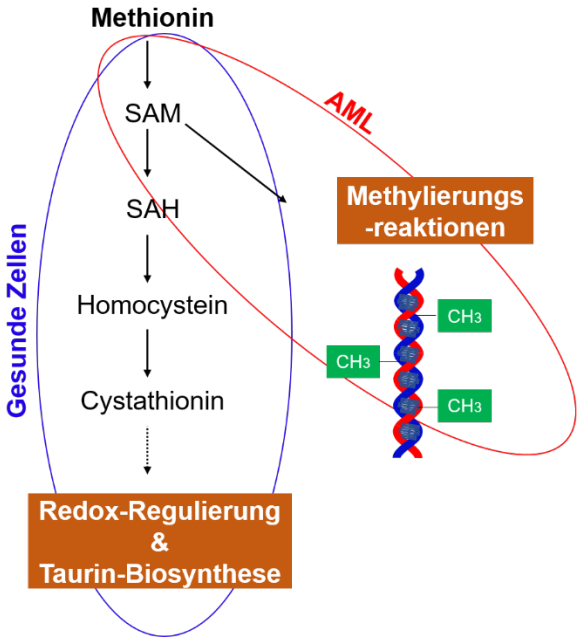


Abbildung Z2: AML-Zellen verwenden Methionin für Methylierungsreaktionen. Eine auf Tracer basierende Untersuchung mittels NMR ergab eine andere Verwendung von Methionin bei der AML im Vergleich zu gesunden Zellen.

Zusätzlich untersuchte diese Arbeit die spezifische Abhängigkeit gegenüber exogenem Methionin trotz der angeborenen intrazellulärem Regenerationsmaschinerie. Bemerkenswerterweise konnte mittels NMR Spektroskopie gezeigt werden, dass bei AML

Zellen im Gegensatz zu gesunden Zellen die Methionin-Recycling-Kapazität aus Homocystein beeinträchtigt ist. Dennoch sind die Daten uneindeutig, da in gesunden Zellen kein Recycling nachgewiesen wurde, was wahrscheinlich auf den Versuchsaufbau zurückzuführen ist, bei dem Methionin in hohen Konzentrationen vorhanden war, wodurch die Notwendigkeit einer de novo Methionin-Regeneration untergraben wurde. Weitere Forschung ist notwendig, um die hier zugrundeliegenden Mechanismen aufzuklären.

Projekt drei: Echtzeit NMR zur Untersuchung des Metabolismus lebender Zellen

Der dritte Teil dieser Arbeit befasst sich mit der Anwendung und Entwicklung von NMR Spektroskopie als Hochdurchsatzmethode für Metabolomikstudien. Traditionelle Metabolismusstudien verwenden Protokolle zur Extraktion von Metaboliten, die Zellen zerstören, hohe Zellzahlen benötigen und lediglich eine Momentaufnahme des Metabolismus liefern. Neuere NMR-Ansätze, im Besonderen die nicht-invasive in-cell NMR, werden zur Untersuchung der intrazellulären, makromolekularen Dynamik eingesetzt. Dieser Arbeit liefert einen parallel durchführbaren, voll automatisierten Ansatz, der die Überwachung des zellulären Metabolismus in Echtzeit mit weniger als einem Zehntel der üblicherweise benötigten Zellzahlen ermöglicht. Konzeptionell beruht diese Methode auf der Messung des Zuflusses/Abflusses extrazellulärer Metabolite im zeitlichen Verlauf ohne Zerstörung der Zellen (Abbildung Z3). Dieser neue NMR Ansatz zeichnet sich durch eine zellfreundliche Matrix, Methylzellulose, aus, die alle bisher beschriebenen Alternativen übertrifft. Es konnte gezeigt werden, dass diese Matrix keinen Einfluss hat auf zelluläre Viabilität hat (erkennbar an den ATP-Spiegeln). Die Zellen erhielten in der Matrix ihre volle Kapazität, auf externe Stimuli und Störungen in Signalwegen zu reagieren. Zudem hält dieser Aufbau physiologische pH und Sauerstoffwerte aufrecht.

Erstmals wurde dieser NMR Ansatz erfolgreich angewendet um die ausgesprochen sensitiven, primären mononukleären Zellen aus dem Knochenmark von AML Patienten zu untersuchen. Diese Zellen zeigten in der entwickelten Versuchsanordnung ein voll aktives und gewöhnliches Verhalten. Die entwickelte Methode wurde weiterhin um die Möglichkeit für Tracer-basierte Assays erweitert. Diese Versuche wurden über Pseudo-2D-Doppelfilter Experimente mit kurzer Messzeit (~7 Minuten) durchgeführt, um den Echtzeitcharakter der Methode zu erhalten. Mit der Fähigkeit, 15 Proben parallel zu analysieren, stellt die hier entwickelte NMR Methode eine hochmoderne, metabolomische Plattformtechnologie dar, die sich robust in der personalisierten Medizin und Diagnostik einsetzen lässt. Die weitere Entwicklung zur Bewertung der Metabolitenwerte von Mitochondrien und des TCA-Zyklus wird die Relevanz und Anwendbarkeit dieser Methode erheblich verbessern.

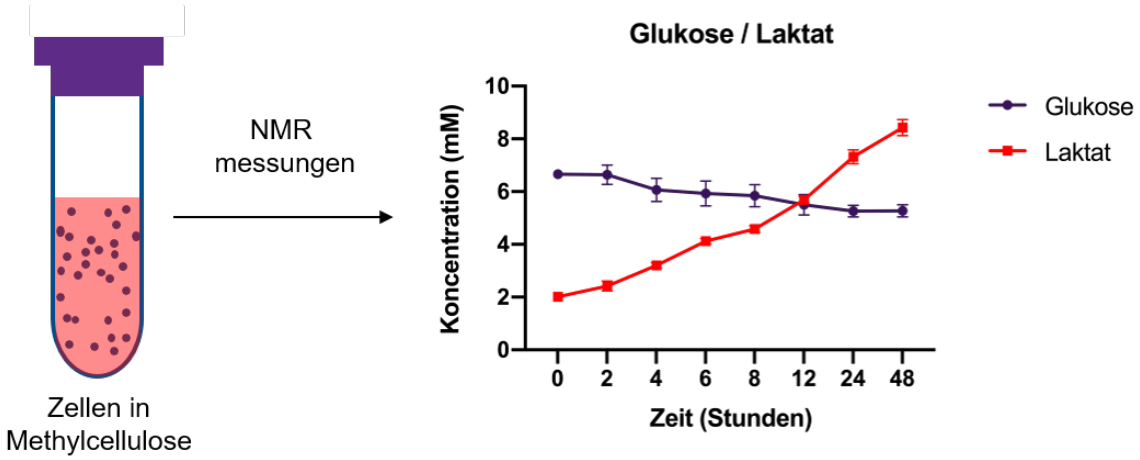


Abbildung Z3: Echtzeit-NMR zur Untersuchung des zellulären Metabolismus. Entwicklung eines zellfreundlichen Ansatzes zur Untersuchung des Metabolismus lebender Zellen.

Table of figures

Figure 1: Genomic alterations in AML. 36
Figure 2: Receptor tyrosine kinase FLT3 structural domains and mutations.....38
Figure 3: Chemical structures of FLT3-inhibitors. The figure shows the chemical structures of both; first generation and second generation FLT3-inhibitors. 41
Figure 4: Core glucose metabolism pathways in the cell.....44
Figure 5: Pyruvate dehydrogenase complex (PDC) regulation of pyruvate fates. 45
Figure 6: Chemical agents developed so far in clinical trials for interrogating OXHPOS and mitochondrial activities in AML. 51
Figure 7 Minimal PDHK1 phosphorylation in FLT3-ITD cells. The western blot shows the relative PDHK1 phosphorylation levels in a variety of cancer cell lines. FLT3-ITD (circled in blue) show relatively low phosphorylation on Y243 and subsequently on S293. Adapted from (Hitosugi et al., 2011) (license obtained). 54
Figure 8: General overview of amino acid metabolism in cancer. 56
Figure 9: Core pathways of methionine metabolism.....57
Figure 10: Metabolomics studies in cancer. 60
Figure 11: Chemical shift assignments of intracellular metabolites. 62
Figure 12: Sample preparation and labelling schemes in NMR-metabolomics. 64
Figure 13: In-cell NMR approach for proteomics and metabolomics on living cells. 65
Figure 14: Seahorse measurement of oxygen consumption rate (OCR) in 32D cells. 71
Figure 15: FACS gating strategy shown on 32D cells transduced with GFP vector. 78
Figure 16: Pseudo 2D GBIRD double-filter 1D NOESY experiment pulse sequence. 88
Figure 17: FLT3-ITD AML cell lines have higher TCA/glycolysis ratio. NMR measurements of higher concentration ratio between 91
Figure 18: 32D model of FLT3-ITD signalling reveals higher TCA cycle and OXPHOS activity. 93
Figure 19: FLT3-ITD activity favours higher pyruvate incorporation into the TCA cycle.....94
Figure 20: TCA cycle supplementation rescues glucose deprivation effects in FLT3-ITD. ...94
Figure 21: FLT3-ITD cells are highly sensitive to mitochondrial inhibition. 95
Figure 22: FLT3-ITD cells are high expressers of PDP1. 96
Figure 23: PDP1 levels correlate with poor overall survival in AML. 97
Figure 24: PDP1 knockdown impairs cellular proliferation of FLT3-ITD cells. 98
Figure 25: PDP1 knockdown impairs FLT3-ITD cell proliferation and synergises with venetoclax *ex vivo*. 99
Figure 26: PDP1 abrogation impairs leukaemia progression *in vivo* 100

Figure 27: Intermediate supplementation of individual mitochondrial pathways is not sufficient to rescue PDP1 knockdown effects. 101
Figure 28: PDP1 knockdown has no impact on cells that are not reliant on OXPHOS (Rho Zero cells). 102
Figure 29: PDP1 overexpression (OE) enhances cellular viability. 103
Figure 30: PDP1 mediates conserved OXPHOS capacity and proliferation capacity upon adaption to hypoxia. 105
Figure 31: PDP1 knockdown synergises with FLT3-inhibition. 106
Figure 32: Higher PDP1 levels are associated with resistance to FLT3-inhibition. 107
Figure 33: PDP1 knockdown sensitizes therapy-resistant AMLs to AC220. 108
Figure 34: PDP1 is upregulated upon FLT3-inhibition. 109
Figure 35: FLT3-inhibition leads to blockade in glucose uptake and can be rescued by pyruvate. 110
Figure 36: Synergism of FLT3-inhibition with venetoclax 111
Figure 38: Gene set enrichment analysis (GSEA) of metabolism-related genes in FLT3-ITD *vs* FLT3-WT AMLs. 114
Figure 38: Methionine is a strong dependency in AML but not healthy cells....122
Figure 39: Methionine starvation leads to global metabolic insufficiency. 123
Figure 40: Methionine dietary restriction impairs leukaemia progression *in vivo*....124
Figure 41: Full panel of untargeted ^{13}C methionine tracing. 125
Figure 42: Minimal methionine-to-cystathionine conversion in AML compared to healthy cells. 126
Figure 43: Methionine depletion impairs DNA methylation and transcription 127
Figure 44: MTR is downregulated in AML. 128
Figure 45: Methionine recycling. 130
Figure 46: Real-time NMR approach design. 136
Figure 47: cell friendly nature of the new real-time NMR setup. 137
Figure 48: Physiological oxygen and pH levels present in the real-time NMR setup. 138
Figure 49: Time course measurements of extracellular metabolites dynamics of primary AML mononuclear cells. 140
Figure 50: Tracer based assay with ^{13}C glucose. 141

List of abbreviation

1D	one dimensional
2D	two dimensional
2-DG	2-deoxy-D-glucose
3-BroP	3-bromopyruvate propylester
AML	Acute myeloid leukaemia
ASL	Argininosuccinate lyase
ASS1	Argininosuccinate synthetase-1
ATP	Adenosine triphosphate
ATRA	All-trans retinoic acid
B_0	External field
BCAA	Branched-chain amino acids
CR	Complete remission
Cri	Complete remission with incomplete hematologic recovery
ddC	2′3′-dideoxycytidine
DSS	Sodium trimethylsilylpropanesulfonate
ECAR	Extracellular acidification rate
EFS	Event-free survival
ELN	European Leukemia Network
EMA	European Medicines Agency
ETC	Electron transport chain
FACS	Florescence-activated cell sorting
FAO	Fatty acid oxidation
FBS	Foetal bovine serum
FCS	Foetal calf serum
FDA	Food and Drug Administration
FLK-2	Foetal Liver Kinase II
FLT3	Fms-Like Tyrosine Kinase III
FLT3L	Fms-Like Tyrosine Kinase III-ligand
FSC	Forward scattered
GBIRD	Gradient Bilinear rotation decoupling
GSEA	Gene set enrichment analysis
HiDAC	High dose Ara-C
HMDB	Human metabolome database
HSA	Highest single agent

HSCs	Hematopoietic stem cells
HSCT	Hematopoietic stem cell transplantations
HSQC	Heteronuclear Single-Quantum Correlation
IC50	Half maximal inhibitory concentration
IDH	Isocitrate dehydrogenase
IL3	Interleukin 3
ITD	Internal tandem duplications
KGDH	α-ketoglutarate dehydrogenase
LDHA	Lactate dehydrogenase A
LSCs	Leukemic stem cells
MS	Mass spectrometry
MTHFD2	Methylenetetrahydrofolate dehydrogenase-cyclohydrolase 2
mTORC1	Mammalian target of rapamycin complex 1
MTR	Methionine Synthase
NMR	Nuclear Magnetic resonance spectroscopy
NOD-SCID	Nonobese diabetic/severe combined immunodeficiency
NOX2	NADPH oxidase-2
NUS	Non-Uniformed Sampling
OCR	Oxygen consumption rate
OS	Overall survival
OXPHOS	Oxidative phosphorylation
PBMSCs	Peripheral blood mononuclear-stem cells
PBS	Phosphate buffer saline
PC	Pyruvate carboxylase
PDC	Pyruvate dehydrogenase complex
PDH	Pyruvate dehydrogenase
PDHE1/ PDHA1	Pyruvate dehydrogenase subunit E1
PDK	Pyruvate dehydrogenase kinases
PDP	Pyruvate dehydrogenase phosphatase
PDX	Patient-derived xenograft
PEI	Polyethylenimine
PET	Positron Emission Tomography
PIA	Plasma inhibitory activity
PKM2	Pyruvate kinase II
PPM	Parts per million
RF	Radio frequency
ROS	Reactive oxygen species

SCF	Stem cell factor
SDS	Sodium dodecyl sulphate
sgRNA	Single guide RNA
shRNA	Short hairpin RNA
siRNA	Small interfering RNA
SSC	Side scattered
SSO	Sorbitan sesquioleate
STAT5	Signal transducer and activator of transcription
STK1	Stem Cell Kinase I
T-ALL	T-cell acute lymphoblastic leukaemia
TCA	Tricarboxylic acid cycle
THF	Tetrahydrofolate
TKD	Tyrosine kinase domain
TKIs	Tyrosine kinase inhibitors
TMSP	Trimethylsilylpropanoic acid
TPO	Thrombopoietin
TPPI	Time-proportional phase incrementation
UTR	Untranslated region
WHO	World health organization
γ	Gyromagnetic ratio

Chapter I

General introduction

Metabolic plasticity in acute myeloid leukaemia and overview of metabolomics platforms

1.1. Altered metabolism in acute myeloid leukaemia

1.1.1. Acute myeloid leukaemia

Haematopoietic stem cells (HSCs) constitute a highly complex machinery for the production of the different types of blood cells in the bone marrow. HSCs are tightly regulated by a balance between proliferation and self-renewal to avoid excessive uncontrolled cellular growth. Dysregulation in these machineries can result in leukaemias and myeloproliferative disorders.

Acute myeloid leukaemia (AML) is a malignant disorder of the haematopoietic system that is mainly caused by genetic alterations in genes regulating cell cycle and differentiation. AML accounts for about 25% of all leukaemias making it the most common form of leukaemia in adults (Estey and Döhner, 2006). AML is particularly associated with poor outcomes in the patients (Daver et al., 2019). The disease is characterised by the presence of malignant non-functional blasts in the bone marrow that are incapable of differentiation and maturation (Passegué et al., 2003). According to the World Health Organization (WHO) classification, AML bone marrow accommodates ≥20% myeloblasts (Arber et al., 2016). The high density of these non-functional myeloblasts ultimately leads to bone marrow failure and haematopoietic insufficiency inflicted by anaemias and higher susceptibility to infection (Deschler and Lübbert, 2006). Therefore, AML patients require infection control, transfusions, as well as anti-proliferation chemotherapeutic agents.

Standard AML chemotherapy involves the administration of cytarabine (Ara-C) and an anthracycline (daunorubicin or idarubicin) on a 7+3-based regimen (7 days cytarabine and 3 days anthracycline) (Dombret and Gardin, 2016). Further targeted therapies are being recently added to the treatment based on the genetic background causing the leukaemia (FLT3-inhibitors, IDH-inhibitors, CD33 antibodies and others) (DiNardo et al., 2018; Döhner et al., 2017; Dombret and Gardin, 2016; Gu et al., 2018; Stein et al., 2017; Stone et al., 2017). Older patients who are unfit for chemotherapy usually receive low intensity chemotherapy together with targeted agents. Novel combination therapies have also shown significantly higher efficacy in treating those patients (namely, the combination of the BCL2-inhibitor venetoclax with the hypomethylating agent azacytidine or decitabine (DiNardo et al., 2019)). Post-remission therapy usually includes intensive high-dose chemotherapy and/or haematopoietic stem cell transplantation, which yields the most durable treatments for AML (Schlenk, 2014). However, therapy choice usually takes into account many factors, mainly the cytogenetics and relapse risk, but also age and patient fitness.

The genetic landscape of the disease is highly heterogeneous with over 5234 known driver mutations in 76 different genes (Papaemmanuil et al., 2016), including epigenetic alterations (Conway O'Brien et al., 2014) (Figure 1). These numbers are constantly increasing with more and more recent reports identifying new genetic alterations that lead to AML.

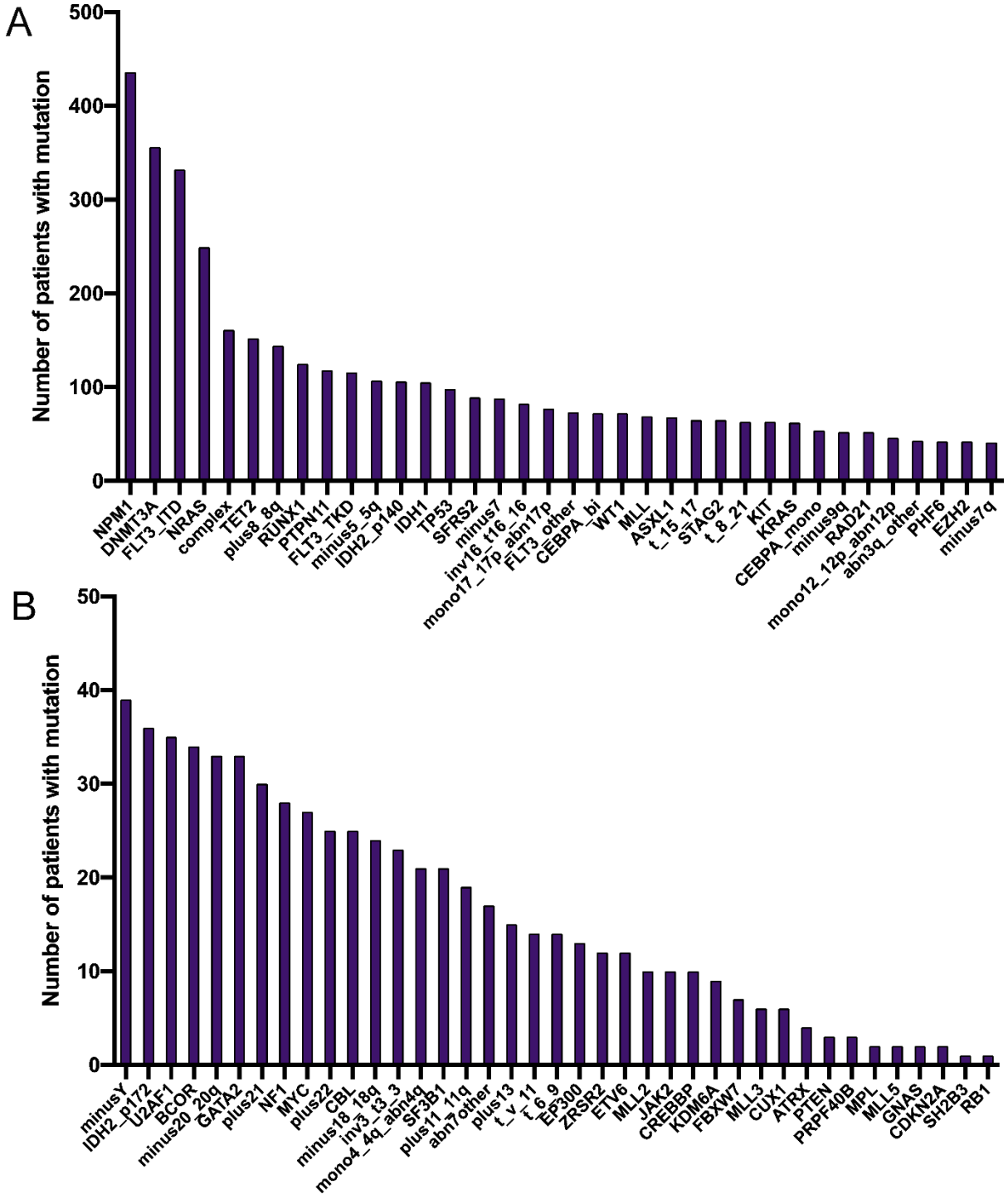


Figure 1: Genomic alterations in AML. Molecular subtypes of 76 different alterations in 1540 sequenced patients are illustrated and classified by this thesis as A. more recurrent (occurring in >40 patients) and B. less recurrent (occurring in <40 patients). Distribution of the molecular lesions entitling genetic mutations, chromosomal aberrations, complex karyotypes and gene fusions is also depicted. Figure was made using data produced by the study of (Papaemmanuil et al., 2016).

Interestingly, AML is different from many other cancers and haematological malignancies in terms of disease evolution. The long standing hypothesis of the 'Two-Hits' model suggests that two genetic alteration (can also be epigenetic) are required for leukaemic transformation to occur (Kelly and Gilliland, 2002; Shih et al., 2012). Indeed, this model is supported by a large-scale sequencing and cytogenetic analysis reporting 86% of the patients to harbor two or more identified genetic alterations (Papaemmanuil et al., 2016). This diversity in the pathophysiology of the disease highlights the need for a more detailed genetic profiling of the patients at diagnosis and implementing it in the therapeutic strategy. In fact, this cornerstone of AML research drove a whole new era of personalized medicine efforts over the last decade. New targeted therapies were developed to specifically target the mutated receptor tyrosine kinases, surface antigens, signaling molecules, cellular enzymes, methyltransferases and other drivers (Lohse et al., 2018).

In order to uniform therapeutic approaches, experts in the field drafted outlines classifying AML by patients' prognosis and risk stratification according to the genetic drivers (2017 European Leukemia Network (ELN) recommendations) (Döhner et al., 2017). This document categorized the molecular background of AML into 3 categories: i) favorable risk, such as biallelic CEBPA mutation and mutated NPM1 without FLT3-ITD or with low allelic ratio FLT3-ITD, ii) intermediate risk group like t(9;11) and *MLLT3-KMT2A*, iii) adverse risk group such as wild type NPM1 with high FLT3-ITD allelic ratio, complex karyotypes and mutated TP53 (Döhner et al., 2017; Papaemmanuil et al., 2016). This standardization resulted in treatment recommendations for the patients with targeted therapies.

1.1.2. Fms-Like Tyrosine Kinase III

FLT3 mutations play a crucial role in patients' outcomes and thus, this section will give more insights into FLT3 pathophysiology in AML. Fms-Like Tyrosine Kinase III (FLT3), also known as Foetal Liver Kinase II (FLK-2) or human Stem Cell Kinase I (STK-1), plays a prominent role in promoting cell proliferation (Hannum et al., 1994; Lyman et al., 1993; Rosnet et al., 1991). FLT3 is normally expressed on primitive haematopoietic stem and progenitor cells (but not mature cells) and plays a role in their survival and maintaining their stemness (deLapeyrière et al., 1995; Hannum et al., 1994; Small et al., 1994). The receptor consists of five domains: extracellular, juxtamembrane, tyrosine kinase, kinase insert and C-terminal domains (Griffith et al., 2004; Kiyoi et al., 2020) (Figure 2).

FLT3 mutations are present in approximately 30% of AML patients and are associated with poor prognosis (Daver et al., 2019). These mutations fall into two categories: i) common

internal tandem duplications (ITDs) in the receptor's juxtamembrane domain (20-25%) and ii) less common point mutations in the activation loop of the tyrosine kinase domain (TKDs) (5-7%) (Daver et al., 2019; Kottaridis et al., 2003; Nagel et al., 2017). FLT3-ITD mutations are usually more common and are associated with non-favorable disease prognosis (Daver et al., 2019; Kiyoi et al., 1999; Kottaridis et al., 2001). TKD mutations, however, are not clearly categorized in terms of their prognostic value, and in fact, one study reported no prognostic association between FLT3-TKD mutations and overall survival (OS) or event free survival (EFS) (Bacher et al., 2008). Nonetheless, TKD mutations have more clinical relevance in the evolution of resistance to FLT3-inhibitors (discussed below) (Bagrintseva et al., 2004; Von Bubnoff et al., 2009; Heidel et al., 2006).

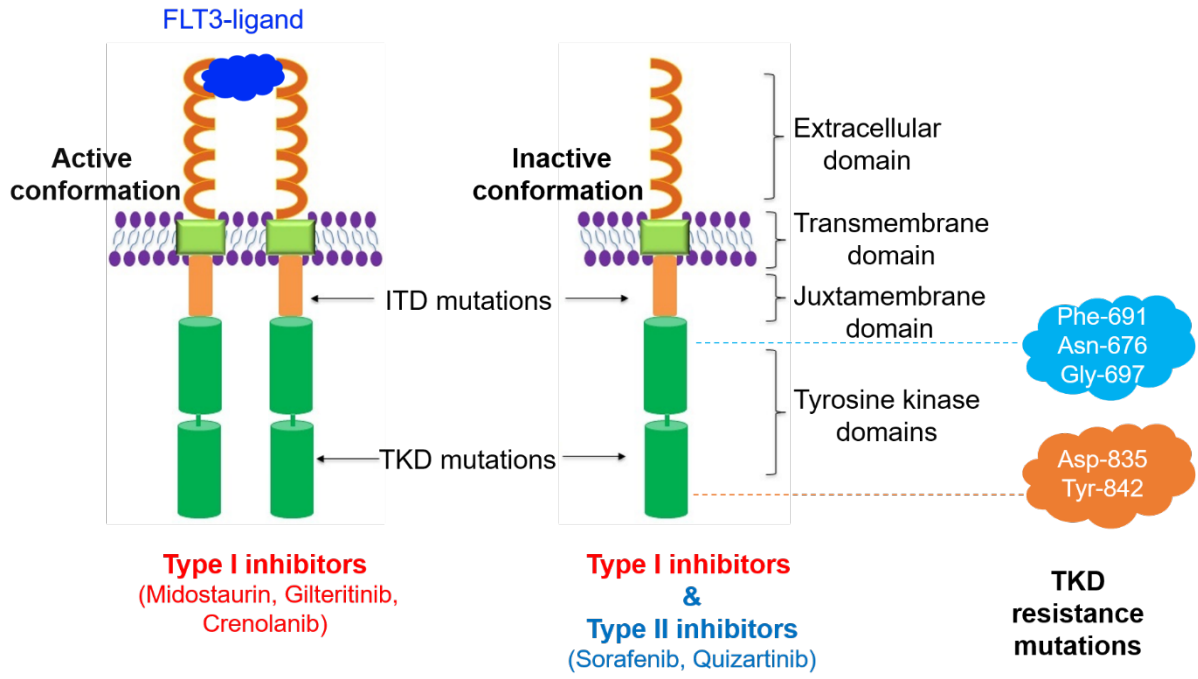


Figure 2: Receptor tyrosine kinase FLT3 structural domains and mutations. The figure shows the structural domains of FLT3-receptor and the location of the occurring mutations. Further, the different conformations of the receptor are shown with indication of FLT3-inhibitors that function in each. Modified after (Kiyoi et al., 2020) (license obtained).

FLT3-ITD mutations were first reported as genetic drivers in AML in 1996 (Nakao et al., 1996). According to their FAB classification, FLT3-muations are usually most recognized within the M5 subtypes, but can still be detected in M2, M3 and M6 (Levis and Small, 2003; Schnittger et al., 2002; Thiede et al., 2002). The average mutation length is between 39 up to 54 base pairs (bp) (ranging from 3-180bp, and up to 400 in some studies) (Schnittger et al., 2002; Thiede et al., 2002). Correlation has been shown between the mutational length and the prognosis and OS, with worse prognosis in the longer ITDs (Liu et al., 2019; Stirewalt et al.,

2006). In addition, higher FLT3-ITD allelic ratio (ITD/WT) is reported as a strong prognostic factor associated with poor survival and increased relapse risk, and thus it is crucially considered in patient's risk classification (Döhner et al., 2017; Kottaridis et al., 2001; Thiede et al., 2002; Whitman et al., 2001). Further, insertion type, karyotype and the co-occurrence of other mutations are also considered as co-determinants of the disease outcome.

In fact, FLT3-ITD mutations tend to occur at high frequency in combination with other mutations, mainly nucleophosmin 1 (NPM1) (Falini et al., 2005). These co-mutations have a strong impact on the patient outcome and plays an important role in treatment options (wild type or mutated NPM1 with FLT3-ITD^{low} classifies favorable risk, NPM1 with FLT3-ITD^{high} classifies intermediate risk while wild type NPM1 with FLT3-ITD^{high} falls into the adverse risk category) (Döhner et al., 2017). Nonetheless, they are also reported to coincide with other mutations such as DNMT3, RUNX1 (Behrens et al., 2017; Ley et al., 2010). Co-occurrence with chromatin-slicing alterations, translocations and gene fusions such as NUP98-NSD1, PML-RARA has also been mapped (Papaemmanuil et al., 2016).

FLT3-ITD (and also TKDs to some extent) can activate the FLT3 kinase and induce autonomous cellular growth (Choudhary et al., 2005, 2007; Daver et al., 2019; Grafone et al., 2012). FLT3-ITD was shown to modulate cell proliferation, survival, and differentiation through constitutive activation of canonical pathways including PI3K/AKT, MAPK/ERK as well as the signal transducer and activator of transcription (STAT5) (Brandts et al., 2005; Mizuki et al., 2000; Murata et al., 2003; Rocnik et al., 2006; Tse et al., 2000). Of particular importance is the role STAT5 plays as a strong driver of cellular proliferation and self-renewal capacity of HSCs (Chung et al., 2005; Wierenga et al., 2006) as well as of leukemic cells (Benekli et al., 2003). Normally, STAT5 activation is mediated by Jak2/ Src family kinases or other receptor tyrosine kinases (Beisenherz-Huss et al., 2001; Chen et al., 1997). Interestingly, FLT3-ITD, but not FLT3-TKD, was reported to directly activate STAT5 signaling pathway independently of the regular STAT5-activation mechanisms (Choudhary et al., 2007). Noteworthy, this activation is usually independent of FLT3-ligand binding (Choudhary et al., 2007; Kiyoi et al., 1998; Mizuki et al., 2000).

This high dependence of FLT3-ITD-positive AML cells to FLT3 signalling was extrapolated and successfully translated into clinical application by developing small molecules inhibiting FLT3 signaling. A handful of first-generation FLT3 inhibitors was developed. However, showed low efficacy and specificity, with only midostaurin being currently used in the clinic with FDA and EMA approval (European Medicines Agency, 2017; USA's Food and Drug Administration, 2017). Second generation inhibitors were more potent; acting in the low nM range with higher

specificity (Table 1) (Chao et al., 2009; Daver et al., 2017, 2019; Kampa-Schittenhelm et al., 2013; Lee et al., 2017b; Levis and Perl, 2020; Maziarz et al., 2016). Based on their binding to the FLT3 receptor, those inhibitors are classified into 'Type 1' which can bind to the active conformation of FLT3 enabling it to inhibit both FLT3-ITD and FLT3-TKD and 'Type 2' which can only bind the inactive form of the receptor resulting in the inhibition of FLT3-ITD only (Daver et al., 2015) (Figure 2). List of FLT3-inhibitors and their chemical structures are shown in (Table 1) (Figure 3).

Table 1: FLT3-inhibitors in development. Modified after the reviews of (Chao et al., 2009; Daver et al., 2017, 2019; Hassanein et al., 2016; Kampa-Schittenhelm et al., 2013; Lee et al., 2017b; Levis and Perl, 2020; Maziarz et al., 2016).

Inhibitor	Generation	Clinical phase	Receptor type	IC50 for FLT3-ITD (nM)
Midostaurin	First-generation	FDA and EMA-approved	10-30	1
Sorafenib	First-generation	III	2	2
Sunitinib	First-generation	II	4	1
Tandutinib	First-generation	Withdrawn	220	2
Lestaurtinib	First-generation	II	3	1
Ponatinib	First-generation	II	4	2
Quizartinib	Second-generation	III	~1	2
Gilteritinib	Second-generation	FDA approved	~1	1
Crenolanib	Second-generation	III	2	1

So far, evaluation of first-generation FLT3 inhibitors as single agent therapy, such as midostaurin, was not very promising suggesting drug combination as the way to go (Fischer et al., 2010; Stone et al., 2005). The RATIFY trial evaluated midostaurin in combination with standard chemotherapy (induction therapy with daunorubicin and cytarabine and consolidation therapy with high-dose cytarabine) which showed significant improvement in the patients' outcome and overall survival (Stone et al., 2017). Interestingly, not only patients with FLT3-ITD benefited from the therapy, but also FLT3-TKD patients, indicating the pan-inhibition activity of midostaurin against RTKs and other oncogenic pathways. Nonetheless, the young age of the patients added to the different clinical presentation of patients with FLT3-TKD (milder compared to the FLT3-ITD patients) can be a confounding factor, raising the need for more detailed and controlled studies. In addition, midostaurin has shown effective as a

maintenance therapy after high dose Ara-C (HiDAC) or hematopoietic stem cell transplantations HSCT (Schlenk et al., 2015).

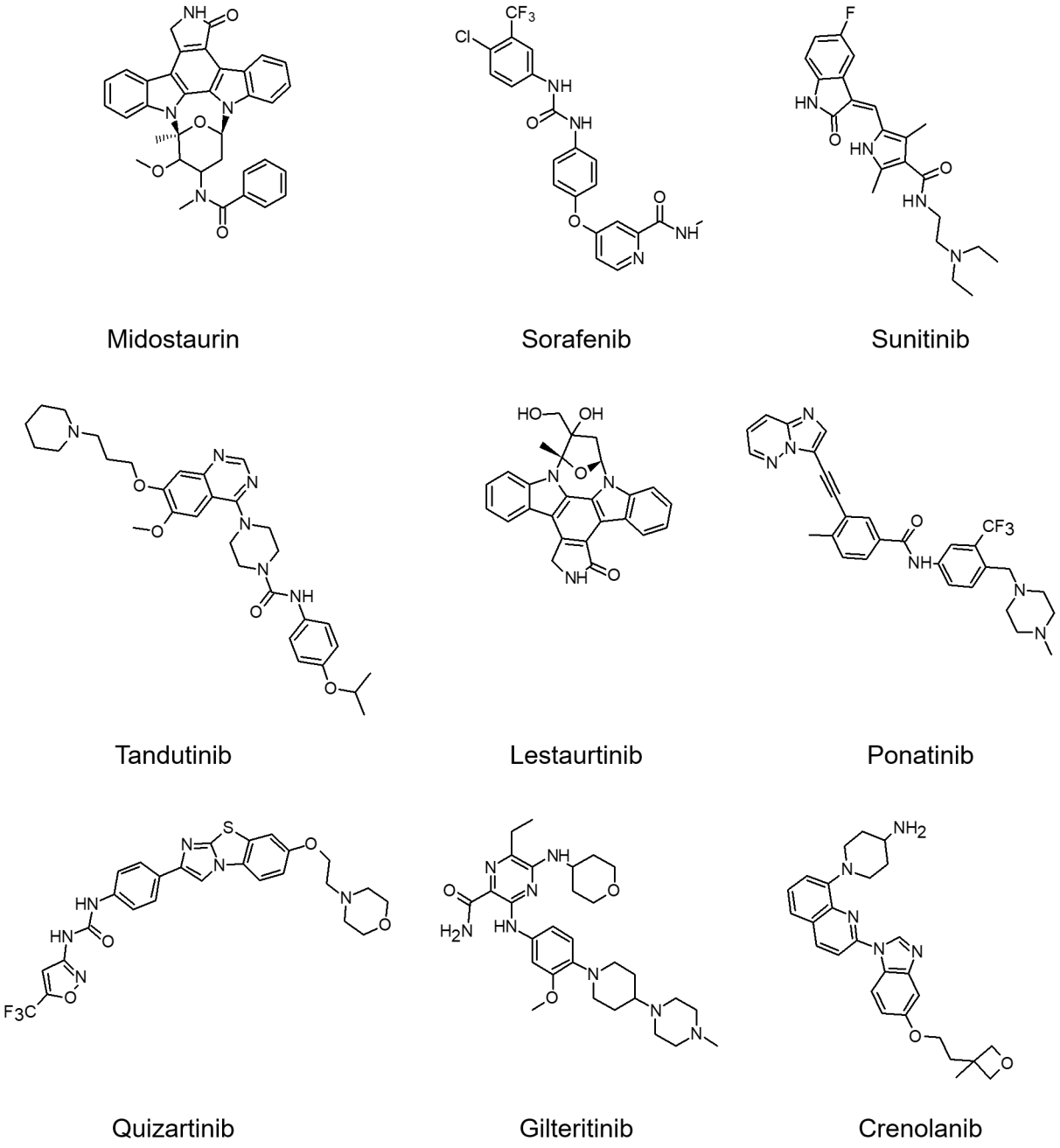


Figure 3: Chemical structures of FLT3-inhibitors. The figure shows the chemical structures of both; first generation and second generation FLT3-inhibitors.

Second generation inhibitors seemed more promising as monotherapy in refractory and relapsed AML. Gilteritinib treatment has induced a response in 40% of the subjects with 8% achieving complete remission (CR) (Perl et al., 2017). Further, crenolanib single agent

treatment has shown efficacy in refractory and relapsed AML patients, with superior responses in patients who did not receive prior TKI treatment (Cortes et al., 2016; Randhawa et al., 2014). Similarly, quizartinib as a single agent has shown advantageous to the patients represented by higher OS and bridge to transplant in relapsed or refractory FLT3-ITD AML patients (Cortes et al., 2018). In fact, quizartinib is currently being evaluated in the QuANTUM-R trial as a monotherapy vs salvage chemotherapy (trial number: NCT02039726).

On the cellular level, FLT3-inhibitors lead to reduced FLT3-phosphorylation without affecting the total FLT3 levels, a finding that was also confirmed *in vivo* by plasma inhibitory activity (PIA) assays (Levis et al., 2006). This inhibitory action is achieved by the binding of the inhibitor to the ATP-binding site of the TKD, and thus suppressing the downstream signaling mechanism activated by the receptor (Larrosa-Garcia and Baer, 2017). FLT3-inhibition showed to efficiently target and eliminate the leukaemic cells by alleviating the blockade in differentiation (Zheng et al., 2002). This phenomenon was also observed *in vivo* in marrow blasts of patients treated with quizartinib (Sexauer et al., 2012). This report has further shown that this differentiation induction leads to impairment of cell proliferation mainly by cell cycle arrest, but also by inducing cell death.

However, the responses to FLT3 inhibitors are transient, lasting for 3 to 6 months owing to the emergence of resistance, which constitutes a significant challenge for a durable response in the patients (Daver et al., 2015, 2019). The primary cause of resistance is the acquisition of point mutations in the ATP-binding domain of the FLT3-TKD (Asp-835, Phe-691, Tyr-842, Asn-676, Gly-697 and others) (Abu-Duhier et al., 2001; Von Bubnoff et al., 2009; Cools et al., 2004; Heidel et al., 2006; Kindler et al., 2005). It is assumed that these mutations alter the conformational state and weaken the binding affinity to FLT3 inhibitors (Daver et al., 2015). Thus, cells become irresponsive to FLT3-inhibitors, especially type II since they only bind the receptor in the inactive state. Furthermore, despite the ability of certain FLT3-inhibitors (such as sorafenib) to suppress FLT3-TKD receptor phosphorylation, no suppression effect was exerted on its downstream signalling mediators, including ERK or AKT/S6K (Zhang et al., 2014).

A variety of other resistance mechanisms have been described. First, persistent exposure to FLT3-inhibitors leads to higher activation of parallel pro-survival signaling pathways including PI3K/AKT and/or RAS/MEK/MAPK (Piloto et al., 2006). Hence, cellular proliferation becomes more dependent of those survival mechanisms and thus, less sensitive to FLT3-inhibitors. Second, cellular microenvironment and interaction with the bone marrow stroma and other cell types were reported to play a role in the resistance process (Sexauer et al., 2012; Yang

et al., 2014). The stroma effect was shown to be driven by several mechanisms such as cell-cell interaction and secretion of different growth factors and cytokines, which hamper the potency of FLT3-inhibition. Last, the levels of FLT3-ligand available to the cells was shown to play an important role in the responses to FLT3-inhibitors. Higher FLT3-ligand levels shift the IC50 of the inhibitor higher and hence, reduce responsiveness (Yang et al., 2014).

Considering the more aggressive proliferation phenotype the resistant cells exert, these cells face higher demands for energy. In fact, some studies have shown metabolic reprogramming to be a critical factor contributing to the evolvement of cancer itself but also, to the evolvement of resistance. The role of metabolic rewiring in AML and FLT3-ITD and also drug resistance will be discussed in detail in the next section.

1.1.3. Cancer and metabolism

Human cells have special dependence on glucose catabolism as the core energy source. Glucose is catabolized via the ten-step glycolysis process, which generates pyruvate (Lehninger et al., 2005). Pyruvate is transported into the mitochondria to feed the tricarboxylic acid cycle (TCA), producing energy precursors (NADH and $FADH_2$). These precursors are then converted to ATP under the activity of the respiratory chain complexes I, II, III and IV. These reactions take place in the inner mitochondrial membrane in a process termed “oxidative phosphorylation” (OXPHOS) (Figure 4A). This process is also termed as “cellular respiration” since it is strictly dependent on the presence of oxygen. When oxygen levels drop in the tissues, cells divert their pyruvate from the TCA cycle towards lactate production (fermentation), which yields substantially lower amounts of ATP (Figure 4B).

The regulation of this switch is tightly controlled by the pyruvate dehydrogenase complex (PDC), downstream of glycolysis. PDC is one of the most important metabolic checkpoints/ regulators in the cell. It consists of a pyruvate dehydrogenase (PDH) which converts pyruvate to Acetyl-CoA under the regulation of 4 different pyruvate dehydrogenase kinases (PDKs), two pyruvate dehydrogenase phosphatase (PDPs) and some other transferases and binding proteins (acetyltransferase (E2p) and E3-binding protein (E3BP)) (Hiromasa et al., 2004; Liu et al., 1995; Patel and Korotchkina, 2001) (Figure 5). The balance of PDH subunit E1 (PDHE1, also known as PDHA1) phosphorylation by PDKs (inhibits the complex) or dephosphorylation by PDP (activates the complex) decides on the metabolic phenotype in the cell (glycolytic or mitochondrial respiration, respectively) (Roche et al., 2001).

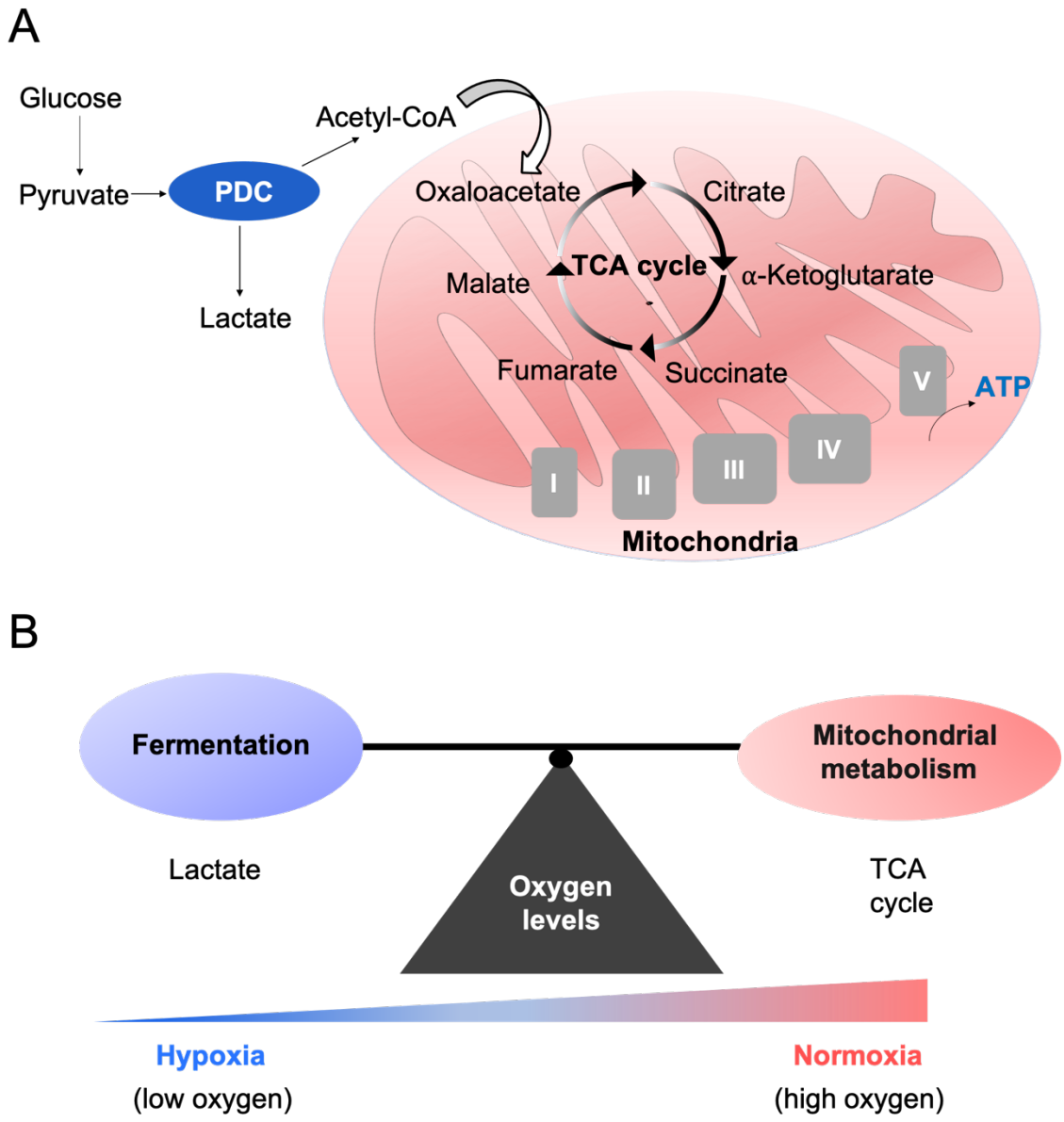


Figure 4: Core glucose metabolism pathways in the cell. A. Glycolysis produces pyruvate that can is incorporated into the TCA cycle then oxidative phosphorylation. Alternatively, pyruvate can be directly converted to lactate (fermentation). B. Oxygen regulation of the metabolic program switch: OXPHOS in the presence of oxygen vs anaerobic fermentation in hypoxic conditions.

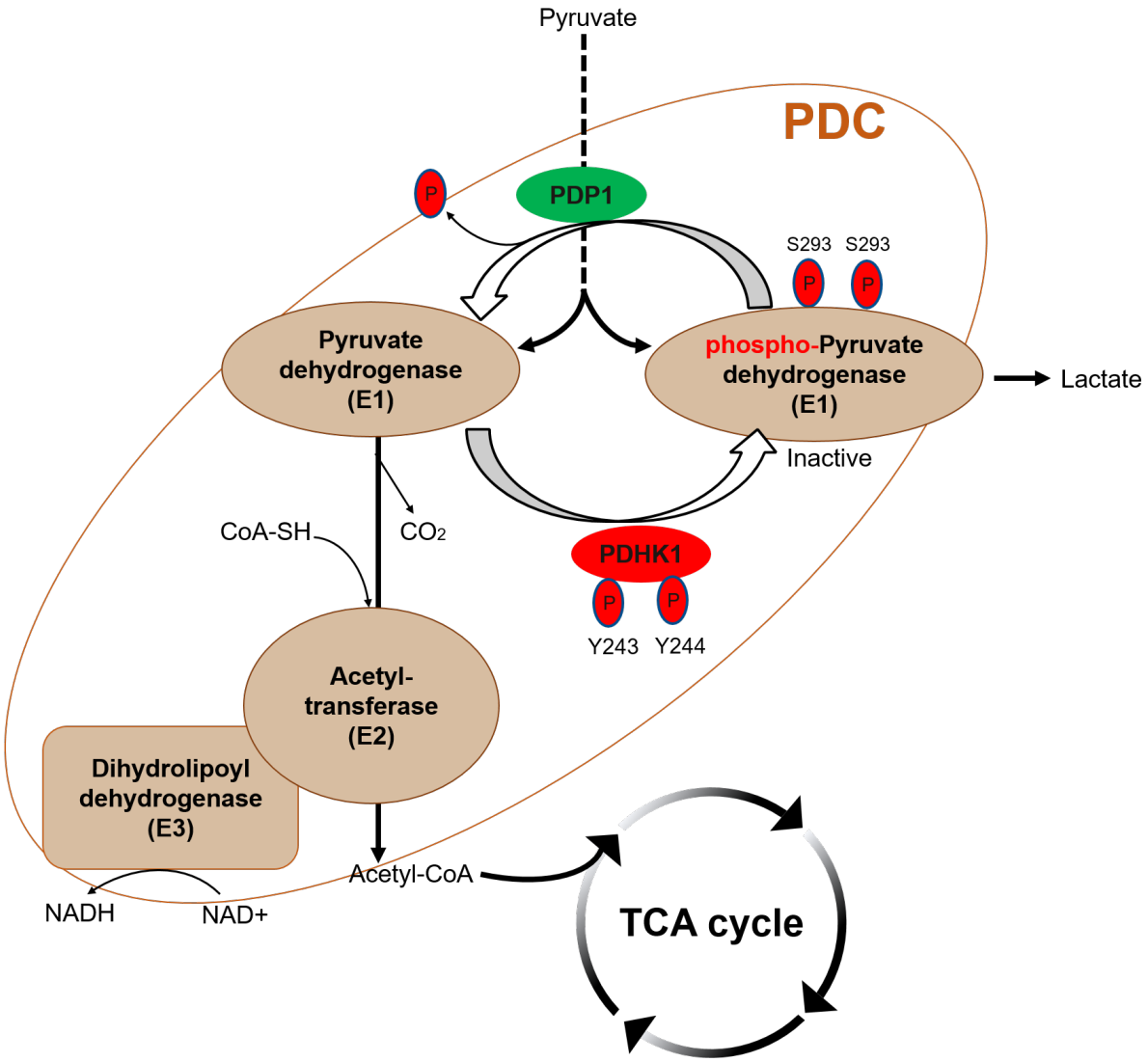


Figure 5: Pyruvate dehydrogenase complex (PDC) regulation of pyruvate fates. Structural illustration of the PDC catalytical subunits (E1, E2 and E3) in metabolising pyruvate. Phosphatase activity of PDP dephosphorylates the pyruvate dehydrogenase E1 subunit (PDHE1) drives the conversion into the TCA cycle while the kinase activity of PDK inactivates PDHE1 and drives lactate production.

Highly proliferative conditions, such as cancer, drive the cells to develop new mechanisms to utilize abundant metabolites in order to cope with their high energy demands. In fact, metabolic rewiring is attracting attention in current cancer research and we have summarized current efforts in AML in a recent review article (Kreitz et al., 2019). Understanding the cancer-specific upregulation or downregulation of different metabolic cycles is becoming a core research area. These research efforts were translated into metabolic targeting approaches based on identifying vulnerabilities that showed effective in targeting cancer cells. In fact, this concept is not new, as metabolic treatment of acute leukaemias by a folic acid antagonist, aminopterin, has been described in 1948 and its antimetabolite derivative, methotrexate, is being used in clinics for decades (Farber and Diamond, 1948). Just in the last decade, several inhibitors of

metabolism have been already approved for AML treatment (venetoclax and isocitrate dehydrogenase (IDH) inhibitors) and some others are currently being evaluated in clinical trials (L-asparaginase and CPI-613) (Kreitz et al., 2019).

The most remarkable discovery in this field has emerged from Otto Warburg's laboratory in the 1920s, when he described the aerobic glycolysis as a cancer cell phenomenon (Warburg et al., 1927). He reported glucose conversion into lactate regardless to oxygen levels in the tumour cells. Later on, he postulated that mitochondrial respiration is generally impaired in cancer cells (Warburg, 1956). Subsequent research in the following decades showed impaired glucose tolerance and altered carbohydrates metabolism in a variety of haematological malignancies (Lisker et al., 1966). Studies with Positron Emission Tomography (PET) imaging with a florescent glucose analogue (^{18}F-fluoro-2-deoxy-D-glucose) have shown significant retention of the glucose analogue in the tumour tissue indicating their high glycolytic activity (Feng et al., 2019; Vansteenkiste and Stroobants, 2001). In fact, observing glucose metabolism has been implemented as a diagnostic approach for detecting solid malignant activity in the tissues.

Abnormal glucose metabolism is similarly considered as a hallmark of AML. High glucose uptake activity was heavily reported in AML patients. In two different studies, analysis of serum glucose metabolism in large AML patients vs healthy individuals cohorts was shown highly altered with increased lactate levels (Chen et al., 2014; Wang et al., 2013). As such, perturbation in glucose metabolism was classified as a strong biomarker and was correlated with poorer prognosis in the patients. The correlation of glycolytic activity with prognosis and responses to chemotherapy was also reported in another study (Herst et al., 2011). Although higher glucose activity was associated with more resistance to ATRA/ ATO treatment, surprisingly, highly glycolytic blasts predicted better overall survival in the patients. Nonetheless, this study is limited by the small sample size and overrepresentation of elderly patients in the moderate glucose metabolism arm. Thus, more elaborate analysis is needed to explore the prognostic value of glucose metabolism in the context of survival and response to chemotherapy.

On the cellular level, this glycolytic behaviour can be mainly attributed to three reasons. First, cancer cells try to fulfil their high energy demands by utilising fast metabolic programs of abundant nutrients. In terms of efficiency, the Warburg style of glucose metabolism is highly inefficient (Vander Heiden et al., 2009; Locasale and Cantley, 2011) (Table 2). Nonetheless, the rate at which one glucose molecule is being fermented is at least 10 times faster compared to that when it is fully metabolised through OXPHOS (Liberti and Locasale, 2016; Shestov et

al., 2014). Second, highly proliferative cells have demands on macromolecules biosynthesis for building blocks that are mainly produced by branching pathways diverted from glycolysis. These include the pentose phosphate pathway (PPP) which produces nucleotides and electron carriers (reviewed in (Hay, 2016)) and the hexosamine pathway which is essential for producing protein glycosylation substrates (reviewed in (Akella et al., 2019)). Third, the tumour microenvironment is generally hypoxic which further promotes this phenotype. Research on solid cancers suggests that more than 90% of tumour tissues are poorly perfused with oxygen (Nordsmark et al., 1996; Shen et al., 2017; Thomlinson and Gray, 1955; Vaupel et al., 1991). In fact, such poor oxygen abundance is also observed in many haematological malignancies, including AML, since they evolve and reside in a relatively hypoxic niche within the bone marrow (endosteal niche) (1-6% O_2) (Fiegl et al., 2009; Harrison et al., 2002; Spencer et al., 2014).

Table 2: Summary of net energy produced from one glucose molecule when metabolised by glycolysis *vs.* OXPHOS. One molecule $FADH_2$ equals 2 ATP and one NADH equals 3 ATP. NADH and $FADH_2$ require the electron transport chain to be converted to ATP.

	Fermentation		**Mitochondrial respiration**	
	Produced	Used (reaction energy)	Produced	Used (reaction energy)
ATP	4	2	6	4
$FADH_2$	0	0	2	0
NADH	2	0	10	0
Total (ATP)	**2**		**36-38**	

To cope with the high glucose demands, cancer cells overexpress their glucose transporters on the plasma membranes (GLUT1 and GLUT3) to increase their glucose uptake (Ancey et al., 2018). Levels of glucose transporters correlated negatively with chemosensitivity in AML patients (Song et al., 2014, 2016). Moreover, AML cells were shown to upregulate their fructose transporters in order to further feed their glycolysis and compensate for any drop in glucose abundance (Chen et al., 2016). Further, leukaemic cells have the capacity to exploit physiological processes in order to monopolize higher glucose levels for themselves. A striking example of this comes from a report elucidating how AML cells block insulin secretion and induce insulin insensitivity in order to minimize glucose uptake by other cells in the body (Ye et al., 2018).

In terms of molecular rearrangements to maximize their glucose utilization towards the Warburg effect, AML cells were shown to upregulate their glycolytic enzymes. Lactate dehydrogenase A (LDHA), the enzyme converting pyruvate to lactate was reported to be overexpressed in AML, especially in association with chemoresistance and bone marrow vascularisation and angiogenesis (Song et al., 2016; Teng et al., 2006; Zhao et al., 2013). Further, LDHA is upregulated under hypoxia (Nina Kurrle, unpublished results), an environment which was shown to prevail with disease progression in the bone marrow (Rytelewski et al., 2020). LDHA depletion impaired leukaemogenesis development in two different oncogenic mouse models (MLL-AF9 and BCR-ABL) (Wang et al., 2014). Similar impact on leukaemia development was also observed when abrogating the upstream enzyme pyruvate kinase II (PKM2) in the same study. Most importantly, cancer cells shift the balance of their pyruvate dehydrogenase complex at the interphase between glycolysis and the TCA cycle. This metabolic switch includes activating the kinase part of the PDC, PDHK1, on the expense of the phosphatase to metabolize more pyruvate towards lactate (Hitosugi et al., 2011). This shift was shown crucial for cancer cells, and interrogating it slowed down tumour growth in nude mice.

Moreover, genomic studies suggest that some metabolic phenotypes can interfere with drug sensitivity in AML. Resistance to tyrosine kinase inhibitors (TKIs) for example, was reported to induce some metabolic rewiring in the cells. In one study, midostaurin- and sorafenib-resistant MV4-11 and BaF3 cells showed an enhanced glycolytic activity and upregulation of glycolysis-related enzymes (hexokinase II, pyruvate kinase II and pyruvate dehydrogenase kinase II), however, with a concomitant suppression of mitochondrial metabolism (downregulation of complexes I, II and III) (Huang et al., 2016). Glycolysis inhibition with 3-bromopyruvate propylester (3-BrOP) or 2-deoxy-D-glucose (2-DG) showed more efficient in eliminating the resistant cells compared to the parental cells.

Nevertheless, the literature seems slightly inconclusive in this regard, with other reports suggesting the opposite. In one study for example, Farge et al. postulated, using an *in vivo* setting, that OXPHOS is the crucial determinant to Ara-C resistance development, as opposed to the long-standing hypothesis of resistance enrichment in the leukemic stem cells (LSCs) fraction (Farge et al., 2017). In their patient-derived xenograft (PDX) model of Ara-C treatment, cells that survived the treatment were selected for their high OXPHOS threshold rather than for being LSCs. These findings were seconded by another study where lowering the OXPHOS threshold in the chemotherapy-resistant cells was capable of sensitizing them to Ara-C (Baccelli et al., 2019). Similar findings were also observed in other cancer entities such as breast cancer, where MCL1 and MYC induced a high mitochondrial respiration phenotype as

part of metabolic rewiring to induce chemoresistance (Lee et al., 2017a). Abrogating this rewiring demolished the chemoresistance in these cells.

Nonetheless, these data suggest a regulated homeostasis between the different metabolic phenotypes in the leukemic cells based on their stemness and genotype. The importance of maintaining the balance between glycolysis and OXPHOS is nicely depicted in the study by Sriskanthadevan et al. that showed that shifting the balance between glycolysis and OXPHOS suppressed leukemic growth (Sriskanthadevan et al., 2015). In fact, such balance exists not only in leukemic cells, but also in the entirety of the haematopoietic hierarchy. Blocking the TCA supply route by inhibiting the mitochondrial phosphatase PTPMT1 attenuated the hematopoietic capacity of normal hematopoietic stem cells (HSCs) and led to hematopoietic failure in PTPMT1 knockout mice (Yu et al., 2013). The following section will try to reconcile these discrepancies and elaborate more on the importance of mitochondrial metabolism.

1.1.4. Mitochondrial metabolism or glycolysis?

While Warburg's observations have guided major research on exploring the exclusive reliance of AML cells on aerobic glycolysis, recent studies have demonstrated the ability of cancer cells to utilise oxygen for oxidative metabolism (Koppenol et al., 2011). Electron transport chain (ETC) and oxidative phosphorylation (OXPHOS) are described as vital for some cancer cells for energy production (Caro et al., 2012; Haq et al., 2013; Weinberg and Chandel, 2015) as well as for cellular biosynthesis (Birsoy et al., 2015; Sullivan et al., 2015). In a very interesting observation, AML cells were shown to utilize NADPH oxidase-2 (NOX2) function to form nanotubes with the surrounding niche cells of the bone marrow to import complete mitochondrial entities (Marlein et al., 2017; Moschoi et al., 2016). This process was shown to be essential to maintain the energy pool of the leukaemic cells. Even in tumours that are highly glycolytic such as BCR-ABL-positive cancers, abrogating alternative mechanisms that feed the TCA cycle such as glutaminase activity showed high therapeutic efficacy (Sontakke et al., 2016).

These studies and others allude to the vulnerable nature of AML to mitochondrial targeting, which has opened a new horizon for metabolic targeting beyond the Warburg metabolism. Several pharmacological inhibitors of mitochondrial targets have been developed (Figure 6). In fact, the efficacy of mitochondrial targeting has been successfully translated in a phase 1 clinical trial. Here, inhibition of OXPHOS by CPI-613 (inhibits PDH and α-ketoglutarate dehydrogenase (KGDH)) showed highly efficacious in combination with chemotherapy (high-dose Ara-C (HiDAC)) and led to higher complete remission (CR)/

complete remission with incomplete hematologic recovery (Cri) in the patients (Pardee et al., 2018). Further, a recent study by Molina et al. reinforced AML susceptibility to mitochondrial targeting by the agent IACS-010759 (complex I inhibitor), which is registered and currently being evaluated in another phase 1 clinical trial (Molina et al., 2018).

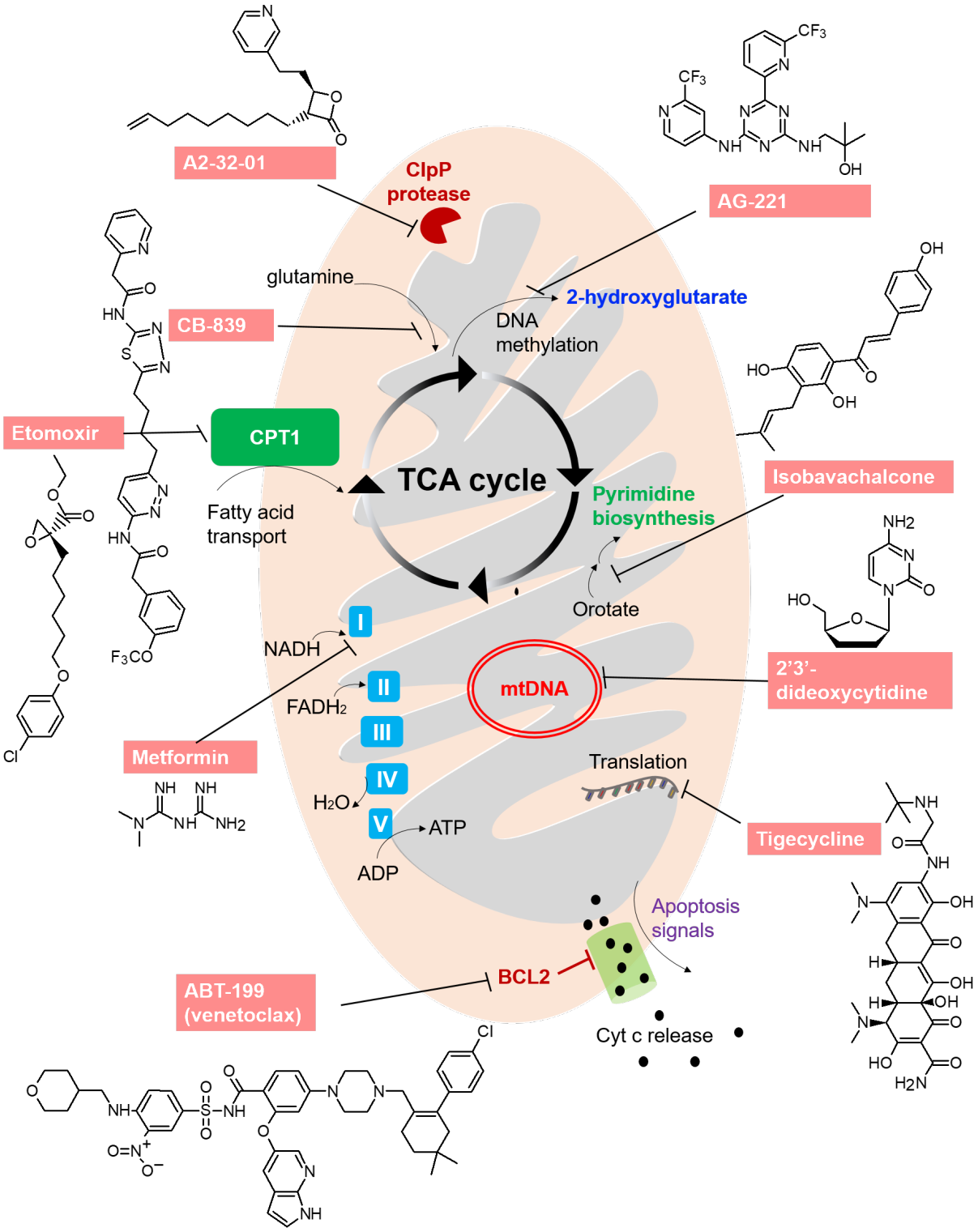


Figure 6: Chemical agents developed so far in clinical trials for interrogating OXHPOS and mitochondrial activities in AML. The figure shows inhibitors acting on the TCA cycle and OXPHOS, fatty acid transport, mitochondrial DNA synthesis, translation, proteases activity, pyrimidine biosynthesis, apoptosis regulation and oncometabolites production for DNA methylation. Modified after (Stuani et al., 2019) (open access article and no licensing for reproduction is required).

Despite their higher mitochondrial mass, AML cells have lower reserve capacity and ETC activity which renders them more sensitive to mitochondrial inhibitors (Sriskanthadevan et al., 2015). This finding has sparked an interest in a variety of different mitochondrial targeting agents. In one study, an elaborate analysis of the function of the mitochondrial protease ClpP positioned it as a targetable vulnerability in AML because of its role in interacting and regulating various ETC proteins and metabolic enzymes (Cole et al., 2015). Cole et al. demonstrated that chemical targeting of ClpP by A2-32-01 in NOD-SCID (Nonobese diabetic/severe combined immunodeficiency) xenograft model lowered the leukaemia engraftment while, interestingly, exerted no effect on normal haematopoiesis. In a different study, targeting mitochondrial translation and biogenesis was also described among the therapeutic strategies. Skrtic et al. demonstrated this vulnerability using the antimicrobial agent, tigecycline, which showed selective AML targeting (including the leukemic stem cell compartment) *in vitro* and in PDX mouse models (Skrtic et al., 2011). Tigecycline, unfortunately, did not translate into significant outcomes in the patients when used in a phase 1 trial. Nevertheless, the researchers attributed these results to the reduced half-life of the drug when measured in the AML patients compared to others (Reed et al., 2016).

One of the most important aspects about mitochondrial therapies is that they can be more efficient at eliminating leukaemic stem cells (LSCs) in comparison to any other metabolic targeting (Skoda et al., 2019). For example, the nucleoside analogue 2′3′-dideoxycytidine (ddC) that inhibits the mitochondrial DNA polymerase and thus, mitochondrial DNA replication has also shown effective in targeting bulk AML cells as well as the LSCs fraction (confirmed by PDX models and secondary transplantations assays) (Liyanage et al., 2017). Similar observations were also reported in other cancers such as pancreatic cancers, where the more primitive cancer stem cells driving the relapse depended on OXPHOS and were very susceptible to mitochondrial inhibitors (Viale et al., 2014).

Interestingly, this special sensitivity of the LSCs was also observed in the metabolic classification concept introduced by Craig Jordan's lab. They postulated that AML compartments can be distinguished based on their OXPHOS status measured by reactive oxygen species (ROS) levels, with LSCs being enriched in the low ROS fraction and crucially reliant on OXPHOS rather than glycolysis (Lagadinou et al., 2013). The low ROS levels are

attributed to their high glutathione levels but also to the metabolic quiescence of LSCs (Lagadinou et al., 2013). The researchers exploited this dependence with the BCL2 inhibitor, venetoclax that disrupts the ETC. In fact, venetoclax sensitivity has been later translated highly successful in a phase 1 clinical trial, where venetoclax synergized with the hypomethylating agent azacytidine in elderly AML patients (DiNardo et al., 2018). The efficacy of this combination was attributed in a paired study to venetoclax effects on disrupting OXPHOS and inhibiting mitochondrial metabolism (Pollyea et al., 2018).

To further emphasize on the plasticity of AML and LSCs metabolism, a recent work by Jones et al. described how LSCs can switch their reliance on metabolic sources to feed their OXPHOS in different cellular contexts. They reported that in *de novo* AML, LSC's OXPHOS metabolism is solely dependent on amino acids, but not glycolysis, fuelling the TCA cycle (Jones et al., 2018). Thus, amino acid deprivation could strongly dismantle the LSCs compartment in colony formation assays and impair their engraftment in PDX models. The very surprising point in this report is that LSCs from relapsed patients cease to depend on amino acids and rather shift to depend on fatty acid oxidation (FAO) to support their TCA cycle. This rewiring was described essential for the LSCs to develop chemotherapy resistance. Combined venetoclax/azacytidine together with inhibiting fatty acid uptake using sorbitan sesquioleate (SSO) showed more efficient in tackling the relapsed LSCs (Jones et al., 2018).

All of these data reflect the massive heterogeneity and plasticity of AML metabolism. Hence, clear understanding and classification needs to be drawn as to what the AML cells need in comparison to normal hematopoietic. In addition, it is important to define and distinguish the homeostasis between the different metabolic programs (namely; glycolysis and OXPHOS) in terms of stemness (LSCs vs bulk AML), adaptation and resistance mechanisms, and also oncogene-specific metabolic reprogramming. The latter is the least explored aspect of metabolic rewiring so far considering the large number of genetic alterations that can drive leukaemia. This thesis postulates that certain oncogenes can promote different metabolic programs. This hypothesis was drawn from existing literature that will be described in the next section in the context of FLT3-ITD.

1.1.5. FLT3-ITD and metabolism

The heterogeneous genetic landscape of AML argues for a limited validity in the generalisation of the Warburg effect as a metabolic fingerprint across the AML disease spectrum. This concept was demonstrated in a recent study where the susceptibility across a cohort of

primary AML blasts against Mubritinib, a complex 1 inhibitor, was evaluated based on the genetic background and chemosensitivity (Baccelli et al., 2019). Here, a variety of different mutations (KIT, RAS/MAPK and others) correlated with cellular insensitivity to mubritinib treatment (suggesting their dependence on the Warburg metabolism). In contrast, FLT3-ITD-positive AML blasts were sensitive to mubritinib and were described to be addicted to OXPHOS. This sensitivity was also confirmed in PDX mouse models *in vivo*, with reduced tumour engraftment in the spleen and BM when treated with mubritinib. Similar to the study cited earlier by (Farge et al., 2017), this current paper has reinforced the essentiality of mitochondrial metabolism for chemotherapy-resistance, with OXPHOS-high samples (including FLT3-ITD) being more chemo-resistant.

In two independent studies, the authors demonstrated that the TCA cycle and mitochondrial metabolism are essential for FLT3-ITD cells under FLT3-inhibition (Gallipoli et al., 2018; Gregory et al., 2018a). They reported on the role 'glutaminase' enzyme plays in catalysing glutamine to glutamate degradation in order to supply the TCA cycle. The authors showed that upon FLT3-inhibition, glutamine becomes a main feeder of the TCA cycle and interrogating this mechanism renders the cells more sensitive to FLT3-inhibition, both, *in vitro* on primary AML blasts and *in vivo* in NSG mouse models (Gallipoli et al., 2018).

Of a special importance to this doctoral thesis are the two studies by (Shan et al., 2014) and (Hitosugi et al., 2011) that emphasise on the role of oncogenes in driving the Warburg effect. The first study demonstrated the general oncogenic activity in suppressing the pyruvate dehydrogenase phosphatase (PDP1) by a Tyr-94 phosphorylation (Shan et al., 2014). In turn, this suppression of PDP1 (which drives mitochondrial metabolism) allows the cells to undergo Warburg metabolism. This ability to suppress PDP1 was demonstrated on several oncogenes including FGFR, JAK2, BCR-ABL and others. However, FLT3-ITD was not reported among these oncogenes and its capacity to suppress PDP1 has not been demonstrated.

The second study by (Hitosugi et al., 2011) is, in fact, complementary to the first study by (Shan et al., 2014). It shows how different oncogenes (including JAK2 V617F, FOP2-FGFR1, BCR-ABL, TEL-TrkC) activate the pyruvate dehydrogenase kinase (PDHK1) (the counter-acting enzyme of PDP1) by a Tyr-243/ Tyr-244 phosphorylation (Figure 7) (See Figure 5 for activity details). In turn, PDHK1 inhibits the activity of the pyruvate dehydrogenase subunit 1 (PDHA1) by a S293 phosphorylation and thus, pyruvate is converted towards lactate production on the expense of the TCA cycle (Warburg metabolism). Interestingly, FLT3-ITD cells exerted very weak PDHK1 Y243 phosphorylation compared to other oncogenes. Subsequently, FLT3-ITD cells also exerted weak PDHA1 phosphorylation. Thus, PDHA1 can

be assumed active within the pyruvate dehydrogenase complex and drives pyruvate conversion to Acetyl-CoA to support the TCA cycle.

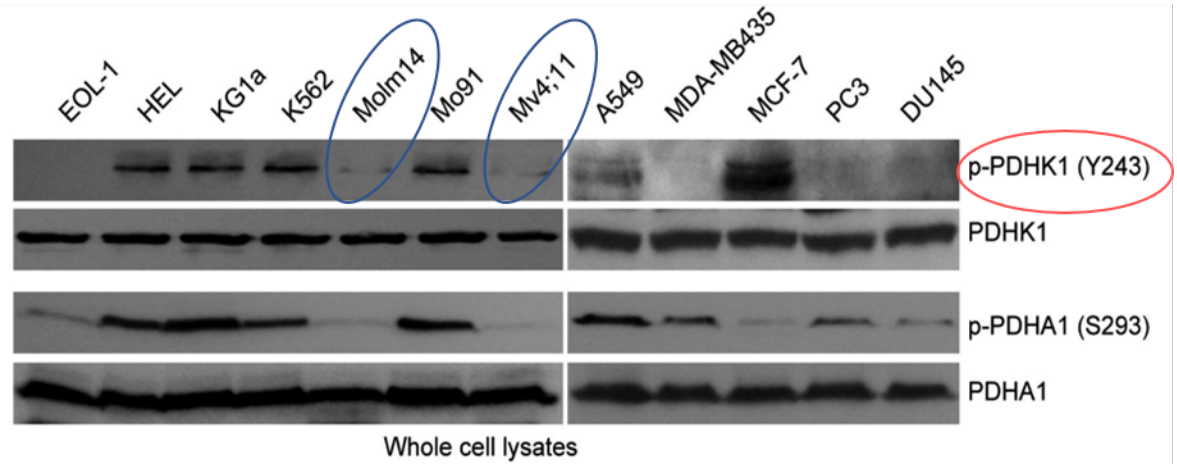


Figure 7 Minimal PDHK1 phosphorylation in FLT3-ITD cells. The western blot shows the relative PDHK1 phosphorylation levels in a variety of cancer cell lines. FLT3-ITD (circled in blue) show relatively low phosphorylation on Y243 and subsequently on S293. Adapted from (Hitosugi et al., 2011) (license obtained).

The findings of these two studies (weak FLT3-ITD ability to suppress PDP1 and activate PDHK1) suggest a different metabolic program being associated with FLT3-ITD-positive AML. With all of this literature in hand, we propose the hypothesis that FLT3-ITD promotes different metabolic dependencies than those observed in most other leukaemia cells (high OXPHOS). Hence, trying to target glycolysis in FLT3-ITD cells would, possibly, not be highly effective. Thus it is important to explore the metabolic reliance in these cells in order to deliver targetable vulnerabilities for preclinical models.

1.1.6. Motivation and project aims (A)

To reconcile the described literatures, this doctoral thesis was carried out with the aim of discerning the detailed OXPHOS program promoted by FLT3-ITD. For this purpose, the current thesis focused on identifying metabolic proteins and enzymes that mediate this OXPHOS phenotype. Functional validation of these targets was planned and included knockouts and overexpression in cell line models, patient-derived primary AML blasts, as well as *in vivo* validation in a xenograft mouse model. Finally, the role of OXPHOS in drug resistance will be investigated.

1.2. Amino acid metabolism and cancer

1.2.1. General amino acid dependencies in AML

While the previous section was narrowed down to investigate the specific metabolic phenotype associated with FLT3-ITD mutations, the second part of this thesis studies general amino acid dependencies in AML. Related literature will be covered in this section with special focus on mechanistic mechanisms of these dependencies.

Distinctive amino acid metabolism has been observed in cancer versus healthy cells (Ananieva, 2015; Lukey et al., 2017) (Figure 8). Most of the studies so far have been focused only on a few amino acids (i.e. glutamine, arginine, cysteine and branched-chain amino acids (BCAA)). The importance of glutamine is among the most studied amino acid metabolism in cancer and AML (Zhang et al., 2017). Glutamine contributes to the production of the TCA cycle substrate alpha-ketoglutarate for energy generation (Bromley-Dulfano et al., 2013; Gallipoli et al., 2018; Gregory et al., 2018a; Gross et al., 2014; Jacque et al., 2015; Matre et al., 2016), redox homeostasis (Gregory et al., 2018b; Zhou et al., 2010), regulation of mammalian target of rapamycin complex 1 (mTORC1) activity and mediating the uptake of other amino acids (Willems et al., 2013; Yang et al., 2017). In addition, glutamine together with aspartate and glycine contribute to pyrimidine synthesis by nitrogen donation (Moffatt and Ashihara, 2002; Zhang et al., 2008).

The role of arginine has also been explored and was demonstrated as a targetable vulnerability in cancer cells. A major aspect of arginine metabolism entitles its role in regulating the urea cycle for ammonia detoxification, a crucial byproduct of protein degradation that occurs at high rates in cancer cells (Keshet et al., 2018). Furthermore, arginine is utilized for proline and glutamate synthesis (Majumdar et al., 2016) as well as polyamines biosynthesis (considered as main contributors to tumorigenesis) (Gerner and Meyskens, 2004). The reliance of AML cells on exogenous arginine has been demonstrated to be mainly related to the low expression levels of the enzymes synthesizing arginine in the cells (argininosuccinate synthetase-1 (ASS1) and argininosuccinate lyase (ASL)) (Miraki-Moud et al., 2015; Mussai et al., 2015a, 2015b).

BCAA amino acid metabolism has also been described in the context of cancer epigenetics. BCAAs play an important role in DNA methylation required for the high proliferative activity of malignant cells (Ananieva and Wilkinson, 2018; Raffel et al., 2017). Last, cysteine has been also explored and shown essential for OXPHOS maintenance through the glutathionylation of

the Succinate Dehydrogenase A (Jones et al., 2019). Nevertheless, the full spectrum of the 20 different amino acids and their importance in AML is yet to be explored.

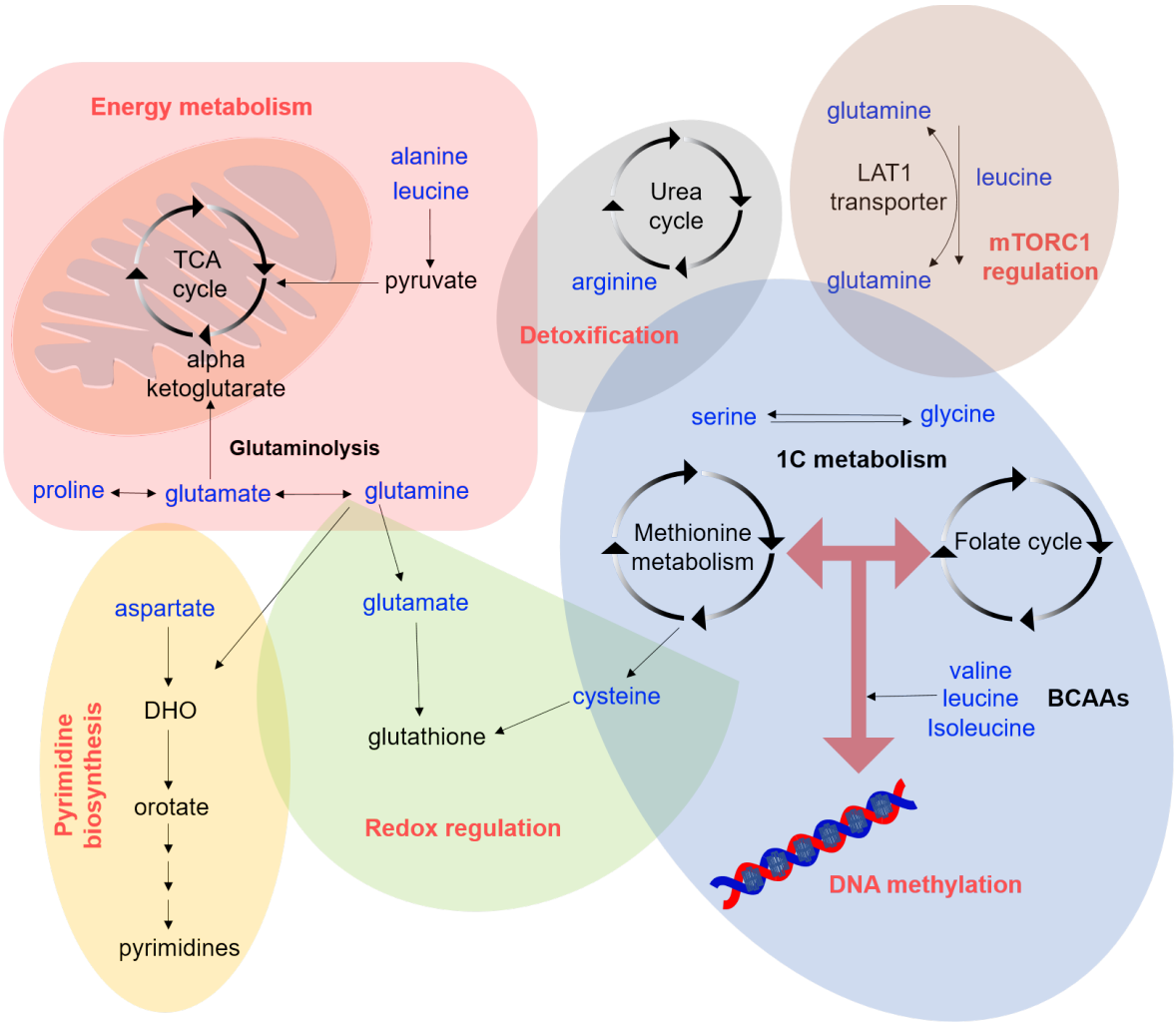


Figure 8: General overview of amino acid metabolism in cancer. Amino acids serve as a source of energy production intermediates. Several amino acids contribute to redox balance and ROS scavenging. Other amino acids regulate Urea cycle in order to detoxify ammonia resulting from protein degradation. Biosynthesis of pyrimidine as building blocks is also depicted. One carbon metabolism and methionine/ folate cycles regulating transmethylation reactions are also illustrated. Role of BCAA in DNA methylation is also shown. Some parts of the graph were modified after (Lieu et al., 2020) (open access article and no licensing for reproduction is required).

1.2.2. Methionine metabolism

The amino acid methionine is not generally well studied in cancer. In the early 50s, the detrimental impact of dietary methionine restriction was described to impair the growth ability in rats (Sugimura et al., 1959). Subsequently, the importance of methionine for healthy cells has been described for embryonic and pluripotent stem cells maintenance and differentiation (Shiraki et al., 2014; Shyh-Chang et al., 2013). In healthy conditions, methionine is utilized for

many functions such as cysteine production to generate glutathione and taurine (Hoffman et al., 2019) (Figure 9). Here, methionine-derived homocysteine is converted to cystathionine via a transsulfuration reaction which will ultimately produce cysteine (Lieu et al., 2020). In addition, methionine plays an essential role in methylation reactions (Hoffman et al., 2019).

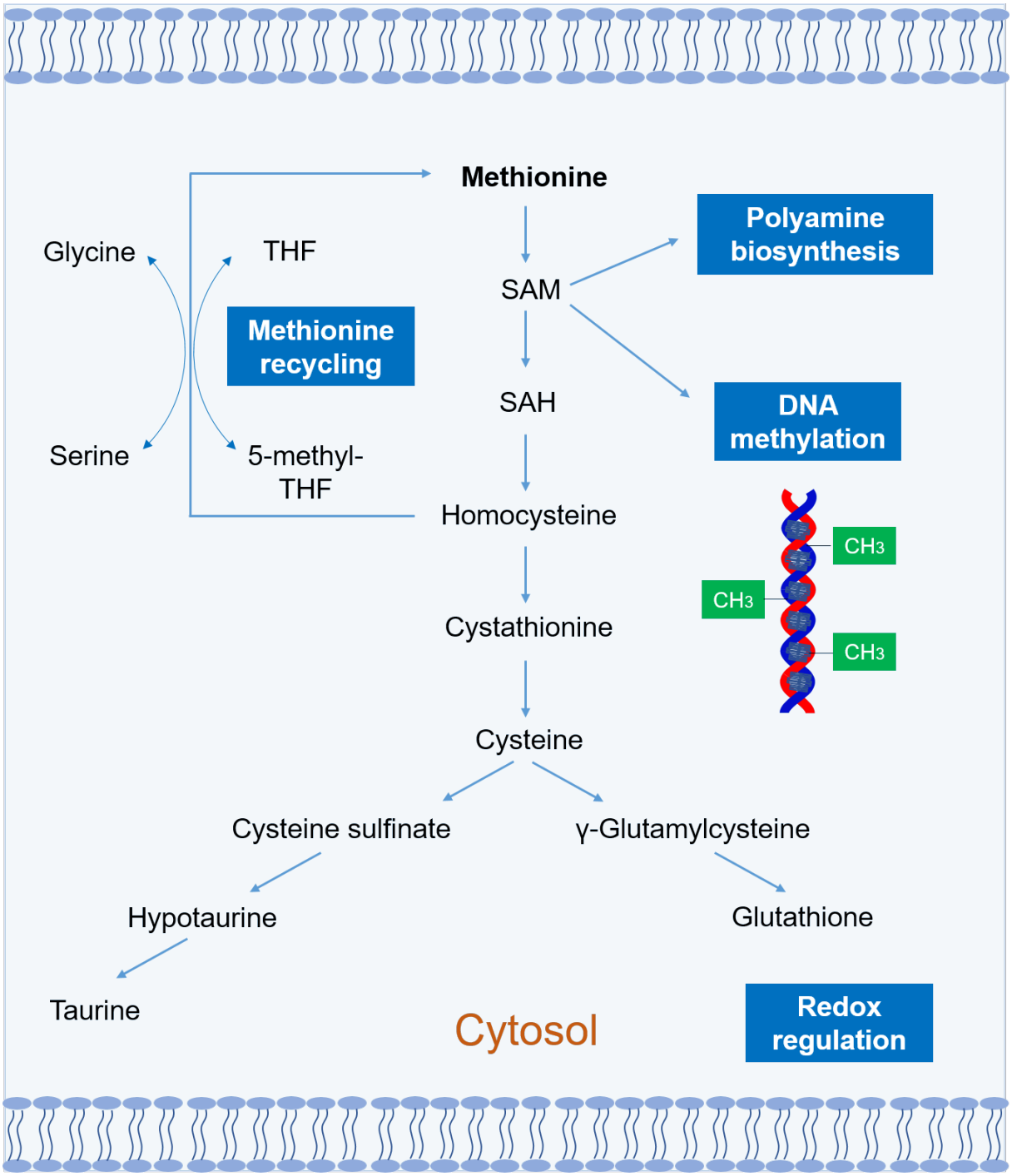


Figure 9: Core pathways of methionine metabolism. Methionine catabolism to produce S-adenosylmethionine (SAM) provides methyl groups for DNA methylation reactions. SAM is further metabolised to S-adenosyl homocysteine (SAH) to produce homocysteine which generates cysteine further downstream to synthesise glutathione and taurine. Methionine Synthase (MTR) recycles

homocysteine back to methionine in conjugation with one carbon metabolism and folate cycle (5-methyltrahydrofolate (5-methyl-THF) to tetrahydrofolate (THF)).

Methionine metabolism is closely entangled with folate and one carbon metabolism. Biochemically, methionine is converted to S-adenosylmethionine (SAM) in a one-step reaction to provide a methyl group for DNA and protein methylation (Mentch et al., 2015; Ulanovskaya et al., 2013). SAM is further converted to homocysteine which is further metabolized to downstream metabolites (i.e. cysteine and glutathione). The remaining homocysteine pool is then used to replenish the methionine reservoir in the cells, a mechanism used to maintain adequate methyl group supply (Lehninger et al., 2005) (Figure 9). Recycling of homocysteine back to methionine is driven by the enzyme methionine synthase (MTR) upon carbon donation from one carbon metabolism (serine-to-glycine conversion) (Lehninger et al., 2005).

As discussed earlier, metabolic alterations are essential to drive epigenetic modulations that lead to cancer and AML development (Kaelin Jr. and McKnight, 2013; Kaelin Jr, 2011; Letouzé et al., 2013; Lu et al., 2012; Xiao et al., 2012). Studies have demonstrated the dysregulation of folate and one carbon metabolism in cancer cells and their role in abrogating DNA methylation (Chaneton et al., 2012; Ducker and Rabinowitz, 2017; Jain et al., 2012; Labuschagne et al., 2014; Maddocks et al., 2016; Newman and Maddocks, 2017). In fact, one study has reported on the importance of methylenetetrahydrofolate dehydrogenase-cyclohydrolase 2 (MTHFD2) (regulates folate and one carbon metabolism) in AML. MTHFD2 plays an essential role in the provision of methionine metabolism in the cells for DNA and histone methylation (Pikman et al., 2016).

Nonetheless, the direct role of methionine in DNA methylation alterations in AML is poorly described and yet to be explored.

1.2.3. Motivation and project aims (B)

The current thesis investigates the dependence of AML cells for each of the 20 proteinogenic amino acids, focusing particularly on methionine. We aimed at elucidating the fates of methionine in the cells. Further, we aimed at understanding its essentiality not only in the bulk AML cells but also in the leukemic stem cell fraction. In addition, this thesis aims at addressing the special dependence on exogenous methionine and the efficacy of methionine recycling machinery in AML vs healthy cells. This project is mainly driven by Alan Cunningham (Group Prof. JJ Schuringa)

1.3. Nuclear magnetic resonance (NMR) spectroscopy for metabolomics studies

The third section of this thesis concerns the development of NMR as a high throughput method for metabolomics studies. Here, current state of methodologies and approaches used for metabolomics studies will be introduced with special focus on NMR

Metabolomics studies, addressing the cellular metabolism, have attracted increasing attention over the last years, especially in cancer research (Figure 10A). Metabolomics usually study metabolic pathways activities and phenotypes associated with different diseases *vs.* physiological conditions. These studies are based on quantifying changes in the small molecules concentrations in biological samples. In addition, methods of metabolites labelling and pathway tracing are utilised to investigate pathway rewiring and metabolic reprograming in the cells.

Metabolites in general are direct indicators of cellular homoeostasis and disease status due to their direct correlation with biological/ biochemical reactivities. Such correlation may not be as straightforward when it comes to genes and proteins due to the complex control layers involved such as epigenetic control, post-transcriptional/ -translational modifications or activity regulation (i.e. phosphorylation) (Patti et al., 2012). Thus, metabolomics studies have been widely implemented for understanding disease pathophysiology, especially in cancer research. In fact, such studies have contributed significantly to understanding cancer biology, by identifying the so called ‘Oncometabolites’. These are metabolic intermediates that can either drive malignancy (i.e. 2-hydroxyglutarate) or contribute to tumour progression (i.e. succinate, fumarate, lactate and others) (Figueroa et al., 2010; Terunuma et al., 2014; Wishart, 2016; Yang et al., 2013).

Two main technology platforms are currently implemented in the metabolomics field: nuclear magnetic resonance (NMR) spectroscopy and mass spectrometry (MS). Each of the two approaches has its own advantages and disadvantages. On one hand, NMR offers a semi-targeted approach for metabolomics studies, while MS, on the other hand, is used for untargeted analysis (Patti et al., 2012; Vignoli et al., 2019). Sensitivity in MS is superior to NMR and is considered as the prime advantage of MS (Pan and Raftery, 2007; Vignoli et al., 2019). Nonetheless, modern NMR spectrometers equipped with high magnetic fields and cryo probe heads have significantly boosted the sensitivity of NMR measurements. Furthermore, the high reproducibility obtained by NMR, together with its quantitative nature, give it higher

preference in metabolomics studies, especially for the multivariate analyses (Emwas et al., 2019a; Pan and Raftery, 2007; Takis et al., 2019).

Moreover, sample preparation for NMR analysis is relatively easy and non-destructive. Unlike MS, it requires no derivatization and thus, allows preserving the samples after the measurements (Lindon and Nicholson, 2008; Takis et al., 2019; Wishart, 2019). Added to that, NMR allows a deeper investigation of chemistry compared to other approaches considering its atomic resolution and its capacity to study different atoms such as ^{1}H, ^{13}C, ^{15}N, ^{19}F and ^{31}P (Emwas et al., 2019a). Finally, developed methods for shortening the measurement time together with the automatability of NMR qualify it as a high-throughput metabolomics platform (Guennec et al., 2014; Vignoli et al., 2019).

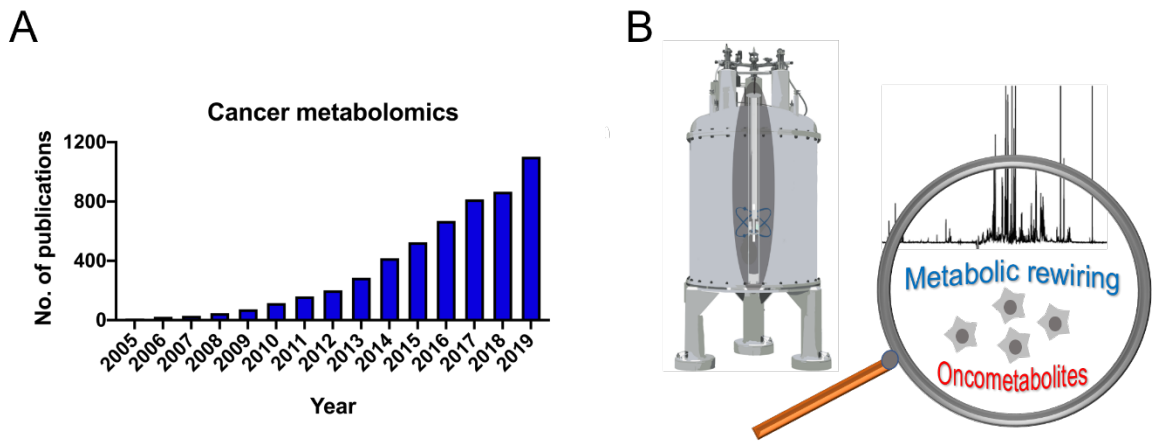


Figure 10: Metabolomics studies in cancer. A. Number of PubMed publications on 'cancer metabolomics' over the last 15 years. B. Graphical illustration of NMR-based metabolomics.

1.3.1. Theoretical principle of NMR

NMR was first discovered in 1946 by two independent groups (Felix Bloch and Edward Purcell) (Bloch et al., 1946; Purcell et al., 1946). For this discovery, both researchers were awarded the Nobel Prize in 1952. Bloch initially described it as the "Nuclear Induction Experiment". The basic theory behind NMR is that due to charge and spin property, a nucleus which has an odd number of protons and/ or an odd number of neutrons, can act as a small magnet.

For the case of a spin quantum number of ½ as it is the case for example for ^{1}H, ^{13}C, ^{15}N or ^{19}F), nuclear spins align in two different directions once put in the static magnetic field of the NMR spectrometer. They could be either parallel to the field or anti-parallel. Here, the

resonance energy (amount of energy between those two states) corresponds to a certain signal on the NMR spectrum. This energy absorption is achieved by excitation with a radio-frequency (RF) pulse and is proportional to the strength of the external field (B_0) and the gyromagnetic ratio (γ) of the atom under investigation (as indicated by the Larmor Equation: $\omega=\gamma B_0$). Additionally, depending on the electronic environment resulting from bonding and atoms surrounding of each molecule, the required energy therefore differs and thus, provides a distinctive signal and insight into the chemical structure of the molecule (Keeler, 2011; Levitt, 2001).

The unique electron shielding resulting from the atoms surroundings in each molecule provides a distinctive resonance signal. This signal gives the atom a sort of a unique identifier termed Chemical Shift, which corresponds to the signal's position in the spectrum (Keeler, 2011; Levitt, 2001). Usually, this position is determined in reference to the signal of a standard compound such trimethylsilylpropanoic acid (TMSP) or sodium trimethylsilylpropanesulfonate (DSS) (Harris et al., 2002). Example chemical shift assignment of different metabolites is shown in (Figure 11).

1.3.2. NMR metabolomics and biological applications

After almost three decades from its discovery, NMR utilisation expanded from biophysical studies to the metabolomics field (reviewed in (Cerdan and Seelig, 1990)). First NMR studies of metabolism started as early as the 70s (Eakin et al., 1972; Hoult et al., 1974; Shulman et al., 1979; Ugurbil et al., 1978b, 1978a). Few years later, NMR was used to profile diabetic patients in one of its first applications in studying human diseases (Nicholson et al., 1984). These studies have opened the doors wide for a plethora of subsequent applications of NMR in metabolic profiling of a wide variety of human tissues and fluids (serum, urine, stool, saliva, cerebrospinal fluid, tissue digests, cell extracts and extracellular excretions) (Takis et al., 2019; Vignoli et al., 2019).

Biomarkers identification for disease screening and metabotyping has also been crucially advanced by NMR (Zhang et al., 2013) in a variety of disorders such as: acute myeloid leukaemia (Musharraf et al., 2016; Wang et al., 2013), inflammatory bowel disease (Stephens et al., 2013), pancreatic ductal adenocarcinoma (Napoli et al., 2012), hepatocellular carcinoma (Nahon et al., 2012) and others. Further, NMR studies have provided predictive insights into the prognostic value of some metabolic phenotypes, like poor OS associated with higher glycolytic activity (Chen et al., 2014; Wang et al., 2013). Moreover, benchtop NMR was implemented to monitor diabetes biomarkers in patients such as glucose and acetone

(Percival et al., 2018). Added to all of that, NMR profiling of urine has been described as a diagnostic/ predictive tool for malignant prostate cancer samples (Cheng et al., 2005).

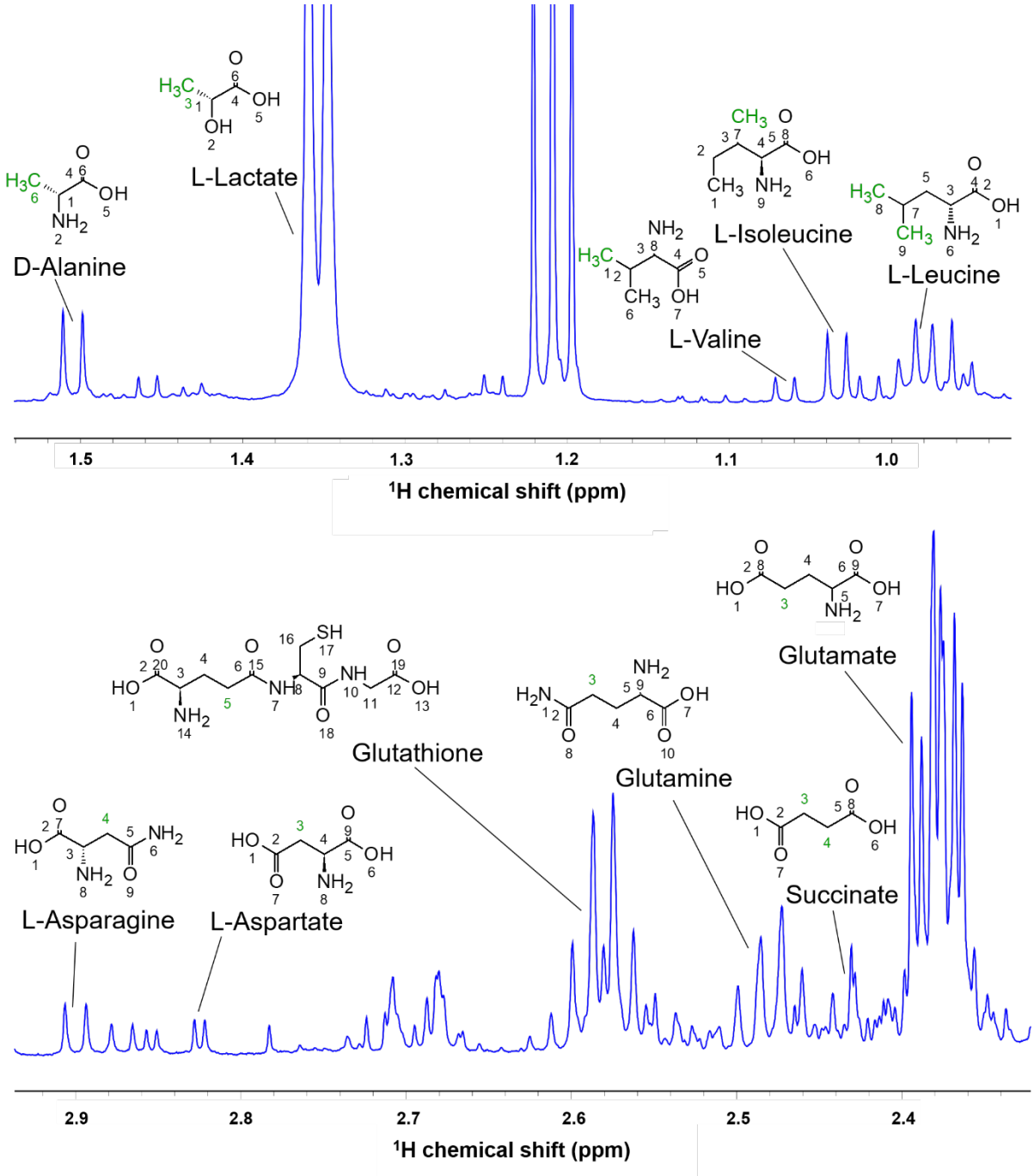


Figure 11: Chemical shift assignments of intracellular metabolites. The figure illustrates 1D ^{1}H-NMR spectrum of some metabolites measured in cellular metabolites extract at 600MHz using the pulse program: NOESYGPPR1D at 25°C). Selected peaks correspond to the atoms labelled in green: succinate is singlet, leucine, isoleucine, valine, lactate, alanine, asparagine and aspartate are doublets, glutamine, glutamate and glutathione are multiplets.

Technically, one dimensional ^{1}H NMR experiments allow for the identification of over 100-160 compounds, depending on the sample type (Bouatra et al., 2013; Takis et al., 2019). These one dimensional ^{1}H NMR experiments are most commonly used experiments in the metabolomics field because of the high sensitivity they provide relative to other atoms such as carbon and nitrogen (Cerdan and Seelig, 1990). The low sensitivity of such atoms is owing to the low natural abundance of their NMR-active isotopes such as ^{13}C (1%) and ^{15}N (0.37%) and their respective smaller gyromagnetic ratios. However, on the downside, ^{1}H spectra are typically dense and crowded. Signals overlap leads to obscuring and overshadowing some low abundance metabolites. Nonetheless, the currently developed protocols of metabolites extraction into polar and non-polar metabolites (McHugh et al., 2018) (Figure 12A) and the use of two dimensional ^{1}H-^{13}C experiments improve the resolution and, therefore, simplify the identification of the signals (Kostidis et al., 2017; Szyperski et al., 1999).

Furthermore, the implementation of isotope-labelled metabolites (^{13}C or ^{15}N) into these two dimensional NMR experiments provides additional pathway analysis. Using such tracer-based assays, the fate of any given metabolite can be traced into the different metabolites intermediates in the cell, providing a detailed picture of the up-/ down-regulation of certain pathways and also the rewiring and cross talk between the different pathways (Carrigan et al., 2016; Szyperski, 1995; Szyperski et al., 1996). Moreover, NMR allows for selective atomic labelling of a given tracer which enables label tracing in a site-specific manner. Labelling can be particularly helpful to examine and differentiate between different enzymatic activities that metabolise a certain metabolite. A typical example is the pyruvate dehydrogenase *vs* pyruvate carboxylase activities in shuttling pyruvate into the TCA cycle (Figure 12B).

A main disadvantage of these two dimensional ^{1}H-^{13}C experiments is the relatively long measurement time caused by the high number of increments recorded in the indirect dimension (Emwas et al., 2019b). This can be an issue when performing real-time experiments with living cells (discussed in the following section). Therefore, development of experiments which would allow to overcome this issue and thus enable a much faster measurement has been the focus of several research groups in recent years. For instance, pseudo-2D double-filtered experiments suggested by Reed et al (Reed et al., 2019) could substantially minimise measurement time. Briefly, such experiments record two different spectra: one standard ^{1}H 1D spectrum and one that applies a gradient that destroys signals originating from protons attached to ^{13}C. The subsequent subtraction of these two spectra allows a more precise quantitation of the ^{13}C label incorporation in the different metabolic pathways (described in detail in the methods section). These experiments hence, provide an

alternative to the long multidimensional experiments and thus this doctoral work seeked their implementation in the real-time NMR studies of metabolism.

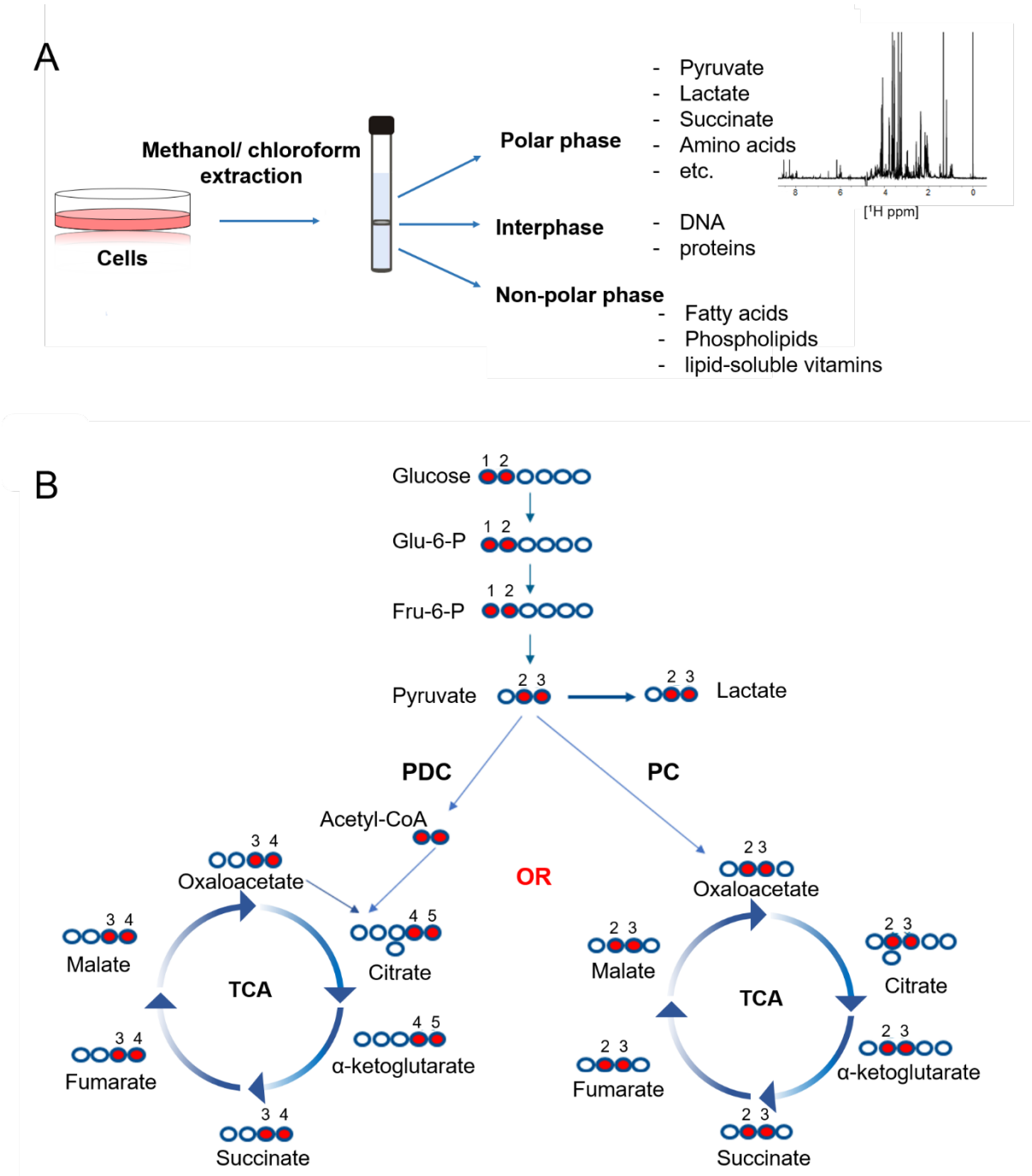


Figure 12: Sample preparation and labelling schemes in NMR-metabolomics. A. Methanol/ chloroform-based metabolite extraction protocol. B. Tracer-based assay with 1, 2-13C glucose. Label incorporation into glycolysis, fermentation and the TCA cycle is illustrated. The different labelling patterns resulting from PDH activity *vs* pyruvate carboxylase (PC) activity is demonstrated. Part (B) of the figure was produced after the same design used for other tracers described in (Carrigan et al., 2016) (open access article and no licensing for reproduction is required).

1.3.3. NMR of live-cells

A very interesting concept that has been developed in the NMR field is the 'in-cell NMR', where NMR studies are designed to observe intracellular activities in a real-time manner. These processes include metabolism, protein folding, post-translational modification, ligand binding, drug discovery and others (Hänsel et al., 2014; Kang, 2019; Luchinat and Banci, 2017) (Figure 13). With certain settings, this method can be non-invasive as it does not lead to cell destruction (Narasimhan et al., 2020). This approach not only allows to study active processes in living cells, but it can also account for the presence of microenvironment for those processes, a crucial factor that is usually obscured in traditional *in-vitro* studies.

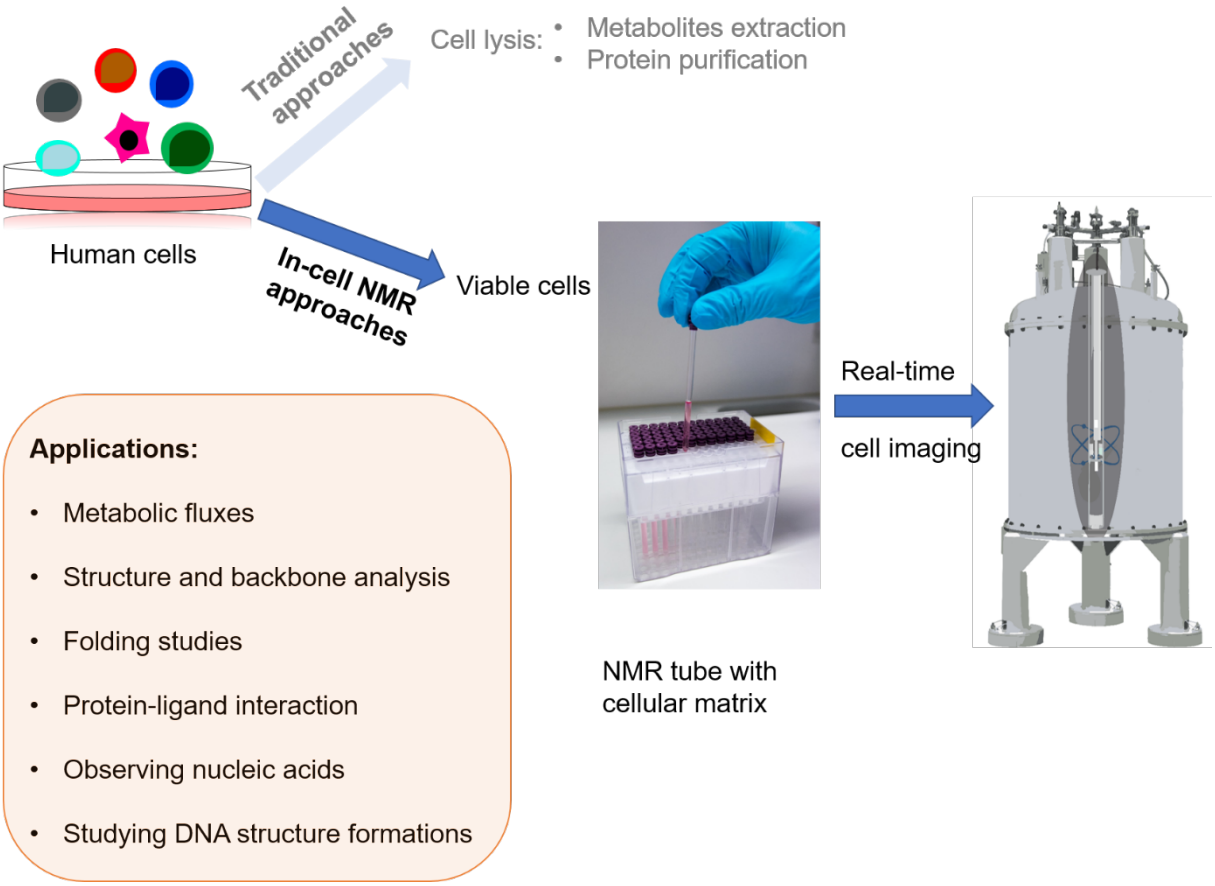


Figure 13: In-cell NMR approach for proteomics and metabolomics on living cells. This approach replaces the invasive methods of cell lysis to extract metabolites or purify proteins by sustaining the cells viability and observing their dynamic processes.

One of the very first reported examples of in-cell NMR was the detection of a ^{15}N labelled protein intracellularly in *Escherichia coli* bacteria (Serber et al., 2001). Few years later, this was described in eukaryotic cells (Sakai et al., 2006). Later on, complete 3D protein structure

assignment was also published (Sakakibara et al., 2009). Subsequent applications expanded to observing nucleic acids (Hänsel et al., 2009) and studying DNA secondary structures (Hänsel et al., 2013). In addition, NMR monitoring of live cell metabolism has been reported in bacteria (Motta et al., 2010) and in human cells (Jeong et al., 2017). More interestingly, *in vivo* applications were described where monitoring of hyperpolarised metabolites was studied in living mice/ rats (Golman et al., 2006; Zacharias et al., 2012).

Nonetheless, the advances made with in-cell NMR in the metabolomics field are relatively limited due to the complexity of the biological requirements and setups. Most of the so far developed in-cell NMR approaches do not provide cell-friendly conditions for the cells. Cells sedimentation in the NMR tube can severely affect the availability of oxygen and comprise cellular viability which can possibly lead to apoptosis. Further, utilised cellular matrices such as agarose (Foxall et al., 1984; Koczula et al., 2016; Lundberg and Kuchel, 1997; Lundberg et al., 1992) can affect protein interactions in the cells, alter cellular microenvironment and hamper metabolites diffusion (Lundberg and Kuchel, 1997; Lundberg et al., 1992). Added to that, multidimensional NMR experiments used for those settings are time consuming, which limits their applicability due to the short life span of the cells under such preparation conditions. These trade-offs are critical in the context of metabolomics studies, mainly because of the resulting stress conditions that can change the metabolic image of the cell by altering the rates of metabolites uptake and excretion.

Overcoming these dilemmas and establishing reliable in-cell NMR approaches for studying metabolism can be substantially advantageous for NMR metabolomics field. These approaches can be especially helpful when studying metabolic processes and adaptions with rapidly changing kinetics. For such studies, metabolic profiling using traditional extraction protocols over a time course can be highly demanding, labour intensive and time consuming. Developed approaches should also address the issue of large cell numbers (˜10 million cells) required for traditional NMR approaches (Kostidis et al., 2017; Saborano et al., 2019)

1.3.4. Motivation and project aims (C)

This part of the doctoral thesis is focused on the development of a new comprehensive high throughput approach that addresses the technical and biological obstacles and builds up on the real-time concept of monitoring metabolism. This approach aims at delivering a method that is suitable for highly sensitive samples in a non-destructive manner, such as patient samples, and can handle low cell numbers, thus can be implemented for diagnostic

procedures. Finally, this work aimed at allowing the feasibility of performing tracer-based assays, a major cornerstone in metabolomics assays.

Chapter II

Materials and methods

2.1. Cellular assays and *in vivo* experiments section

2.1.1. Cell culture and maintenance

Human AML cell lines were obtained from the DSMZ (Deutsche Sammlung von Mikroorganismen und Zellkulturen GmbH). Cytogenetics are described in (Table 3). Cells were cultured in RPMI 1640 medium (Gibco, ThermoFisher, USA, catalogue number 11875) supplemented with 10% Foetal bovine serum (FBS) (Sigma-Aldrich, USA), 100 IU/ml penicillin and 100 ug/ml streptomycin (Gibco, ThermoFisher, USA) at 37°C in a humidified 5% CO_2 incubator. Molm13 Rho Zero cells were similarly maintained, however, with addition of 1 mM pyruvate (ThermoFisher, USA) and 50 µg/ml uridine (Sigma-Aldrich, USA). HEK T293 cells were maintained similar to the AML cell lines, however with DMEM medium (Gibco, ThermoFisher, USA). Murine haematopoietic progenitor 32D cells were maintained in standard 10% FCS RPMI media containing 1 ng/ml murine interleukin 3 (mIL3) (Peprotech, USA). These cells were originally isolated from haematopoietic myeloid progenitor cells. FLT3-ITD positive 32D cells were previously generated by Hubert Serve's group as described (Mizuki et al., 2000, 2003). A new batch of the cells was kindly provided by Prof. Christian Brandts.

Mononuclear cells from bone marrow were purified by Ficoll-Paque™ Premium gradient centrifugation according to the manufacturer's instructions (GE Healthcare, USA) and immediately stored in liquid nitrogen. An exception to this was the samples of the AC220-resistant patient where the samples were from obtained from peripheral blood and plated for experiment immediately without freezing. The bone marrow biopsies/ peripheral blood aspirates from the patients were obtained and collected pre-treatment (apart from the AC220-resistant patient where the samples were taken after induction therapy/HDAC/AC220 and Litalir treatment) (Appendix Table A1). The patients gave informed consent according to the Declaration of Helsinki to participate in the collection of samples. The use of bone marrow aspirates was approved by the Ethics Committee of Frankfurt University Hospital (approval no. SHN-11-2016/SHN-09-2019). The blasts were thawed for the experiments and were cultivated in X-vivo 10 medium (Lonza, Switzerland) supplemented with 10% HyClone FCS (GE Healthcare, USA), 4 mM L-glutamine (ThermoFisher, USA) and cytokines cocktail (25 ng/ml human thrombopoietin (hTPO), 50 ng/ml human stem cell factor (hSCF), 50 ng/ml human FLT3-ligand (hFLT3L) and 20 ng/ml human interleukin 3 (hIL3) (all from Peprotech, USA)).

2.1.2. Hypoxic cell culture

Hypoxia experiments were performed in a hypoxia chamber (BioSpherix Medical, USA) with 1% O_2 and 5% CO_2 levels. Cells were maintained in a humidified incubator in the chamber at 37°C. Cells were allowed to adapt to a chronic hypoxic state for 7 days before carrying out the experiments. Media was adapted in the chamber overnight before usage to equilibrate the dissolved O_2 to 1%.

Table 3: Cytogenetics of AML cell lines used.

Cell line	Cytogenetics
Molm13	FLT3-ITD; MLL-AF9 (KMT2A-MLLT3)
MV4-11	FLT3-ITD, MLL-AF4 (KMT2A-AFF1)
Molm14	FLT3-ITD; MLL-AF9 (KMT2A-MLLT3)
PL21	FLT3-ITD, NRAS
THP1	NRAS G12D, TP53 R174Fs, MLL-AF9 (KMT2A-MLLT3)
HEL	JAK2 V617F, P53 M133K
HL60	Amplified cMYC
U937	t(10;11)(p13;q14)
NB-4	t(15;17) PML-RARA fusion gene
K-562	BCR-ABL1 e14-a2 (b3-a2) fusion gene

2.1.3. Inhibitors, reagents and chemicals

AC220, midostaurin and venetoclax were bought from Selleckchem, USA. HEPES buffer, rotenone, 2-Dimethyl 2-oxoglutarate, sodium palmitate, uridine and polyethylenimine (PEI) were bought from Sigma-Aldrich, USA. Labelled isotopes (^{13}C glucose and ^{13}C, ^{15}N methionine) were also bought from Sigma-Aldrich, USA. Puromycin was bought from InvivoGen.

2.1.4. Seahorse measurement

The XFe96 Extracellular Flux Assay Kit was incubated overnight before the experiment with Agilent seahorse XF calibrant to allow the cartridge to hydrate. Cells were washed and resuspended in KHB buffer (composition in Table 4) containing 5 mM glucose and 1 mM glutamine (pH 7.4). Cells were seeded at a density of 1 x 10^5 cells/well for the AML cell lines and at a density of 3 x 10^5 cells/well for the 32D cells with 200 µl buffer in the seahorse plate.

The reagents for the Mito-stress assay were added to the XFe96 Extracellular Flux Assay Kit (concentrations in Table 5). All of the mitostress reagents were bought from Cayman Chemicals, USA, except for Antimycin which was bought from Sigma Aldrich, USA. The plate was then measured on an XF96 Aglient Seahorse reader with OCR and ECAR readouts. Mito-stress assay readout is illustrated in (Figure 14).

Table 4: Seahorse KHB buffer composition.

Component	Amount
ddH_2O	1000 ml
NaCl	6.27 g
KCl	0.347 g
$MgSO_4*7H_2O$	0.462 g
$Na_2HPO_4*2H_2O$	0.198 g

Table 5: Mito-stress inhibitors.

Component	Concentration
Oligomycin	25 µM
CCCP	10 µM
Rotenone	10 µM
Antimycin	10 µM

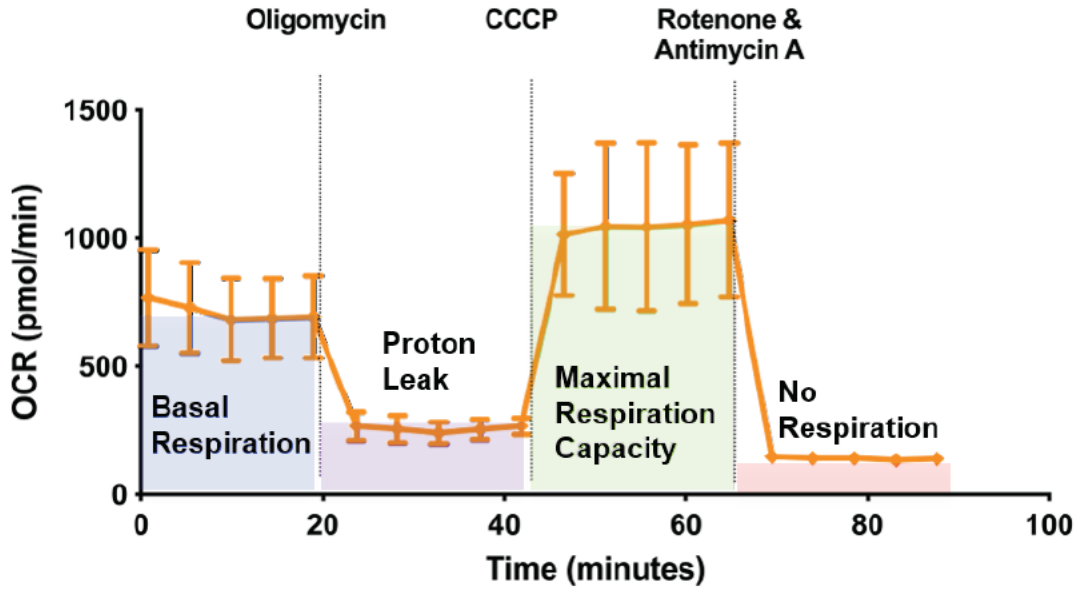


Figure 14: Seahorse measurement of oxygen consumption rate (OCR) in 32D cells. The figure illustrates the Mito-stress test inhibitors and readout. The seahorse graph was recorded for 32D cells. Figure's details were adapted after Agilent's seahorse XFe96 user guide.

2.2. Gene editing section

2.2.1. Generation of gRNA-expressing vectors

Oligonucleotides corresponding to the target guide RNA were cloned into the backbone vector (detailed in Table 9). Initially, oligonucleotides (sense/ anti-sense) were annealed by mixing and incubation at 95°C for 5 minutes. Next, oligonucleotides were cloned into the vector by restriction and ligation reaction with the reagents specified in (Table 6) according to the program specified in (Table 7).

Table 6: Component reagents for restriction and ligation for cloning

Component	Amount
Vector (150 ng stock)	1 µl
Annealed primers	5 µl
T4 ligase buffer (10X) (NEB, USA)	2 µl
T4 DNA ligase (NEB, USA)	0.5 µl
BsmBI restriction enzyme (NEB, USA)	1 µl

Table 7: Reaction steps for restriction and ligation reactions.

Step	Temperature	Time
1. Restriction	37 C	5 min
2. Ligation	16 C	10 min
3. Eliminate empty vectors	37 C	15 min
4. Enzymes inactivation	80 C	5 min

2.2.2. Transformation

Transformation was done in competent bacterial cells (E. *coli* DH5α). Plasmid DNA was mixed with competent cells for 30 minutes on ice then heat-shocked at 42°C for 45 seconds. Samples were incubated on ice again for 2 minutes before spreading on LB agar plates (supplemented with 100 µg/ ml ampicillin) (media composition in Appendix Table A2).

2.2.3. Mini-preparation

Bacterial colonies were picked and propagated overnight in 4 ml LB medium (composition in Appendix Table A3). Bacterial cells were spun down at 15000 xg for 5 minutes, resuspended

in 100 µl resuspension buffer (all reagents from Macherey-Nagel, Germany). 200 µl of lysis buffer was added followed by 150 µl neutralization buffer. Samples were then spun down at 15000 xg for 5 minutes. Supernatant was transferred in a new Eppendorf tube, mixed with 1 ml 100% ethanol and centrifuged at 15000 xg for 5 minutes. Supernatant was discarded and the pellet was washed with 70% ethanol, centrifuged at 15000 xg for 1 minute and allowed to dry at room temperature. Plasmid DNA was resuspended in 50 µl H_2O and an aliquot was sent for sequencing for clone validation (SeqLab, Germany).

2.2.4. Midi-preparation

A single bacterial colony was picked and grown overnight in 200 ml LB medium supplemented with 100 µg/ ml ampicillin. Bacteria were then harvested, spun down, and resuspended in resuspension buffer according to the manufacturer instructions (NucleoSpin DNA, MACHEREY-NAGEL, Germany). Next, cells were lysed with lysis buffer, mixed with neutralisation buffer then loaded on a column filter. Columns were equilibrated then discarded. The membrane is then washed and the plasmid is eluted with elution buffer. The flow through was mixed with isopropanol and spun down at 6000 xg for 90 minutes at 4 °C. The pellet was washed in 70% ethanol then dried and reconstituted in water. DNA concentration was measured on a NanoDrop 2000c device (PeQlab, ThermoFisher, USA).

2.2.5. Lentivirus production in Hek293T cells

Hek293T cells were seeded 24 hours before the experiment at a density of $4*10^5$ cell/ml in 15cm petri dishes ($11*10^6$ cells in total before transfection). On the day of transfection, two mixes were prepared and incubated separate at room temperature for 5 minutes (Table 8). The first mix contains the plasmid DNA of the gene of interest and the viral proteins (packaging Gag-Pol (psPAX) and envelop plasmid VSV-G (pMD2.G)). The second mixture contains 1x polyethylenimine (PEI) (1 µg/µl) as a transfection reagent. The two mixtures are then mixed and incubated at room temperature for 20 minutes before being added to the cells. 24 hours later, media was changed to allow virus production in fresh media. 72 hours later, virus was harvested and filtered via 0.45-micrometre filters and either used for a transduction or frozen down in -80°C freezer. A list of all vectors used for plasmid generation are shown in (Table 9). Backbone maps of all vectors are shown in (Appendix 3). Vector maps were designed in SnapGene® software (GSL Biotech, USA).

Table 8: Transfection mixture per 15cm petri dish.

Component	Amount
Mix (I)	
Serum free DMEM	1900 µL
Plasmid DNA	11.3 µg
psPAX	10.5 µg
pMD2.G	5.8 µg
Mix (II)	
Serum free DMEM	1760 µL
PEI	140 µL

Table 9: vectors

Gene editing	Vector	Marker/ resistance cassette
PDP1 knockdown (human)	pLKO.1_puro	Puromycin resistance
PDP1 knockdown (mouse)	pLKO.1_puro	Puromycin resistance
PDP1 knockout (human)	pLentiCRISPRv2_ EGFP_ ΔCAS9	GFP
PDP1 overexpression (1) (human)	SIGW (PDP1)	GFP
PDP1 overexpression (2) (human)	SIHW (PDP1)	Hygromycin resistance
Hygromycin empty vector	SIHW (Mock)	Hygromycin resistance
GFP empty vector	pHR`SINcPPT_SEW	GFP
Gamma polymerase knockout (Rho Zero cells generation)	pLentiCRISPRv2_ BFP_ΔCAS9	BFP

2.2.6. shRNA PDP1 knockdown transduction

shRNA bacterial glycerol stocks were bought from Sigma-Aldrich, USA (Table 10). Midi-prep was performed and the plasmid was isolated as described in section 2.2.4. Virus was produced in HEK T293 cells as described in section 2.2.5. For the transduction, cells were then seeded in a 6-well plate at a density of 3 x 10^5 cells/ well with 500 µl virus (depending on the cell line), 1:1000 polybrene (hexadimethrine bromide) (Fluka BioChemika, Switzerland) (final concentration 8 µg/µl) and 1.5 ml fresh media. Puromycin selection was done with 2 µg/ml for 48 hours, 3 days after the transduction.

Table 10: PDP1 shRNA sequences.

shRNA	Sequence
Human shPDP1 (1) (TRCN0000356073)	CCGGCACTGGTGAGTCGACTGATATCTCGAGATATCAGTCGACTCACCAGTGTTTTTG
Human shPDP1 (2) (TRCN0000003081)	CCGGGCTGTGTGTAGTCTCTTGGTTCTCGAGAACCAAGAGACTACACACAGCTTTTT
Mouse shPDP1 (1) (TRCN0000081381)	CCGGGCAGAATCTATGGCACTGCATCTCGAGATGCAGTGCCATAGATTCTGCTTTTTG
Mouse shPDP1 (2) (TRCN0000081382)	CCGGCGCCATGCTGTAGGCAATAATCTCGAGATTATTGCCTACAGCATGGCGTTTTTG

2.2.7. PDP1 knockout

PDP1 knockout cells were generated by a CRISPR Cas9 strategy. sgRNAs against human PDP1 were designed by Frank Schnuetgen (sequences are shown in Table 11). Vector details are shown in Table 9, Appendix 3. Virus production and transduction were done similarly as described above (section 2.2.5). Transduction efficiency was assessed by GFP-positivity measured 3 days after the transduction.

Table 11: PDP1 guide RNAs sequences.

sgRNA	Sequence
sgRNA 1 (s)	CACCGctctgaggaatgtacgatg
sgRNA 1 (as)	AAACcatcgtacattcctcagagC
sgRNA 2 (s)	CACCGgtgtgaggtaaaatttctg
sgRNA 2 (as)	AAACcagaaattttacctcacacC

2.2.8. siRNA PDP1 KD

PDP1 siRNAs (Sigma-Aldrich, USA) (sequences in (Table 12)) and Trilencer-27 Universal scrambled negative control siRNA duplex (Origene, USA) were prepared in duplex re-suspension buffer (Origene, USA). 100 nM was used as a final transfection concentration. Cells were plated at a density of 1 x 10^5 cells/ml in a 96-well plate and transfection was done using the transfection reagent (Viromere Green) (Biozyme, USA) according to the manufacturer's instructions. Luminescence was measured 72 hours later with CellTiter-Glo as described in section (2.4.1).

Table 12: PDP1 siRNA sequence.

shRNA	Sequence
Human siPDP1 (s)	CGGUAUUUGAGGAUCAGAA
Human siPDP1 (as)	UUCUGAUCCUCAAAUACCG

2.2.9. PDP1 overexpression

Coding sequence of PDP1 cDNA was amplified from RPMI 8226 cells via a standard PCR reaction using the primers shown in (Table 13). The PCR product was cloned into two different PDP1 overexpression (OE) vectors (hygromycin (SIHW) or GFP (SIGW) selection cassettes) via BamHI and NruI restriction sites as specified in Appendix 3. Virus production and transduction were done similarly as described above (section 2.2.5). Hygromycin selection was done with 400 µg/ml for 3 days. GFP-transduced cells were FACS sorted 3 days after the transduction as described in the Flow cytometry section (2.3.1).

Table 13: Primers sequences of human PDP1 cDNA cloning

Primer	Sequence
PDP1 OE (s)	gggggggatccaccggtcgccaccATGCCAGCACCAACTCAACTG
PDP1 OE (as)	GGGCGTCGCGActcaTTCTTGGTTTTGATACGCCCC

2.2.10. Generation of Rho Zero cells

Molm13 Rho Zero cells were generated by a knockout of the mitochondrial gamma polymerase in spCas9-positive+ Molm13 cells (vector details in Table 9, Appendix 3). sgRNA sequences used are shown in (Table 14). Single clones were generated, and the knockout was confirmed on the protein level before using them for further analysis. These cells were generated by Dr. Frank Schnuetgen (Goethe University Hospital Frankfurt, Germany).

Table 14: Gamma polymerase guide RNAs sequences (Rho Zero cells generation).

sgRNA	Sequence
Gamma polymerase sgRNA (s)	CACCGctgcaccaggaatacctga
Gamma polymerase sgRNA (as)	AAACtcaggtattcctggtgcagC

2.3. Flow cytometry section

2.3.1. Fluorescence-activated cell sorting (FACS)

After staining procedures or transductions, cells were washed and then resuspended with phosphate buffer saline (PBS) in FACS tubes. Cells were then analysed on BD LSR Fortessa analyser (BD Biosciences, USA). A total of 10,000 events were recorded per sample. Fluorescence-activated cell sorting (FACS) of cells with low transduction efficiency was done on a FACS Aria II sorter (BD Biosciences, USA).

2.3.2. Gating strategy

Initial gating was done to define the living cells with the parameters side scattered light (SSC-A) and forward scattered light (FSC-A) (Figure 15A). SSC-A reflects on the cellular granularity and complexity while FSC-A is a measure of cell size (Adan et al., 2017). Next, single cells were gated out of the living cell population by the FSC parameters of Height vs Area (FSC-H vs FSC-A) (Figure 15B). Usually doublet cells have the same height as single cells but the area is bigger and thus they are distinguished and excluded on the FSC-A scale. Finally, the desired fluorochrome/ dye is measured out of the single cell population with the corresponding laser (Table 15). An example gating strategy of GFP is shown in (Figure 15C) and depicted differently as a histogram in (Figure 15D)

Table 15: Lasers used for fluorochromes measured on the LSR Fortessa analyser.

Fluorochrome	Laser	Filter
Hoechst	UV 355 nm	450/50
GFP	Blue 488 nm	V530/30
7-AAD	Yellow Green 561 nM	G610/20
Annexin V APC	Red 635 nm	R670/30
eFlour	Red 635 nm	R780/60

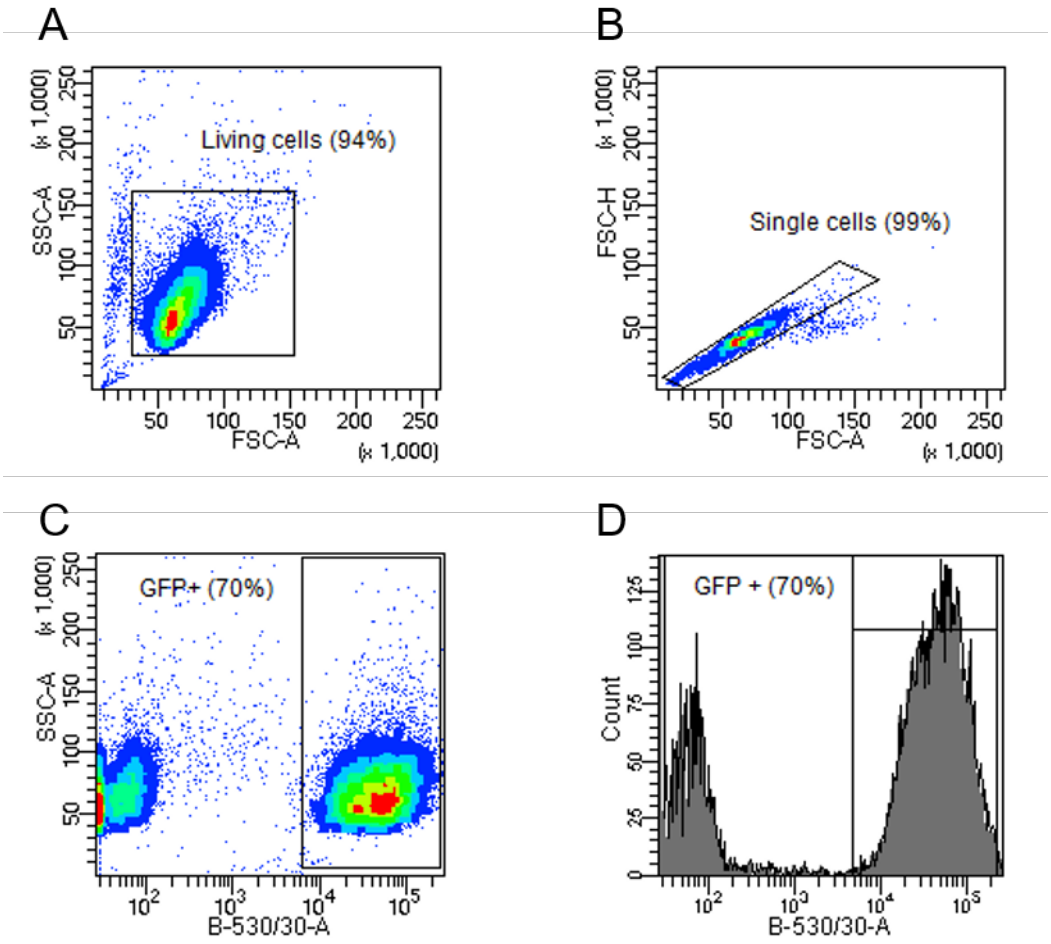


Figure 15: FACS gating strategy shown on 32D cells transduced with GFP vector. Gating of A. living cells and B. single cells is depicted. C. Gating for GFP positivity is plotted. D. Same GFP-positive population is shown as histogram.

2.4. Proliferation and viability assays

2.4.1. Cellular ATP assays

Cellular viability measured by ATP levels was done using CellTiter-Glo (Promega, USA). The assay readout was regarded as 'Relative survival' when using inhibitors that lead to cell death (AC220, venetoclax and rotenone). When assessing growth capacity of the cells with certain knockdown or the addition of cell culture supplementation, the readout was labelled as 'Proliferation". 10000 cells were plated per well in a 96-well flat while plate (Greiner bio-one, Austria) and 30 µl of the reagent were added and incubated at 37°C for 10 minutes. Luminescence was measured using a Tecan reader (Infinite M200 Pro, TECAN, Switzerland) with a time of one second flash (reading) per well.

2.4.2. Competition growth assay

Transduced cells were mixed with GFP-positive cells (50:50) and then maintained in culture. GFP-positive cells were produced by the transduction with SEW virus (pHR`SINcPPT-SEW vector) produced as described by (Demaison et al., 2002). The virus was kindly provided by Dr. Frank Schnuetgen (Goethe University Hospital Frankfurt, Germany). FACS samples were taken every 48 hours for the experimental time of 14 days. FACS analysis of GFP was done according to the specified parameters described in section (2.3.2) (Table 15).

2.4.3. Cumulative growth assay

Cells were originally plated at a density of 2.5 x 10^5 cells/ ml in 12-well plates. Cell counting was done regularly every 48 hours. Cells were then reseeded with fresh media to the original density and counted for 12 days. Counting was performed on an automatic cell counter (CASY, OMNI Life Science, Germany).

2.4.4. Apoptosis assay

Cell were treated with AC220 for 24 hours, then a total of 1 x 10^5 cells were washed with cold PBS and resuspended in 100 µl 1x binding buffer. Cells were then stained with 5 µl Annexin-APC (BD Biosciences, USA) and incubatedd for 20 min at room temperature in the dark. They were then analyzed by FACS with the specified parameters described in section (2.3.2) (Table 15).

2.4.5. Dead-cell staining (eFlour)

1 x 10^5 cells were washed and resuspended with PBS then the eFlour 780 dye (eBiosciences, USA) was added (1:10000 dilution) and incubated for 30 minutes in the dark at 37°C. Cells were then washed and FACS analysed with the specified parameters described in section (2.3.2) (Table 15). Unstained cells were used as a negative control.

2.4.6. Cell cycle assay

Cells were synchronized 24 hours before the experiment in G0 using 1 mM thymidine (Sigma-Aldrich, USA) as described before (Chen and Deng, 2018). Cells were incubated with thymidine for 16 hours followed by extensive washing. 1 x 10^5 cells were stained with Hoechst dye (bisBenzimide H 33342 trihydrochloride) (Sigma-Aldrich, USA) at a final concentration of 9 µM for 30 minutes in the dark at 37°C with 5% CO_2. The staining solution was then washed

out and cells were resuspended with PBS and measured on FACS with the specified parameters described in section (2.3.2) (Table 15). Unstained cells were used as a negative control for gating.

2.4.7. Synergy assays

For detection of synergism, 25,000 cells/96 well were seeded in increasing concentrations of AC220 {vertical layer} and venetoclax {horizontal layer} arranged in a checkerboard pattern. After 72 hours, ATP levels were measured using CellTiter-Glo reagent as a readout (described in section 2.4.1). Dose-response curves, IC_{50} values and analysis of fixed combinations could be analyzed from these data. Single combinations with fixed doses of venetoclax (10 nM) and AC220 (1 nM) were also performed. Analysis of synergism according to the highest single agent (HSA) reference model (Berenbaum, 1989) was performed with the open access platform SynergyFinder (Ianevski et al., 2017). This work was performed with the help of Philipp Makowka and Karoline Stoschek (Group of Prof. Hubert Serve, Goethe University Hospital Frankfurt, Germany).

2.4.8. Glucose consumption assay

Glucose consumption was measured using a colorimetric assay of hexokinase/ glucose-6-phosphate dehydrogenase coupled enzymatic reactions (accompanied by equimolar NAD+ to NADH reduction) (Glucose HK Assay Kit GAHK20, Sigma-Aldrich, USA). Media samples were collected from drug-treated cells and plated in 96-well flat bottom transparent polystyrene plate (Greiner bio-one, Austria). Absorbance was measured at 340 nm wavelength using a Tecan reader (Infinite M200 Pro, TECAN, Switzerland).

2.5. *In vivo* experiments

2.5.1. Xenotransplantation mouse experiments

Ten to fourteen-week old, non-irradiated NSG (NOD SCID gamma) mice (with interleukin-2 receptor knockout) were transplanted intravenously with 1 x 10^5 Molm13 cells (PDP1 knockdown shRNA or non-target shRNA). Prior to transplantation, cells were transduced with either NTC or PDP1 shRNA. Three days post-transduction, the cells were selected with puromycin (2 μg/ml) for 48 hours. Cells were then extensively washed from puromycin and debris before the transplantation. Disease course was followed by analysing human CD45+ cells in peripheral blood by flow cytometry (BD Biosciences, USA). The last three mice in the PDP1 knockdown group that did not develop leukaemia were sacrificed at day 60. The *in vivo*

work was done by Dr. Rahul Kumar in Prof. Daniela Krause lab (Georg Speyer-House, Frankfurt, Germany).

2.5.2. Ethical and regulatory information

The mice were bred in the animal facility of Georg-Speyer-Haus, Frankfurt. All animal studies were approved by the local German government (Regierungspräsidium Darmstadt) in Hessen, Germany. Project approved: Metabolismus- und Hypoxie-assoziierte Target-Gene bei der AML, FK/1117).

2.6. Protein and RNA section

2.6.1. Western blotting

Protein lysates were harvested in a RIPA buffer (150 mM sodium chloride, 1% Triton X-100, 0.5% sodium deoxycholate, 0.1% SDS (sodium dodecyl sulphate) and 50 mM Tris-HCL, pH= 7.5). The buffer was freshly supplemented with EDTA-free proteinase inhibitor (Merck, Germany), 5 mM NAF (Sigma Aldrich, USA) and 1 mM NA_3VO_4 and Pierce Nuclease (0.5µl/1 ml buffer) (ThermoFisher, USA). One million cells were harvested and lysed with the buffer, vortexed, incubated on ice for 20 minutes then at 37°C for 5 minutes (for the nuclease activity) and then centrifuged for 10 minutes at 15000 xg. Protein concentrations were measured using Bradford assay with 5X Roti-Quant reagent (Carl Roth, Germany). Lysates were then prepared with 4X loading dye (Carl Roth, Germany) and boiled for 5 minutes at 94°C.

Protein lysates were run on a 10% agarose gel using MOPS SDS running buffer (Invitrogen, USA) at 150 Volts. Gels were then blotted on a nitrocellulose membrane (0.2 µM pore size) (Bio-Rad, USA) using a transfer buffer (Novex NuPAGE 20X Transfer buffer (ThermoFisher, USA) prepared in H_2O and 10% methanol) for 2.5 hours at 35 Volts. Membranes were then blocked with 5% milk (Carl Roth, Germany). Primary antibodies (Table 16) were applied overnight at 4°C. After thorough washing from the primary antibody with Tris-Wash buffer (TBS) (Zytomed, Germany), secondary antibodies (HRP anti-rabbit IgG or HRP anti-mouse IgG, both at 1:10,000 dilution) (Santa Cruz Biotechnology, USA) were applied for 1 hour at room temperature. Membranes were then visualised on a LI-COR imager (Biosciences GmbH, Germany) using SuperSignal™ West Femto and PICO chemiluminescence substrates (ThermoFisher, USA). Image quantification was done using Image Studio software.

Table 16: Primary antibodies for western blot. Abbreviations: mAB: monoclonal antibody.

Antibody	Brand	Species	Dilution
PDP1	Cell signalling, USA	Rabbit (mAB)	1:1,000
Vinculin	Sigma-Aldrich, USA	Mouse (mAB)	1:1,000
Beta-Actin	Cell signalling, USA	Rabbit (mAB)	1:1,000
PDHA1	Molecular Probes, USA	Mouse (mAB)	1:500
pPDHA1 (S293)	Merck, Germany	Rabbit (mAB)	1:1,000

2.6.2. RNA extraction and reverse transcription

Cells were homogenised and lysed by cell lysis buffer then mercaptoethanol was added and DNA was removed by a DNA-binding column (NucleoSpin). RNA was then washed on a silica membrane and eluted in RNAse-free H_2O according to the manufacturer's instructions (NucleoSpin® RNA, MACHEREY-NAGEL). cDNA was prepared with 0.5 μg RNA mixed with 1 μl random primers (ThermoFisher, USA) and 7 μl RNAse free water (Mix (I)), heated for 5 minutes at 65°C (annealing) then incubated on ice. A second mix of strand buffer, DTT, dNTP, RNAse inhibitor and reverse transcriptase (SuperScript, ThermoFisher, USA) was then added to the RNA-primers mix (Table 17). The mix was then run in a PCR machine for cDNA synthesis (reverse transcription) as detailed in (Table 18). The end cDNA product was filled up to 100 μl RNAse-free H_2O and frozen down at -80°C.

Table 17: cDNA synthesis master mix (per one reaction).

Component	Amount
Mix (I)	
RNA	0.5 μg
RNAse-free water	7 μl
random primers	1 μl
Mix (II)	
1st strand buffer (5X)	4 μl
Dithiothreitol (DTT)	1 μl
deoxynucleoside triphosphates (dNTPs)	1 μl
RNAse inhibitor (RNAsin)	1 μl
Reverse transcriptase	1 μl

Table 18: cDNA synthesis (reverse transcription) reaction.

Step	Temperature	Time
Annealing	65 C	5 min
cDNA synthesis	25 C	10 min
	42 C	60 min
	70 C	15 min

2.6.3. qPCR measurement

qPCR mix was prepared with Syber green (Sigma-Aldrich, USA), PDP1 primers (Sigma-Aldrich, USA), RNAse free water and cDNA (Table 19). PDP1 primers sequences are shown in (Table 20). Samples were vortexed and then measured on a quantitative PCR instrument (Opticon reader (MJ research, USA)) with the program detailed in (Table 21). ddCT was calculated to identify relative differences in RNA levels. The experiment was done in 2 biological replicates with 3 technical replicates each.

Table 19: qPCR master mix (per one reaction).

Component	Amount
cDNA	5 µl
Syber green	12.5 µl
PDP1 primers	1 µl
RNAse-free water	6.5 µl

Table 20: PDP1 qPCR primer sequence.

Primer	Sequence
Human PDP1 (s)	ctcgtcgggaagaatcgtt
Human PDP1 (as)	GTGGTGGCAGTAACATGCAG
Mouse PDP1 (s)	tgctgagtgagggaaggac
Mouse PDP1 (as)	CACAGTTACGGACGAGAGGA

Table 21: qPCR reaction setup.

Step	Temperature	Time	Cycle
1. Initial denaturation	95 C	15 min	
2. Denaturation	95 C	30 sec	
3. Annealing	60 C	30 sec	
4. Synthesis	72 C	20 sec	39 (steps 2-4)

2.7. Metabolomics and NMR section

2.7.1. Metabolites extraction and sample preparation

Cells were plated 24 hours before the experiment in fresh media. A highly reproducible extraction protocol was followed as described previously (Madji Hounoum et al., 2015). 1 x 10^7 cells were harvested, washed with (PBS) at 37°C and spun down for 20 seconds at 16000 g. PBS was removed and cells were vortexed for 10 seconds after adding pre-chilled HPLC-grade methanol (VWR Chemicals International, USA) (amounts specified in Table 22). Double distilled H_2O and pre-chilled HPLC-grade chloroform (Carl Roth, Germany) were added to each sample and vortexed for 40 seconds. Samples were placed on ice for 10 minutes and then centrifuged at 5000 xg for 10 minutes at 4°C in a swingout rotor. 500 µl were taken from the upper (polar) layer and then dried using a Concentrator Plus vacuum dryer (Eppendorf, Germany) at 4°C for 4 hours.

Table 22: Chemicals used for metabolites extraction.

Material	Volume per sample (10 million cells)
PBS	1 ml
HPLC-grade methanol	400 µl
Distilled water	325 µl
HPLC-grade chloroform	400 µl

The metabolites extracts were then resuspended in 190 µl of NMR phosphate buffer (pH=7). The buffer is composed of 100 mM sodium phosphate (PO_4) dissolved in 100% D_2O (Deutero, Germany) supplemented with 0.5 mM trimethylsilylpropanoic acid (TMSP) (Merck, Germany) as a reference compound. Samples were then sonicated for 10 minutes and loaded in the NMR tubes (3 mm tubes, Norell, HT version or the new 96-tubes racks).

2.7.2. Tracer-based assay

For the glucose labelling experiments, cells were plated 24 hours before extraction in glucose-free RPMI 1640 medium (Gibco, ThermoFisher, USA) (similar composition to standard RPMI medium but without glucose, catalogue number 11879) supplemented with 11 mM uniformly ^{13}C-labelled glucose (Sigma-Aldrich, USA). For methionine tracers, cells were plated 12 hours before the experiment in a homemade media (prepared by Alan Cunningham with the same composition of Gibco RPMI 1640 media as reported on their website (Appendix Table A4) supplemented with 0.1 mM ^{13}C-labelled methionine (Sigma-Aldrich, USA). Samples were processed similarly to the 1D extracts, however, the methionine tracers were prepared with only 60 µl of the NMR buffer and loaded in 3 mm Shigemi tubes (Cortecnet, France) for sensitivity enhancement.

2.7.3. Real-time NMR cell culture and sample preparation

Cells were maintained in IMDM medium (Sigma-Aldrich, USA) prepared with 40% methylcellulose (R&D systems, USA), 10% fetal bovine serum (Sigma-Aldrich, USA) and 1% penicillin and streptomycin (Gibco, ThermoFisher, USA). For the viability assays (ATP levels), cells were plated in a 96-well plate (50000 cell/ well) and luminescence was similarly measured 48 hours using CellTiter-Glo® (Promega, USA) (as described in section 2.4.1). For the determination of oxygen levels, an OxyScan300 device (UMS, Germany) was used on samples prepared in 8 mm NMR tubes. pH values were determined in 5 mm NMR tubes using SI Analytics pH meter.

Sample preparation was done with 5 x 10^5 Molm13 cells or 1 x 10^6 primary AML blasts per sample. Cells were washed and resuspended in 40% methylcellulose media containing 10% D_2O, 0.5 mM TMSP and cytokines cocktail (see chapter 2.1.1). For the tracer-based assay, the cells were instantly supplemented with a 1:1 mixture of ^{12}C and ^{13}C glucose. Samples were then loaded in 5 mm NMR tubes using Hamilton Gilson syringe and then transferred to the spectrometer's sample changer (SampleJet, Bruker, USA). Sample preparation and storage in-between the measurements was at 37°C.

2.7.4. NMR data acquisition

Most of the samples were measured on a Bruker 600MHz AVIIIHD spectrometer equipped with a nitrogen-cooled triple resonance probe head (5 mm TCI Prodigy, ^{1}H, ^{13}C, ^{15}N Z-GRD), unless specified otherwise in the results section. The spectrometer is equipped with

SampleJet that loads and alternates the samples automatically. Tuning and matching were performed automatically using the (ATMA) command (automatic tuning and matching). Shimming was usually performed with an optimised shim file on a standard sucrose sample. Methionine tracing samples were measured on a Bruker 800MHz AVIIIHD with a cryo probe head (5 mm TCI cryo ^{1}H, ^{13}C, ^{15}N Z-GRD) to obtain higher sensitivity. Tuning and matching were performed manually.

One-dimensional experiments were mainly recorded using either NOESYGPPR1D or ZGESGPPS pulse sequences (parameters in Table 23). NOESYGPPR1D is a standard Bruker pulse sequence for 1D NOESY experiments. This sequence implements water suppression by pre-saturation during the relaxation delay with a continuous low power pulse on water region. The second pulse sequence (ZGESGPPS) is a modified standard Bruker (ZGESGP) for double solvent suppression (water suppression with Excitation Sculpting) (Hwang and Shaka, 1995).

Table 23: One dimensional ^{1}H NMR experimental parameters.

Experiment/ parameter	**NOESYGPPR1D** (standard Bruker)	**ZGESGPPS** (Hwang and Shaka, 1995)
Number of points	32768	32768
Number of scans	512	128
Frequency offset (ppm)	4.696	4.7
Spectral width (ppm)	12	16
Acquisition time (sec)	2.27	1.7
Spectrometer (^{1}H resonance frequency (MHz))	600	600
Temperature (C)	25	25

For the two-dimensional measurements, ^{1}H–^{13}C Heteronuclear Single-Quantum Correlation (HSQC) spectra were recorded using the phase sensitive standard Bruker pulse program HSQCPHPRSP.UG4 with States-TPPI acquisition mode (experimental parameters are shown in (Table 24)). Some parts of the data was recorded with either of the standard Bruker pulse programs HSQCETGPSP.2 or HSQCETGPSISP2.2 with Echo-Antiecho acquisition mode. These two pulse program incorporate time-proportional phase incrementation (TPPI) gradient selection during the echoes. This is achieved by adiabatic pulses for inversion and refocusing. Phase error in these two pulse programs was corrected for (see Appendix 6).

These HSQC experiments were recorded with Non-Uniformed Sampling (NUS) function (10%) in order to reduce the number of increments recorded in the indirect dimension without losing the resolution and therefore the spectral information (Barna et al., 1987; Zambrello et al., 2018). This allows to increase the resolution without increasing the measurement time.

Table 24: Two dimensional ^{1}H–^{13}C HSQC experimental parameters.

Parameter	**HSQCETGPSP.2**		**HSQCPHPRSP.UG4**			
	^{13}C Glucose tracer		^{13}C Methionine tracer			
Spectrometer (^{1}H resonance frequency (MHz))	600		600 (K562)		800 (Molm13 and MV4-11 and healthy PBMSCs)	
Temperature (C)	25		25		25	
Number of scans	128		128		64	
	^{1}H	**^{13}C**	**^{1}H**	**^{13}C**	**^{1}H**	**^{13}C**
Number of points	2048	2048	1024	2048	1024	4096
NUS		10%		10%		10%
Frequency offset (ppm)	4.696	85	4.7	82.5	4.7	85
Spectral width (ppm)	12	170	12	165	12	170
Acquisition time (sec)	0.142	0.04	0.07	0.04	0.053	0.06
Resolution (Hz)	7.04	25.05	14.08	24.31	18.78	16.69

2.7.5. Real-time NMR experimental setup and measurement

Cells were loaded in the NMR tubes after methylcellulose preparation (see chapter 2.7.3) at 37°C. Samples were transferred to the spectrometer's sample changer (pre-warmed to 37°C). Automatic setup was performed with a series of time course measurements in an interleaved manner where every sample was measured every 2 hours for the first 12 hours, with further measurements at 24, 36 and 48 hours.

Standard 1D measurements were recorded with ZGESGP pulse sequence. Double-filter pseudo-2D measurements were recorded for the tracer-based assays, as described previously (Reed et al., 2019). This is originally a NOESYGPPR1D pulse sequence modified by integrating a "Gradient Bilinear Rotation Decoupling" (GBIRD) filter as described in (Heikkinen and Kilpeläinen, 1999) (Figure 16). This GBIRD filter is designed after the original BIRD method published by (Garbow et al., 1982). The sequence allows to record two datasets;

one standard 1D dataset for the total proton signals and another ^{13}C-filtered with integrated gradients that destroys signals originating from ^{13}C-bound protons. By changing the phase of the ^{1}H pulse, ^{13}C-bound proton signal get destroyed because, unlike those bound to ^{12}C, they do not change magnetization sign as it gets through the GBIRD, which doesn't allow it to defocus and get refocussed again by the gradients. Experimental parameters are detailed in (Table 25).

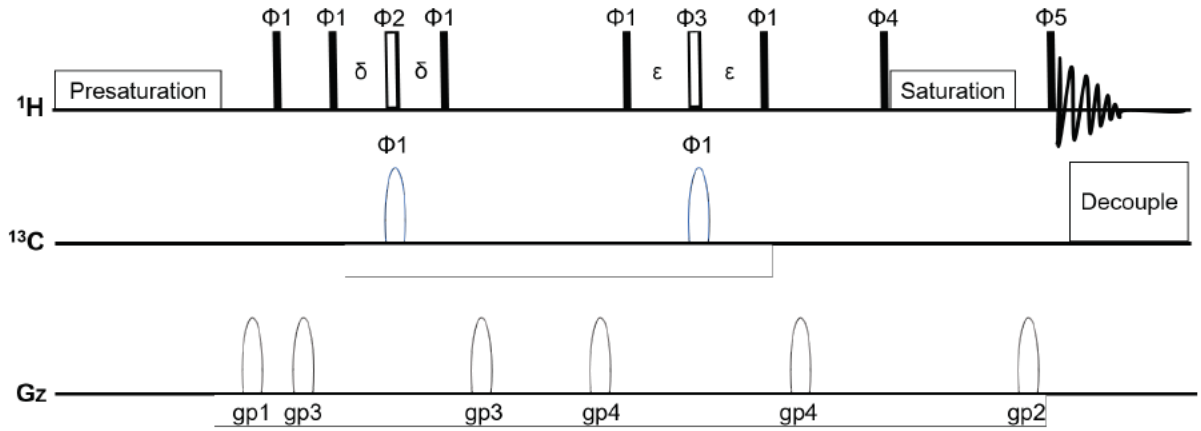


Figure 16: Pseudo 2D GBIRD double-filter 1D NOESY experiment pulse sequence. The gradients implemented eliminate signals originating from protons attached to ^{13}C because their magnetisation sign does not change as they get through the BIRD. Only protons attached to ^{12}C can change the sign and thus get refocused by the gradients. The figure was modified after (Reed et al., 2019) (license obtained).

Table 25: Pseudo-two-dimensional GBIRD double filtered experimental parameters.

Parameter	**GBIRD filtered experiments**	
Spectrometer (^{1}H resonance frequency (MHz))	600	
Temperature (C)	27	
Number of scans	32	
	^{1}H	**Pseudo second dimension**
Number of points	8192	2
Frequency offset (ppm)	4.698	4.698
Spectral width (ppm)	12	12
Acquisition time (sec)	0.568	

2.7.6. NMR Data analysis

For the one dimensional ^{1}H data, spectral processing (phasing, baseline correction and referencing to TMSP peak) was performed in NMRLab (MATLAB-based) (Ludwig and Günther, 2011). Metabolites identification was performed using Chenomx profiler software (Chenomx Inc. Edmonton, Alberta, Canada) as described previously (Alshamleh et al., 2020) (Appendix Table A5). This was confirmed with the Human Metabolome Data Base (HMDB) (Wishart et al., 2007). Metabolites quantification was performed in NMRLab and intensities were normalized according to TMSP peak.

NUS reconstitution of the two dimensional $^{1}H–^{13}C$ data was performed in NMRPipe (Delaglio et al., 1995). Spectra were then phased and referenced to lactate peak (C3) in NMRLab. Metabolites assignment and label incorporation analysis was performed in NMRLab for the metabolites available in its library, and the rest of the metabolites were analysed in Sparky 3.114 (UCSF) software (Goddard and Kneller).

Processing the pseudo 2D-double filtered experiments was done in Topspin 3.5. The AU-program (proc_std with the relax option) separated the 2 datasets and generated 2 spectra: total protons and protons attached to ^{12}C. The ^{13}C-attached protons spectra were generated from the difference between the total protons and ^{12}C protons spectra using the AU-program (proc_std). Spectra were phased and baseline was corrected in Topspin. Metabolites integrals calculation was performed in Topspin 3.5.

2.8. Statistical analysis

Data plotting and graphs generation was performed in GraphPad Prism 8 (GraphPad Software, USA). Statistical analysis of two groups was done using unpaired Student's t-test with confidence interval of 95% and P=0.05 significance level, while for multiple groups analysis was done using one/ two-way ANOVA with Bonferroni's multiple comparisons. Survival curves comparison was performed using Gehan-Breslow-Wilcoxon test with P=0.0332 significance level. IC_{50} determination was performed by nonlinear regression analysis of dose response curves.

Chapter III

PDP1 is a key metabolic gatekeeper and modulator of drug resistance in FLT3-ITD-positive AML

PDP1 drives dependence on OXHPOS metabolism

3.1. Results

3.1.1. FLT3-ITD-positive AML cells exhibit dominant mitochondrial metabolism

The metabolic phenotypes of different AML cell lines with different genetic backgrounds was investigated. Using NMR spectroscopy, a panel of eight different AML cell lines was screened to compare their mitochondrial TCA cycle activity with their glycolytic activity. This was assessed by taking the ratio of the concentrations of the two TCA cycle intermediates succinate (Figure 17A) and fumarate (Figure 17B) to lactate concentration. Interestingly, 1.5 to 2-fold higher TCA/glycolysis ratio was observed in FLT3-ITD cells in comparison to their FLT3-WT counterparts, suggesting higher mitochondrial metabolism.

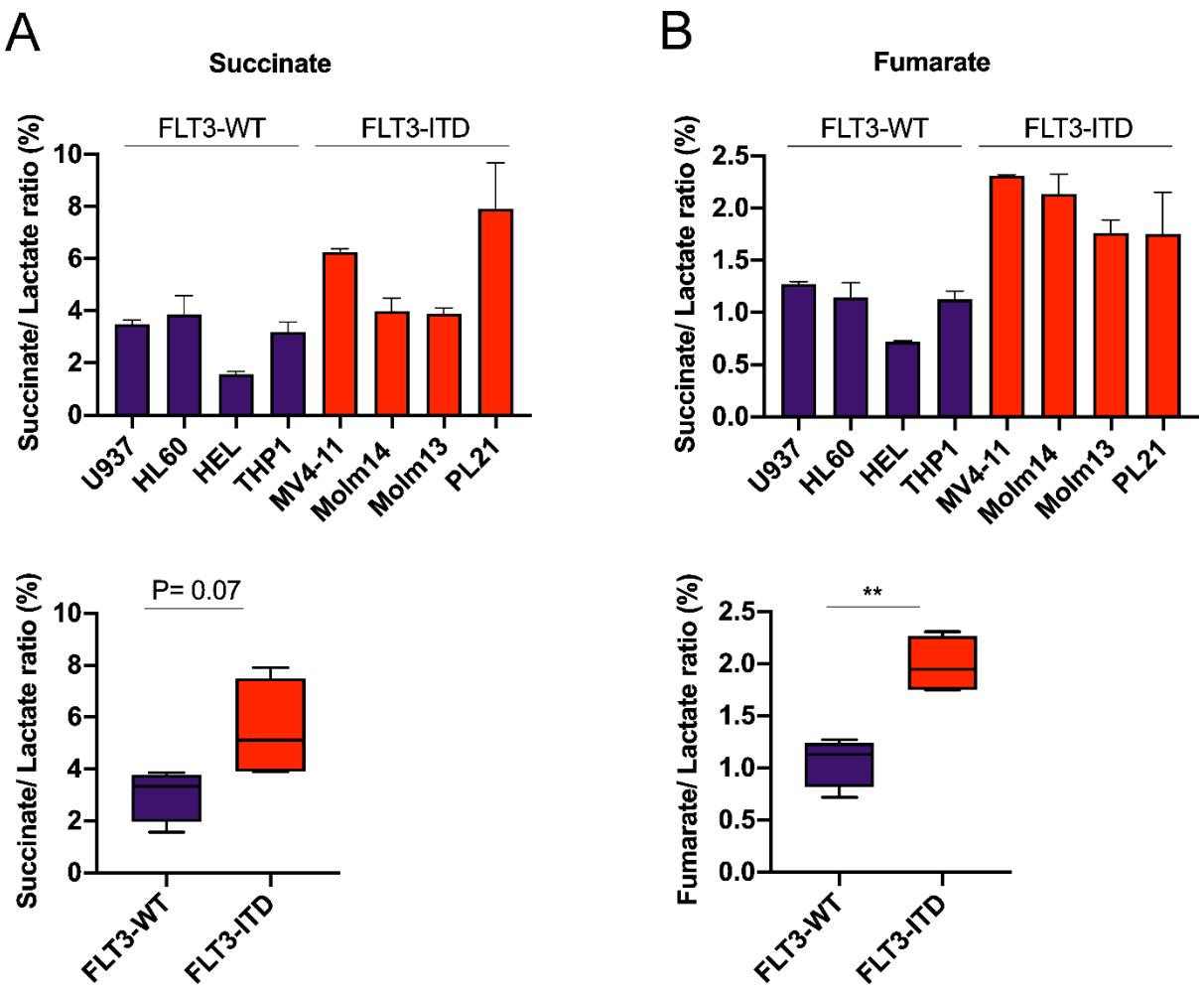


Figure 17: FLT3-ITD AML cell lines have higher TCA/glycolysis ratio. NMR measurements of higher concentration ratio between A. succinate/ lactate and B. fumarate/ lactate in FLT3-ITD *vs* FLT3-WT AML cell lines. Statistical analysis was performed using unpaired Student's t-test. ** P≤ 0.01.

Considering the multi-mutational nature of the cell line models, a more comprehensive metabolic profiling was carried out in cytokine-dependent hematopoietic progenitor 32D cells. These cells were originally established by transducing them with FLT3-ITD construct which can sustain cellular proliferation independently of cytokines (Choudhary et al., 2005; Mizuki et al., 2000). This allows to directly compare the metabolic consequences of FLT3-ITD signalling in cellular settings with identical genetic background. For a controlled comparison of the metabolic behaviour driven by FLT3-ITD kinase activity, two main conditions were used; no growth factors (FLT3-ITD) *vs* IL3 signalling (combined with AC220 to block FLT3-ITD signalling). An extra condition of IL3 alone (without AC220) was also used as a control (both; IL3 and FLT3-ITD oncogene are active). No FLT3-ligand was added since FLT3-ITD signalling is ligand independent (Kiyoi et al., 1998). Cells were adapted to FLT3-ITD signalling for five days before the experiment to avoid artefacts of acute transition from IL3 to FLT3-ITD signalling.

Similar to the cell lines results, NMR measurements of intracellular metabolites levels revealed reduced lactate production when cells were under the influence of FLT3-ITD signalling in comparison to IL3 stimulation (Figure 18A). However, succinate and fumarate levels were clearly elevated under FLT3-ITD signalling (Figure 18B, C) (correspondent NMR spectrum is shown for each metabolite). FLT3-inhibition with AC220 (highly potent FLT3-inhibitor (Kampa-Schittenhelm et al., 2013; Zarrinkar et al., 2009) led to a strong reduction in lactate levels, but also succinate and fumarate. These results again indicate a more dominant mitochondrial metabolism rather than glycolysis under FLT3-ITD activity.

To get mechanistical insights on the dynamics at the interphase between glycolysis and the TCA cycle, a tracer-based assay using ^{13}C-glucose was performed. This allowed for observing the change in the balance of glucose-derived pyruvate fates upon signalling manipulation. Consistent with lactate levels measurements, FLT3-ITD did not promote strong pyruvate conversion into lactate (relative to IL3) (Figure 19A). Instead, the balance was shifted towards the TCA cycle, as reflected by the sustained ^{13}C label incorporation into succinate (Figure 19B). Altogether, ^{13}C labelling ratio between succinate *vs* lactate was increased under FLT3-ITD kinase activity compared to IL3 stimulation (Figure 19C). Interestingly, AC220 led to even higher TCA/glycolysis ratio, and this will be presented later in the context of PDP1 upregulation under AC220 treatment (Figure 34C).

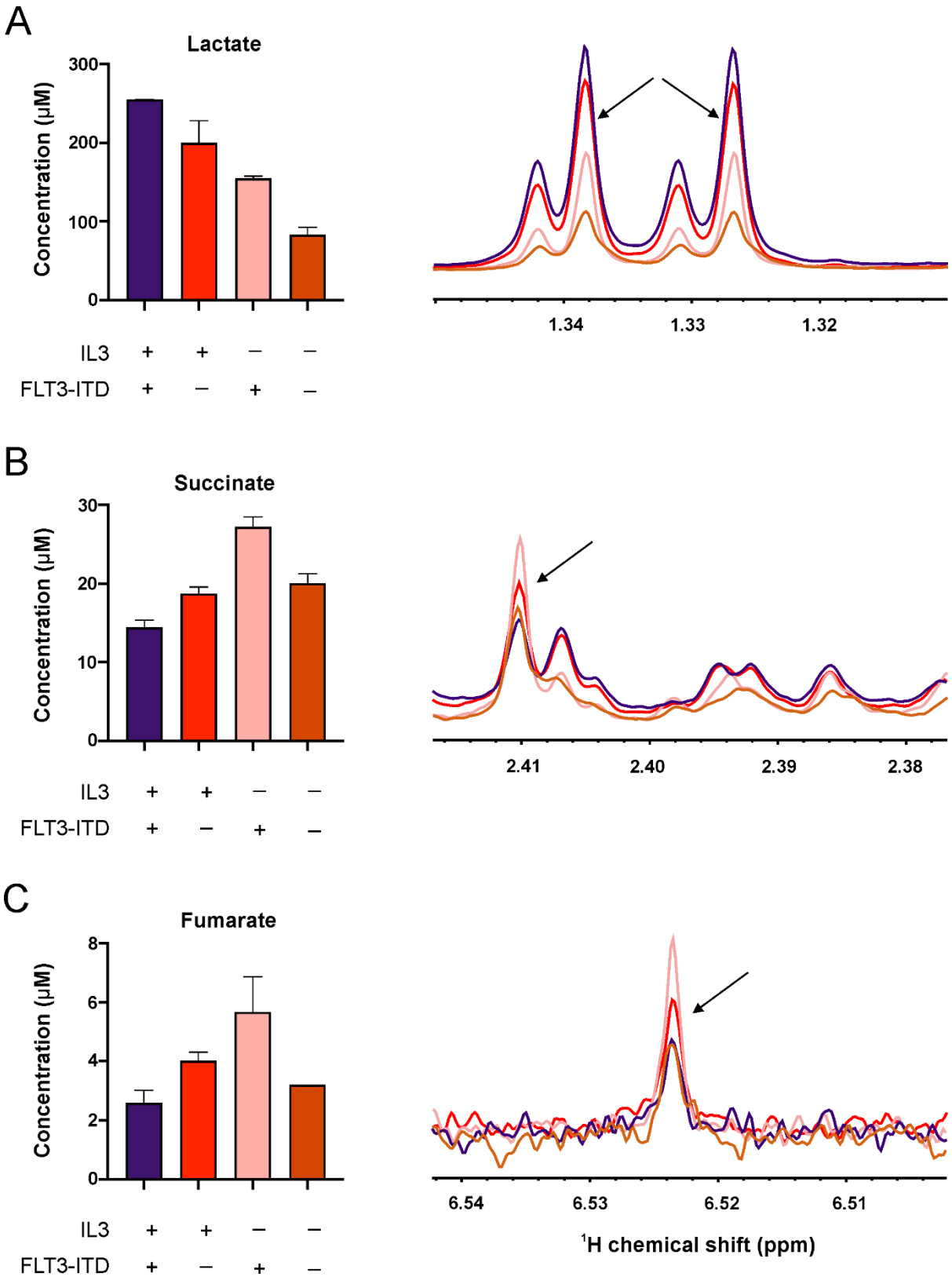


Figure 18: 32D model of FLT3-ITD signalling reveals higher TCA cycle and OXPHOS activity. The figure shows NMR measurements of A. reduced intracellular lactate levels under FLT3-ITD signalling in comparison to IL3, however, increased levels of the TCA cycle metabolites B. succinate and C. fumarate. n=2. For each metabolite, 1D ^{1}H-NMR spectrum is shown for an individual replicate (measured at 600MHz using the pulse program: NOESYGPPR1D at 25°C). For detailed atoms assignment, refer to (Figure 11).

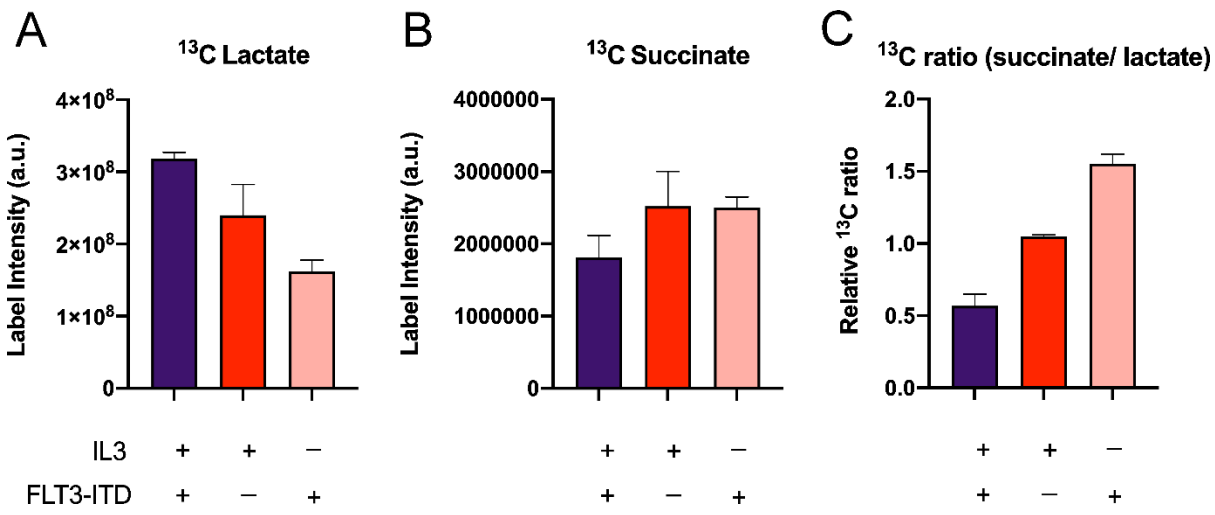


Figure 19: FLT3-ITD activity favours higher pyruvate incorporation into the TCA cycle. Tracer-based assay using NMR shows A. lower ^{13}C label incorporation into lactate while B. sustained ^{13}C intensity in succinate after 24 hours of tracing with ^{13}C-labelled glucose. C. Higher ^{13}C ratio observed between succinate and lactate under FLT3-ITD activity. n=2.

Considering these findings of higher mitochondrial metabolism in FLT3-ITD-positive cells, a nutrient deprivation experiment was performed aiming at assessing the relative mitochondrial fitness. 32D cells were deprived from glucose (glucose-free medium RPMI, detailed in section 2.7.2) and alternatively provided with a precursor of the TCA cycle metabolite alpha ketoglutarate (2-dimethyl 2-oxoglutarate). Interestingly, under FLT3-ITD, but not IL3 signalling, alpha ketoglutarate fully sustained cellular proliferation by shifting the cellular reliance to the TCA cycle (Figure 20). These results further indicate higher mitochondrial fitness in FLT3-ITD cells, which comes in line with their dominant mitochondrial phenotype.

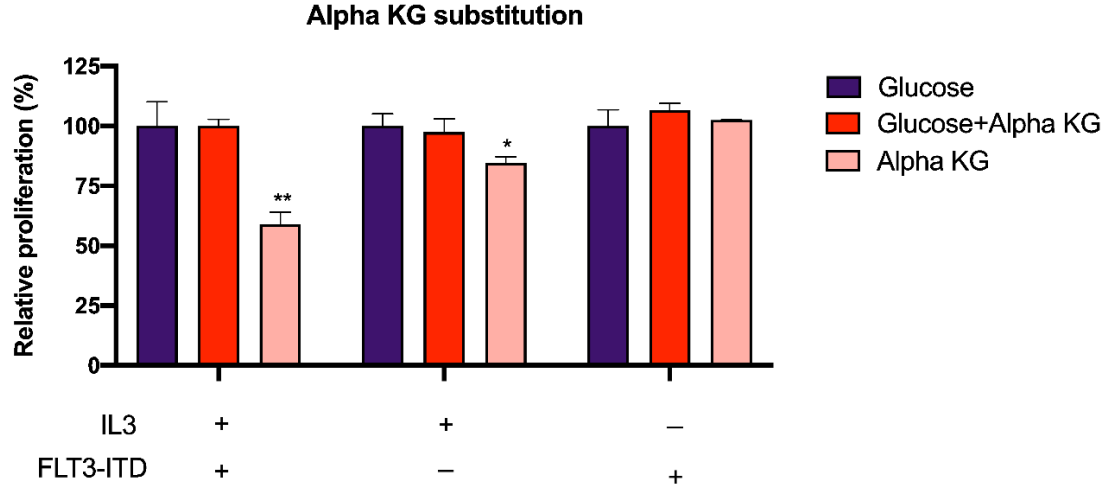


Figure 20: TCA cycle supplementation rescues glucose deprivation effects in FLT3-ITD. Glucose substitution with the precursor of the TCA cycle metabolite Alpha KG (alpha-ketoglutarate (added as 2-Dimethyl 2-oxoglutarate)) can maintain full metabolic activity and proliferation in FLT3-ITD but not FLT3-WT cells. Statistical analysis was performed using two-way ANOVA with Bonferroni's multiple comparisons. ** P≤ 0.0021, * P≤0.0332.

3.1.2. FLT3-ITD cells are highly sensitive to OXPHOS perturbations

To further elucidate the importance of OXPHOS to FLT3-ITD-positive AML cells in comparison to other AML genetic backgrounds, the relative sensitivity of a panel of AML cell lines was determined against the BCL2-inhibitor venetoclax (Souers et al., 2013) (also inhibits OXPHOS (Pollyea et al., 2018; Roca-Portoles et al., 2020). Clear differential sensitivities to venetoclax were observed. While FLT3-ITD cells (Molm13, Molm14 and MV4-11) had IC_{50} values in the lower nanomolar range, FLT3-WT cells (HEL and THP1) were less sensitive with IC_{50} values in the micromolar range (Figure 21A). These findings were confirmed in patient-derived primary AML blasts where FLT3-ITD-positive samples were pronouncedly more sensitive to venetoclax treatment (Figure 21B) (patient characteristics are detailed in Appendix Table A1). Similarly, rotenone, inhibitor of complex 1 of the electron transport chain (ETC), showed higher impact on FLT3-ITD cells in comparison to their FLT3-WT counterparts (Figure 21C).

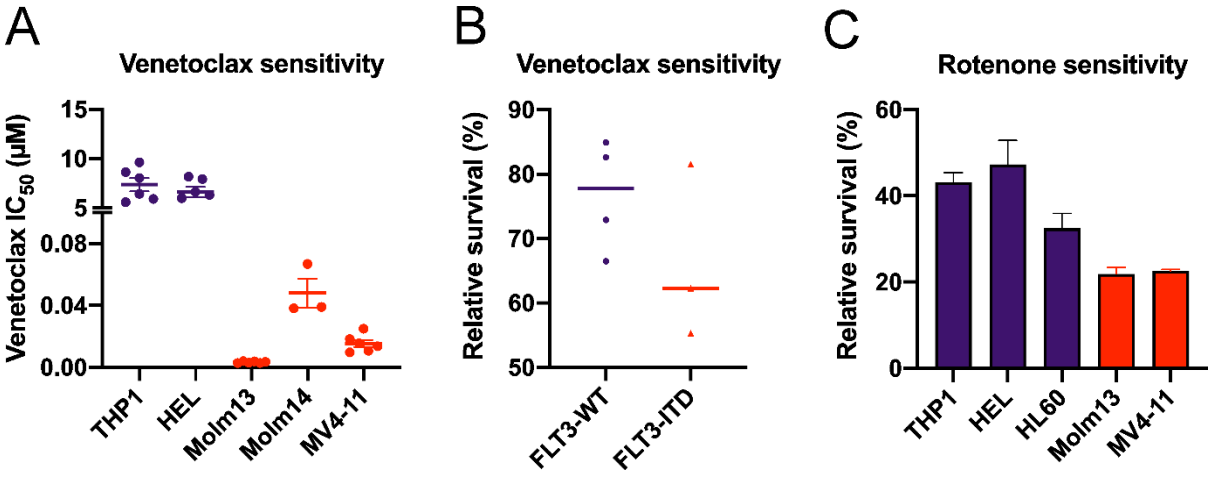


Figure 21: FLT3-ITD cells are highly sensitive to mitochondrial inhibition. A. IC_{50} determination of venetoclax shows FLT3-ITD cells to be highly sensitive (nM range) while FLT3-WT cells are less sensitive (µM range) after 48 hours of treatment[1]. B. Venetoclax treatment (50 nM for 72 hours) exerts higher impact on FLT3-ITD-positive primary AML blasts in comparison to their FLT3-WT counterparts. C. FLT3-ITD cells are more sensitive to rotenone treatment than FLT3-WT cells (500 nM for 24 hours).

3.1.3. FLT3-ITD cells express high PDP1 levels

With these data in hand, the molecular mechanism by which FLT3-ITD promotes this OXPHOS phenotype was investigated. Potential metabolic players and enzymes that regulate and drive TCA cycle activity were investigated, mainly components of the pyruvate dehydrogenase complex (PDC) (at the interphase between glycolysis and the TCA cycle (see (Figure 5)). Interestingly, pyruvate dehydrogenase phosphatase 1 (PDP1) (which promotes

[1] The IC_{50} experiment and its part of the figure was performed and provided by Philipp Makowka (Prof. Serve lab, MED2, Goethe-University Hospital Frankfurt, Germany).

pyruvate conversion to acetyl-CoA) was found at higher levels (2.6 folds) in 32D cells under FLT3-ITD signalling compared to IL3 stimulation (Figure 22A). Similarly, FLT3-ITD-positive AML cell lines had significantly higher PDP1 protein levels compared to their FLT3-WT counterparts (approximately double the amounts) (Figure 22B). Moreover, mass-spectrometry-based proteomics analysis of a cohort of 166 newly-diagnosed AML patients revealed higher PDP1 levels in samples with FLT3-ITD mutations (Figure 22C)[2]. Consequently, the high PDP1 levels were associated with high PDH activity (represented by lower S293 inhibitory phosphorylation (Figure 22D)).

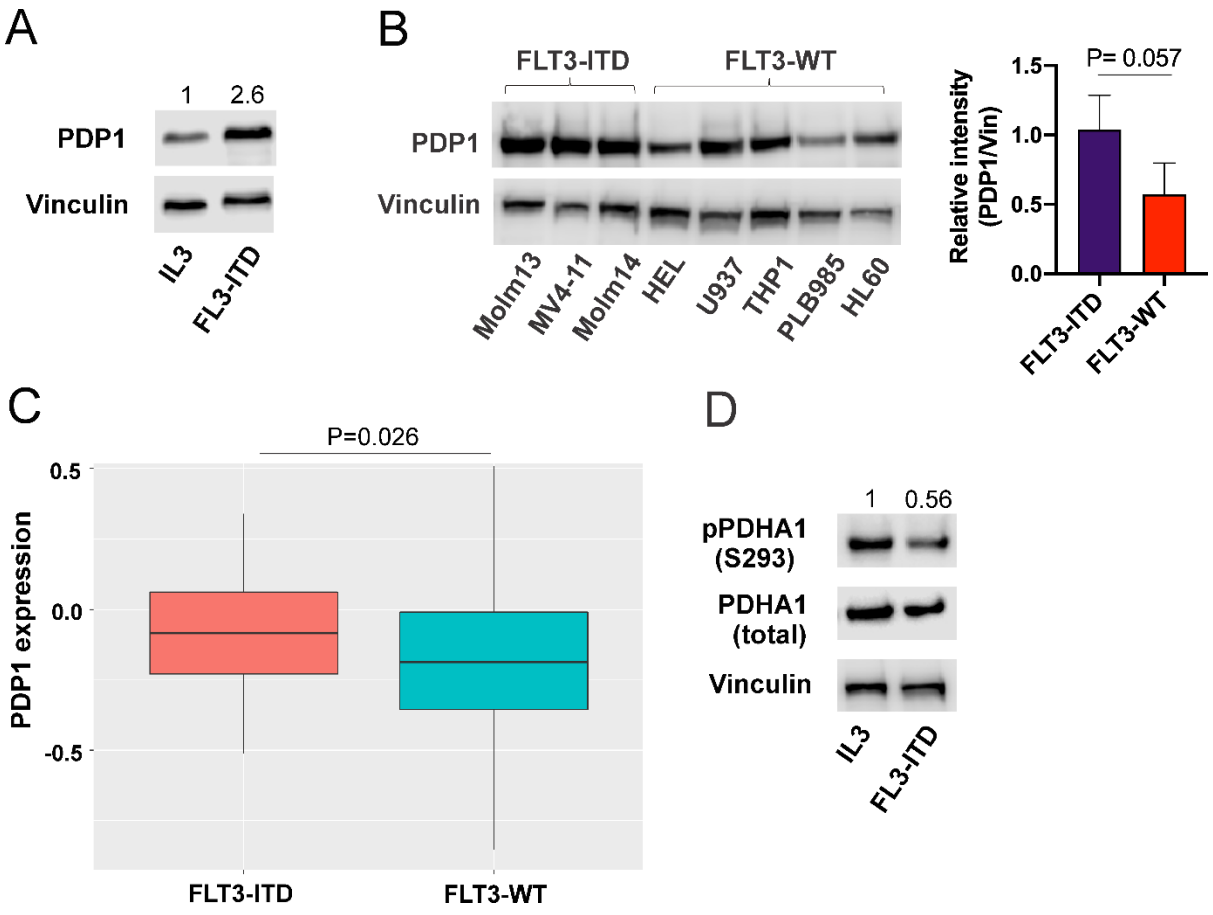


Figure 22: FLT3-ITD cells are high expressers of PDP1. A. Higher PDP1 levels are observed under FLT3-ITD *vs* IL3 signalling in 32D cells. B. Higher PDP1 protein levels in a set of FLT3-ITD-positive AML cell lines in comparison to their FLT3-WT counterparts. Statistical analysis was performed using unpaired Student's t-test. * P≤ 0.05. C. Proteomic analysis of higher PDP1 levels in FLT3-ITD-positive (n=37) compared to FLT3-ITD-negative (n=129) primary AML blasts from a cohort of newly diagnosed AML patients[2]. Statistical analysis was performed using unpaired Student's t-test. * P≤ 0.05. D. Lower inhibitory PDHA1 S293 phosphorylation under FLT3-ITD signalling in 32D cells.

[2] The proteomics study and its part of the figures were performed and provided by the group of Prof. Thomas Oellerich (MED2, Goethe-University Hospital Frankfurt, Germany).

Furthermore, to investigate whether the high PDP1 levels are clinically relevant in AML patients, online-available databases on gene expression correlations with patients' survival were visited (Genomic Data Commons database https://gdc.cancer.gov/). Interestingly, high PDP1 gene expression levels were associated with poorer prognosis and overall survival in the patients (Figure 23).

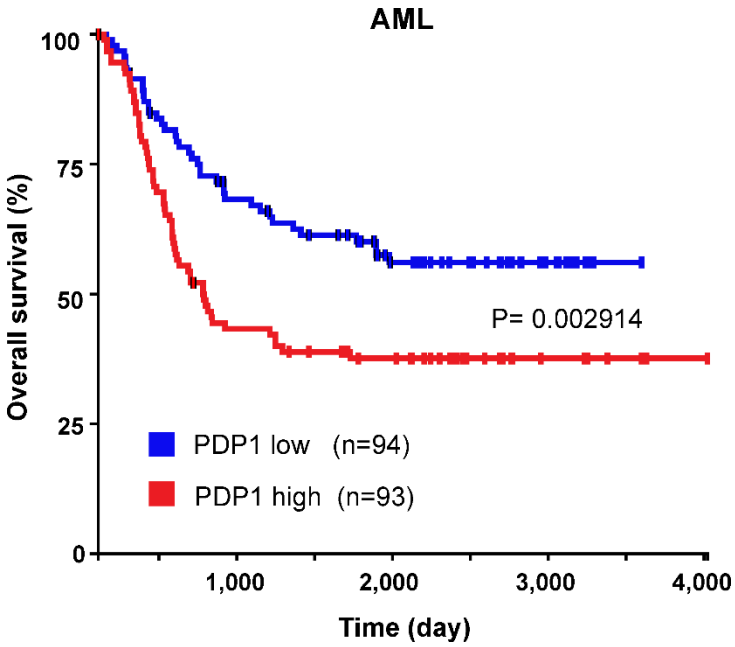
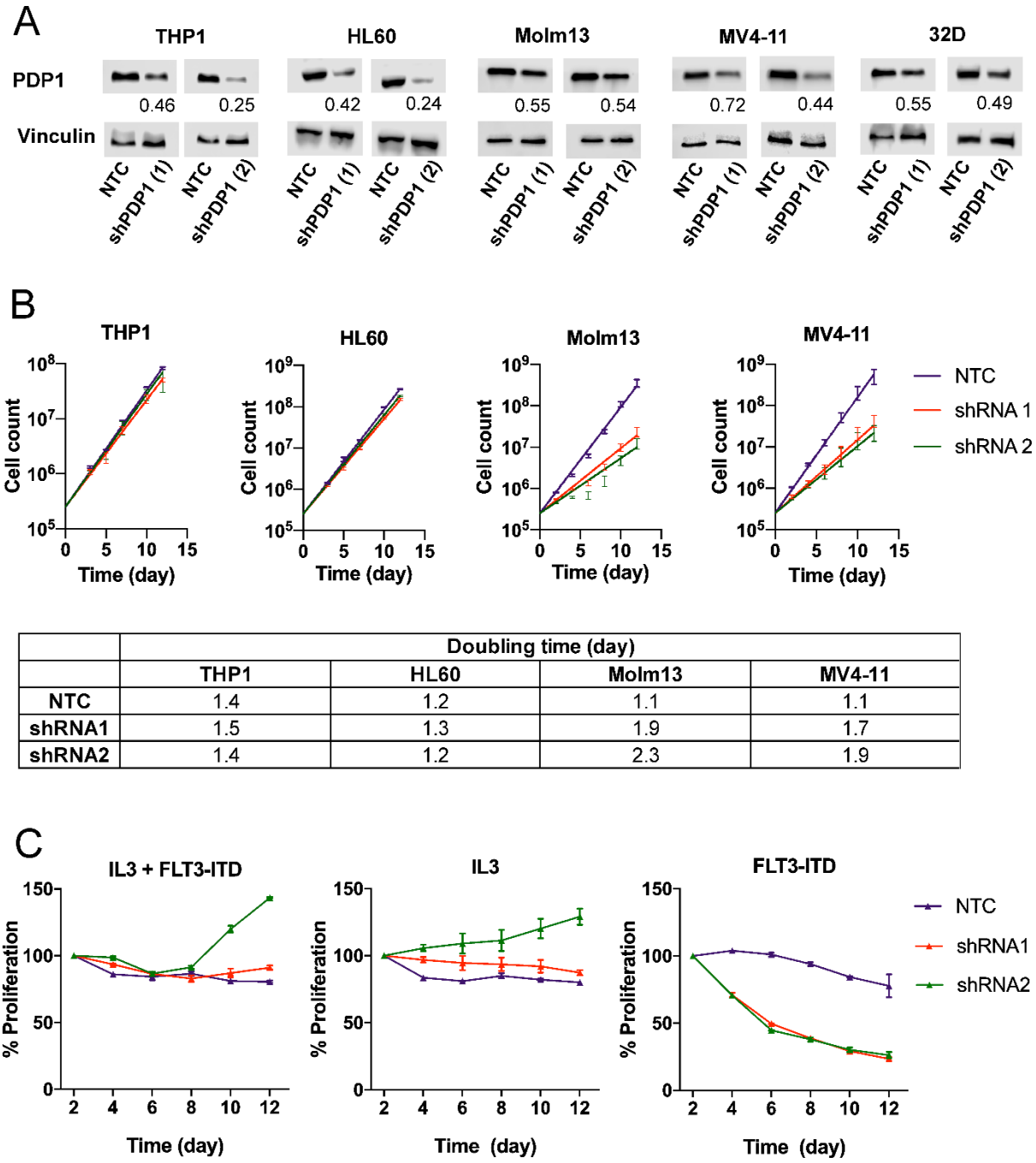


Figure 23: PDP1 levels correlate with poor overall survival in AML. The figure shows the overall survival in AML patients classified based on their PDP1 gene expression levels (low vs high) (Genomic Data Commons database https://gdc.cancer.gov/).

3.1.4. PDP1 is a targetable vulnerability in FLT3-ITD-positive AML

With these data in hand, the targetability of PDP1 in FLT3-ITD-positive AML cells was investigated. To get functional insights about PDP1 importance in the cells, CRISPR-Cas9 knockout of PDP1 was performed, however, it was fatal (Appendix Figure A4). Hence, a knockdown approach was taken since no commercial PDP1 inhibitor was available. Two short hairpin RNAs (shRNAs) were used to knockdown PDP1 in 2 FLT3-WT (THP1 and HL60) and two FLT3-ITD cell lines (Molm13 and MV4-11). A knockdown efficiency of around 50% was achieved (variable among the different cell lines) (Figure 24A). The effect of PDP1 loss-of-function was evaluated by a cumulative growth assay. A strong growth disadvantage was observed in FLT3-ITD-positive cell lines, however, FLT3-WT cell lines were almost unaffected (Figure 24B). Doubling times are indicated in the table of the same figure. The growth disadvantage was correlative with the knockdown efficacy (shRNA 2 showed relatively stronger knockdown, possibly due to its binding to the untranslated region (UTR) of PDP1

mRNA). These findings were further confirmed in a competitive growth assay in 32D FLT3-ITD cells. Here, PDP1-knockdown cells were mixed in a (50:50) ratio with GFP-positive control cells. GFP percentage was followed over a time course of twelve days as an indication of proliferation. Cells signalling with FLT3-ITD but not IL3, were severely disadvantaged by the knockdown, which comes in line with the cumulative growth assay results (Figure 24C).



	Doubling time (day)			
	THP1	HL60	Molm13	MV4-11
NTC	1.4	1.2	1.1	1.1
shRNA1	1.5	1.3	1.9	1.7
shRNA2	1.4	1.2	2.3	1.9

Figure 24: PDP1 knockdown impairs cellular proliferation of FLT3-ITD cells. A. Western blot of PDP1 levels after PDP1 knockdown using two different PDP1-shRNAs in THP1, HL60, Molm13, MV4-11 and 32D FLT3-ITD cells. B. Cumulative growth assays in AML cell lines showing a prominent growth disadvantage in FLT3-ITD cells (Molm13 and MV4-11), while the effect is not apparent in FLT3-WT

cells (THP1 and HL60). C. Competitive growth assay of exclusive growth disadvantage under FLT3-ITD but not IL3 signalling upon PDP1 knockdown in 32D cells.

These findings were confirmed in primary patient-derived AML blasts using small interfering RNAs (siRNAs) targeting PDP1 (patient characteristics are detailed in Appendix Table A1). Due to the challenging transducability of primary AML blasts, only 22% PDP1 knockdown efficiency could be achieved (as measured representatively for one AML patient (patient 6)) (Figure 25A). Nevertheless, FLT3-ITD-positive blasts were more sensitive to PDP1 knockdown compared to FLT3-WT blasts (Figure 25B). Furthermore, combined mitochondrial targeting by venetoclax together with PDP1 knockdown showed significantly higher potency in FLT3-ITD-positive blasts (Figure 25C).

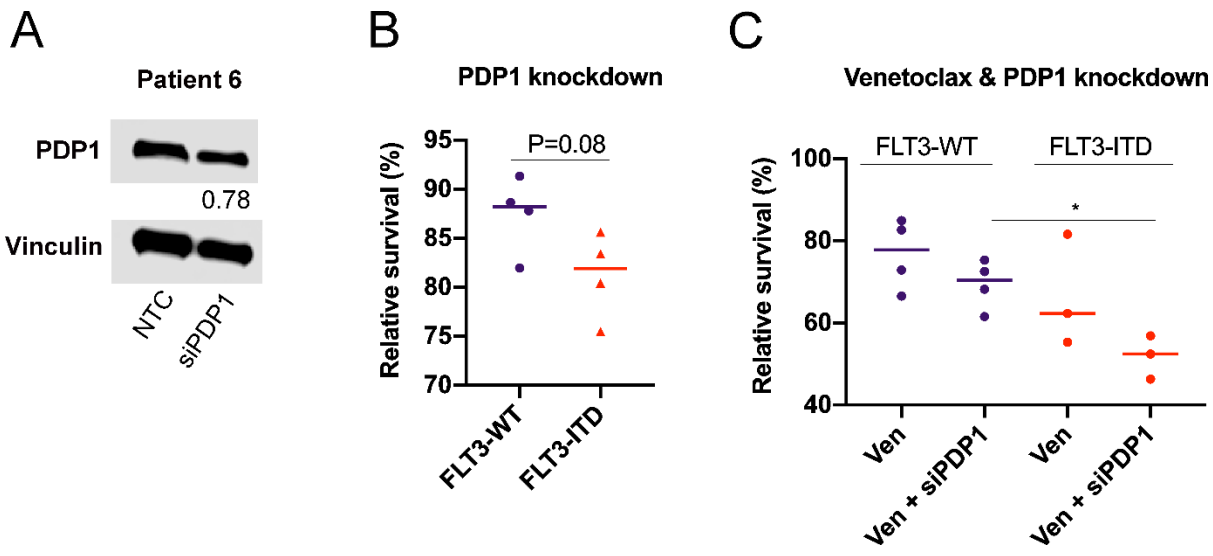


Figure 25: PDP1 knockdown impairs FLT3-ITD cell proliferation and synergises with venetoclax *ex vivo*. A. Western blot of PDP1 knockdown using PDP1-siRNA in primary AML blasts derived from an AML patient. B. PDP1 knockdown has stronger impact on the proliferation capacity of primary AML blasts with FLT3-ITD mutations in comparison to FLT3-WT blasts. C. Stronger combinatorial effect of PDP1 knockdown and venetoclax (50 nM for 72 hours) observed in FLT3-ITD compared to FLT3-WT AML blasts. Statistical analysis was performed using one-way ANOVA with Bonferroni's two comparisons. * P≤ 0.0332.

To validate PDP1 role in FLT3-ITD-positive leukaemia maintenance and development *in vivo*, a xenotransplantation mouse model of PDP1 knockdown was performed. Molm13 cells transduced with either NTC-shRNA or PDP1-shRNA were transplanted into two groups of immunocompromised NOD-SCID mice (n=8 per group). The knockdown was confirmed by western blot prior to the transplantation (Figure 26A). Disease progression was followed up by human CD45 levels in the peripheral blood. Leukaemia developed early on, with CD45 positivity detected in the peripheral blood as early as day 13 post-transplantation (Figure 26B).

Consistent with the *in vitro* data, PDP1 knockdown slowed leukaemia progression and significantly prolonged the overall survival of the mice (Figure 26C). Intriguingly, three out of the eight mice in the knockdown group did not succumb to leukaemia and were sacrificed at day 60 (more than double the control's overall survival). Of note, these mice showed successful transplantation and had leukaemia engraftment, since CD45 positivity persisted in the peripheral blood up to when it was last assessed at day 50 (41-45%). Finally, even when the leukaemia developed in the PDP1 knockdown group, the disease phenotype was less aggressive with less sarcoma-like tissues being formed in mice of this group (Figure 26D).

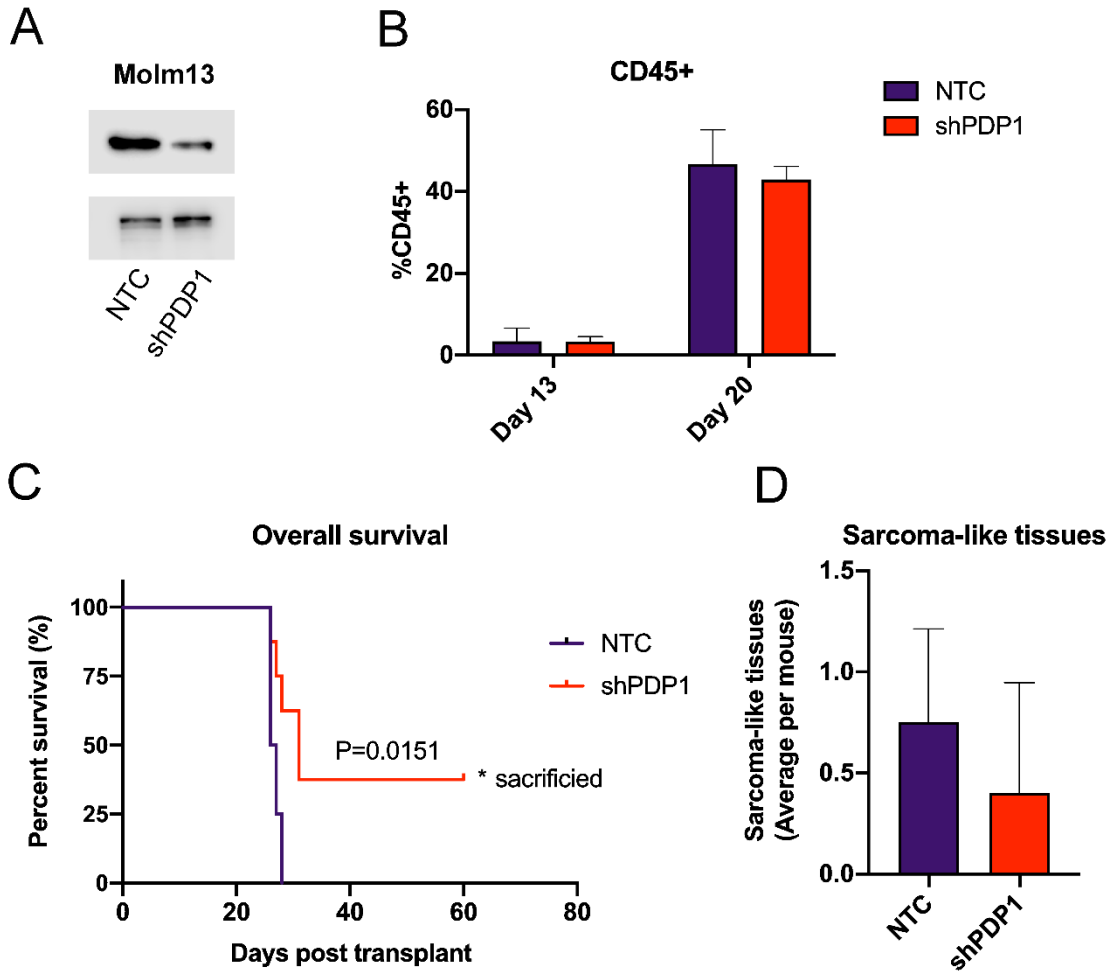


Figure 26: PDP1 abrogation impairs leukaemia progression *in vivo*[3]. A. Western blot of PDP1 knockdown in the transplanted Molm13 cells. B. Human CD45 levels in the peripheral blood of the mice after transplantation. C. Survival curve of prolonged overall survival of mice transplanted with PDP1-knockdown Molm13 cells in comparison to PDP1-WT group. Three mice did not succumb to leukaemia in the PDP1 knockdown group and were sacrificed at day 60. Statistical analysis was performed using Gehan-Breslow-Wilcoxon test. * P≤ 0.0332. D. Average number of sarcoma-like tissues quantified in the 2 transplantation groups (average per mouse).

[3] This *in vivo* experiment was performed by Dr. Rahul Kumar (group of Prof. Daniella Krause, Georg-Speyer-House, Frankfurt, Germany).

Finally, the question arose as to the cause of the growth disadvantage upon PDP1 knockdown. Considering PDP1 functions in fuelling mitochondrial metabolism, it was hypothesized that the growth disadvantage observed is mainly due to the metabolic insufficiency induced by PDP1 abrogation. Initially, a rescue experiment was performed by providing a precursor of the downstream TCA cycle metabolite alpha ketoglutarate (2-dimethyl oxygluterate). Enhanced cellular proliferation was observed in Molm13 cells, however in both; the NTC and PDP1 knockdown cells (Figure 27A), suggesting no rescue but rather a general growth advantage due to alpha ketoglutarate supplementation. Alternatively, rescue by compensating for other pathways fed by PDP1 activity was investigated. Similarly, neither addition of palmitate (fatty acid oxidation precursor) (Figure 27B), nor of uridine (precursor for pyrimidine biosynthesis pathway) (Figure 27C) rescued PDP1 growth disadvantage.

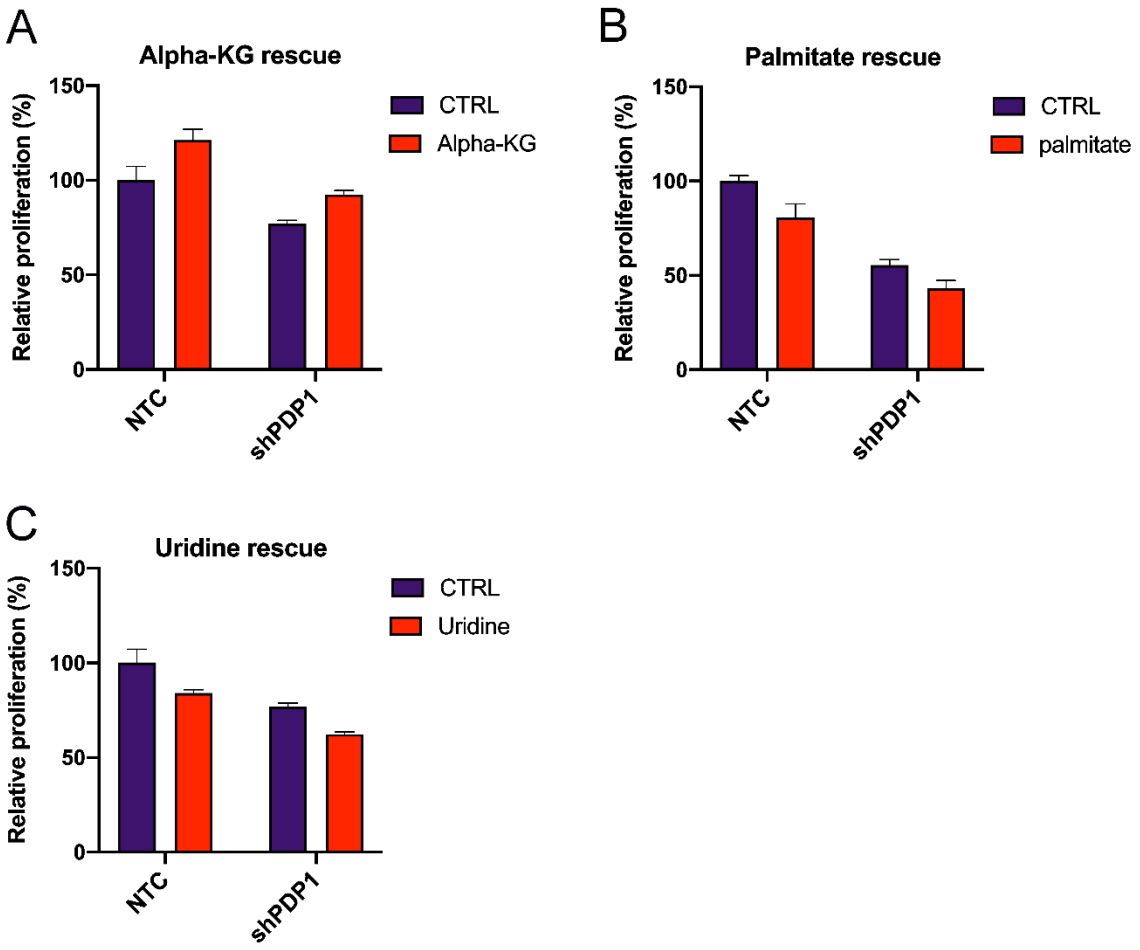


Figure 27: Intermediate supplementation of individual mitochondrial pathways is not sufficient to rescue PDP1 knockdown effects. A. Attempted rescue with supplementation of 1 mM Alpha-KG (alpha ketoglutarate) precursor (2-dimethyl oxygluterate) in Molm13 cells. B. Addition of 20 µM palmitate could not rescue PDP1 knockdown effects in Molm13 cells. C. Addition of 200 µM uridine did not lead to any rescue of PDP1 knockdown in Molm13 cells.

Acknowledging the several roles PDP1 plays in mitochondrial metabolism, it was anticipated that rescue of some pathways would not be enough to rescue the growth disadvantage. Thus, a different approach was taken using Rho Zero Molm13 cells (kindly provided by Dr. Frank Schnuetgen). These cells lack mitochondrial polymerase gamma and thus, mitochondrial respiratory chain activity (detailed in section 2.2.10). After adaption, they grow independently of mitochondrial respiration. PDP1 knockdown was performed in these cells (Figure 28A), and expectedly, it did not have any impact on their growth behaviour as evaluated by the cumulative growth assay (Figure 28B). These findings suggest that PDP1 knockdown does not have any impact on cells that are reliant on glycolysis but not OXPHOS. Thus, it can be concluded that the growth disadvantage associated by PDP1 abrogation is caused by mitochondrial metabolic insufficiency.

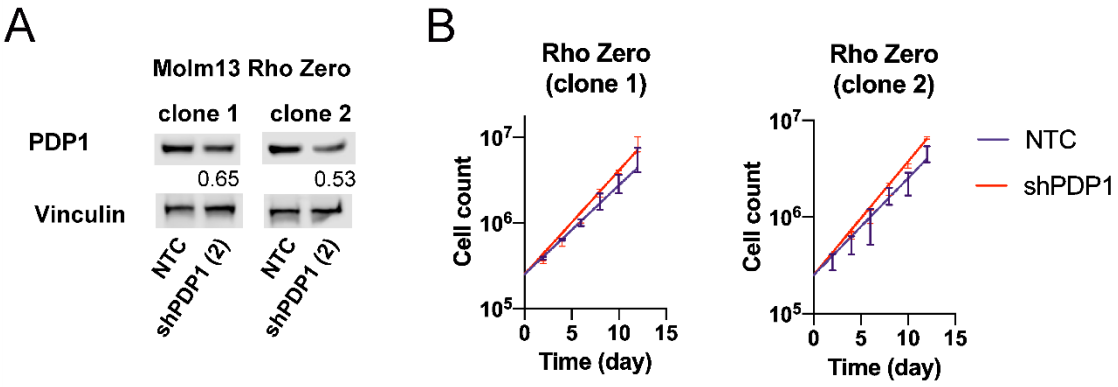


Figure 28: PDP1 knockdown has no impact on cells that are not reliant on OXPHOS (Rho Zero cells). A. Western blot of PDP1 knockdown (shRNA2) in two clones of Molm13 Rho Zero cells. B. Cumulative growth assay in Molm13 Rho Zero cells showing no impact of PDP1 knockdown on their proliferation.

Considering the dependence of FLT3-ITD cells on PDP1, the functions of PDP1 in the cells were investigated. Three main roles of PDP1 were identified. These include: i) enhancing ATP generation, ii) facilitating metabolic adaption under hypoxia to sustain the ability to switch to OXPHOS and start proliferation upon oxygen availability and iii) mediating resistance to FLT3-inhibition. These aspects will be addressed in detail in the following sections.

3.1.5. High PDP1 levels boost energy generation

To further emphasize on PDP1 metabolic functions, PDP1 was overexpressed in a panel of two FLT3-ITD cells lines (Molm13 and MV4-11) and five FLT3-WT cell lines (THP1, HL60, HEL, NB4 and U937) (Figure 29A). Interestingly, PDP1 overexpression resulted in an elevated

intracellular ATP pool in FLT3-ITD cells, while FLT3-WT cells remained unchanged (Figure 29B).

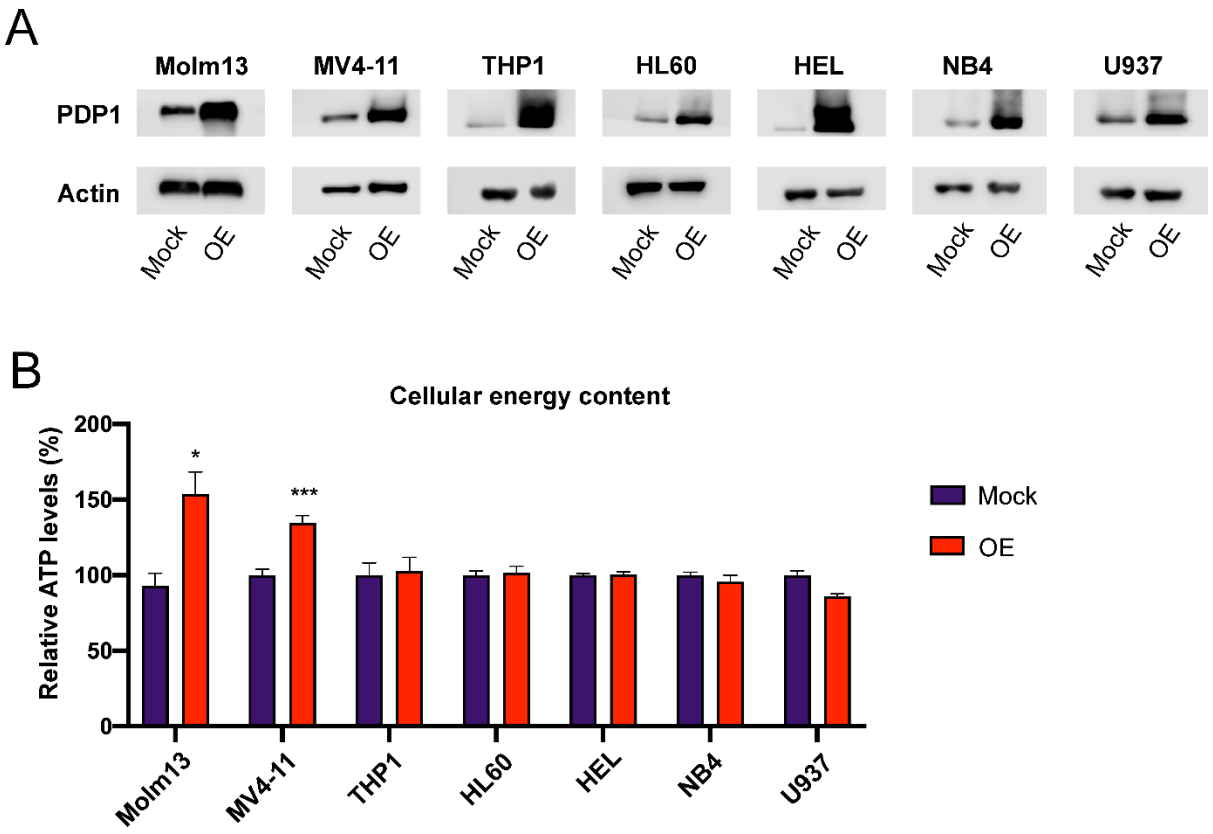
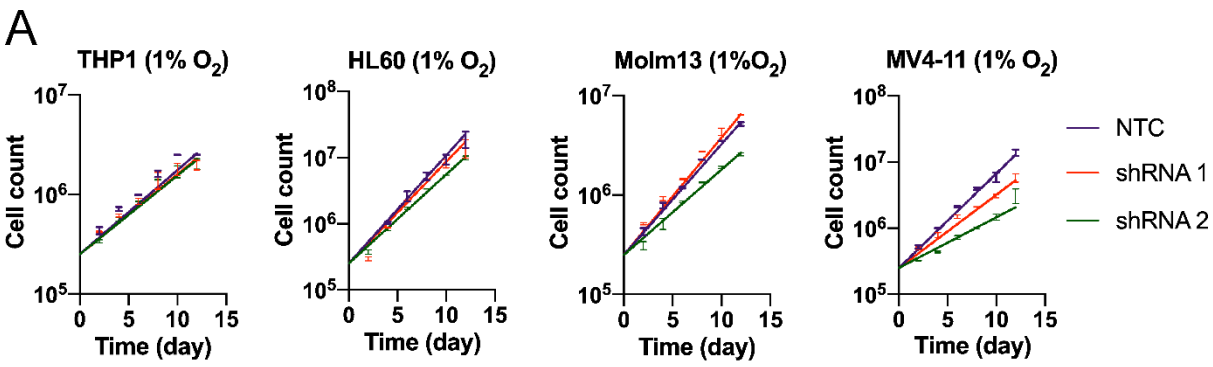


Figure 29: PDP1 overexpression (OE) enhances cellular viability. A. Western blot of PDP1 OE (SIGW construct) in two FLT3-ITD cell lines (Molm13 and MV4-11) and 5 FLT3-WT cell lines (THP1, HL60, HEL, NB4 and U937) (All PDP1 OE experiments in this figure were made with PDP1 SIGW construct). B. Enhanced cellular viability in FLT3-ITD but not FLT3-WT cells upon PDP1 overexpression (depicted by higher ATP levels) (measured 72 hours after plating the same number of cells) (n=3). Statistical analysis was performed using unpaired Student's t-test. *** P≤ 0.001, * P≤ 0.05.

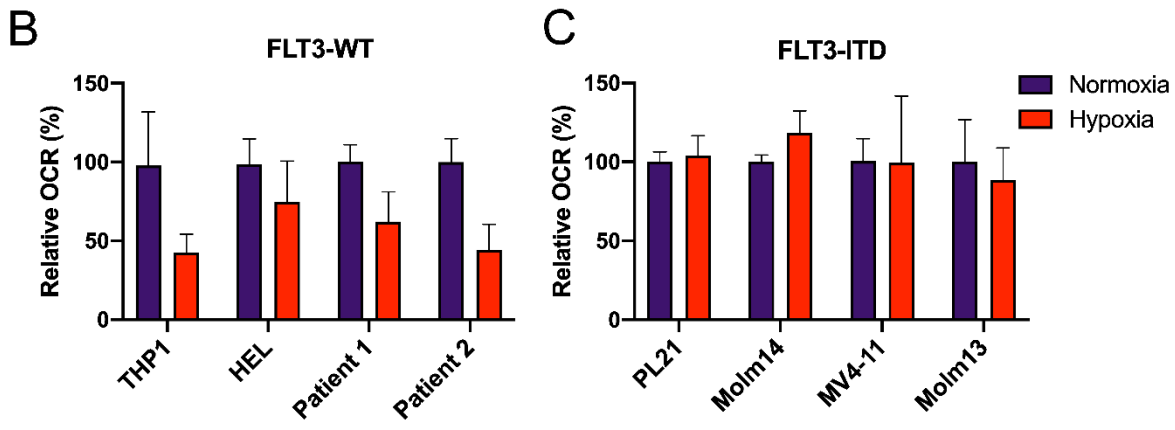
3.1.6. PDP1 provides cellular flexibility for metabolic adaption under oscillating oxygen conditions

The second function of PDP1 involves its role in the metabolic flexibility of FLT3-ITD-positive cells and their adaption to semi-physiological hypoxic oxygen conditions (1% O_2). To investigate PDP1 importance under hypoxia, cumulative growth assays upon PDP1 knockdown were performed. Interestingly, the effect of PDP1 knockdown persisted under hypoxic conditions despite the oxygen scarcity that favours glycolysis (Figure 30A). FLT3-WT cells however, remained unaffected by PDP1 knockdown. This persistent importance of PDP1 under hypoxia, although OXPHOS is minimal, led to the hypothesis that PDP1 is essential for OXPHOS switch in FLT3-ITD-positive cells upon exposure to oxygen. To investigate this hypothesis, seahorse measurements were performed on different AML cell lines and primary

patient-derived AML blasts which were adapted to hypoxia and then exposed to oxygen. Expectedly, FLT3-WT cells were unable to immediately restore their respiration capacity (Figure 30B). On the other hand, FLT3-ITD cells, surprisingly, retained sustained respiration capacity regardless to the prior adaption to hypoxia and were able to restore this respiration capacity upon re-oxygenation (Figure 30C). To confirm the role of PDP1 in facilitating this rapid OXPHOS switch, prior PDP1-depletion was performed in Molm13 cells and then their OCR was measured upon reoxygenation. Expectedly, PDP1 knockdown abrogated the capacity of Molm13 cells to restore respiration (Figure 30D) and entering cell cycle upon oxygen availability (Figure 30E).



	Doubling time (day)			
	THP1	HL60	Molm13	MV4-11
NTC	3.6	1.8	2.7	2.1
shRNA1	3.7	1.9	2.6	2.7
shRNA2	3.8	2.2	3.5	3.9



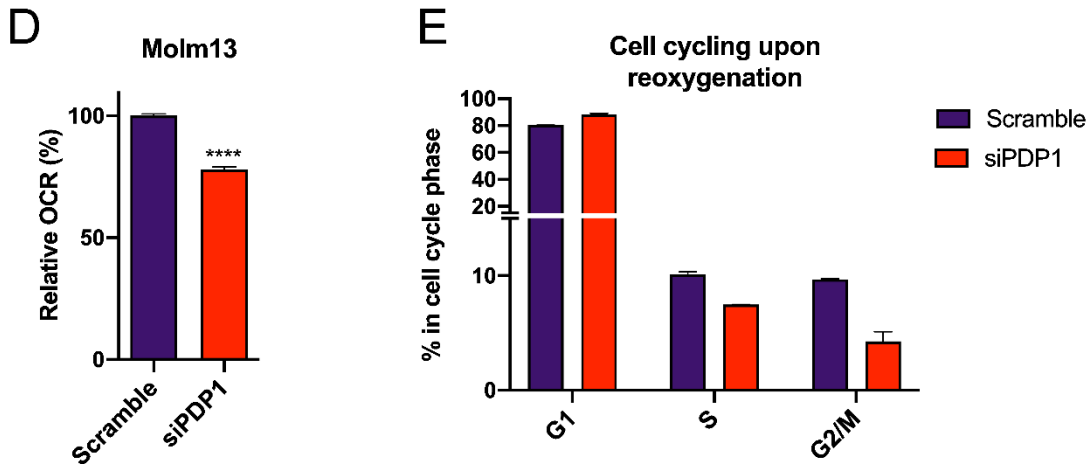


Figure 30: PDP1 mediates conserved OXPHOS and proliferation capacity upon adaption to hypoxia. A. Cumulative growth assay under hypoxia showing strong effects of PDP1 knockdown on FLT3-ITD cells however, the effects are minimal in FLT3-WT cells. Seahorse measurements of oxygen consumption rates (OCR) in B. two FLT3-WT cell lines (THP1 and HEL) and two primary FLT3-WT AML blasts and C. four different FLT3-ITD cell lines under 21% *vs* 1% O_2 (measured upon reoxygenation). D. Seahorse measurements of reduced respiration capacity of hypoxia-adapted cells upon PDP1 knockdown with PDP1-siRNA. Statistical analysis was performed using unpaired Student's t-test. **** P≤ 0.0001. E. Cell cycle analysis in Molm13 cells showing impaired ability to enter the cell cycle upon exposure to oxygen (reoxygenation) when PDP1 is abrogated.

3.1.7. PDP1 mediates resistance to FLT3-inhibition

Another aspect of PDP1 functions was investigated in the context of cellular response to FLT3-inhibition. First, considering the reliance of FLT3-ITD cells on PDP1, a possible synergy between PDP1 knockdown and FLT3-inhibiton was investigated. Interestingly, PDP1 knockdown exerted a strong combinatorial effect with AC220 treatment in Molm13, MV4-11 and 32D FLT3-ITD cells (Figure 31A). Furthermore, PDP1 knockdown primed FLT3-ITD cells to apoptosis induced by FLT3-inhibition (Figure 31B). This priming effect was observed at low doses of AC220 (1 nM) that do not usually induce apoptosis within 24 hours of treatment.

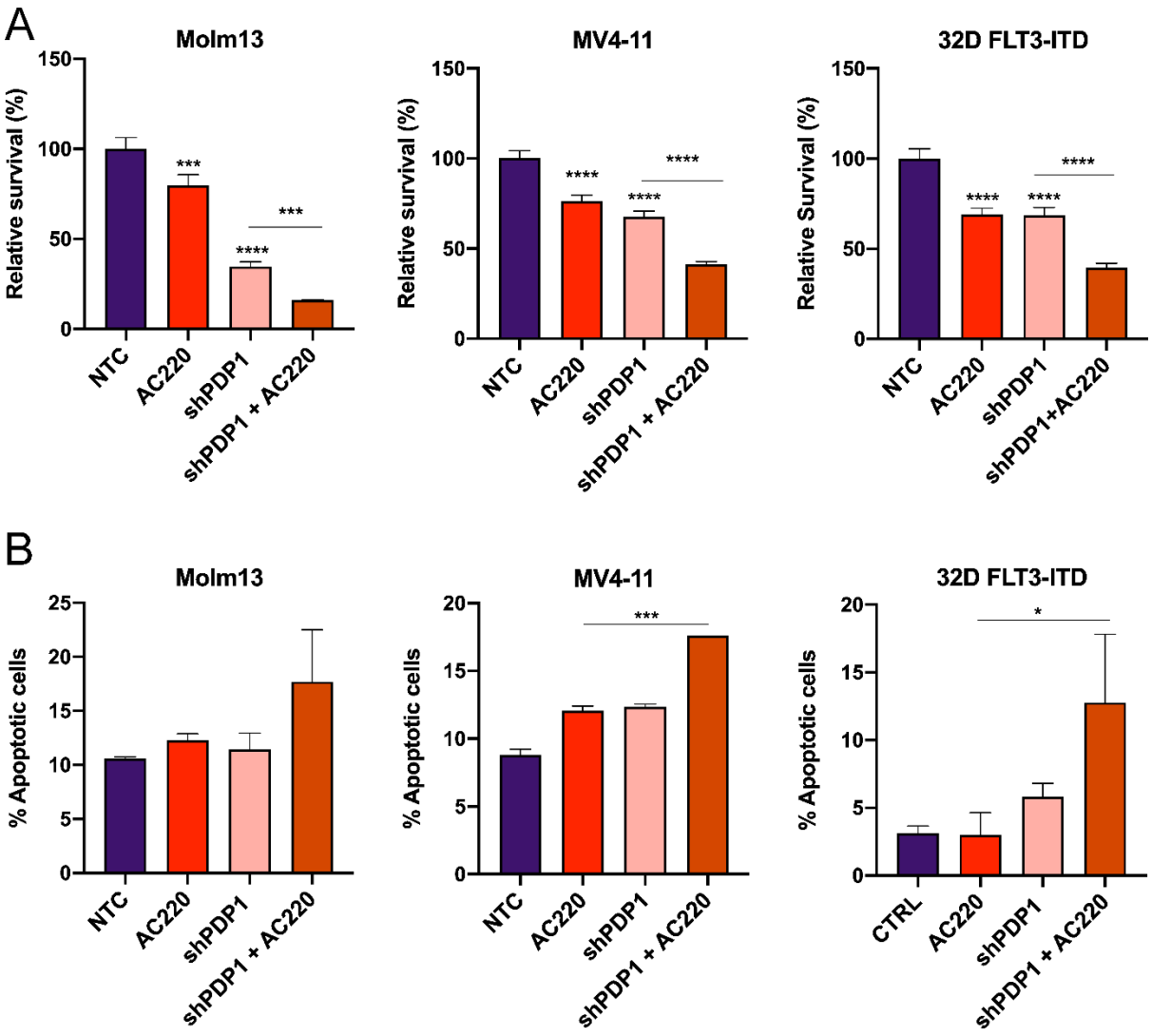


Figure 31: PDP1 knockdown synergises with FLT3-inhibition. A. Combinatorial effect of PDP1 knockdown and FLT3-inhibition by 1 nM AC220 in Molm13, MV4-11 and 32D cells. B. PDP1 knockdown induces apoptosis when combined with AC220 treatment in Molm13, MV4-11 (1 nM) and 32D FLT3-ITD cells (5 nM) for 24 hours. Statistical analysis was performed using one-way ANOVA with Bonferroni's multiple comparisons. **** P≤ 0.0001, *** P≤ 0.0002, ** P≤ 0.0021.

To further validate the role of PDP1 in responses to FLT3-inhibtion, PDP1 was overexpressed in FLT3-ITD cells (Molm13 and MV4-11) and their sensitivity towards AC220 was evaluated. Interestingly, PDP1 overexpression increased resistance against AC220. PDP1 overexpression shifts the IC_{50} curves of both Molm13 and MV4-11 to the right (resistance effect) with approximately 20-30% increase in the IC_{50} values (Figure 32A). Correspondently, a lesser impact of FLT3-inhibition on cellular proliferation was observed (Figure 32B).

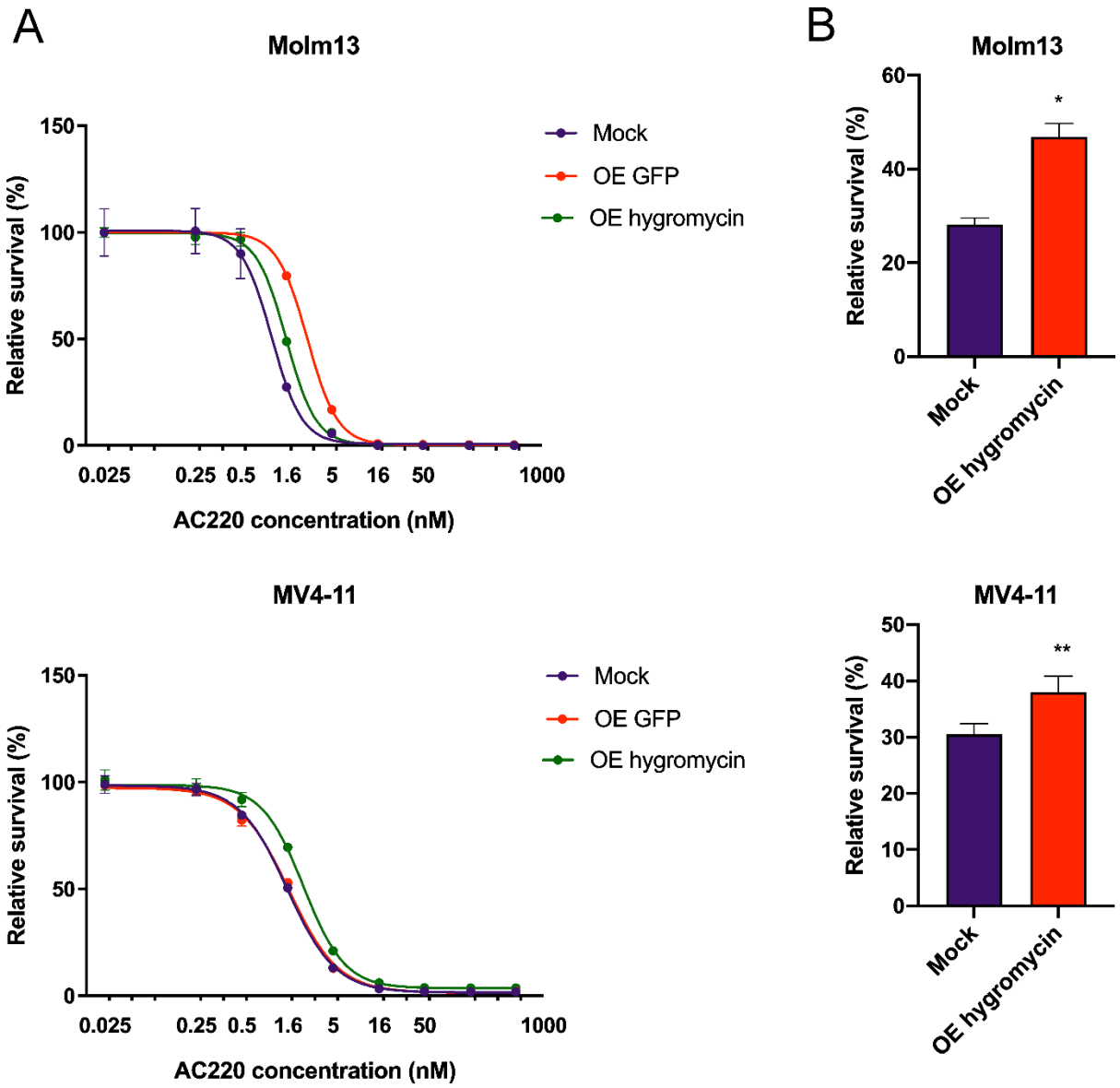


Figure 32: Higher PDP1 levels are associated with resistance to FLT3-inhibition. A. Dose response curve of reduced AC220 sensitivity (72 hours treatment) upon PDP1 overexpression in Molm13 and MV4-11 cells (SIGW and SIHW constructs). B. PDP1 overexpression desensitises the cells to AC220 (1.6nM for 72 hours). Statistical analysis was performed using unpaired Student's t-test. ** P≤ 0.01, * P≤ 0.05.

More interestingly, the relevance of PDP1 in primary blasts (peripheral blood-derived) from an AC220-resistant FLT3-ITD positive AML patient was evaluated (patient characteristics are detailed in Appendix Table A1). Initially, an AC220 dose-response curve was performed and the cells were unresponsive even at very high doses (Figure 33A). Strikingly, PDP1 knockdown restored cellular sensitivity towards AC220 (Figure 33B), which further confirms its role in modulating drug responses.

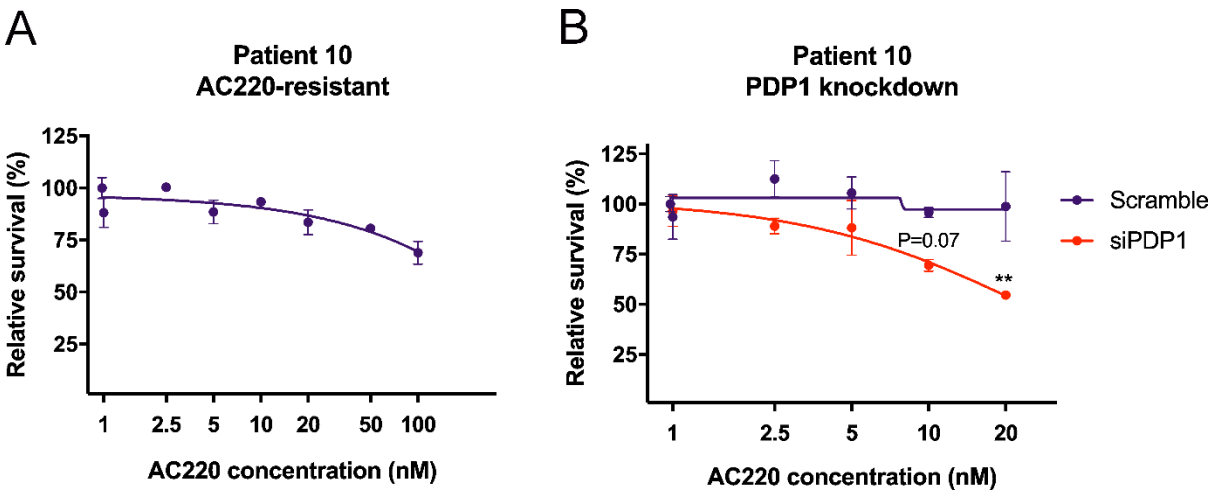


Figure 33: PDP1 knockdown sensitizes therapy-resistant AMLs to AC220. A. AC220 response curve in peripheral blood aspirate from an AC220-resistant AML patient (48 hour treatment). B. PDP1 knockdown by PDP1-siRNA sensitizes the cells to AC220 (24 hours after the induction of PDP1 knockdown, AC220 was added for another 48 hours). Statistical analysis was performed using two-way ANOVA with Bonferroni's multiple comparisons. ** P≤ 0.0021, * P≤ 0.0332.

Considering these findings on PDP role in desensitising against AC220, the dynamics of PDP1 were investigated upon FLT3-inhibition. Interestingly, PDP1 levels were elevated in all the four different FLT3-ITD-positive cell lines when treated with low doses of AC220 (1-2 nM) (Figure 34A). This elevation was observed as early as 24 hours in both Molm13 and Molm14 cells with 1 nM AC220 while in MV4-11 and 32D FLT3-ITD cells, this was observed after 48 hours (approximately 1.5-2 folds elevation). PDP1 elevation was similarly confirmed at the mRNA level with qPCR measurements 24 hours post-treatment (Figure 34B). These findings suggested that PDP1 antagonizes AC220 by further shifting the cells towards mitochondrial metabolism which has a cytotoxic-protective nature. This can explain the modulation of AC220 sensitivity upon PDP1 knockdown/ overexpression. To validate this hypothesis, a tracer-based assay with ^{13}C-glucose was performed in 32D FLT3-ITD-positive cells. Under AC220 treatment, a significant shift in the fate of glucose-derived pyruvate in favour of the TCA cycle was observed, presumably driven by PDP1 upregulation (Figure 34C).

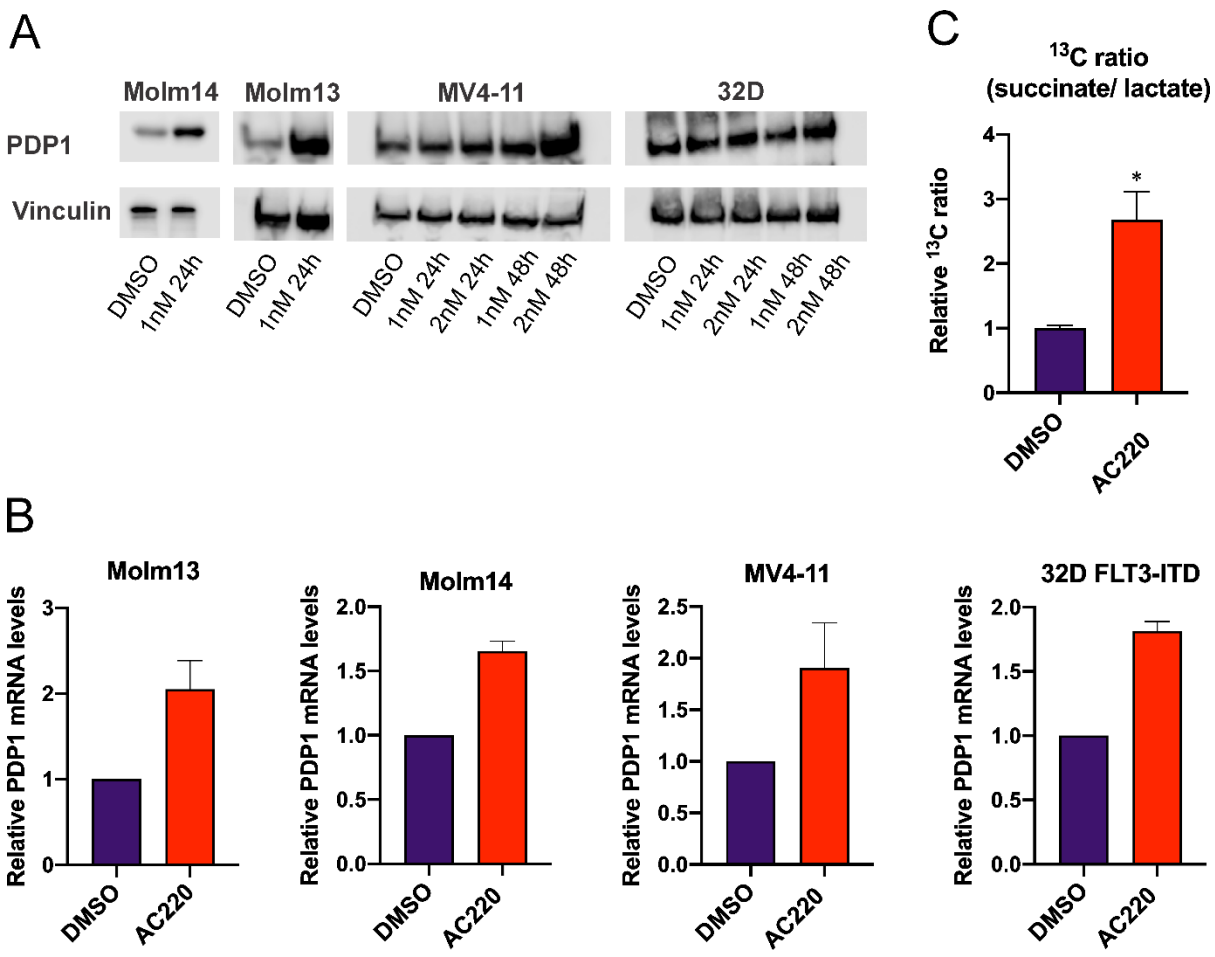


Figure 34: PDP1 is upregulated upon FLT3-inhibition. A. Western blotting of PDP1 upregulation upon FLT3-inhibition with different concentrations of AC220 in Molm14, Molm13, MV4-11 and 32D FLT3-ITD cells. B. qPCR measurement of elevated PDP1 mRNA levels upon FLT3-inhibition (normalised to RPII levels). C. Tracer-based assay with ^{13}C-glucose in 32D FLT3-ITD cells revealing higher shuffling of pyruvate into the TCA cycle upon FLT3-inhibition. Statistical analysis was performed using unpaired Student's t-test. * P≤ 0.05.

To further validate PDP1 as the driver of this rescue, the cells were provided with PDP1 substrate, pyruvate[4]. Strikingly, pyruvate addition rendered FLT3-ITD cells less sensitive to FLT3-inhibition at low AC220 doses (0.5 nM) (Figure 35). This effect varied between the cell lines from partial to full rescue.

[4] Added as sodium pyruvate. Hereafter referred to as ´pyruvate´.

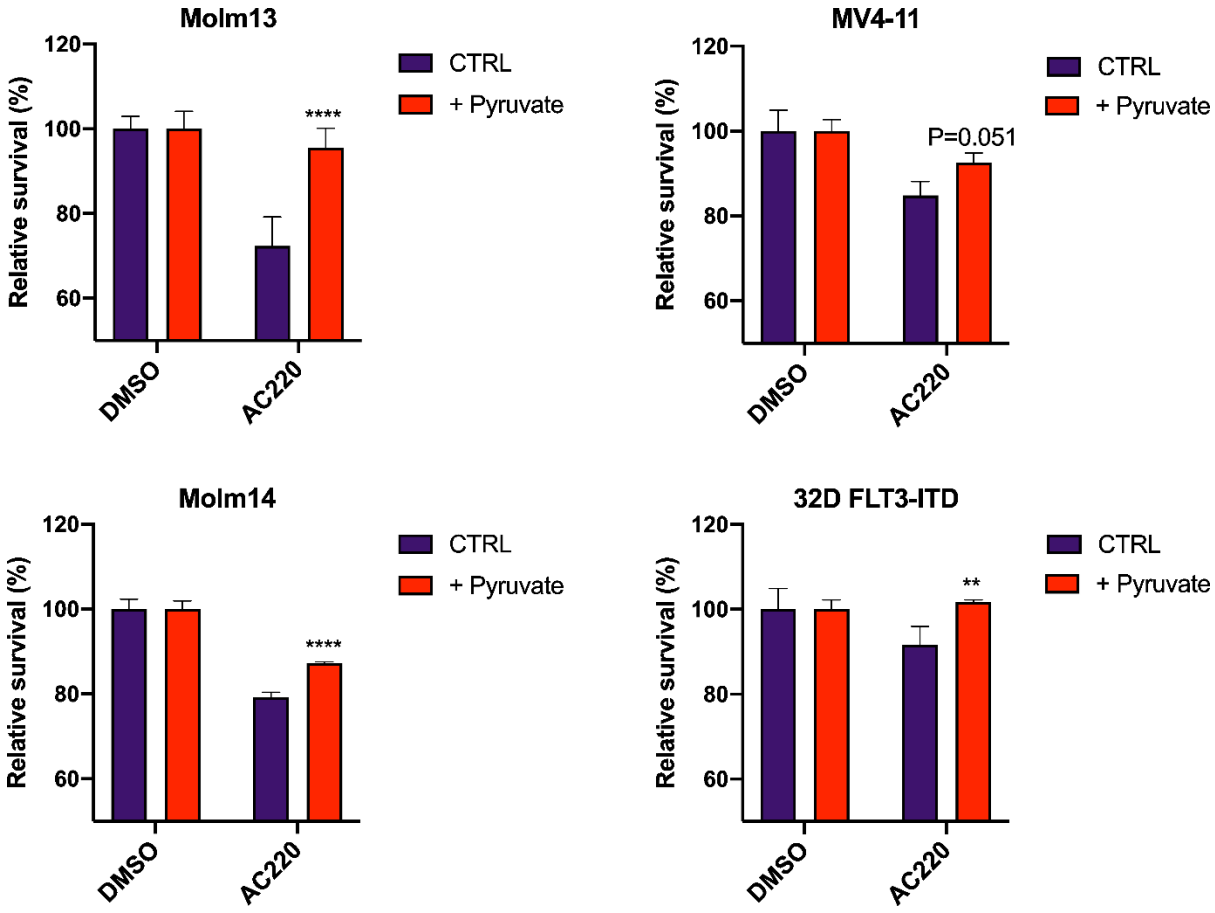


Figure 35: FLT3-inhibition leads to blockade in glucose uptake and can be rescued by pyruvate. Rescue of FLT3-inhibition (0.5 nM AC220) by the addition of 10 mM sodium pyruvate for 24 hours. Statistical analysis was performed using two-way ANOVA with Bonferroni's multiple comparisons. **** P≤ 0.0001, ** P≤ 0.0021, * P≤ 0.0332.

Altogether, previous data demonstrate the importance of PDP1-driven OXPHOS in FLT3-ITD cells and its role in their response to FLT3-inhibition. Therefore, the synergy between FLT3-inhibtion and mitochondrial targeting was investigated. Using the Highest Single Agent (HSA) reference model (Berenbaum, 1989), mitochondrial targeting with venetoclax was shown to synergize with FLT3-inhibition by AC220 in Molm14 cells (Figure 36A). This effect was also observed in Molm13 and MV4-11 cells (Appendix Figures A1-3). The average synergistic value was around HSA=3 with the strongest value being around 9.97. This synergistic/additive effect is shown in a relatively stretched range of around 0.5-2 nM AC220 with 5-50 nM venetoclax. The combined effect of the drugs is observed best at 1 nM AC220 and 10 nM venetoclax (below the IC_{50} concentration of each) (Figure 36B). This synergy leads to a sensitisation effect of both drugs as illustrated in the dose response curve (Figure 36C) where venetoclax addition shifts the IC_{50} curve of AC220 to the left.

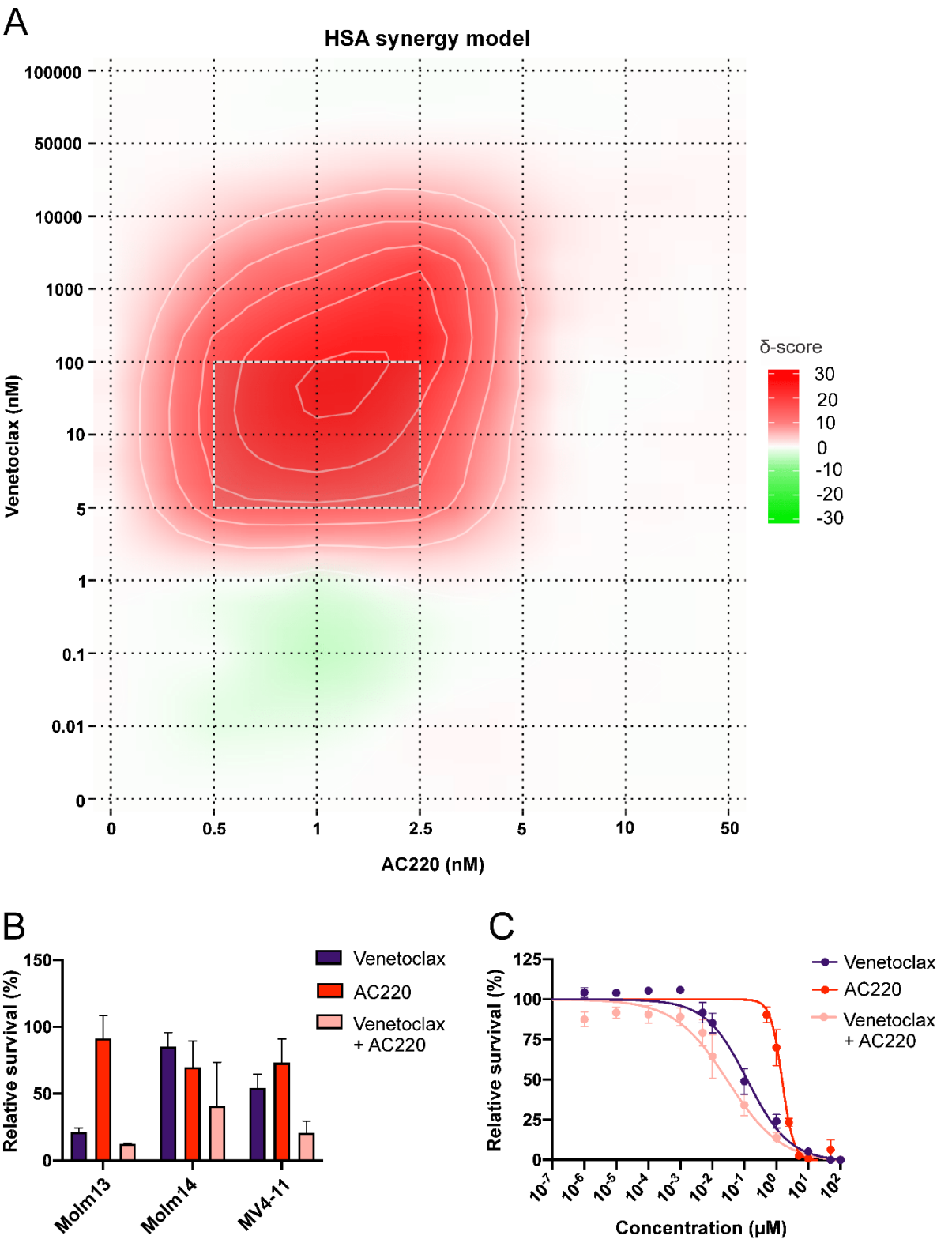


Figure 36: Synergism of FLT3-inhibition with venetoclax[5]**.** A. HSA reference model of synergy between venetoclax and AC220 in Molm14 cells with a synergy score of 3.96. B. Combined effect of venetoclax (10 nM) and FLT3-inhibiton using AC220 (1 nM) in Molm13, Molm14 and MV4-11 for 72 hours. C. Dose response curve of the two drugs combination in Molm14 cells.

[5] These experiments and figure were performed and provided by Philipp Makowka (Prof. Serve lab, MED2, Goethe-University Hospital Frankfurt, Germany).

3.2. Discussion

The current work highlights the importance of studying AML metabolic dependencies and their potentials as therapeutic targets. For a long time, it has been accepted that cancer cells in general exert the Warburg effect which entitles metabolising glucose into lactate, regardless of oxygen levels (Warburg, 1956; Warburg et al., 1927). In fact, many studies have identified some genes involved in promoting the Warburg effect and they were evaluated as metabolic vulnerabilities in AML (i.e. HKII, PKMII, LDHA) (Huang et al., 2016; Wang et al., 2014). This glycolytic behaviour was shown to be controlled by proteins at the interphase between glycolysis and the TCA cycle via the kinase arm of the pyruvate dehydrogenase complex (PDC). In particular, pyruvate dehydrogenase kinase 1 (PDHK1) was exploited as a key metabolic dependence among a variety of cancer cells (Hitosugi et al., 2011).

Nevertheless, high glycolysis does not necessarily imply impaired mitochondrial metabolism. In fact, recent literature suggests the efficacy of mitochondrial targeting (Kreitz et al., 2019; Molina et al., 2018; Škrtić et al., 2011; Sriskanthadevan et al., 2015). On the same line, this thesis reports on a non-Warburg style of metabolism in a specific subtype of AML. Metabolic profiling of FLT3-ITD-positive AML cells unravelled OXPHOS reliance and thus, sensitivity to OXHPOS inhibition. Detailed experiments suggested that this mitochondrial reliance is driven by high PDP1 levels in FLT3-ITD-positive cells. These high levels are a result of either FLT3-ITD induction of PDP1 expression or its weak oncogenic ability to promote a dominant Warburg style of metabolism. A variety of *in vitro*, *ex vivo* and *in vivo* experiments positioned PDP1 as a putative target in FLT3-ITD-positive AML. Further discussion on these findings will be addressed in detail in the following sections.

3.2.1. FLT3-ITD and the OXPHOS phenotype

This doctoral thesis took a focused approach and shed some light on the metabolic program of FLT3-ITD-driven leukaemia. Screening the metabolic phenotype of a panel of AML cell lines using NMR revealed a higher tendency towards a mitochondrial OXPHOS metabolism in FLT3-ITD-positive cells. This was observed by higher ratio of TCA cycle metabolites to lactate (Figure 17). Considering the multi-oncogene nature of the available cell lines, it is appreciated that the results carry more of a correlative rather than causative value. Thus, the results were confirmed in the 32D FLT3-ITD model (Figure 18) which allowed for metabolic comparison with identical cellular background (Choudhary et al., 2005; Mizuki et al., 2000). The main advantage of this model is the ability to turn on/off a single oncogene (FLT3-ITD in this case) through cytokine modulation and then assess metabolic changes. These observations were

fostered by a tracer-based assay which mechanistically demonstrated how FLT3-ITD signalling shifted the fate of pyruvate labelling from lactate into the TCA cycle (Figure 19). The results of the glucose deprivation experiment support these findings by illustrating the metabolic fitness of FLT3-ITD cells which allowed them to switch their reliance to TCA cycle activity in the absence of glucose (Figure 20). Altogether, these results suggest that a major use of glucose in FLT3-ITD cells is to feed the TCA cycle. It is particularly interesting that, even when adapted to hypoxic oxygen levels, FLT3-ITD cells do not lose their capacity to promptly restore respiration and OXPHOS metabolism (Figure 30C), which further suggests it as their main metabolic reliance.

These results support very recent literature that emerged concurrently with the current study. In the study by (Baccelli et al., 2019), the authors categorized AML subtypes based on their metabolic reliance. In agreement with our findings, FLT3-ITD-positive AML scored among the OXPHOS-high AML cells. Similar findings of high OXPHOS activity in the FLT3-ITD cell lines (Molm14 and MV4-11) were also reported by (Farge et al., 2017). In another study that assessed online available whole genome and exome sequencing data from AML patient samples (Cancer Genome Atlas Research Network et al., 2013; Verhaak et al., 2009; Whitman et al., 2010), strong enrichment for OXPHOS profile in the FLT3-ITD cells was observed (Figure 37). This data however, also shows high expression levels of glycolysis-related genes in the FLT3-ITD cells. Nevertheless, it is plausible to propose the importance of the high glycolytic activity to lie in supplying the TCA cycle and driving mitochondrial metabolism rather than lactate production. This assumption is supported by two main facts. First, although this gene set enrichment analysis (GSEA) shows high enrichment for glycolysis, it shows higher enrichment score for mitochondrial ETC-related genes (NES= 1.79 vs 2.55, respectively) (Figure 37). Second, the findings in this thesis of high PDP1 levels in FLT3-ITD cells (Figure 22) anticipate the high production of pyruvate (high glycolysis) to be utilised for fuelling the TCA cycle, and not lactate production. This is clearly illustrated by the tracer-based assay where FLT3-ITD signalling directs the fate of glucose towards TCA cycle metabolites (Figure 19).

These findings/interpretations also reconcile the findings of this thesis with the report by Ju et al. which suggests FLT3-ITD to promote high expression of glycolytic enzymes (hexokinase II and pyruvate kinase II) (Ju et al., 2017). In conclusion, our findings dismiss the misconception on Warburg metabolism and high glycolysis to be exclusively meant to produce lactate, and this occurs to be in agreement with the emerging scientific opinion (DeBerardinis and Chandel, 2020).

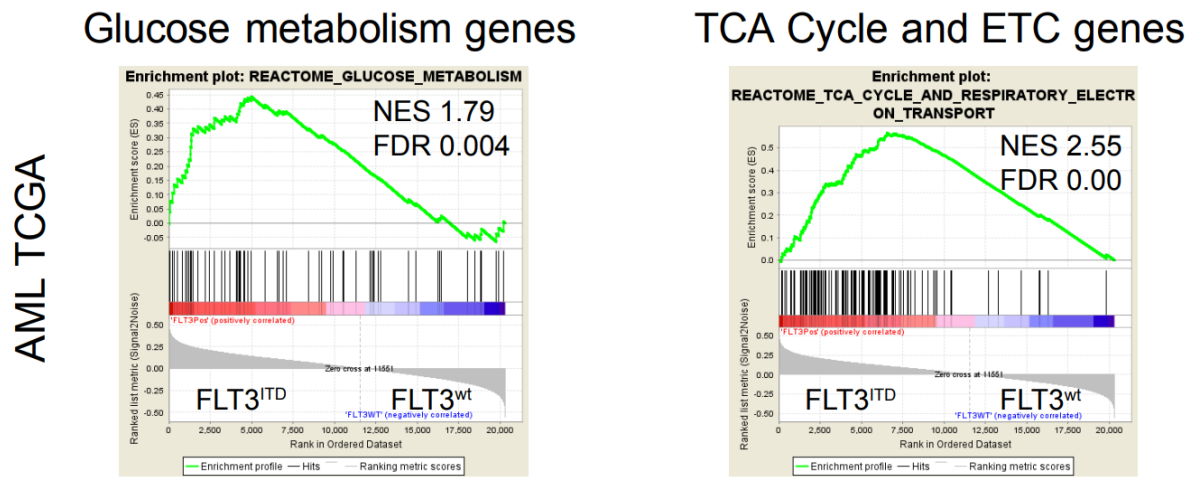


Figure 37: Gene set enrichment analysis (GSEA) of metabolism-related genes in FLT3-ITD *vs* FLT3-WT AMLs. The figure shows higher enrichment for both glycolysis-related genes, and to a higher extent, TCA cycle- and ETC-related genes. Adapted from (Gallipoli et al., 2018) (license obtained).

A very important aspect that was addressed in this doctoral work was confirming that the OXPHOS phenotype was not just a commonly active pathway in FLT3-ITD-AML cells, but rather an indispensable metabolic reliance. By the utilisation of different mitochondrial component inhibitors (venetoclax and rotenone), it was shown that FLT3-ITD cells are generally more sensitive to the disruption of mitochondrial metabolism (Figure 21A). These findings come in agreement with Baccelli et al. findings of FLT3-ITD cells being more sensitive to complex 1 inhibitor mubritinib than many other genotypes (Baccelli et al., 2019).

Of note regarding venetoclax, it is appreciated that it mainly targets BCL2 (Souers et al., 2013). Nevertheless, recent literature suggests venetoclax potency to be partially due to mitochondrial disruption (Pollyea et al., 2018). This mitochondrial effect of venetoclax was also confirmed to be independent of BCL2-inhibition (Roca-Portoles et al., 2020). This thesis provides more evidence of a metabolic aspect to high venetoclax sensitivity, where OXPHOS-high FLT3-ITD cells were generally more sensitive to venetoclax compared to OXPHOS-low FLT3-WT cells (Figure 21). Added to that, PDP1 abrogation synergised with venetoclax suggesting a common mode of action (presumably against mitochondrial metabolism) (Figure 25).

3.2.2. Metabolic consequences of FLT3-ITD/ PDP1 signalling axis

The observed OXPHOS phenotype was mostly attributed to a sort of regulation at the interphase of glycolysis with the TCA cycle. Intuitively, the main protein that promotes the conversion of pyruvate into Acetyl-CoA to feed the TCA cycle (PDP1) was evaluated which

revealed it to be the key player responsible for driving energy production in FLT3-ITD cells (Figure 22). These high PDP1 levels were concretely demonstrated in the 32D FLT3-ITD model, AML cell lines and also in the proteome study on the AML patients' cohort (Figure 22). In effect, these high PDP1 levels were shown to influence cellular metabolism by inducing higher PDH activity (lower inhibitory PDHA1 S293 phosphorylation (Figure 22)).

These findings are especially interesting considering previous literature that suggests AML cells to suppress PDP1 in order to promote Warburg metabolism (Fan et al., 2014; Shan et al., 2014). These high PDP1 levels in FLT3-ITD cells can be attributed to either i) induction of PDP1 by FLT3-ITD or ii) weak oncogenic capacity of FLT3-ITD in suppressing PDP1. The second hypothesis is supported by several pieces of literature. It is well established that FLT3-ITD has a weak leukaemogenic capacity and several reports showed it to be a relatively weak oncogene in inducing leukaemia in comparison to other oncogenes, such as MLL-AF9 (Stubbs et al., 2008), Nup98-HoxD13 (Greenblatt et al., 2012) and C/EBPα mutations (Reckzeh et al., 2012). The implications of its weak oncogenic capacity on metabolism can be observed in the study by Hitosugi et al. This study demonstrated that oncogenes in general activate PDHK1 which in turn, shifts pyruvate fates towards lactate (Warburg metabolism) (Figure 7) (Hitosugi et al., 2011). Interestingly, FLT3-ITD was among the weakest oncogenic activators of PDHK1. Together, the low induction of PDHK1 and the weak suppression of PDP1 argue for FLT3-ITD to be a weak inducer of the Warburg effect. Nevertheless, this hypothesis requires further molecular studies on the exact transcriptional and post-translational mechanisms of PDP1 regulation.

3.2.3. PDP1 targetability and clinical relevance

Regarding the reliance on PDP1, the current thesis showed that PDP1 abrogation is significantly disadvantageous to FLT3-ITD but not FLT3-WT cells (Figure 24, Figure 25). The strength of the growth impairment correlated with the knockdown efficiency. The exclusivity of growth disadvantage under FLT3-ITD signalling was demonstrated in the competition growth assay of 32D cells (Figure 24). The same differential sensitivity was observed in patient-derived primary AML blasts (FLT3-ITD vs FLT3-WT) and this effect was apparent in spite of the weak PDP1 knockdown efficiency (22% only) (Figure 25).

The importance of PDP1 for the development of AML with FLT3-ITD background was also demonstrated *in vivo*. PDP1 knockdown reduced leukemic burden, delayed disease onset and prolonged the mice survival despite the aggressive nature of this leukaemia (kills the mice within less than 4 weeks with 25 days survival on average) (Figure 26). The disease phenotype

was less aggressive with less sarcoma-like tissues occurring in the PDP1 knockdown group (Figure 26). It is particularly interesting that three out of the eight mice did not succumb to leukaemia and were sacrificed on day 60 (more than double the control survival). In fact, similar observations in Molm13 NSG model are reported in literature with a proportion of mice within the same group not developing leukaemia at all (Park et al., 2019). Nevertheless, the transplantation was successful and the control mice died within 26 days after transplantation which comes in agreement with literature about Molm13 xenotransplantation in NSG mice (Tzelepis et al., 2018).

Concerning the homing of the cells after injection, there seems to be immediate engraftment in the bone marrow of these mice. This is assumed because the human CD45 (hCD45) marker was not positive in peripheral blood up to day 13 after the transplantation (Figure 26). Nevertheless, this assumption cannot be confirmed since the homing of the cells was not tracked. Concerning the three mice that did not develop leukaemia, similar hCD45 positivity was observed in the peripheral blood during the course of the experiment compared to the other mice, meaning that leukemic cells did survive the transplantation and resided in the mice. This can be comprehended from the persistence of hCD45 in the peripheral blood of those mice (41-45%), from day 13 until day 50 (Figure 26).

Nevertheless, by scarification at day 60, these mice seemed to have had lost the transplant, indicated by the plunged hCD45 positivity (<1%). Several hypotheses can explain this observation. It can be argued that those cells struggled with engrafting in the bone marrow with its hypoxic environment (Spencer et al., 2014). This explanation is supported by the strong effect observed in the cumulative growth assays of PDP1 knockdown under hypoxia (Figure 30). That being so, a combination of PDP1 ablation and the scarcity of oxygen in the bone marrow might have been detrimental for their OXPHOS and caused cell depletion on the long run. Other explanations cannot be excluded such as altered homing and migration capacity however, a more elaborate mouse model is needed to investigate these aspects.

Beyond the *in vivo* data, the clinical relevance of PDP1 is manifested by the correlation between high PDP1 gene expression levels and poor overall survival in AML patients (Genomic Data Commons database) (Figure 23). Nonetheless, due to the small overall sample size, no focused analysis on FLT3-ITD *vs* FLT3-WT could be done. Further proteomics/ transcriptomics analyses are needed on a bigger cohort of patients to validate the clinical relevance of PDP1 levels in patients with FLT3-ITD background. In conclusion, this study here provides a prognostic predictor in AML based on a metabolic biomarker.

It is to be mentioned that it was challenging to successfully rescue PDP1 knockdown in the cells and thus relay the growth disadvantage to metabolic impairment. All potential pathways activated by PDP1 were investigated and boosted with intermediate metabolites in order compensate for PDP1 loss, however with no success (Figure 27). Combination rescues with intermediates of the TCA cycle, fatty acid oxidation, redox control and pyrimidine biosynthesis similarly failed. This is mainly attributed to the different metabolic entanglements relying on PDC/ PDP1 activity, such as energy production (Li et al., 2020; Love et al., 2011), lipid biosynthesis (Chen et al., 2018) and redox balance (Fisher-Wellman et al., 2015). In addition, it seems that PDP1 has a far-reaching effect in functionally promoting OXPHOS by mechanistically interacting with other mitochondrial proteins such as: mitochondrial IDH2, Aconitase, NADH dehydrogenase, Succinate dehydrogenase as suggested by interactome databases (BioGRID database (Stark et al., 2006), http://www.thebiogrid.org/). These explanations are supported by the experiment with Rho Zero cells where PDP1 knockdown had no effect on the proliferation of cells that are not reliant on mitochondrial metabolism (Figure 28). Hence, there is a strong evidence to suggest PDP1 knockdown to primarily disadvantage the cells by abrogating energy balance.

3.2.4. PDP1 roles in therapeutic responses and metabolic flexibility

As described in the results sections 3.1.5, 3.1.6 and 3.1.7, PDP1 plays three main functions in FLT3-ITD-positive AML cells. First, due to their assumed weak induction of the Warburg effect, FLT3-ITD cells shift to depend on mitochondrial metabolism mediated by PDP1. Thus, higher PDP1 levels would boost energy metabolism in FLT3-ITD cells, which was confirmed by PDP1 overexpression experiment (Figure 29). Nonetheless, PDP1 overexpression did not enhance ATP production in FLT3-WT cells because they depend on the Warburg metabolism. Another explanation for their inability to benefit from PDP1 overexpression would be their low mitochondrial fitness, due to their higher persistent reliance on glycolysis. Thus, even if the TCA cycle was boosted by PDP1 overexpression, FLT3-WT cells would probably not have enough respiration capacity to produce ATP from the resulting energy intermediates.

The second function of PDP1 involves its role in the metabolic flexibility in FLT3-ITD cells. As demonstrated by the OCR measurements, even when they are put under hypoxic conditions (an environment that does not allow for OXPHOS and favours fermentation), FLT3-ITD cells do not lose their capacity to perform mitochondrial metabolism (Figure 30). PDP1 mediates this ability by retaining basal OXPHOS levels, which explains the growth disadvantage upon PDP1 knockdown under hypoxia as shown by the cumulative growth assay (Figure 30). More importantly is the function of PDP1 in the switch to mitochondrial metabolism upon exposure

to oxygen. PDP1 enabled FLT3-ITD cells to immediately restore respiration when re-oxygenated and PDP1 knockdown abrogated this ability. This metabolic switch is not only important for energy production, but also for cellular proliferation as indicated by the cell cycle assay. This can have important role and implications on AML biology in the bone marrow. As literature suggests, bone marrow has two main niches; central niche where the bulk AML blasts reside and endosteal niche where the leukemic stem cells (LSCs) reside (mainly the chemotherapy-resistant fraction) (Ishikawa et al., 2007; Lane et al., 2011; Méndez-Ferrer et al., 2020). LSCs migrate between the niches and thus require to metabolically adapt, potentially via PDP1 activity. Further studies are required to address this aspect of PDP1 functions, especially in the context of disease relapse.

Third, the remarkable finding of the role of PDP1 in therapeutic responses is very important considering the challenging aspect of drug resistance in clinical outcomes (Figure 32, Figure 33). Not only it induced growth disadvantage, PDP1 knockdown synergized with FLT3-inhibition and exerted a strong effect on the cells, further supporting the importance of mitochondrial metabolism for FLT3-ITD cell survival. Interestingly, on its own, PDP1 knockdown was not enough to induced apoptosis, however, it primed the cells to apoptosis induced by low doses of AC220 (Figure 31). This can be of a special importance considering the dose-limiting toxicity of AC220 treatment in the patients (Fletcher et al., 2020). Clinically, this would possibly mean enhanced potency of FLT3-inhibitors in the patients at lower doses when combined with PDP1 targeting. Vice versa, PDP1 overexpression experiments confirmed the role of PDP1 in resistance to FLT3-inhibiton (Figure 32). Furthermore, the potency of PDP1 abrogation in restoring AC220-sensitivity in primary blasts from an AC220-resistant patient presents another striking evidence on the modulatory role of PDP1 in this context (Figure 33). The later finding is extremely important considering the therapeutic value of sensitising agents in drug-resistant patients. These findings come in line with other studies showing that OXPHOS enriches for chemotherapy resistance and that targeting OXPHOS leads to higher sensitivity to chemotherapy and targeted therapies (Baccelli et al., 2019; Farge et al., 2017; Henkenius et al., 2017).

Data produced in this thesis provides insights into the mechanistics of this role. As detailed earlier, FLT3-inhibition leads to elevation in PDP1 on the mRNA and protein levels (Figure 34). This elevation in PDP1 is functionally important to alleviate the effects of AC220 (supported by the results of pyruvate rescue upon FLT3-inhibition (Figure 35)). The tracer-based assay proved PDP1 to be the key driver of this rescue represented by significantly higher glucose shuffling into the TCA cycle upon AC220 treatment (Figure 34).

Chapter IV

Methionine metabolism in AML

Divergent methionine utilization and impaired recycling

4.1. Results

4.1.1. Methionine dependence in AML

In order to understand the level of dependency of AML cells for each of the different amino acids, a single amino acid dropout assay was performed, where individual amino acid depletion settings were carried out for all of the 20 different amino acids (Figure 38A)[6]. This was done in different cellular subtypes in order to get a general dependency overview (Molm13 and HL60 cell lines (data not shown) and primary bone marrow-derived AML blasts). Primary AML blasts were divided into two subpopulations: the bulk tumor cells (CD34+/ CD38+) and the presumed stem cell fraction (CD34+/ CD38-). Among the amino acids on which AML cells were most dependent was methionine. This was observed across the cell lines with different genetic backgrounds (Figure 38B) and also the presumed stem and progenitor fractions from the primary AML samples (Figure 38C). To investigate the AML exclusivity of this dependence, the dropouts were also performed on a set of CD34+ hematopoietic stem and progenitor cells isolated from the bone marrow of healthy donors. Interestingly, methionine depletion had no impact on healthy stem and progenitors isolated from bone marrow (Figure 38D). This suggests methionine targeting to be potent strategy against AML without impacting normal hematopoiesis.

To assess the general impact of methionine depletion on cellular metabolism, total metabolites levels were quantified by NMR upon 24 hours of methionine starvation. A significant reduction in the concentrations of several metabolites was observed in both, Molm13 (Figure 39A) and HL60 cell lines (Figure 39B). Metabolites affected were related to energy metabolism (lactate, succinate, fumarate and ADP), glutaminolysis and redox control (glutamine, glutamate and glutathione) and other metabolites related to methionine metabolism (taurine and phosphocholine).

To further investigate the essentiality of methionine for AML development, *in vivo* studies were performed[7]. Here, different groups of NSG mice were transplanted with Molm13 cells and then the groups were allocated to either full diet or methionine-depleted diet (either initial depletion or after a specific time point). Interestingly, methionine depletion perturbed leukaemia development and prolonged the overall survival of the mice (Figure 40A). Moreover, methionine restriction impaired leukaemia engraftment in the bone marrow and spleen (Figure 40B).

[6] These experiments were performed by A. Cunningham (group of Prof. JJ Schuringa, University of Groningen, Netherlands).

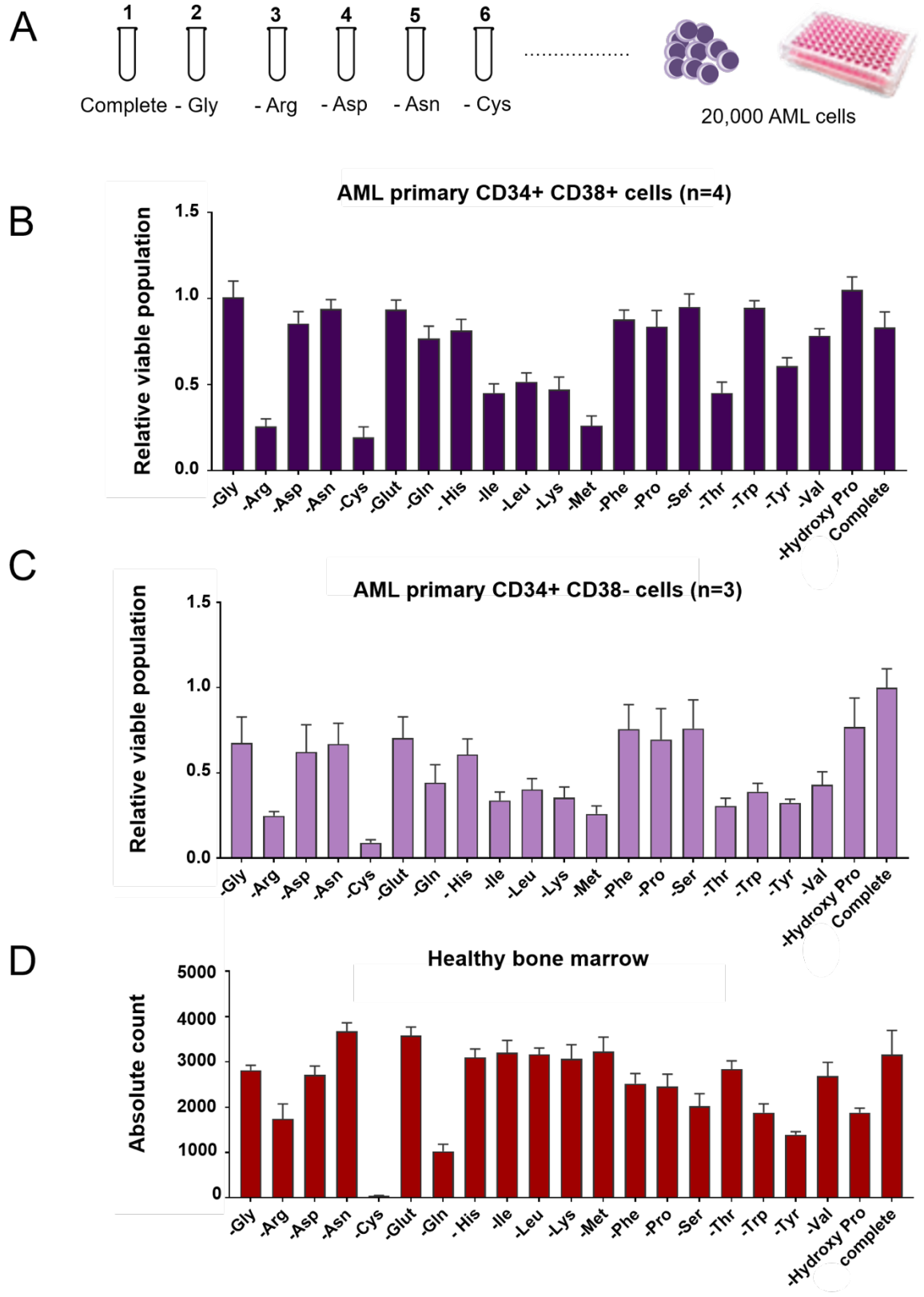


Figure 38: Methionine is a strong dependency in AML but not healthy cells[7]**.** A. Experimental layout of individual amino acid dropout showing strong growth impairment upon methionine depletion in: B. progenitor AML blasts and C. presumed leukemic stem cells sorted for CD34+/ CD38- expression (isolated from patients) but not in D. healthy donor CD34+ hematopoietic stem cells.

[7] This figure and experiments were performed by A. Cunningham (group of Prof. JJ Schuringa).

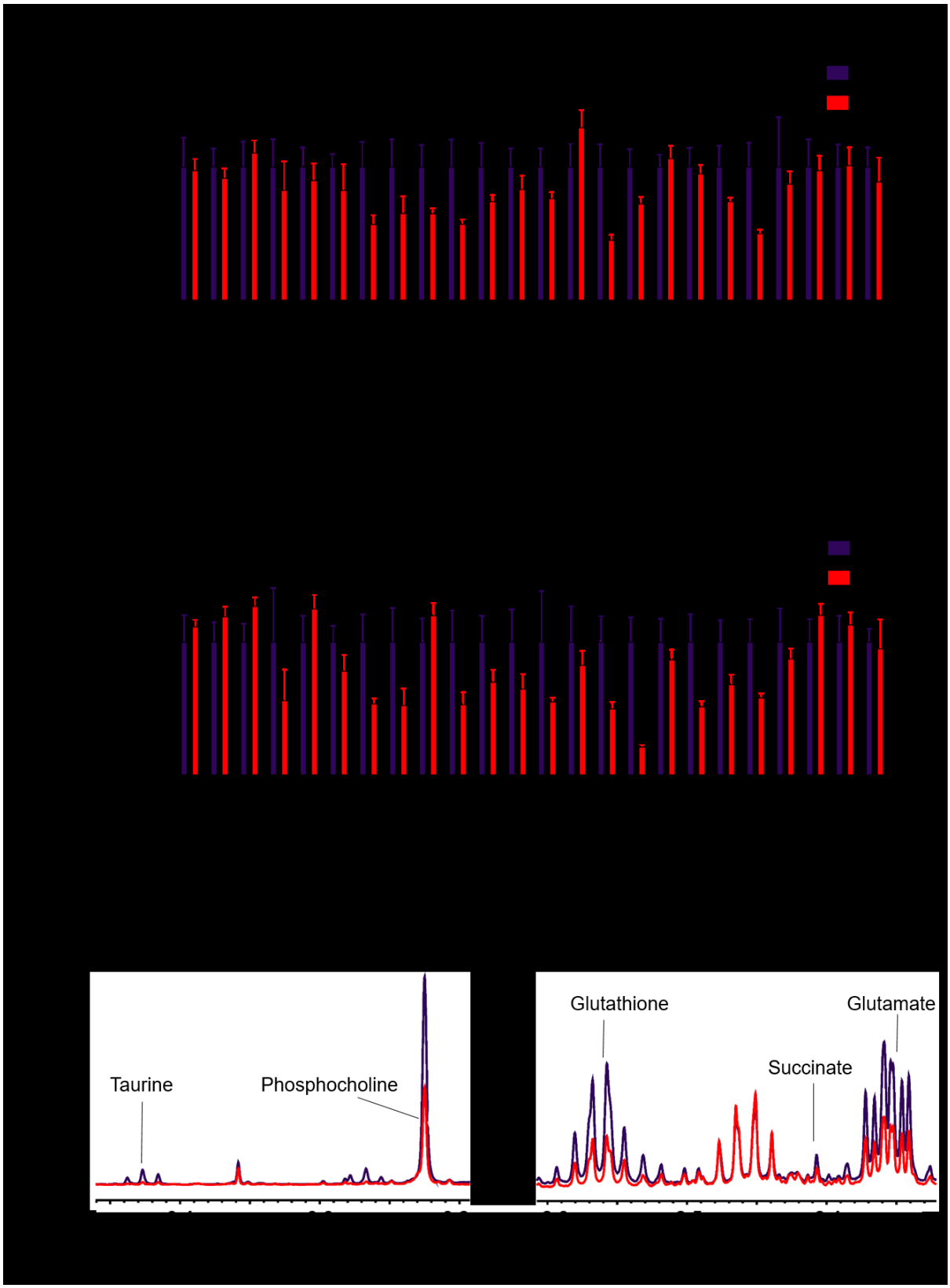


Figure 39: Methionine starvation leads to global metabolic insufficiency. Fold change of metabolites levels upon methionine depletion for 24 hours in A. Molm13 and B. HL60 cells. C. 1D ^{1}H-NMR spectrum of some of the most affected metabolites upon methionine depletion (red) in HL60 cells. Spectrum was measured on a Bruker 600MHz AVIIIHD spectrometer with the pulse program: NOESYGPPR1D at 25°C. For atoms assignment, refer to Figure 11.

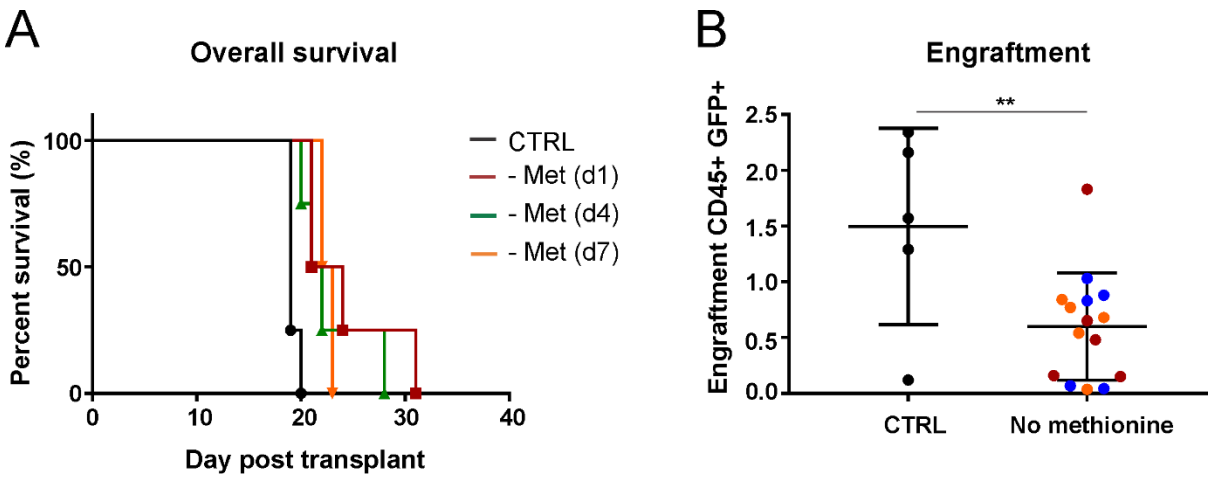


Figure 40: Methionine dietary restriction impairs leukaemia progression *in vivo*[8]. A. Methionine restriction diets prolonged the overall survival in a Molm13 luciferase NSG mouse model. B. Methionine depletion reduces total engraftment of leukemic cells in the mice bone marrow and spleen.

4.1.2. Methionine utilization and DNA methylation

To understand this dependence and the fate of methionine in AML cells, a tracer-based assay with ^{13}C isotope-labeled methionine was carried out in K562 (Figure 41A), MV4-11 (Figure 41B) and Molm13 (Figure 41C) cell lines. Label tracing analysis was performed in an untargeted approach to identify label incorporation not only in the known pathways of methionine metabolism, but also in any other metabolite where labelling could be observed. No label incorporation was detected in the redox regulation pathway (methionine conversion towards cysteine and glutathione production) suggesting no contribution of methionine to redox control in AML (Figure 41). In fact, addition of N-acetyl cysteine or glutathione did not rescue methionine depletion in our settings (data not shown). Similarly, no label incorporation was found in taurine.

The last trackable fate of methionine ^{13}C label was detected in cystathionine, downstream of homocysteine. To assess the proportion of methionine being converted to cystathionine, a direct comparison of ^{13}C label intensity ratio on C_4 of cystathionine *vs* C_4 of methionine was performed in AML *vs* healthy peripheral blood mononuclear-stem cells (PBMSCs) (Figure 42A, B, C). This ratio was at relatively low levels in all of the AML cell lines (less than 50%, down to 5% in MV4-11) (Figure 42D), as opposed to healthy PBMSCs where the incorporation ratio was at significantly higher levels (Figure 42E). These results indicate that only a minor fraction of methionine is being converted to cystathionine in AML, anticipating different methionine utilisation upstream of cystathionine.

[8] This figure and experiments were performed by A. Cunningham (group of Prof. JJ Schuringa, University of Groningen, Netherlands).

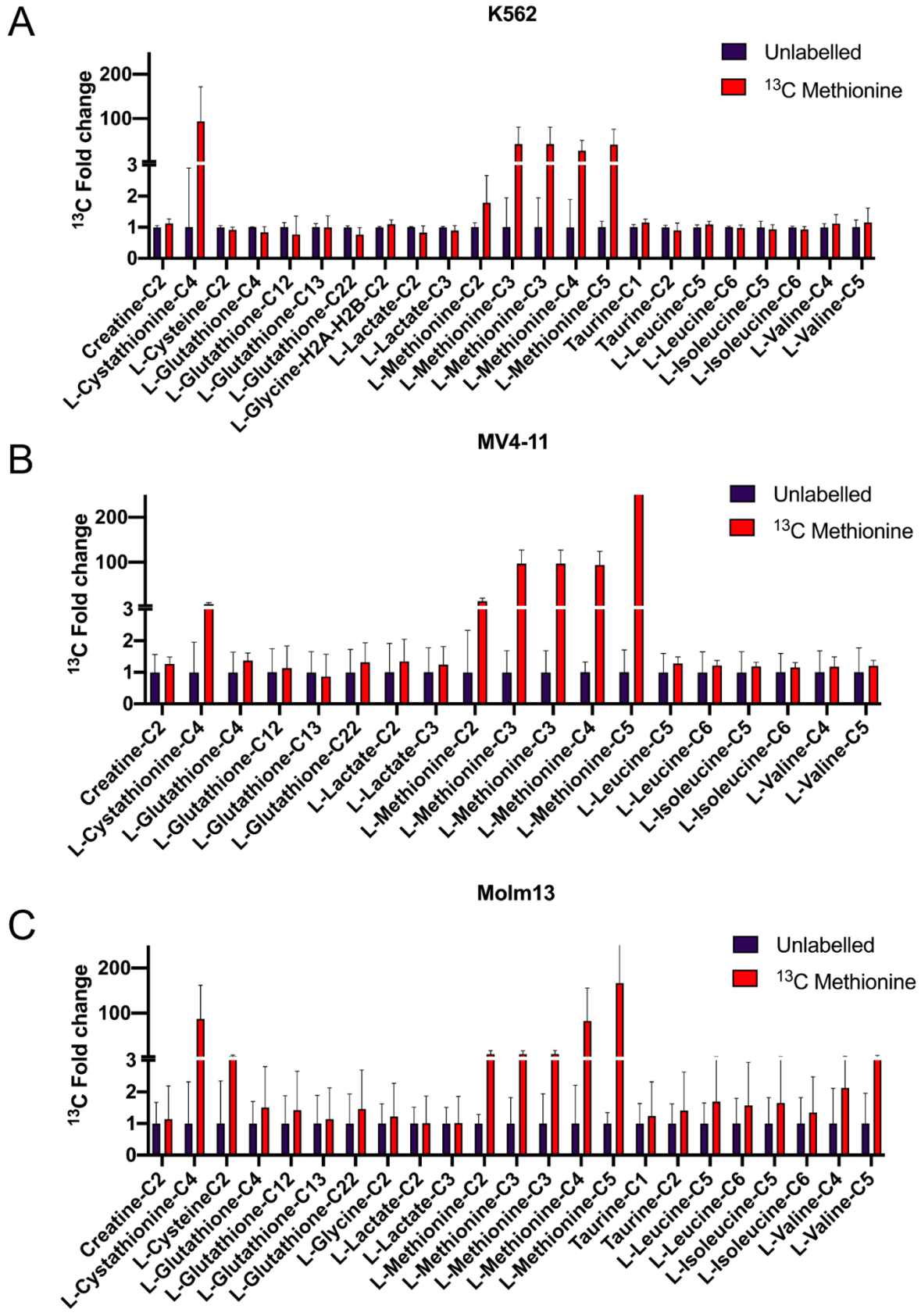


Figure 41: Full panel of untargeted ^{13}C methionine tracing. The figure shows label incorporation upon 12 hour of labelling with ^{13}C methionine in A. K562, B. MV4-11 and C. Molm13 cell lines.

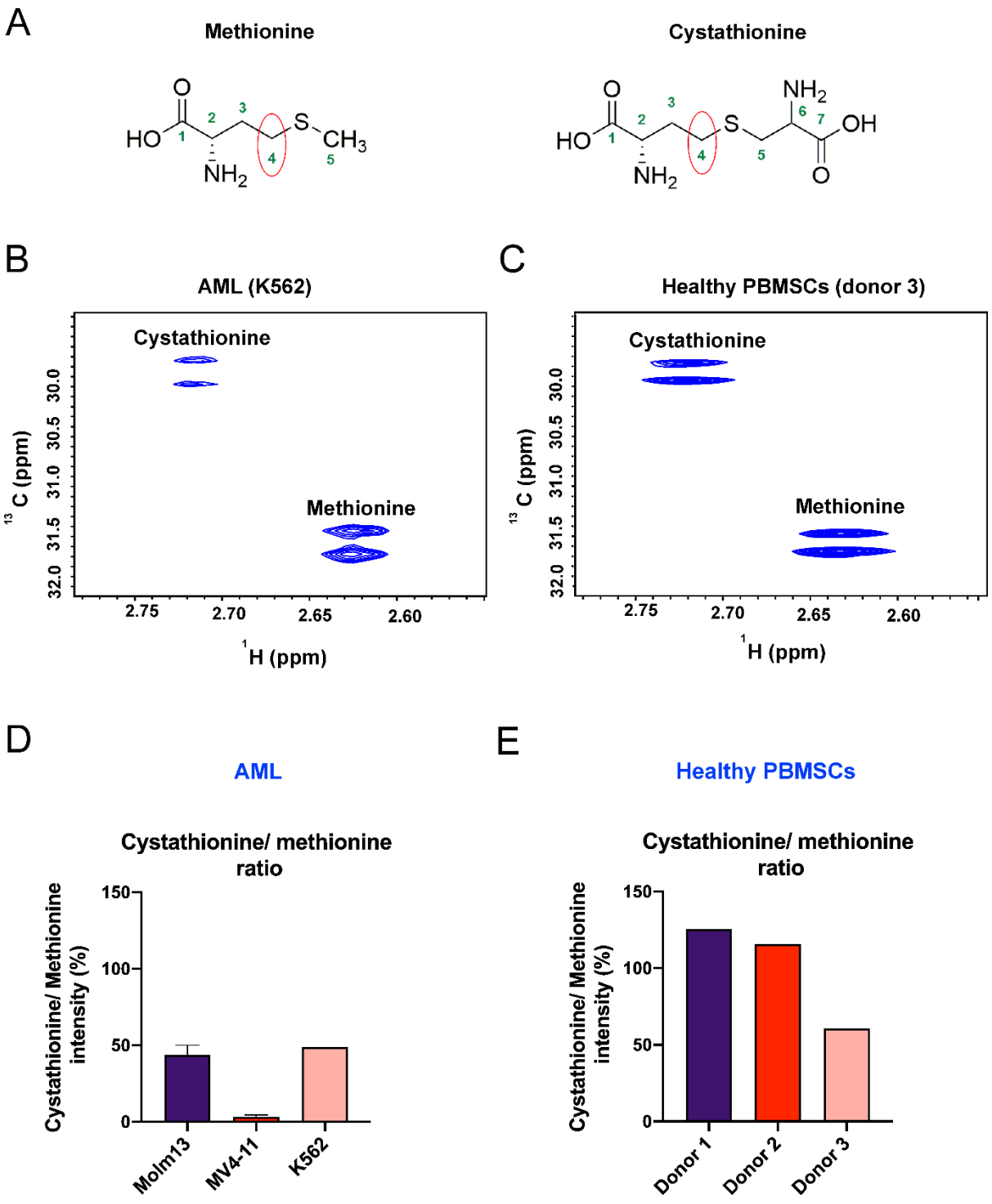


Figure 42: Minimal methionine-to-cystathionine conversion in AML compared to healthy cells. A. Chemical structure of methionine and cystathionine with marked C_4 in methionine that ends up as C_4 in Cystathionine. ^{1}H-^{13}C HSQC NMR spectra of methionine (C_4) and cystathionine (C_4) from B. K562 and C. Healthy PBMSCs. Both spectra were measured at 25°C with HSQCPHPRSP.UG4 pulse sequence. K562 spectrum was recorded on a Bruker 600MHz AVIIIHD spectrometer, while the healthy PBMSCs spectrum was recorded on a Bruker 800MHz AVIIIHD spectrometer. D. Low methionine-to-cystathionine conversion ratio in AML cell lines Molm13, MV4-11 and K562 (measured by ^{13}C intensity on C_4 of both metabolites). E. High methionine-to-cystathionine conversion ratio in healthy PBMSCs from 3 different donors.

The low label incorporation in cystathionine suggests that methionine is being predominantly utilized upstream to produce S-adenosylmethionine in a reaction that will donate a methyl group (CH_3) for methylation reactions. This utilization was confirmed by evaluating different histone methylation marks upon methionine depletion. Clear differences were observed between various histones marks with H3K36me3, a transcriptional activation and elongation mark, being significantly impacted whereas H3K4me3 was only marginally affected at 48 hours and H3K37me3 being unaffected (Figure 43A). Subsequently, methionine depletion resulted in reduced total cellular RNA levels (Figure 43B). Similarly, polysomal profiling revealed impaired protein translation (data not shown). Altogether, these results suggest that the necessity of methionine in the cells relay to the provision of methyl-groups donation for methylation reactions.

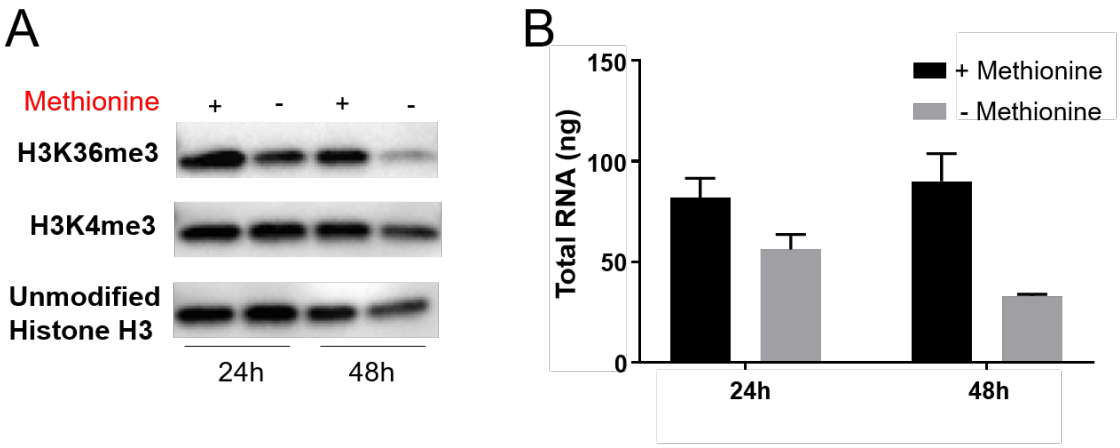


Figure 43: Methionine depletion impairs DNA methylation and transcription[9]**.** A. Methionine depletion generally reduces histone methylation, with a prominent impact on H3K36me3 mark in HL60 cells. B. Methionine depletion impairs transcription as depicted by reduced total RNA levels.

4.1.3. Methionine recycling

After establishing the difference in methionine utilization of between AML and healthy cells, the question arose as to the mechanism by which AML cells and perhaps cancer cells in general have an increased dependency for exogenous methionine supply (compared to healthy cells). First, online databases were examined for the expression levels of all genes related to methionine, folate and polyamine biology and were compared between AML and healthy cells. Interestingly, the main enzyme responsible for methionine de novo synthesis from homocysteine, Methionine Synthase (MTR), was downregulated in AML compared to healthy hematopoietic stem cells according to BloodSpot database (Bagger et al., 2016)

[9] This figure and experiments were performed and provided by A. Cunningham (group of Prof. JJ Schuringa, University of Groningen, Netherlands).

(http://www.bloodspot.eu/) (Figure 44). This suggested that the increased dependency of AML cells for methionine is possibly due to the reduced capacity to recycle homocysteine to methionine and indicated perhaps an imbalance in the methionine recycling capacity between AML cells and their healthy counterparts (*In silico* analysis was done by A. Cunningham (group of Prof. JJ Schuringa, University of Groningen, Netherlands)).

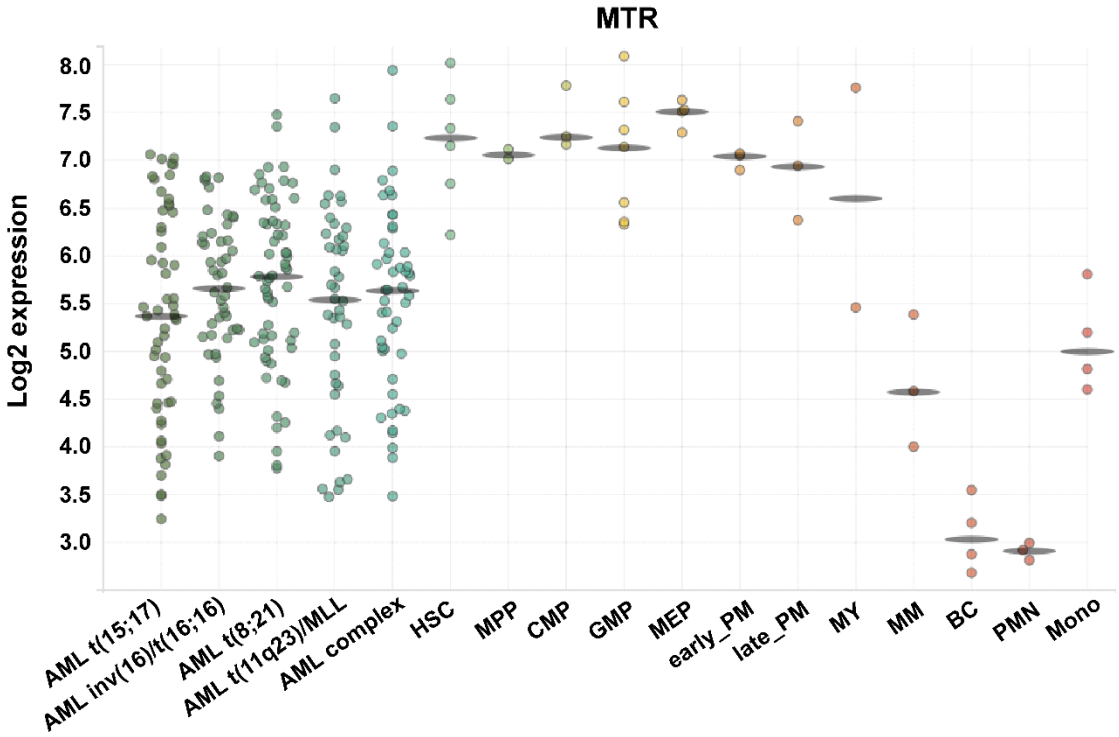


Figure 44: MTR is downregulated in AML. Low Methionine Synthase (MTR) gene expression levels in AML *vs* healthy CD34 stem cells (BloodSpot database (Bagger et al., 2016) (http://www.bloodspot.eu/)).

To gain mechanistic insights on MTR activity in catalysing homocysteine-to-methionine recycling, a tracer-based assay using uniformly ^{13}C-labelled methionine was performed. During the conversion to homocysteine, the CH_3 group of methionine is released (specifically upon the conversion of S-Adenosylmethionine (SAM) to S-Adenosylhomocysteine (SAH)), leaving homocysteine with four carbons all uniformly ^{13}C-labelled. Upon the recycling of homocysteine back to methionine, an extra carbon is donated (mainly by serine/glycine one-carbon metabolism). This additional carbon is hence unlabelled (^{12}C). Thus, in case of active methionine recycling machinery, two methionine pools are present in the cell: uniformly ^{13}C-labelled pool (original tracer imported to the cells) and a second pool without ^{13}C-label on the methyl group (C_5) (Figure 45A). In this case, the ratio of ^{13}C-label between methionine's C_4

and C_5 is anticipated to increase because of the second methionine pool that has unlabelled C_5. First, this ratio was identified to be around '1.3' in a plain 100% uniformly ^{13}C-labelled methionine sample (without cells). Upon measuring this ratio in AML cell lines, no significant increase in the ratio was found in any of the cell lines, suggesting no recycling (Figure 45B, C). Nevertheless, no recycling was detected in healthy PBMSCs either. Although no difference was observed between AMLs and healthy PBMSCs in terms of their recycling (in spite of the lower MTR levels in AML), this discrepancy, can be attributed to high abundance of methionine in the media (approximately 3 folds higher than human serum (Cantor et al., 2017)), which might undermine the need for recycling (addressed in detail in the discussion section).

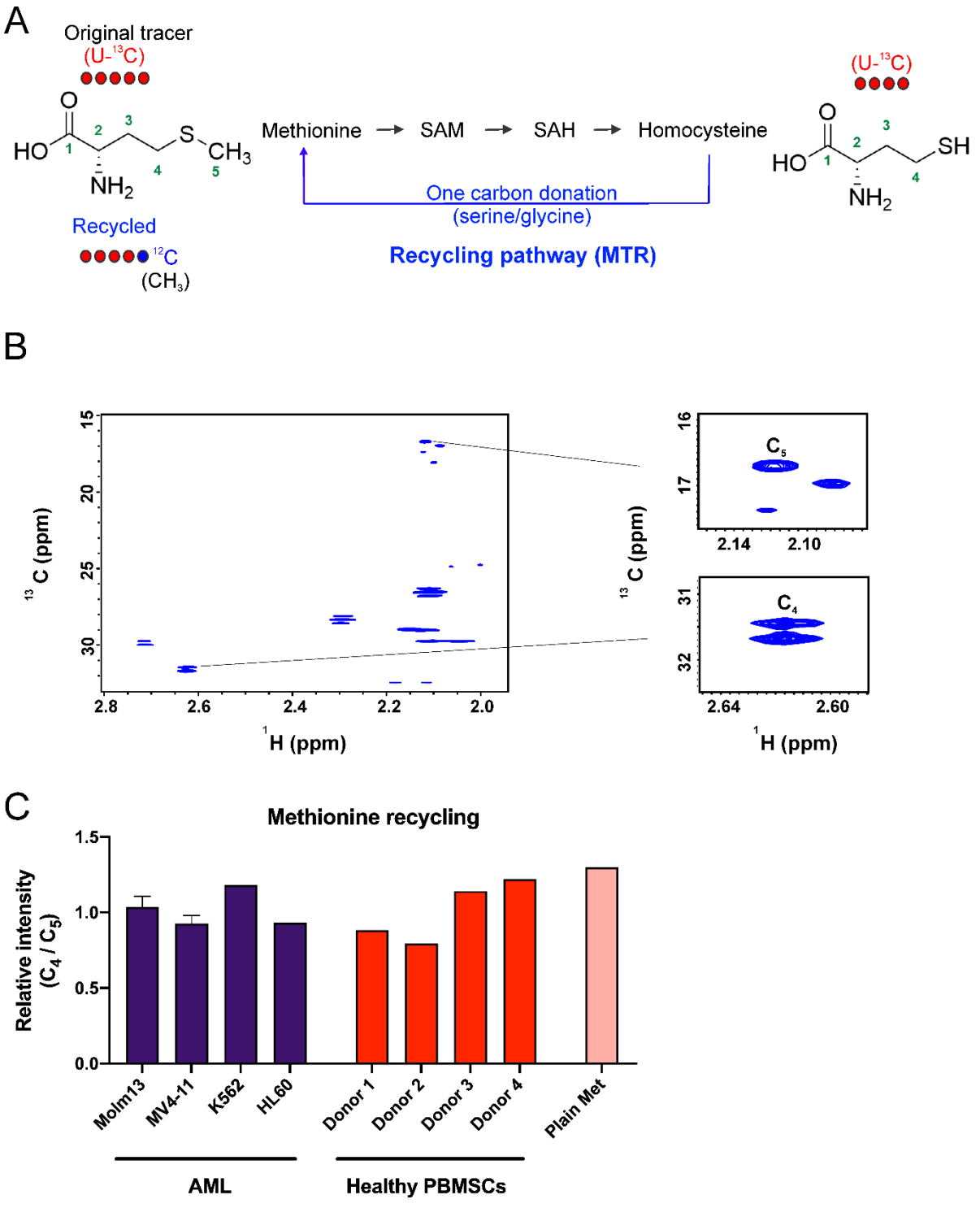


Figure 45: Methionine recycling. A. Methionine recycling pathway from homocysteine via MTR produces an extra methionine pool without ^{13}C label on C_5. B. ^{1}H-^{13}C HSQC NMR spectrum of methionine C_4 and C_5 in K562 cells measured with HSQCPHPRSP.UG4 pulse sequence and recorded on a Bruker 600MHz AVIIIHD spectrometer at 25°C. C. Relative ^{13}C intensity ratio between methionine's C_4 and C_5 in four different AML cell lines (Molm13, MV4-11, K562 and HL60) in comparison to a plain ^{13}C methionine sample implies poor methionine recycling in AML. Similarly, healthy PBMSCs show poor methionine recycling.

4.2. Discussion

Altered amino acid metabolism is recognized as a hallmark of cancer cells (Ananieva, 2015; Kreitz et al., 2019; Lukey et al., 2017; Miraki-Moud et al., 2015; Mussai et al., 2015a, 2015b; Zhang et al., 2017). However, the dependency of AML cells for only a few of the coded amino acids has been studied thoroughly while many others are yet to be explored (Castro et al., 2019; Kreitz et al., 2019). Initial work by Prof. JJ Schuringa's group addressed the relative amino acid dependencies in a dropout assay which revealed methionine as a strong metabolic dependency in AML. Such role was poorly described in cancer in general, and not described at all in AML in particular.

The broad importance of methionine in AML is seen by its dependency across the different genetic backgrounds in AML with relatively similar sensitivities observed (performed in 4 different cell lines, primary bone-marrow AML progenitor blasts and leukemic stem cells). Evidence was provided on the role of methionine in leukaemia development *in vivo*. Methionine dietary starvation in mice delayed leukaemia onset in a cell line model. Such a strategy can hold significant therapeutic potential in patients due to the feasibility of dietary restrictions without the need for specific pharmacological targeting of methionine metabolism pathways. Furthermore, a unique aspect of methionine targeting is the exclusive AML toxicity without affecting the healthy hematopoietic stem cells. This specificity is pivotal in the therapeutic context.

Methionine has many roles in the cell such as maintaining pluripotency, DNA methylation and glutathione, cysteine and taurine production (Hoffman et al., 2019; Shiraki et al., 2014; Shyh-Chang et al., 2013). The tracer-based assay with ^{13}C isotope-labelled methionine elucidated different methionine utilization in AML. Given that no label incorporation was detected in the redox regulation intermediates (cysteine and glutathione), that cysteine was present in the methionine dropout condition and that N-acetyl cysteine addition did not rescue methionine depletion, it could be asserted that the dependency is not related to redox control in AML. This in fact is in agreement with literature attributing redox control in AML to other amino acids such as glutamine and cysteine (Gregory et al., 2018b; Jones et al., 2019; Zhou et al., 2010).

The unique approach of comparing ^{13}C label on C_4 of cystathionine to that of methionine C_4 allowed for accurate quantification of methionine-to-cystathionine conversion ratio (direct derivative). On average, less than half of the methionine was converted to cystathionine in AML, unlike healthy stem cells where the majority of methionine was converted to cystathionine and downstream intermediates. With these data in hand, it is plausible to

propose the central role of methionine to be predominantly producing S-adenosyl methionine (SAM) in a reaction that donates a methyl group (CH3) for methylation reactions. This is supported by the reduced histone methylation, particularly to H3K36 tri-methylation, a transcriptional activation and elongation mark which was consistent with reduced cellular RNA levels, impaired protein translation and a cell cycle blockade (data not shown) upon methionine depletion.

In fact, while the current study was being conducted, another group elucidated the reliance of lung cancer cells on exogenous methionine. The authors reported the pivotal importance of the first enzyme in the methionine cycle, adenosyltransferase II alpha (MAT2A) (converts methionine to SAM), in maintaining proliferation and stemness of lung adenocarcinoma cells by maintaining DNA methylation (Wang et al., 2019). This report is consistent with the findings of the current chapter on methionine. However, it does not provide mechanistic insights on the reason behind the reliance on exogenous methionine, another aspect that was addressed by this thesis.

Evolution has equipped cells with recycling and salvage mechanisms to ensure adequate metabolite supply during periods of exogenous shortage. An example of this is glutamate production from glutamine (Tohyama et al., 2016). The same is the case for methionine which can be recycled back from homocysteine or recovered from polyamines in the salvage pathway. We hypothesized based on reduced MTR expression at the transcriptome level (BloodSpot) that AML cells would have a higher dependency on exogenous methionine due to reduced capacity to recover methionine from homocysteine. In fact, such dependencies were described for other amino acids in AML and were also shown to be a result of dysfunctional recycling of these amino acids. For example, poor regeneration of arginine was observed in AML and was demonstrated to be mediated by the lack of expression of the synthesizing enzyme argininosuccinate synthetase-1 (ASS1) (Miraki-Moud et al., 2015; Mussai et al., 2015a).

The novel NMR approach developed for this purpose allowed for the differentiation between the two methionine pools present in the cell; imported *vs* recycled (^{13}C *vs* ^{12}C ratio on the CH_3 group of methionine). In fact, about 90-95% of the intracellular methionine in all of the cell lines was imported, indicating poor/ no homocysteine-to-methionine recycling in AML. Nevertheless, no recycling was observed in healthy PBMSCs either. Whether this observation reflects no recycling of methionine in both, healthy and AML cells is yet unclear and cannot be concluded. However, the differential MTR expression between AML and healthy remains a significant finding and clearly points to recycling differences. One explanation for this

discrepancy might be the excessive methionine levels present in cell culture medium (almost three folds higher than methionine level in human serum (Cantor et al., 2017)) which might undermine the cellular need for *de novo* methionine generation and recycling. Thus, further experiments are needed and they should include ^{13}C-methionine tracing under methionine restriction conditions (or full depletion) to tease out the recycling capacity of both healthy and AML cells when challenged with methionine scarcity.

Altogether, this data explains the dependence of AML cells on methionine uptake for the provision of methyl groups for methylation reactions. It is however, important to further assess primary AML blasts and not only cell lines, considering the excessive proliferation capacity of cell lines in comparison to primary AML blasts and healthy cells. The reliance on exogenous methionine is believed to be due to the compromised methionine recycling machinery in AML. Nevertheless, the experiments done so far are not sufficient to show the difference in methionine recycling capacity in AML compared to healthy cells, and further experiments are needed. Similar tracing with ^{13}C-serine would also help to elucidate methionine recycling machinery by directly detecting the additional carbon provided by one carbon metabolism. This helps expanding the existing knowledge on the role of one carbon metabolism in the context of methionine metabolism (Ducker and Rabinowitz, 2017; Kaelin Jr. and McKnight, 2013), especially because alterations in this pathways were reported in AML (such as MTHFD2) (Pikman et al., 2016).

Chapter V

Real-time NMR for studying metabolism

Development of a novel cell-friendly NMR approach for studying live cell metabolism

5.1. Results

Most of the described in-cell NMR approaches rely on manual handling of the samples and measurements. Here, an automated NMR approach for studying metabolism of living cells in a real-time manner is introduced. Automation of the process was achieved by installing a sample changer with temperature control option that allows for sustaining the cells at a physiological temperature (Figure 46A). This ensures that the metabolic readout of the cells is physiological and not affected by temperature-induced stress. The sample changer alternates the samples in an automated fashion upon setup, where around 15 samples can be run per hour with short measurement times. The full capacity is up to 96 samples, which makes it a high throughput platform for metabolic profiling.

For each sample, several measurements are recorded over a time course corresponding to extracellular metabolites. The spectra are then overlaid to calculate the difference in intensities and determine the rates of metabolites influx such as glucose and efflux such as lactate (Figure 46B) (shown for 48 hour time course). Example 1D ^{1}H-NMR spectrum of the real-time NMR measurement is shown in (Figure 46C). Number of cells required is considerably low, with only 5 x 10^5 cells per sample (less than a tenth of the cell numbers required for the traditional approaches (Saborano et al., 2019)).

5.1.1. Optimisation towards a cell-friendly approach

As discussed in Chapter 1.3.3, in-cell NMR enables studying cellular activities with more physiological relevance. Here, we build up on existing approaches to improve the cellular environment and minimise its effects on the studied activities. In preparation for a cellular scaffold (to sustain the cells in suspension and prevent their aggregation), different materials that were described for in-cell NMR setups were evaluated. The impact of the most reported substance in the in-cell NMR literature (agarose) on the cellular viability and ATP content was evaluated in a viability assay. These agarose-based matrices significantly abrogated the cellular viability (around 60% ATP reduction) and thus, were excluded (Figure 47A). Next, methylcellulose was investigated, a material that is used for highly sensitive stem cells setups and colony-formation assays. Interestingly, methylcellulose-based media showed no impact at all on the metabolic integrity or the cellular ATP pool (Figure 47A). Further, this matrix was non-invasive as cells retained full viability throughout the measurements and when they were put back in culture, they exerted normal growth behaviour. Thus, 40% methylcellulose IMDM medium was considered for the real-time NMR settings.

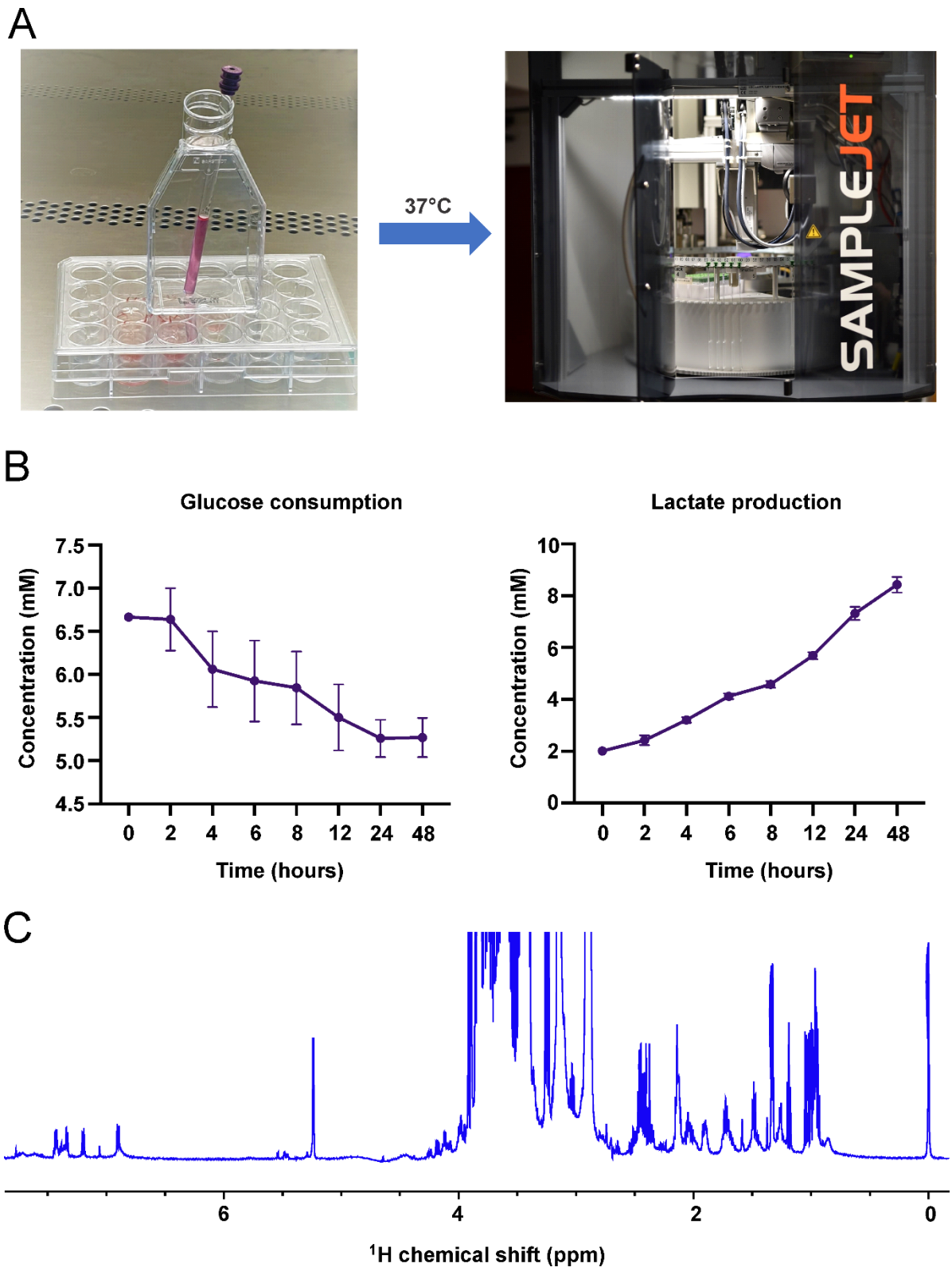


Figure 46: Real-time NMR approach design. A. The illustration elucidates cell preparation in the NMR tube which is then maintained in the spectrometer's sample changer at 37°C. B. Example of monitoring cellular metabolic activity represented by glucose uptake and lactate secretion. C. Example 1D ^{1}H-ZGESGPPS NMR spectrum (water suppression with Excitation Sculpting) of living cells maintained in methylcellulose media recorded on a Bruker 600MHz AVIIIHD spectrometer at 27°C.

With all of the basic setups established, cellular responsiveness and metabolic adaptions to external stimuli were further assessed to ensure normal cellular functionality. Cells were treated with the FLT3-inhibitor midostaurin that has been shown earlier to block glucose uptake (see chapter 3.1.7) (also reported in previous literature (Gallipoli et al., 2018; Ju et al., 2017)). Interestingly, cells in methylcellulose media in the NMR tube responded normally to midostaurin-induced metabolic changes by a blockade in their glucose consumption rate (higher extracellular glucose pool) (Figure 47B).

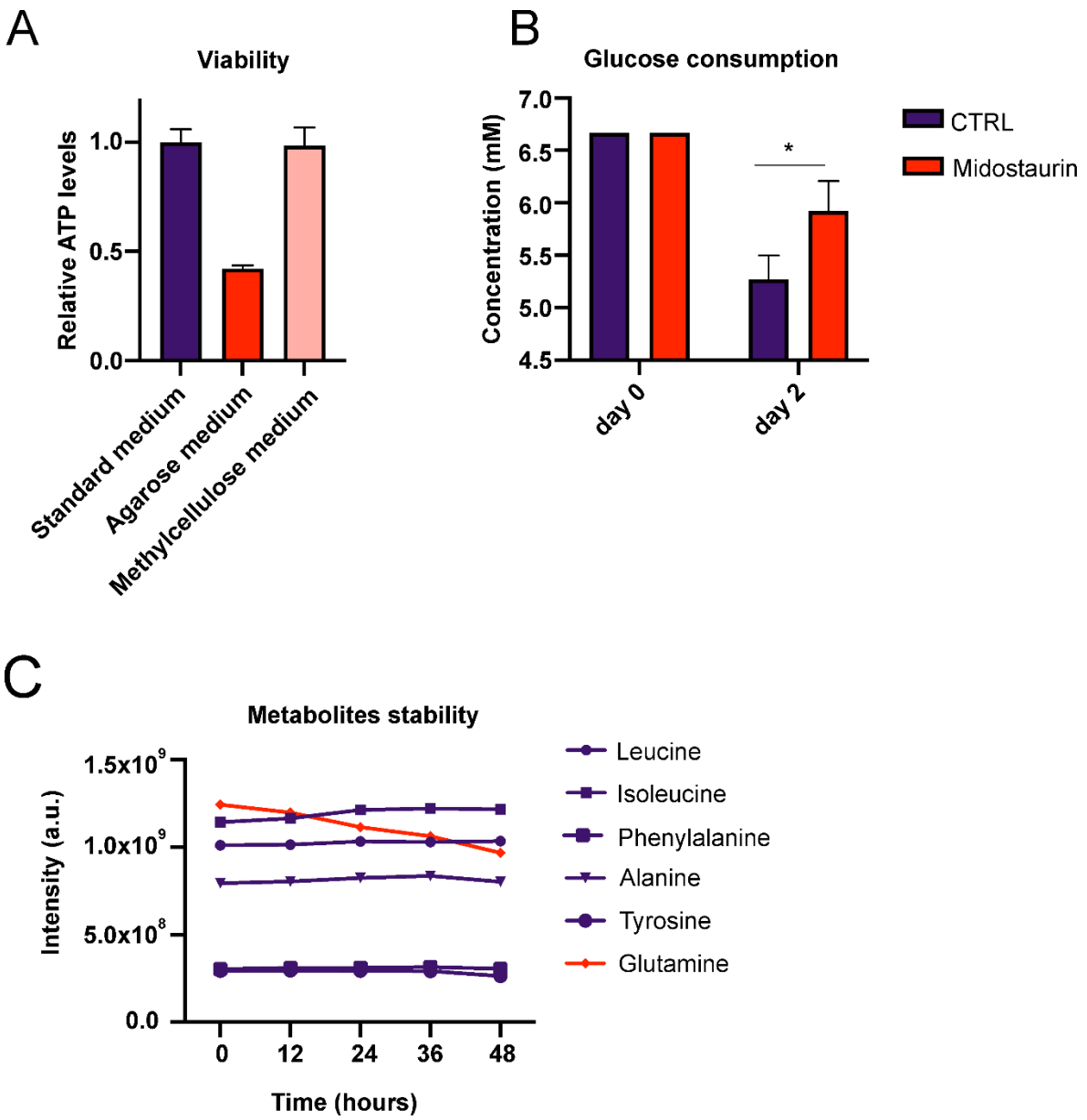


Figure 47: cell friendly nature of the new real-time NMR setup. A. Cellular viability of Molm13 cells when grown in standard medium *vs* agarose or methylcellulose-based medium (measured by total ATP levels). B. NMR measurements of glucose uptake upon treatment with 30 nM midostaurin (~ IC_{50}). Glucose levels indicated were measured in the media (extracellular glucose). C. Metabolites stability of a plain media sample (no cells) in the NMR tube over a period of 48 hours. Statistical analysis was performed using unpaired Student's t-test. P≤ 0.05.

In addition, metabolites stability was evaluated to investigate any undesired degradation within the setup. For this purpose, a plain methylcellulose media sample was measured every 12 hours over a period of 48 hours. No metabolites degradation was seen in any of the metabolites apart from glutamine (Figure 47C). Glutamine degradation however, is not due to our setup but rather to its instability as reported in literature (Heeneman et al., 1993; Jagušić et al., 2016) and will be addressed in detail in the discussion section.

To ensure the presence of physiological cell-friendly environment, we investigated both, oxygen availability and the pH of the media after 48 hours of sample preparation. Oxygen levels varied between (1.4-3.2 %) across the tube with the highest rates detected around the surface (12 %) (Figure 48A). These levels in general fall within the physiological bone marrow oxygen atmosphere (1-6 % O_2) (Fiegl et al., 2009; Harrison et al., 2002; Spencer et al., 2014). Similarly, pH levels fluctuated with 0.1 reduction from the standard pH value of fresh media (pH= 7.4) (Figure 48B). These pH values in fact are similar to normal blood pH (Singh et al., 2013). With all of these optimisations, a highly reliable approach was developed and can be used for more sophisticated and sensitive cellular systems, as described in the next section.

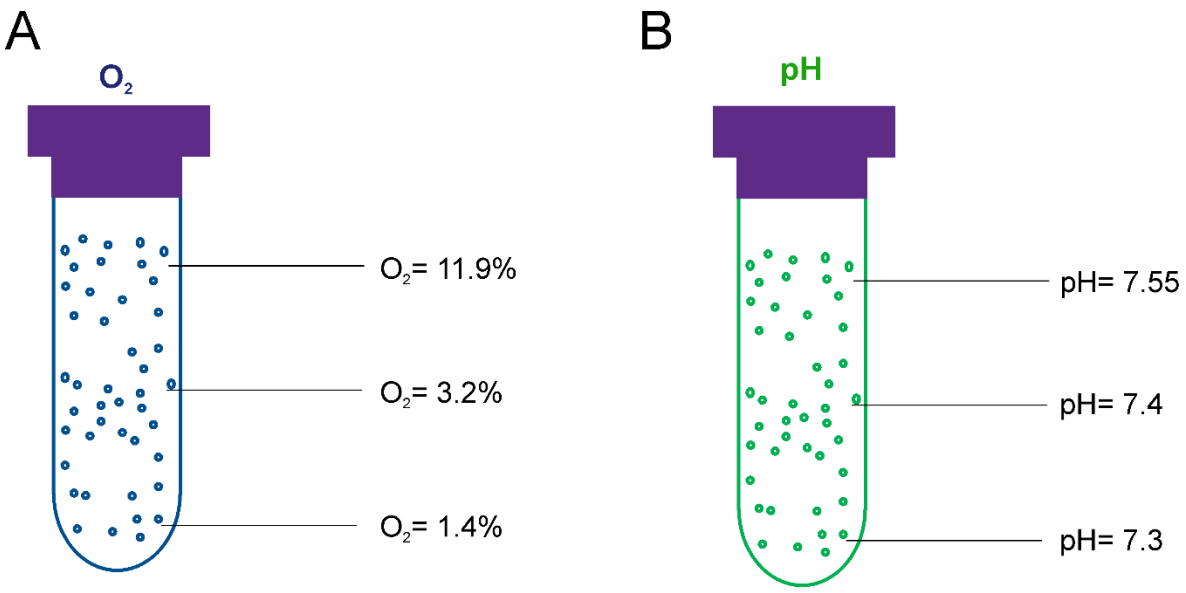


Figure 48: Physiological oxygen and pH levels present in the real-time NMR setup. A. Oxygen and B. pH levels measurements of real-time NMR samples 48 hours after preparation. Standard O_2 levels in cell culture media are around 12% and standard pH value is around 7.4 (Singh et al., 2013).

5.1.2. Application on sensitive cellular entities

With all these validations, this real-time NMR setup was considered suitable to provide reliable metabolic measurements. Hence, it was tested on primary mononuclear cells isolated from an AML patient's bone marrow. These cells are often difficult to maintain in culture without optimised cell culture conditions and require special supplementation. Interestingly, the primary AML blasts exerted normal metabolic activity. The cells grew and exchanged nutrients with the media. They consumed glucose and secreted lactate. As seen in (Figure 49), it was not only glycolytic activity, but the cells further consumed amino acids for energy production such as glutamine and alanine, branched chain amino acids for biosynthesis and DNA methylation and others. Similar to cell lines, low cell number was required (1 x 10^6 cells were used per sample to observe clearer rate changes). For ethical considerations in handling primary patient samples, only one sample was used as a proof of concept.

5.1.3. Incorporation of tracer-based assays

Lastly, to advance our approach as a fully robust metabolomics platform, it was enabled with a tracer-based assay. Considering the long measurement time required for a standard HSQC experiment (typically used for tracer-based assays), pseudo-2D filter experiments were implemented in order to speed up the acquisition time (Reed et al., 2019). Briefly, these experiments allow the differentiation between total protons and protons that are attached to ^{13}C atoms (see chapter 2.7.5). This allows to reduce the measurement time to around 7 minutes per sample and thus, retaining the real-time characteristics of this approach. Using uniformly-labelled ^{13}C glucose as a tracer, we followed the uptake of the tracer over a time course with recordings every 12 hours (Figure 50A). Label incorporation in downstream metabolites such as lactate (Figure 50B) and alanine (Figure 50C) was monitored upon their secretion to the media.

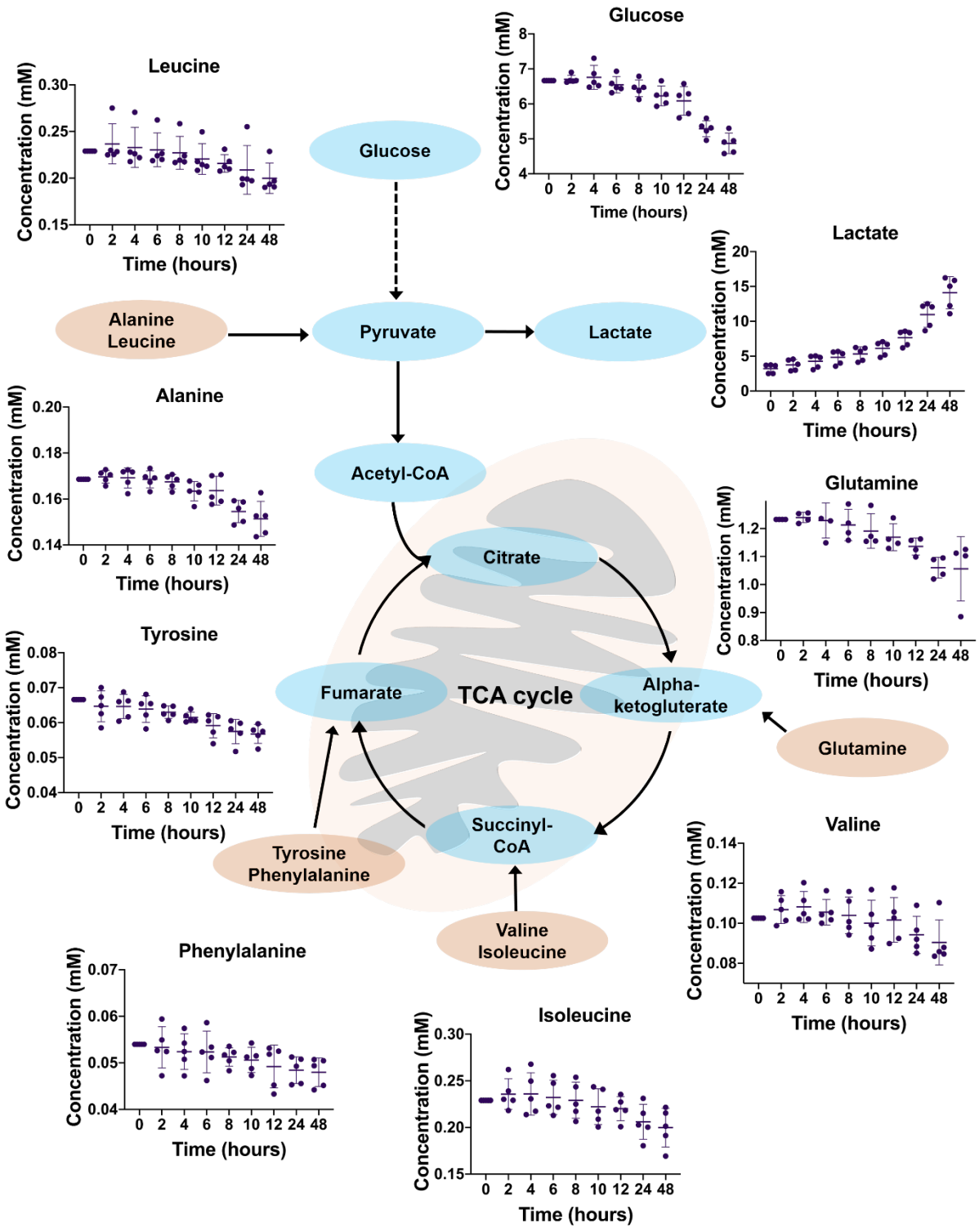


Figure 49: Time course measurements of extracellular metabolites dynamics of primary AML mononuclear cells. Intermediates of the core metabolic cycles such as glycolysis, TCA cycle and amino acids are plotted. (n=5 technical replicates). Adapted from the original publication (Alshamleh et al., 2020) (open access article and no licensing for reproduction is required).

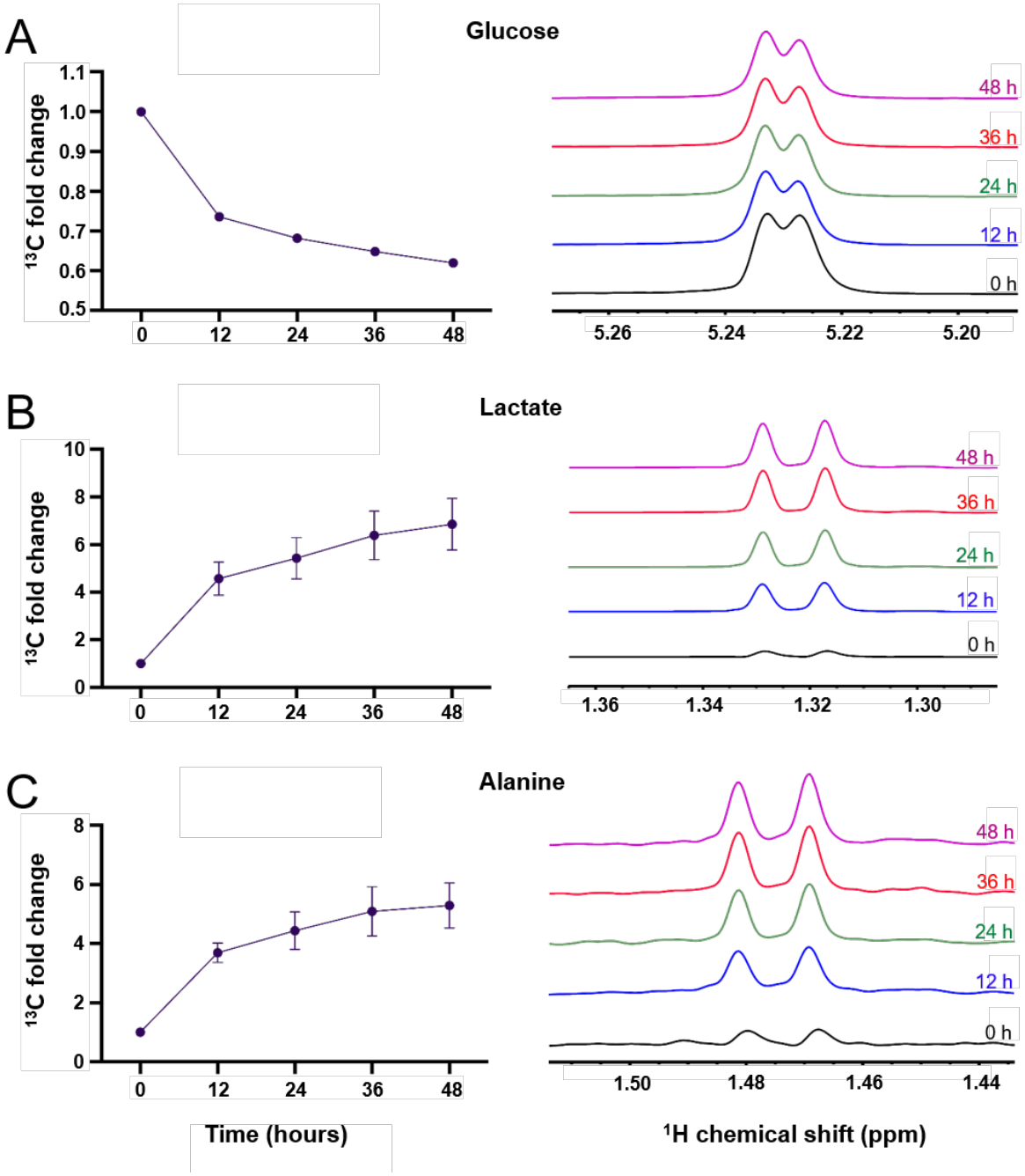


Figure 50: Tracer based assay with ^{13}C glucose. A. The figure shows the uptake of ^{13}C glucose into the cells (depicted by reduced extracellular levels). Fluxes are illustrated for label incorporation into B. lactate and C. Alanine. The corresponding spectra for each metabolite are also shown (Pseudo-2D experiments recorded with double GBIRD filter on a Bruker 600MHz AVIIIHD spectrometer at 27°C). Different scaling is applied for each metabolite. Adapted from the original publication (Alshamleh et al., 2020) (open access article and no licensing for reproduction is required).[10]

[10] Experiments in this chapter have been performed together with the bachelor student Nina Krause.

5.2. Discussion

Metabolomics studies have gained a significant research interest due to their contribution to understanding disease physiology. These studies mainly concern biomarker identification, metabolic fingerprinting, drug responses, quantitation of metabolites changes and pathway analysis. Nevertheless, in spite of the intensive research, only around 10% of the overall human metabolome has been explored and studied so far (according to the HMDB (Human Metabolome Data Base) (Wishart et al., 2007)). Further developments in metabolomics platforms and technology can help bridge this gap and enable more integrative metabolomics studies. Advances in NMR spectroscopy over the last years as a core metabolomics technique have boosted its applicability and reliability in studying biological processes. In-cell NMR approaches have been advanced and widely implemented for studying intracellular activities. This entitles structural and folding studies, ligand interactions, posttranslational modifications and others (Kang, 2019; Koczula et al., 2016; Luchinat and Banci, 2017; Lundberg and Kuchel, 1997). The ability to observe such processes intracellularly implicates a more physiological relevance of NMR studies. Nevertheless, not much of a progress has been made in the context of in-cell NMR and metabolism. This mostly owes to the liability of metabolic processes to the environmental stress induced by the experimental setup, a matter that has not been fully addressed in the in-cell NMR field. Developments in the experimental setups are needed to facilitate such implementation.

This doctoral thesis explored and built up on the already established in-cell NMR approaches for developing a state-of-the-art metabolomics platform with a non-invasive nature. By observing the influx of nutrients from the media and the extracellular efflux of metabolites over a time course, the metabolic activity of the cells could be determined. Although the introduced approach measures extracellular, but not intracellular, metabolites levels, it still reflects on the general cellular metabolism, considering the complementary homeostasis in the cells between metabolites uptake and excretion.

In comparison to the very few other approaches utilized in metabolomics studies such as mass spectrometry (MS) and seahorse, real-time NMR is superior in terms of applicability and detailed profiling provided. Unlike NMR, MS for example cannot be implemented for real-time kind of analysis due to the derivatization process required for sample measurement (Pan and Raftery, 2007; Takis et al., 2019). Furthermore, as opposed to seahorse technique, real-time NMR reports on the rates of the individual metabolite concentrations rather than measuring indirect general indicators such as oxygen consumption rate (OCR) (the readout of seahorse experiments) (Yépez et al., 2018). Not to mention, such indicators entitle some confounding

factors, with the example of extracellular acidification rate (ECAR) that measures the media acidification as a reporter of glycolysis/ lactate levels. This readout can be significantly obscured by CO_2 levels (constantly produced by several metabolic activities in the cell) (Mookerjee et al., 2015).

5.2.1. Bridging closer to physiological conditions

In the context of existing in-cell NMR approaches to study cellular processes, anticipating a cell friendly matrix where cells can reside unstressed remains a challenging aspect for studying metabolism. The current approach utilizes a cell-friendly substance, methylcellulose, as a matrix for the cells to prevent their sedimentation and aggregation in the NMR tube. The advantages of methylcellulose are reflected by its wide use for highly sensitive cells such as stem cells assays (Eaves and Lambie, 1995; Kaufman et al., 2001; Sarma et al., 2010). In fact, a simultaneously emerging report with the current thesis illustrated similar cell-friendly characteristics of methylcellulose in studying protein interactions (Mateos et al., 2020).

Methylcellulose was demonstrated to have no influence on cell growth or responses to stimuli. Superior to other approaches such as agarose (Foxall et al., 1984; Koczula et al., 2016), methylcellulose had no impact on the intracellular ATP pool. Furthermore, the active metabolites consumption rates suggest that methylcellulose does not affect metabolites diffusion or abundance (a disadvantage reported on agarose gels (Lundberg and Kuchel, 1997; Lundberg et al., 1992)).

To further assure a physiological microenvironment, pH and oxygen levels were monitored. No significant pH fluctuation in the samples was observed. This ruled out the need for CO_2 perfusion in the settings (usually present in cell culture incubators for pH maintenance). In fact, pH levels were within the normal range present in blood (Singh et al., 2013). Concerning oxygenation, no anoxic spots were detected, as oxygen was present across the different regions of the NMR tube. This was especially interesting because the distribution of oxygen in the tube was very similar to that of the bone marrow endosteal niche where leukemic cells reside (1.5-3%) (Fiegl et al., 2009; Spencer et al., 2014).

Metabolite stability was not compromised, with the only exception of glutamine. This however, is not due to the experimental settings but rather due to the unstable decomposing nature of glutamine into glutamate and ammonia, which is well documented in literature (Heeneman et al., 1993; Jagušić et al., 2016; Ozturk and Palsson, 1990). NMR reference (TMSP) and lock compounds utilized were shown in literature to be non-toxic at the used concentrations (Chun and Mun, 2015; Kwak et al., 2012).

The semi-physiological and cell friendly nature of this approach was reflected by the predictable cellular responses to interferences with signalling pathways. This was represented by the tested example of FLT3-inhibition where an expected blockade in glucose consumption was observed (as suggested by earlier findings (see chapter 3.1.7), also reported in literature (Gallipoli et al., 2018; Ju et al., 2017)).

Moreover, this approach enabled the maintenance of highly sensitive patient-derived primary AML mononuclear cells in the NMR tube viable for 48 hours with a stable and active metabolic behaviour (no fluctuations in the metabolic phenotype). The cells consumed glucose and excreted lactate. They consumed other amino acids as well, indicating the activity and functionality of essential pathways such as building blocks biosynthesis and DNA methylation activity. In fact, this is the first successful utilisation of NMR for studying metabolism of such bone marrow aspirates in a real-time manner.

5.2.2. Technicalities, applications and limitations

This approach overcomes the labour-intensive nature of standard in-cell NMR approaches. Technically, it is unique in terms of being fully automated in alternating the samples, inter-measurement storage and the setup of the time-course acquisition. This was achieved by installing a sample changer on the spectrometer that provides temperature control during storage and transport (37°C), an essential factor for a stable cellular metabolic activity.

The ability to do time-course measurements with this approach facilitates to observe the dynamicity of the metabolic processes in the cells over time. This can be especially helpful in cancer studies considering the rapid kinetics and fluctuation in metabolic processes and adaptions in the cells. Studying such processes using existing extraction protocols over a time course is highly demanding, labour intensive and time consuming. The capacity of this method to process 10-15 samples simultaneously qualifies it as a high-throughput technology for metabolomics studies. Therefore, real-time NMR can be highly suitable for implementation in personalised medicine and diagnostic settings.

Importantly, this approach is convenient in regards to handling low cell numbers, which can often be a problem when studying patient-derived samples. Often, these samples, such as AML blasts, are obtained with low numbers that are not enough to perform standard NMR metabolomic profiling (approximately 10 million cells are required (Kostidis et al., 2017; Saborano et al., 2019)). In addition, certain cells grow generally slower and hence, have low rates of metabolic processes/ activities. Therefore, higher cell numbers are needed to observe

such low pace activities. The current approach overcomes these obstacles with its capability to process as low as 5 x 10^5 cell (less than a tenth of the numbers required for the traditional approaches). It even allows to preserve those cells for further analyses or required diagnostic procedures. In fact, samples were successfully plated back in culture after the NMR experiments without affecting their viability or proliferation capacity.

Another important aspect of this approach lies in equipping it with a tracer-based assay. With a modified version of pseudo-2D double-filter experiments (Reed et al., 2019), ^{13}C levels could be calculated to assess the isotope fate within the different metabolic cycles in the cells. With the short measurement time required (7 minutes), this pulse sequence overcomes the issues associated with the long measurement time required for a standard HSQC experiment. Such long measurement time can undermine the real-time characteristics of this approach. These experiments were demonstrated on ^{13}C glucose as a tracer but can also be implemented with other tracers such as glutamine and alanine to study energy metabolism, aspartate to study building blocks biosynthesis or methionine/ branched-chain amino acids to study DNA methylation.

Nonetheless, some aspects remain to be improved to further bring real-time NMR from bench to bedside. A challenging aspect of this method lies in its inability to assess metabolites of the TCA cycle and mitochondrial metabolism which cannot cross the plasma membrane such as succinate and malate. Combining real-time NMR with other methods/ traditional NMR experiments that detect intracellular metabolites can be highly informative. Developing additional cell-friendly matrices/ NMR tubes that suit adherent cells will boost the universality of this approach. Finally, a very interesting addition in future research would be to implement it on co-cultures of different cell types or even organoids. This utilization will help studying cell-cell interactions and metabolites exchange.

Concluding remarks

PDP1 importance in FLT3-ITD-positive AML

The paramount significance of this PhD thesis stems from the effectively established strategy of metabolic targeting in AML based on the molecular background of the leukaemia. FLT3-ITD-positive AML cells were shown to depend on mitochondrial metabolism rather than the Warburg metabolism. This mitochondrial reliance translated into a strong susceptibility to a wide range of mitochondrial inhibitors. Combination of mitochondrial targeting and FLT3-inhibition shows strong synergism which can be of a clinical relevance.

Concerning the molecular players involved in this mitochondrial dependency, this thesis suggests that, unlike most other oncogenes, FLT3-ITD is a weak inducer of the Warburg effect. High PDP1 levels result in higher shuttling of pyruvate into the TCA cycle. PDP1 was verified as a targetable vulnerability in FLT3-ITD but not FLT3-WT AML. This targetability was proven *in vitro*, *ex vivo* and *in vivo*. Therapeutically, a combination of both, PDP1 suppression and FLT3-inhibition exerted a strong efficacy in eliminating the leukemic cells, suggesting therapeutic potentials.

Finally, PDP1 not only mediates energy production in FLT3-ITD cells, but also contributes to drug responses and can be exploited as a sensitising factor. Strikingly, targeting PDP1 restored the sensitivity to AC220 in cells from a patient with clinical resistance to AC220. Moreover, PDP1 allows for metabolic flexibility and enables cellular adaptions and proliferation capacity upon changes in oxygen conditions. Altogether, these findings indicate PDP1 to be a crucial safeguard of FLT3-ITD oncogenesis. Further research is needed to understand the mechanism by which FLT3-ITD mechanistically regulates PDP1 expression and function.

Methionine metabolism in AML

AML cells have a high level of dependence on methionine metabolism. Unlike healthy cells, the majority of methionine is utilised for methylation reactions and protein translation. Methionine restriction reduces histone and DNA methylation and RNA transcription activity. The special dependence on exogenous methionine is mainly attributed to the impaired recycling capacity of homocysteine to methionine in AML and further research is needed to address this aspect.

Real-time NMR

The current thesis presented a high throughput platform that allows for studying metabolism of living cellular systems. This approach is fully automated in terms of sample storage and time course measurements. This method enables for metabolism imaging in a real-time manner with a non-invasive nature. Methylcellulose was used as a cellular matrix due to its cell-friendly characteristics. The use of methylcellulose eliminated external stress impacting the cells, a common problem encountered by other materials described in literature. A main development here was the ability to sustain full viability and normal metabolic activity of the cells for over 48 hours. For the first time, NMR was demonstrated to be applicable to highly sensitive materials such as primary AML blasts. Furthermore, this new approach was enabled with isotope-tracing experiments for pathway analysis. Together, all these developments and optimisations boost NMR reliability and utilisation in the metabolomics field.

References

Abu-Duhier, F.M., Goodeve, A.C., Wilson, G.A., Care, R.S., Peake, I.R., and Reilly, J.T. (2001). Identification of novel FLT-3 Asp835 mutations in adult acute myeloid leukaemia. Br. J. Haematol. *113*, 983–988.
Adan, A., Alizada, G., Kiraz, Y., Baran, Y., and Nalbant, A. (2017). Flow cytometry: basic principles and applications. Crit. Rev. Biotechnol. *37*, 163–176.
Akella, N.M., Ciraku, L., and Reginato, M.J. (2019). Fueling the fire: emerging role of the hexosamine biosynthetic pathway in cancer. BMC Biol. *17*, 52.
Alshamleh, I., Krause, N., Richter, C., Kurrle, N., Serve, H., Günther, U.L., and Schwalbe, H. (2020). Real-Time NMR Spectroscopy for Studying Metabolism. Angew. Chemie Int. Ed. *59*, 2304–2308.
Ananieva, E. (2015). Targeting amino acid metabolism in cancer growth and anti-tumor immune response. World J. Biol. Chem. *6*, 281–289.
Ananieva, E.A., and Wilkinson, A.C. (2018). Branched-chain amino acid metabolism in cancer. Curr. Opin. Clin. Nutr. Metab. Care *21*, 64–70.
Ancey, P.B., Contat, C., and Meylan, E. (2018). Glucose transporters in cancer – from tumor cells to the tumor microenvironment. FEBS J. *285*, 2926–2943.
Arber, D.A., Orazi, A., Hasserjian, R., Thiele, J., Borowitz, M.J., Le Beau, M.M., Bloomfield, C.D., Cazzola, M., and Vardiman, J.W. (2016). The 2016 revision to the World Health Organization classification of myeloid neoplasms and acute leukemia. Blood *127*, 2391–2405.
Baccelli, I., Gareau, Y., Lehnertz, B., Gingras, S., Spinella, J.-F., Corneau, S., Mayotte, N., Girard, S., Frechette, M., Blouin-Chagnon, V., et al. (2019). Mubritinib targets the electron transport chain complex I and reveals the landscape of OXPHOS dependency in acute myeloid leukemia. Cancer Cell *36*, 84-99.e8.
Bacher, U., Haferlach, C., Kern, W., Haferlach, T., and Schnittger, S. (2008). Prognostic relevance of FLT3-TKD mutations in AML: the combination matters—an analysis of 3082 patients. Blood *111*, 2527–2537.
Bagger, F.O., Sasivarevic, D., Sohi, S.H., Laursen, L.G., Pundhir, S., Sønderby, C.K., Winther, O., Rapin, N., and Porse, B.T. (2016). BloodSpot: a database of gene expression profiles and transcriptional programs for healthy and malignant haematopoiesis. Nucleic Acids Res. *44*, D917-24.
Bagrintseva, K., Schwab, R., Kohl, T.M., Schnittger, S., Eichenlaub, S., Ellwart, J.W., Hiddemann, W., and Spiekermann, K. (2004). Mutations in the tyrosine kinase domain of FLT3 define a new molecular mechanism of acquired drug resistance to PTK inhibitors in FLT3-ITD–transformed hematopoietic cells. Blood *103*, 2266–2275.
Barna, J.C.J., Laue, E.D., Mayger, M.R., Skilling, J., and Worrall, S.J.P. (1987). Exponential sampling, an alternative method for sampling in two-dimensional NMR experiments. J. Magn. Reson. *73*, 69–77.
Behrens, K., Maul, K., Tekin, N., Kriebitzsch, N., Indenbirken, D., Prassolov, V., Müller, U., Serve, H., Cammenga, J., and Stocking, C. (2017). RUNX1 cooperates with FLT3-ITD to induce leukemia. J. Exp. Med. *214*, 737–752.
Beisenherz-Huss, C., Mundt, M., Herrala, A., Vihko, P., Schubert, A., and Groner, B. (2001). Specific DNA binding and transactivation potential of recombinant, purified Stat5. Mol. Cell. Endocrinol. *183*, 101–112.
Benekli, M., Baer, M.R., Baumann, H., and Wetzler, M. (2003). Signal transducer and activator of transcription proteins in leukemias. Blood *101*, 2940–2954.
Berenbaum, M.C. (1989). What is synergy? Pharmacol. Rev. *41*, 93 LP – 141.
Birsoy, K., Wang, T., Chen, W.W., Freinkman, E., Abu-Remaileh, M., and Sabatini, D.M. (2015). An essential role of the mitochondrial electron transport chain in cell proliferation is to enable sspartate synthesis. Cell *162*, 540–551.
Bloch, F., Hansen, W.W., and Packard, M. (1946). The Nuclear Induction Experiment. Phys. Rev. *70*, 474–485.

Bouatra, S., Aziat, F., Mandal, R., Guo, A.C., Wilson, M.R., Knox, C., Bjorndahl, T.C., Krishnamurthy, R., Saleem, F., Liu, P., et al. (2013). The Human Urine Metabolome. PLoS One *8*, e73076.
Brandts, C.H., Sargin, B., Rode, M., Biermann, C., Lindtner, B., Schwäble, J., Buerger, H., Müller-Tidow, C., Choudhary, C., McMahon, M., et al. (2005). Constitutive activation of Akt by Flt3 internal tandem duplications is necessary for increased survival, proliferation, and myeloid transformation. Cancer Res. *65*, 9643 LP – 9650.
Bromley-Dulfano, S., Demo, S., Janes, J., Gross, M., Lewis, E., MacKinnon, A., Rodriguez, M., Yang, J., Zhao, F., and Bennett, M. (2013). Antitumor activity of the glutaminase inhibitor CB-839 in hematological malignances. Blood *122*.
Von Bubnoff, N., Engh, R.A., Åberg, E., Sänger, J., Peschel, C., and Duyster, J. (2009). FMS-like tyrosine kinase 3-internal tandem duplication tyrosine kinase inhibitors display a nonoverlapping profile of resistance mutations in vitro. Cancer Res. *69*, 3032 LP – 3041.
Cancer Genome Atlas Research Network, Ley, T.J., Miller, C., Ding, L., Raphael, B.J., Mungall, A.J., Robertson, A.G., Hoadley, K., Triche, T.J., Laird, P.W., et al. (2013). Genomic and epigenomic landscapes of adult de novo acute myeloid leukemia. N. Engl. J. Med. *368*, 2059–2074.
Cantor, J.R., Abu-Remaileh, M., Kanarek, N., Freinkman, E., Gao, X., Louissaint Jr, A., Lewis, C.A., and Sabatini, D.M. (2017). Physiologic Medium Rewires Cellular Metabolism and Reveals Uric Acid as an Endogenous Inhibitor of UMP Synthase. Cell *169*, 258-272.e17.
Caro, P., Kishan, A.U., Norberg, E., Stanley, I.A., Chapuy, B., Ficarro, S.B., Polak, K., Tondera, D., Gounarides, J., Yin, H., et al. (2012). Metabolic Signatures Uncover Distinct Targets in Molecular Subsets of Diffuse Large B Cell Lymphoma. Cancer Cell *22*, 547–560.
Carrigan, J.B., Reed, M.A.C., Ludwig, C., Khanim, F.L., Bunce, C.M., and Günther, U.L. (2016). Tracer-Based Metabolic NMR-Based Flux Analysis in a Leukaemia Cell Line. Chempluschem *81*, 453–459.
Castro, I., Sampaio-Marques, B., and Ludovico, P. (2019). Targeting Metabolic Reprogramming in Acute Myeloid Leukemia. Cells *8*, 967.
Cerdan, S., and Seelig, J. (1990). NMR Studies of Metabolism. Annu. Rev. Biophys. Biophys. Chem. *19*, 43–67.
Chaneton, B., Hillmann, P., Zheng, L., Martin, A.C.L., Maddocks, O.D.K., Chokkathukalam, A., Coyle, J.E., Jankevics, A., Holding, F.P., Vousden, K.H., et al. (2012). Serine is a natural ligand and allosteric activator of pyruvate kinase M2. Nature *491*, 458–462.
Chao, Q., Sprankle, K.G., Grotzfeld, R.M., Lai, A.G., Carter, T.A., Velasco, A.M., Gunawardane, R.N., Cramer, M.D., Gardner, M.F., James, J., et al. (2009). Identification of N-(5-tert-Butyl-isoxazol-3-yl)-N′-{4-[7-(2-morpholin-4-yl-ethoxy)imidazo[2,1-b][1,3]benzothiazol-2-yl]phenyl}urea Dihydrochloride (AC220), a Uniquely Potent, Selective, and Efficacious FMS-Like Tyrosine Kinase-3 (FLT3) Inhibitor. J. Med. Chem. *52*, 7808–7816.
Chen, G., and Deng, X. (2018). Cell synchronization by double thymidine block. Bio-Protocol *8*, e2994.
Chen, J., Sadowski, H.B., Kohanski, R.A., and Wang, L.H. (1997). Stat5 is a physiological substrate of the insulin receptor. Proc. Natl. Acad. Sci. U. S. A. *94*, 2295–2300.
Chen, J., Guccini, I., Di Mitri, D., Brina, D., Revandkar, A., Sarti, M., Pasquini, E., Alajati, A., Pinton, S., Losa, M., et al. (2018). Compartmentalized activities of the pyruvate dehydrogenase complex sustain lipogenesis in prostate cancer. Nat. Genet. *50*, 219–228.
Chen, W.-L., Wang, J., Zhao, A.-H., Xu, X., Wang, Y.Y.Y.-Y.Y.-H., Chen, T., Li, J.-M.J.-Y.J., Mi, J.-Q., Zhu, Y.-M., Liu, Y.-F., et al. (2014). A distinct glucose metabolism signature of acute myeloid leukemia with prognostic value. Blood *124*, 1645–1654.
Chen, W.L., Wang, Y.Y., Zhao, A., Xia, L., Xie, G., Su, M., Zhao, L., Liu, J., Qu, C., Wei, R., et al. (2016). Enhanced fructose utilization mediated by SLC2A5 is a unique metabolic feature of acute myeloid leukemia with therapeutic potential. Cancer Cell *30*, 779–791.
Cheng, L.L., Burns, M.A., Taylor, J.L., He, W., Halpern, E.F., McDougal, W.S., and Wu, C.-L. (2005). Metabolic characterization of human prostate cancer with tissue magnetic resonance spectroscopy. Cancer Res. *65*, 3030 LP – 3034.
Choudhary, C., Schwäble, J., Brandts, C., Tickenbrock, L., Sargin, B., Kindler, T., Fischer, T.,

Berdel, W.E., Müller-Tidow, C., and Serve, H. (2005). AML-associated Flt3 kinase domain mutations show signal transduction differences compared with Flt3 ITD mutations. Blood *106*, 265–273.
Choudhary, C., Brandts, C., Schwable, J., Tickenbrock, L., Sargin, B., Ueker, A., Böhmer, F.-D., Berdel, W.E., Müller-Tidow, C., and Serve, H. (2007). Activation mechanisms of STAT5 by oncogenic Flt3-ITD. Blood *110*, 370 LP – 374.
Chun, S.-I., and Mun, C.-W. (2015). Cytotoxicity of TSP in 3D Agarose Gel Cultured Cell. PLoS One *10*, e0128739.
Chung, K.Y., Morrone, G., Schuringa, J.J., Wong, B., Dorn, D.C., and Moore, M.A.S. (2005). Enforced expression of an Flt3 internal tandem duplication in human CD34+ cells confers properties of self-renewal and enhanced erythropoiesis. Blood *105*, 77–84.
Cole, A., Wang, Z., Coyaud, E., Voisin, V., Gronda, M., Jitkova, Y., Mattson, R., Hurren, R., Babovic, S., Maclean, N., et al. (2015). Inhibition of the mitochondrial protease ClpP as a therapeutic strategy for human acute myeloid leukemia. Cancer Cell *27*, 864–876.
Conway O'Brien, E., Prideaux, S., and Chevassut, T. (2014). The Epigenetic Landscape of Acute Myeloid Leukemia. Adv. Hematol. *2014*, 103175.
Cools, J., Mentens, N., Furet, P., Fabbro, D., Clark, J.J., Griffin, J.D., Marynen, P., and Gilliland, D.G. (2004). Prediction of resistance to small molecule FLT3 inhibitors: implications for molecularly targeted therapy of acute leukemia. Cancer Res. *64*, 6385–6389.
Cortes, J.E., Kantarjian, H.M., Kadia, T.M., Borthakur, G., Konopleva, M., Garcia-Manero, G., Daver, N.G., Pemmaraju, N., Jabbour, E., Estrov, Z., et al. (2016). Crenolanib besylate, a type I pan-FLT3 inhibitor, to demonstrate clinical activity in multiply relapsed FLT3-ITD and D835 AML. J. Clin. Oncol. *34*, 7008.
Cortes, J.E., Tallman, M.S., Schiller, G.J., Trone, D., Gammon, G., Goldberg, S.L., Perl, A.E., Marie, J.-P., Martinelli, G., Kantarjian, H.M., et al. (2018). Phase 2b study of 2 dosing regimens of quizartinib monotherapy in FLT3-ITD–mutated, relapsed or refractory AML. Blood *132*, 598–607.
Daver, N., Cortes, J., Ravandi, F., Patel, K.P., Burger, J.A., Konopleva, M., and Kantarjian, H. (2015). Secondary mutations as mediators of resistance to targeted therapy in leukemia. Blood *125*, 3236–3245.
Daver, N., Pollyea, D.A., Rizzieri, D.A., Palmer, J., Rampal, R.K., Dinner, S., Bixby, D.L., Percival, M.-E.M., Kovacsovics, T., Begna, K.H., et al. (2017). A Phase I Study of FLX925, a Dual FLT3 and CDK4/6 Inhibitor in Patients with Relapsed or Refractory Acute Myeloid Leukemia (AML). Blood *130*, 1343.
Daver, N., Schlenk, R.F., Russell, N.H., and Levis, M.J. (2019). Targeting FLT3 mutations in AML: review of current knowledge and evidence. Leukemia *33*, 299–312.
DeBerardinis, R.J., and Chandel, N.S. (2020). We need to talk about the Warburg effect. Nat. Metab. *2*, 127–129.
Delaglio, F., Grzesiek, S., Vuister, G.W., Zhu, G., Pfeifer, J., and Bax, A. (1995). NMRPipe: A multidimensional spectral processing system based on UNIX pipes. J. Biomol. NMR *6*, 277–293.
deLapeyrière, O., Naquet, P., Planche, J., Marchetto, S., Rottapel, R., Gambarelli, D., Rosnet, O., and Birnbaum, D. (1995). Expression of Flt3 tyrosine kinase receptor gene in mouse hematopoietic and nervous tissues. Differentiation *58*, 351–359.
Demaison, C., Parsley, K., Brouns, G., Scherr, M., Battmer, K., Kinnon, C., Grez, M., and Thrasher, A.J. (2002). High-level transduction and gene expression in hematopoietic repopulating cells using a human imunodeficiency virus type 1-based lentiviral vector containing an internal spleen focus forming virus promoter. Hum. Gene Ther. *13*, 803–813.
Deschler, B., and Lübbert, M. (2006). Acute myeloid leukemia: Epidemiology and etiology. Cancer *107*, 2099–2107.
DiNardo, C.D., Pratz, K.W., Letai, A., Jonas, B.A., Wei, A.H., Thirman, M., Arellano, M., Frattini, M.G., Kantarjian, H., Popovic, R., et al. (2018). Safety and preliminary efficacy of venetoclax with decitabine or azacitidine in elderly patients with previously untreated acute myeloid leukaemia: a non-randomised, open-label, phase 1b study. Lancet Oncol. *19*, 216–228.

DiNardo, C.D., Pratz, K., Pullarkat, V., Jonas, B.A., Arellano, M., Becker, P.S., Frankfurt, O., Konopleva, M., Wei, A.H., Kantarjian, H.M., et al. (2019). Venetoclax combined with decitabine or azacitidine in treatment-naive, elderly patients with acute myeloid leukemia. Blood *133*, 7–17.
Döhner, H., Estey, E., Grimwade, D., Amadori, S., Appelbaum, F.R., Büchner, T., Dombret, H., Ebert, B.L., Fenaux, P., Larson, R.A., et al. (2017). Diagnosis and management of AML in adults: 2017 ELN recommendations from an international expert panel. Blood *129*, 424–447.
Dombret, H., and Gardin, C. (2016). An update of current treatments for adult acute myeloid leukemia. Blood *127*, 53–61.
Ducker, G.S., and Rabinowitz, J.D. (2017). One-Carbon Metabolism in Health and Disease. Cell Metab. *25*, 27–42.
Eakin, R.T., Morgan, L.O., Gregg, C.T., and Matwiyoff, N.A. (1972). Carbon-13 nuclear magnetic resonance spectroscopy of living cells and their metabolism of a specifically labeled 13C substrate. FEBS Lett. *28*, 259–264.
Eaves, C., and Lambie, K. (1995). Atlas of human hematopoietic colonies. STEMCELL technologies. Inc., Vancouver, BC.
Emwas, A.-H., Roy, R., McKay, R.T., Tenori, L., Saccenti, E., Gowda, G.A.N., Raftery, D., Alahmari, F., Jaremko, L., Jaremko, M., et al. (2019a). NMR Spectroscopy for Metabolomics Research. Metabolites *9*, 123.
Emwas, A.-H.M., Alghrably, M., Al-Harthi, S., Gabriel Poulson, B., Szczepski, K., Chandra, K., and Jaremko, M. (2019b). New Advances in Fast Methods of 2D NMR Experiments. Nucl. Magn. Reson. [Working Title].
Estey, E., and Döhner, H. (2006). Acute myeloid leukaemia. Lancet *368*, 1894–1907.
European Medicines Agency (2017). Rydapt midostaurin. *1*, 1–2.
Falini, B., Mecucci, C., Tiacci, E., Alcalay, M., Rosati, R., Pasqualucci, L., La Starza, R., Diverio, D., Colombo, E., Santucci, A., et al. (2005). Cytoplasmic Nucleophosmin in Acute Myelogenous Leukemia with a Normal Karyotype. N. Engl. J. Med. *352*, 254–266.
Fan, J., Shan, C., Kang, H.-B., Elf, S., Xie, J., Tucker, M., Gu, T.-L., Aguiar, M., Lonning, S., Chen, H., et al. (2014). Tyr phosphorylation of PDP1 toggles recruitment between ACAT1 and SIRT3 to regulate the pyruvate dehydrogenase complex. Mol. Cell *53*, 534–548.
Farber, S., and Diamond, L.K. (1948). Temporary remissions in acute leukemia in children produced by folic acid antagonist, 4-aminopteroyl-glutamic acid. N. Engl. J. Med. *238*, 787–793.
Farge, T., Saland, E., de Toni, F., Aroua, N., Hosseini, M., Perry, R., Bosc, C., Sugita, M., Stuani, L., Fraisse, M., et al. (2017). Chemotherapy-resistant human acute myeloid leukemia cells are not enriched for leukemic stem cells but require oxidative metabolism. Cancer Discov. *7*, 716–735.
Feng, H., Wang, X., Chen, J., Cui, J., Gao, T., Gao, Y., and Zeng, W. (2019). Nuclear imaging of glucose metabolism: beyond 18F-FDG. Contrast Media Mol. Imaging *2019*, 7954854.
Fiegl, M., Samudio, I., Clise-Dwyer, K., Burks, J.K., Mnjoyan, Z., and Andreeff, M. (2009). CXCR4 expression and biologic activity in acute myeloid leukemia are dependent on oxygen partial pressure. Blood *113*, 1504–1512.
Figueroa, M.E., Abdel-Wahab, O., Lu, C., Ward, P.S., Patel, J., Shih, A., Li, Y., Bhagwat, N., Vasanthakumar, A., Fernandez, H.F., et al. (2010). Leukemic IDH1 and IDH2 mutations result in a hypermethylation phenotype, disrupt TET2 function, and impair hematopoietic differentiation. Cancer Cell *18*, 553–567.
Fischer, T., Stone, R.M., DeAngelo, D.J., Galinsky, I., Estey, E., Lanza, C., Fox, E., Ehninger, G., Feldman, E.J., Schiller, G.J., et al. (2010). Phase IIB Trial of Oral Midostaurin (PKC412), the FMS-Like Tyrosine Kinase 3 Receptor (FLT3) and Multi-Targeted Kinase Inhibitor, in Patients With Acute Myeloid Leukemia and High-Risk Myelodysplastic Syndrome With Either Wild-Type or Mutated FLT3. J. Clin. Oncol. *28*, 4339–4345.
Fisher-Wellman, K.H., Lin, C.-T., Ryan, T.E., Reese, L.R., Gilliam, L.A.A., Cathey, B.L., Lark, D.S., Smith, C.D., Muoio, D.M., and Neufer, P.D. (2015). Pyruvate dehydrogenase complex and nicotinamide nucleotide transhydrogenase constitute an energy-consuming redox circuit. Biochem. J. *467*, 271–280.

Fletcher, L., Joshi, S.K., and Traer, E. (2020). Profile of Quizartinib for the Treatment of Adult Patients with Relapsed/Refractory FLT3-ITD-Positive Acute Myeloid Leukemia: Evidence to Date. Cancer Manag. Res. *12*, 151–163.
Foxall, D.L., Cohen, J.S., and Mitchell, J.B. (1984). Continuous perfusion of mammalian cells embedded in agarose gel threads. Exp. Cell Res. *154*, 521–529.
Gallipoli, P., Giotopoulos, G., Tzelepis, K., Costa, A.S.H., Vohra, S., Medina-Perez, P., Basheer, F., Marando, L., Lisio, L. Di, Dias, J.M.L., et al. (2018). Glutaminolysis is a metabolic dependency in FLT3ITDacute myeloid leukemia unmasked by FLT3 tyrosine kinase inhibition. Blood *131*, 1639–1653.
Garbow, J.R., Weitekamp, D.P., and Pines, A. (1982). Bilinear rotation decoupling of homonuclear scalar interactions. Chem. Phys. Lett. *93*, 504–509.
Gerner, E.W., and Meyskens, F.L. (2004). Polyamines and cancer: old molecules, new understanding. Nat. Rev. Cancer *4*, 781–792.
Goddard, Td., and Kneller, D.G. Sparky 3. Univ. California, San Fr.
Golman, K., in 't Zandt, R., and Thaning, M. (2006). Real-time metabolic imaging. Proc. Natl. Acad. Sci. *103*, 11270 LP – 11275.
Grafone, T., Palmisano, M., Nicci, C., and Storti, S. (2012). An overview on the role of FLT3-tyrosine kinase receptor in acute myeloid leukemia: biology and treatment. Oncol. Rev. *6*.
Greenblatt, S., Li, L., Slape, C., Nguyen, B., Novak, R., Duffield, A., Huso, D., Desiderio, S., Borowitz, M.J., Aplan, P., et al. (2012). Knock-in of a FLT3/ITD mutation cooperates with a NUP98-HOXD13 fusion to generate acute myeloid leukemia in a mouse model. Blood *119*, 2883–2894.
Gregory, M.A., Nemkov, T., Reisz, J.A., Zaberezhnyy, V., Hansen, K.C., D'Alessandro, A., and DeGregori, J. (2018a). Glutaminase inhibition improves FLT3 inhibitor therapy for acute myeloid leukemia. Exp. Hematol. *58*, 52–58.
Gregory, M.A., Nemkov, T., Zaberezhnyy, V., Park, H.J., Gehrke, S., Hansen, K.C., Alessandro, A.D., DeGregori, J., Zaberezhnvv, V., Gehrke, S., et al. (2018b). Targeting glutamine metabolism and redox state for leukemia therapy. Clin. Cancer Res. *25*, 4079–4090.
Griffith, J., Black, J., Faerman, C., Swenson, L., Wynn, M., Lu, F., Lippke, J., and Saxena, K. (2004). The Structural Basis for Autoinhibition of FLT3 by the Juxtamembrane Domain. Mol. Cell *13*, 169–178.
Gross, M.I., Demo, S.D., Dennison, J.B., Chen, L., Chernov-Rogan, T., Goyal, B., Janes, J.R., Laidig, G.J., Lewis, E.R., Li, J., et al. (2014). Antitumor activity of the glutaminase inhibitor CB-839 in triple-negative breast cancer. Mol. Cancer Ther. *13*, 890–901.
Gu, R., Yang, X., and Wei, H. (2018). Molecular landscape and targeted therapy of acute myeloid leukemia. Biomark. Res. *6*, 32.
Guennec, A. Le, Giraudeau, P., and Caldarelli, S. (2014). Evaluation of Fast 2D NMR for Metabolomics. Anal. Chem. *86*, 5946–5954.
Hannum, C., Culpepper, J., Campbell, D., McClanahan, T., Zurawski, S., Kastelein, R., Bazan, J.F., Hudak, S., Wagner, J., Mattson, J., et al. (1994). Ligand for FLT3/FLK2 receptor tyrosine kinase regulates growth of haematopoietic stem cells and is encoded by variant RNAs. Nature *368*, 643–648.
Hänsel, R., Foldynová-Trantírková, S., Löhr, F., Buck, J., Bongartz, E., Bamberg, E., Schwalbe, H., Dötsch, V., and Trantírek, L. (2009). Evaluation of parameters critical for observing nucleic acids inside living Xenopus laevis oocytes by in-cell NMR spectroscopy. J. Am. Chem. Soc. *131*, 15761–15768.
Hänsel, R., Löhr, F., Trantirek, L., and Dötsch, V. (2013). High-resolution insight into G-overhang architecture. J. Am. Chem. Soc. *135*, 2816–2824.
Hänsel, R., Luh, L.M., Corbeski, I., Trantirek, L., and Dötsch, V. (2014). In-cell NMR and EPR spectroscopy of biomacromolecules. Angew. Chemie Int. Ed. *53*, 10300–10314.
Haq, R., Shoag, J., Andreu-Perez, P., Yokoyama, S., Edelman, H., Rowe, G.C., Frederick, D.T., Hurley, A.D., Nellore, A., Kung, A.L., et al. (2013). Oncogenic BRAF Regulates Oxidative Metabolism via PGC1α and MITF. Cancer Cell *23*, 302–315.
Harris, R.K., Becker, E.D., Cabral de Menezes, S.M., Goodfellow, R., and Granger, P. (2002).

NMR Nomenclature: Nuclear Spin Properties and Conventions for Chemical Shifts: IUPAC Recommendations 2001. Solid State Nucl. Magn. Reson. *22*, 458–483.
Harrison, J.S., Rameshwar, P., Chang, V., and Bandari, P. (2002). Oxygen saturation in the bone marrow of healthy volunteers. Blood *99*, 394.
Hassanein, M., Almahayni, M.H., Ahmed, S.O., Gaballa, S., and El Fakih, R. (2016). FLT3 Inhibitors for Treating Acute Myeloid Leukemia. Clin. Lymphoma, Myeloma Leuk. *16*, 543–549.
Hay, N. (2016). Reprogramming glucose metabolism in cancer: Can it be exploited for cancer therapy? Nat. Rev. Cancer *16*, 635–649.
Heeneman, S., Deutz, N.E.P., and Buurman, W.A. (1993). The concentrations of glutamine and ammonia in commercially available cell culture media. J. Immunol. Methods *166*, 85–91.
Heidel, F., Solem, F.K., Breitenbuecher, F., Lipka, D.B., Kasper, S., Thiede, M.H., Brandts, C., Serve, H., Roesel, J., Giles, F., et al. (2006). Clinical resistance to the kinase inhibitor PKC412 in acute myeloid leukemia by mutation of Asn-676 in the FLT3 tyrosine kinase domain. Blood *107*, 293–300.
Vander Heiden, M.G., Cantley, L.C., and Thompson, C.B. (2009). Understanding the Warburg effect: the metabolic requirements of cell proliferation. Science (80-.). *324*, 1029 LP – 1033.
Heikkinen, S., and Kilpeläinen, I. (1999). Gradient BIRDR: a method to select uncoupled magnetization. J. Magn. Reson. *137*, 93–99.
Henkenius, K., Greene, B.H., Barckhausen, C., Hartmann, R., Marken, M., Kaiser, T., Rehberger, M., Metzelder, S.K., Parak, W.J., Neubauer, A., et al. (2017). Maintenance of cellular respiration indicates drug resistance in acute myeloid leukemia. Leuk. Res. *62*, 56–63.
Herst, P.M., Howman, R.A., Neeson, P.J., Berridge, M. V., and Ritchie, D.S. (2011). The level of glycolytic metabolism in acute myeloid leukemia blasts at diagnosis is prognostic for clinical outcome. J. Leukoc. Biol. *89*, 51–55.
Hiromasa, Y., Fujisawa, T., Aso, Y., and Roche, T.E. (2004). Organization of the cores of the mammalian pyruvate dehydrogenase complex formed by E2 and E2 plus the E3-binding protein and their capacities to bind the E1 and E3 components. J. Biol. Chem. *279*, 6921–6933.
Hitosugi, T., Fan, J., Chung, T.-W., Lythgoe, K., Wang, X., Xie, J., Ge, Q., Gu, T.-L., Polakiewicz, R.D., Roesel, J.L., et al. (2011). Tyrosine phosphorylation of mitochondrial pyruvate dehydrogenase kinase 1 is important for cancer metabolism. Mol. Cell *44*, 864–877.
Hoffman, R.M., Yano, S., and Igarashi, K. (2019). Methionine dependence of cancer and aging, methods and protocols.
Hoult, D.I., Busby, S.J.W., Gadian, D.G., Radda, G.K., Richards, R.E., and Seeley, P.J. (1974). Observation of tissue metabolites using 31P nuclear magnetic resonance. Nature *252*, 285–287.
Huang, A., Ju, H.-Q., Liu, K., Zhan, G., Liu, D., Wen, S., Garcia-Manero, G., Huang, P., and Hu, Y. (2016). Metabolic alterations and drug sensitivity of tyrosine kinase inhibitor resistant leukemia cells with a FLT3/ITD mutation. Cancer Lett. *377*, 149–157.
Hwang, T.L., and Shaka, A.J. (1995). Water suppression that works. Excitation sculpting using arbitrary wave-forms and pulsed-field gradients. J. Magn. Reson. Ser. A *112*, 275–279.
Ianevski, A., He, L., Aittokallio, T., and Tang, J. (2017). SynergyFinder: a web application for analyzing drug combination dose-response matrix data. Bioinformatics *33*, 2413–2415.
Ishikawa, F., Yoshida, S., Saito, Y., Hijikata, A., Kitamura, H., Tanaka, S., Nakamura, R., Tanaka, T., Tomiyama, H., Saito, N., et al. (2007). Chemotherapy-resistant human AML stem cells home to and engraft within the bone-marrow endosteal region. Nat. Biotechnol. *25*, 1315–1321.
Jacque, N., Ronchetti, A.M., Larrue, C., Meunier, G., Birsen, R., Willems, L., Saland, E., Decroocq, J., Maciel, T.T., Lambert, M., et al. (2015). Targeting glutaminolysis has antileukemic activity in acute myeloid leukemia and synergizes with BCL-2 inhibition. Blood *126*, 1346–1356.
Jagušić, M., Forčić, D., Brgles, M., Kutle, L., Šantak, M., Jergović, M., Kotarski, L., Bendelja, K., and Halassy, B. (2016). Stability of Minimum Essential Medium functionality despite L-

glutamine decomposition. Cytotechnology *68*, 1171–1183.
Jain, M., Nilsson, R., Sharma, S., Madhusudhan, N., Kitami, T., Souza, A.L., Kafri, R., Kirschner, M.W., Clish, C.B., and Mootha, V.K. (2012). Metabolite Profiling Identifies a Key Role for Glycine in Rapid Cancer Cell Proliferation. Science (80-.). *336*, 1040 LP – 1044.
Jeong, S., Eskandari, R., Park, S.M., Alvarez, J., Tee, S.S., Weissleder, R., Kharas, M.G., Lee, H., and Keshari, K.R. (2017). Real-time quantitative analysis of metabolic flux in live cells using a hyperpolarized micromagnetic resonance spectrometer. Sci. Adv. *3*, e1700341.
Jones, C.L., Stevens, B.M., D'Alessandro, A., Reisz, J.A., Culp-Hill, R., Nemkov, T., Pei, S., Khan, N., Adane, B., Ye, H., et al. (2018). Inhibition of amino acid metabolism selectively targets human leukemia stem cells. Cancer Cell *34*, 724-740.e4.
Jones, C.L., Stevens, B.M., D'Alessandro, A., Culp-Hill, R., Reisz, J.A., Pei, S., Gustafson, A., Khan, N., DeGregori, J., Pollyea, D.A., et al. (2019). Cysteine depletion targets leukemia stem cells through inhibition of electron transport complex II. Blood blood.2019898114.
Ju, H.-Q.Q., Zhan, G., Huang, A., Sun, Y., Wen, S., Yang, J., Lu, W.H., Xu, R.H., Li, J., Li, Y., et al. (2017). ITD mutation in FLT3 tyrosine kinase promotes Warburg effect and renders therapeutic sensitivity to glycolytic inhibition. Leukemia *31*, 2143–2150.
Kaelin Jr., W.G., and McKnight, S.L. (2013). Influence of Metabolism on Epigenetics and Disease. Cell *153*, 56–69.
Kaelin Jr, W.G. (2011). Cancer and altered metabolism: potential importance of hypoxia-inducible factor and 2-oxoglutarate-dependent dioxygenases. Cold Spring Harb. Symp. Quant. Biol. *76*, 335–345.
Kampa-Schittenhelm, K.M., Heinrich, M.C., Akmut, F., Döhner, H., Döhner, K., and Schittenhelm, M.M. (2013). Quizartinib (AC220) is a potent second generation class III tyrosine kinase inhibitor that displays a distinct inhibition profile against mutant-FLT3, -PDGFRA and -KIT isoforms. Mol. Cancer *12*, 19.
Kang, C. (2019). Applications of In-Cell NMR in Structural Biology and Drug Discovery. Int. J. Mol. Sci. *20*, 139.
Kaufman, D.S., Hanson, E.T., Lewis, R.L., Auerbach, R., and Thomson, J.A. (2001). Hematopoietic colony-forming cells derived from human embryonic stem cells. Proc. Natl. Acad. Sci. *98*, 10716 LP – 10721.
Keeler, J. (2011). Understanding NMR Spectroscopy (Wiley).
Kelly, L.M., and Gilliland, D.G. (2002). GENETICS OF MYELOID LEUKEMIAS. Annu. Rev. Genomics Hum. Genet. *3*, 179–198.
Keshet, R., Szlosarek, P., Carracedo, A., and Erez, A. (2018). Rewiring urea cycle metabolism in cancer to support anabolism. Nat. Rev. Cancer *18*, 634–645.
Kindler, T., Breitenbuecher, F., Kasper, S., Estey, E., Giles, F., Feldman, E., Ehninger, G., Schiller, G., Klimek, V., Nimer, S.D., et al. (2005). Identification of a novel activating mutation (Y842C) within the activation loop of FLT3 in patients with acute myeloid leukemia (AML). Blood *105*, 335–340.
Kiyoi, H., Towatari, M., Yokota, S., Hamaguchi, M., Ohno, R., Saito, H., and Naoe, T. (1998). Internal tandem duplication of the FLT3 gene is a novel modality of elongation mutation which causes constitutive activation of the product. Leukemia *12*, 1333–1337.
Kiyoi, H., Naoe, T., Nakano, Y., Yokota, S., Minami, S., Miyawaki, S., Asou, N., Kuriyama, K., Jinnai, I., Shimazaki, C., et al. (1999). Prognostic Implication of FLT3 and N-RAS Gene Mutations in Acute Myeloid Leukemia. Blood *93*, 3074–3080.
Kiyoi, H., Kawashima, N., and Ishikawa, Y. (2020). FLT3 mutations in acute myeloid leukemia: Therapeutic paradigm beyond inhibitor development. Cancer Sci. *111*, 312–322.
Koczula, K.M., Ludwig, C., Hayden, R., Cronin, L., Pratt, G., Parry, H., Tennant, D., Drayson, M., Bunce, C.M., Khanim, F.L., et al. (2016). Metabolic plasticity in CLL: adaptation to the hypoxic niche. Leukemia *30*, 65–73.
Koppenol, W.H., Bounds, P.L., and Dang, C. V (2011). Otto Warburg's contributions to current concepts of cancer metabolism. Nat. Rev. Cancer *11*, 325–337.
Kostidis, S., Addie, R.D., Morreau, H., Mayboroda, O.A., and Giera, M. (2017). Quantitative NMR analysis of intra- and extracellular metabolism of mammalian cells: A tutorial. Anal. Chim. Acta *980*, 1–24.

Kottaridis, P., Gale, R.E., and Linch, D.C. (2003). Flt3 mutations and leukaemia. Br. J. Haematol. *122*, 523–538.
Kottaridis, P.D., Gale, R.E., Frew, M.E., Harrison, G., Langabeer, S.E., Belton, A.A., Walker, H., Wheatley, K., Bowen, D.T., Burnett, A.K., et al. (2001). The presence of a FLT3 internal tandem duplication in patients with acute myeloid leukemia (AML) adds important prognostic information to cytogenetic risk group and response to the first cycle of chemotherapy: analysis of 854 patients from the United King. Blood *98*, 1752–1759.
Kreitz, J., Schönfeld, C., Seibert, M., Stolp, V., Alshamleh, I., Oellerich, T., Steffen, B., Schwalbe, H., Schnütgen, F., Kurrle, N., et al. (2019). Metabolic Plasticity of Acute Myeloid Leukemia. Cells *8*, 805.
Kwak, S.Y., Jang, M.Y., and Mun, C.W. (2012). Cytotoxicity evaluation of TSP and D2O in nuclear magnetic resonance spectroscopy. TISSUE Eng. Regen. Med. *9*, S81–S85.
Labuschagne, C.F., van den Broek, N.J.F., Mackay, G.M., Vousden, K.H., and Maddocks, O.D.K. (2014). Serine, but Not Glycine, Supports One-Carbon Metabolism and Proliferation of Cancer Cells. Cell Rep. *7*, 1248–1258.
Lagadinou, E.D., Sach, A., Callahan, K., Rossi, R.M., Neering, S.J., Minhajuddin, M., Ashton, J.M., Pei, S., Grose, V., O'Dwyer, K.M., et al. (2013). BCL-2 inhibition targets oxidative phosphorylation and selectively eradicates quiescent human leukemia stem cells. Cell Stem Cell *12*, 329–341.
Lane, S.W., Wang, Y.J., Lo Celso, C., Ragu, C., Bullinger, L., Sykes, S.M., Ferraro, F., Shterental, S., Lin, C.P., Gilliland, D.G., et al. (2011). Differential niche and Wnt requirements during acute myeloid leukemia progression. Blood *118*, 2849–2856.
Larrosa-Garcia, M., and Baer, M.R. (2017). FLT3 inhibitors in acute myeloid leukemia: current status and future directions. Mol. Cancer Ther. *16*, 991–1001.
Lee, K. min, Giltnane, J.M., Balko, J.M., Schwarz, L.J., Guerrero-Zotano, A.L., Hutchinson, K.E., Nixon, M.J., Estrada, M. V., Sánchez, V., Sanders, M.E., et al. (2017a). MYC and MCL1 cooperatively promote chemotherapy-resistant breast cancer stem cells via regulation of mitochondrial oxidative phosphorylation. Cell Metab. *26*, 633-647.e7.
Lee, L.Y., Hernandez, D., Rajkhowa, T., Smith, S.C., Raman, J.R., Nguyen, B., Small, D., and Levis, M. (2017b). Preclinical studies of gilteritinib, a next-generation FLT3 inhibitor. Blood *129*, 257–260.
Lehninger, A.L., Nelson, D.L., and Cox, M.M. (2005). Lehninger principles of biochemistry (New York: W.H. Freeman).
Letouzé, E., Martinelli, C., Loriot, C., Burnichon, N., Abermil, N., Ottolenghi, C., Janin, M., Menara, M., Nguyen, A.T., Benit, P., et al. (2013). SDH Mutations Establish a Hypermethylator Phenotype in Paraganglioma. Cancer Cell *23*, 739–752.
Levis, M., and Perl, A.E. (2020). Gilteritinib: potent targeting of FLT3 mutations in AML. Blood Adv. *4*, 1178–1191.
Levis, M., and Small, D. (2003). FLT3: ITDoes matter in leukemia. Leukemia *17*, 1738–1752.
Levis, M., Brown, P., Smith, B.D., Stine, A., Pham, R., Stone, R., DeAngelo, D., Galinsky, I., Giles, F., Estey, E., et al. (2006). Plasma inhibitory activity (PIA): a pharmacodynamic assay reveals insights into the basis for cytotoxic response to FLT3 inhibitors. Blood *108*, 3477–3483.
Levitt, M.H. (2001). Spin Dynamics: Basics of Nuclear Magnetic Resonance (Wiley).
Ley, T.J., Ding, L., Walter, M.J., McLellan, M.D., Lamprecht, T., Larson, D.E., Kandoth, C., Payton, J.E., Baty, J., Welch, J., et al. (2010). DNMT3A Mutations in Acute Myeloid Leukemia. N. Engl. J. Med. *363*, 2424–2433.
Li, Y., Shen, J., Cheng, C., Gao, H., Zhao, J., and Chen, L. (2020). Overexpression of pyruvate dehydrogenase phosphatase 1 promotes the progression of pancreatic adenocarcinoma by regulating energy-related AMPK/mTOR signaling. Cell Biosci. *10*, 95.
Liberti, M. V, and Locasale, J.W. (2016). The Warburg Effect: How Does it Benefit Cancer Cells? Trends Biochem. Sci. *41*, 211–218.
Lieu, E.L., Nguyen, T., Rhyne, S., and Kim, J. (2020). Amino acids in cancer. Exp. Mol. Med. *52*, 15–30.
Lindon, J.C., and Nicholson, J.K. (2008). Spectroscopic and Statistical Techniques for

Information Recovery in Metabonomics and Metabolomics. Annu. Rev. Anal. Chem. *1*, 45–69.
Lisker, B.Y., Brody, J., and Beiyer, L. (1966). Abnormal carbohydrate metabolism in patients with malignant blood dyscrasias. Am J Med Sci *252*, 282.
Liu, S.-B., Dong, H.-J., Bao, X.-B., Qiu, Q.-C., Li, H.-Z., Shen, H.-J., Ding, Z.-X., Wang, C., Chu, X.-L., Yu, J.-Q., et al. (2019). Impact of FLT3-ITD length on prognosis of acute myeloid leukemia. Haematologica *104*, e9 LP-e12.
Liu, S., Baker, J.C., and Roche, T.E. (1995). Binding of the pyruvate dehydrogenase kinase to recombinant constructs containing the inner lipoyl domain of the dihydrolipoyl acetyltransferase component. J. Biol. Chem. *270*, 793–800.
Liyanage, S.U., Hurren, R., Voisin, V., Bridon, G., Wang, X., Xu, C., MacLean, N., Siriwardena, T.P., Gronda, M., Yehudai, D., et al. (2017). Leveraging increased cytoplasmic nucleoside kinase activity to target mtDNA and oxidative phosphorylation in AML. Blood *129*, 2657–2666.
Locasale, J.W., and Cantley, L.C. (2011). Metabolic Flux and the Regulation of Mammalian Cell Growth. Cell Metab. *14*, 443–451.
Lohse, I., Statz-Geary, K., Brothers, S.P., and Wahlestedt, C. (2018). Precision medicine in the treatment stratification of AML patients: challenges and progress. Oncotarget *9*, 37790–37797.
Love, L.K., LeBlanc, P.J., Inglis, J.G., Bradley, N.S., Choptiany, J., Heigenhauser, G.J.F., and Peters, S.J. (2011). The relationship between human skeletal muscle pyruvate dehydrogenase phosphatase activity and muscle aerobic capacity. J. Appl. Physiol. *111*, 427–434.
Lu, C., Ward, P.S., Kapoor, G.S., Rohle, D., Turcan, S., Abdel-Wahab, O., Edwards, C.R., Khanin, R., Figueroa, M.E., Melnick, A., et al. (2012). IDH mutation impairs histone demethylation and results in a block to cell differentiation. Nature *483*, 474–478.
Luchinat, E., and Banci, L. (2017). In-cell NMR: a topical review. IUCrJ *4*, 108–118.
Ludwig, C., and Günther, U.L. (2011). MetaboLab - advanced NMR data processing and analysis for metabolomics. BMC Bioinformatics *12*, 366.
Lukey, M.J., Katt, W.P., and Cerione, R.A. (2017). Targeting amino acid metabolism for cancer therapy. Drug Discov. Today *22*, 796–804.
Lundberg, P., and Kuchel, P.W. (1997). Diffusion of solutes in agarose and alginate gels: 1H and 23Na PFGSE and 23Na TQF NMR studies. Magn. Reson. Med. *37*, 44–52.
Lundberg, P., Berners-Price, S.J., Roy, S., and Kuchel, P.W. (1992). NMR studies of erythrocytes immobilized in agarose and alginate gels. Magn. Reson. Med. *25*, 273–288.
Lyman, S.D., James, L., Bos, T. Vanden, de Vries, P., Brasel, K., Gliniak, B., Hollingsworth, L.T., Picha, K.S., McKenna, H.J., Splett, R.R., et al. (1993). Molecular cloning of a ligand for the flt3 flk-2 tyrosine kinase receptor: A proliferative factor for primitive hematopoietic cells. Cell *75*, 1157–1167.
Maddocks, O.D.K., Labuschagne, C.F., Adams, P.D., and Vousden, K.H. (2016). Serine Metabolism Supports the Methionine Cycle and DNA/RNA Methylation through De Novo ATP Synthesis in Cancer Cells. Mol. Cell *61*, 210–221.
Madji Hounoum, B., Blasco, H., Nadal-Desbarats, L., Diémé, B., Montigny, F., Andres, C.R., Emond, P., and Mavel, S. (2015). Analytical methodology for metabolomics study of adherent mammalian cells using NMR, GC-MS and LC-HRMS. Anal. Bioanal. Chem. *407*, 8861–8872.
Majumdar, R., Barchi, B., Turlapati, S.A., Gagne, M., Minocha, R., Long, S., and Minocha, S.C. (2016). Glutamate, Ornithine, Arginine, Proline, and Polyamine Metabolic Interactions: The Pathway Is Regulated at the Post-Transcriptional Level . Front. Plant Sci. *7*, 78.
Marlein, C.R., Zaitseva, L., Piddock, R.E., Robinson, S.D., Edwards, D.R., Shafat, M.S., Zhou, Z., Lawes, M., Bowles, K.M., and Rushworth, S.A. (2017). NADPH oxidase-2 derived superoxide drives mitochondrial transfer from bone marrow stromal cells to leukemic blasts.
Mateos, B., Sealey-Cardona, M., Balazs, K., Konrat, J., Staffler, G., and Konrat, R. (2020). NMR characterization of surface receptor protein interactions in live cells using methylcellulose hydrogels. Angew. Chem. Int. Ed. Engl. *59*, 3886–3890.
Matre, P., Velez, J., Jacamo, R., Qi, Y., Su, X.X.X.X.X., Cai, T., Chan, S.M., Lodi, A., Sweeney, S.R., Ma, H., et al. (2016). Inhibiting glutaminase in acute myeloid leukemia:

metabolic dependency of selected AML subtypes.
Maziarz, R.T., Patnaik, M.M., Scott, B.L., Mohan, S.R., Deol, A., Rowley, S.D., Kim, D.D.H., Haines, K., Bonifacio, G., Rine, P., et al. (2016). Radius: A Phase 2, Randomized Trial of Standard of Care (SOC) with or without Midostaurin to Prevent Relapse Following Allogeneic Hematopoietic Stem Cell Transplant (alloHSCT) in Patients (pts) with FLT3-Itd-Mutated Acute Myeloid Leukemia (AML). Blood *128*, 2248.
McHugh, C.E., Flott, T.L., Schooff, C.R., Smiley, Z., Puskarich, M.A., Myers, D.D., Younger, J.G., Jones, A.E., and Stringer, K.A. (2018). Rapid, Reproducible, Quantifiable NMR Metabolomics: Methanol and Methanol: Chloroform Precipitation for Removal of Macromolecules in Serum and Whole Blood. Metabolites *8*, 93.
Méndez-Ferrer, S., Bonnet, D., Steensma, D.P., Hasserjian, R.P., Ghobrial, I.M., Gribben, J.G., Andreeff, M., and Krause, D.S. (2020). Bone marrow niches in haematological malignancies. Nat. Rev. Cancer *20*, 285–298.
Mentch, S.J., Mehrmohamadi, M., Huang, L., Liu, X., Gupta, D., Mattocks, D., Gómez Padilla, P., Ables, G., Bamman, M.M., Thalacker-Mercer, A.E., et al. (2015). Histone Methylation Dynamics and Gene Regulation Occur through the Sensing of One-Carbon Metabolism. Cell Metab. *22*, 861–873.
Miraki-Moud, F., Ghazaly, E., Ariza-McNaughton, L., Hodby, K.A., Clear, A., Anjos-Afonso, F., Liapis, K., Grantham, M., Sohrabi, F., Cavenagh, J., et al. (2015). Arginine deprivation using pegylated arginine deiminase has activity against primary acute myeloid leukemia cells in vivo. Blood *125*, 4060–4068.
Mizuki, M., Fenski, R., Halfter, H., Matsumura, I., Schmidt, R., Müller, C., Grüning, W., Kratz-Albers, K., Serve, S., Steur, C., et al. (2000). Flt3 mutations from patients with acute myeloid leukemia induce transformation of 32D cells mediated by the Ras and STAT5 pathways. Blood *96*, 3907–3914.
Mizuki, M., Schwable, J., Steur, C., Choudhary, C., Agrawal, S., Sargin, B., Steffen, B., Matsumura, I., Kanakura, Y., Bohmer, F.D., et al. (2003). Suppression of myeloid transcription factors and induction of STAT response genes by AML-specific Flt3 mutations. Blood *101*, 3164–3173.
Moffatt, B.A., and Ashihara, H. (2002). Purine and pyrimidine nucleotide synthesis and metabolism. Arab. B. *1*, e0018–e0018.
Molina, J.R., Sun, Y., Protopopova, M., Gera, S., Bandi, M., Bristow, C., Mcafoos, T., Morlacchi, P., Ackroyd, J., Agip, A.A., et al. (2018). An inhibitor of oxidative phosphorylation exploits cancer vulnerability. Nat. Med. *24*.
Mookerjee, S.A., Goncalves, R.L.S., Gerencser, A.A., Nicholls, D.G., and Brand, M.D. (2015). The contributions of respiration and glycolysis to extracellular acid production. Biochim. Biophys. Acta - Bioenerg. *1847*, 171–181.
Moschoi, R., Imbert, V., Nebout, M., Chiche, J., Mary, D., Prebet, T., Saland, E., Castellano, R., Pouyet, L., Collette, Y., et al. (2016). Protective mitochondrial transfer from bone marrow stromal cells to acute myeloid leukemic cells during chemotherapy. Blood *128*, 253–264.
Motta, A., Paris, D., and Melck, D. (2010). Monitoring Real-Time Metabolism of Living Cells by Fast Two-Dimensional NMR Spectroscopy. Anal. Chem. *82*, 2405–2411.
Murata, K., Kumagai, H., Kawashima, T., Tamitsu, K., Irie, M., Nakajima, H., Suzu, S., Shibuya, M., Kamihira, S., Nosaka, T., et al. (2003). Selective cytotoxic mechanism of GTP-14564, a novel tyrosine kinase inhibitor in leukemia cells expressing a constitutively active Fms-like tyrosine kinase 3 (FLT3). J. Biol. Chem. *278*, 32892–32898.
Musharraf, S.G., Siddiqui, A.J., Shamsi, T., Choudhary, M.I., and Rahman, A.-U. (2016). Serum metabonomics of acute leukemia using nuclear magnetic resonance spectroscopy. Sci. Rep. *6*, 30693.
Mussai, F., Egan, S., Higginbotham-Jones, J., Perry, T., Beggs, A., Odintsova, E., Loke, J., Pratt, G., U, K.P., Lo, A., et al. (2015a). Arginine dependence of acute myeloid leukemia blast proliferation: a novel therapeutic target. Blood *125*, 2386–2396.
Mussai, F.J., Booth, S., Vardon, A., Ng, M., Cheng, P., and De Santo, C. (2015b). Cytotoxicity of the recombinant human arginase (BCT-100) against acute lymphoblastic leukaemia (ALL). Blood *126*, 4916.

Nagel, G., Weber, D., Fromm, E., Erhardt, S., Lübbert, M., Fiedler, W., Kindler, T., Krauter, J., Brossart, P., Kündgen, A., et al. (2017). Epidemiological, genetic, and clinical characterization by age of newly diagnosed acute myeloid leukemia based on an academic population-based registry study (AMLSG BiO). Ann. Hematol. *96*, 1993–2003.
Nahon, P., Amathieu, R., Triba, M.N., Bouchemal, N., Nault, J.-C., Ziol, M., Seror, O., Dhonneur, G., Trinchet, J.-C., Beaugrand, M., et al. (2012). Identification of serum proton NMR metabolomic fingerprints associated with hepatocellular carcinoma in patients with alcoholic cirrhosis. Clin. Cancer Res. *18*, 6714 LP – 6722.
Nakao, M., Yokota, S., Iwai, T., Kaneko, H., Horiike, S., Kashima, K., Sonoda, Y., Fujimoto, T., and Misawa, S. (1996). Internal tandem duplication of the flt3 gene found in acute myeloid leukemia. Leukemia *10*, 1911–1918.
Napoli, C., Sperandio, N., Lawlor, R.T., Scarpa, A., Molinari, H., and Assfalg, M. (2012). Urine Metabolic Signature of Pancreatic Ductal Adenocarcinoma by 1H Nuclear Magnetic Resonance: Identification, Mapping, and Evolution. J. Proteome Res. *11*, 1274–1283.
Narasimhan, S., Folkers, G.E., and Baldus, M. (2020). When Small becomes Too Big: Expanding the Use of In-Cell Solid-State NMR Spectroscopy. Chempluschem *85*, 760–768.
Newman, A.C., and Maddocks, O.D.K. (2017). One-carbon metabolism in cancer. Br. J. Cancer *116*, 1499–1504.
Nicholson, J.K., O'Flynn, M.P., Sadler, P.J., Macleod, A.F., Juul, S.M., and Sönksen, P.H. (1984). Proton-nuclear-magnetic-resonance studies of serum, plasma and urine from fasting normal and diabetic subjects. Biochem. J. *217*, 365–375.
Nordsmark, M., Overgaard, M., and Overgaard, J. (1996). Pretreatment oxygenation predicts radiation response in advanced squamous cell carcinoma of the head and neck. Radiother. Oncol. *41*, 31–39.
Ozturk, S.S., and Palsson, B.O. (1990). Chemical Decomposition of Glutamine in Cell Culture Media: Effect of Media Type, pH, and Serum Concentration. Biotechnol. Prog. *6*, 121–128.
Pan, Z., and Raftery, D. (2007). Comparing and combining NMR spectroscopy and mass spectrometry in metabolomics. Anal. Bioanal. Chem.
Papaemmanuil, E., Gerstung, M., Bullinger, L., Gaidzik, V.I., Paschka, P., Roberts, N.D., Potter, N.E., Heuser, M., Thol, F., Bolli, N., et al. (2016). Genomic classification and prognosis in acute myeloid leukemia. N. Engl. J. Med. *374*, 2209–2221.
Pardee, T.S., Anderson, R.G., Pladna, K.M., Isom, S., Ghiraldeli, L.P., Miller, L.D., Chou, J.W., Jin, G., Zhang, W., Ellis, L.R., et al. (2018). A phase I study of CPI-613 in combination with high-dose cytarabine and mitoxantrone for relapsed or refractory acute myeloid leukemia. Clin. Cancer Res. *24*, 2060–2073.
Park, S.-M., Cho, H., Thornton, A.M., Barlowe, T.S., Chou, T., Chhangawala, S., Fairchild, L., Taggart, J., Chow, A., Schurer, A., et al. (2019). IKZF2 Drives Leukemia Stem Cell Self-Renewal and Inhibits Myeloid Differentiation. Cell Stem Cell *24*, 153-165.e7.
Passegué, E., Jamieson, C.H.M., Ailles, L.E., and Weissman, I.L. (2003). Normal and leukemic hematopoiesis: Are leukemias a stem cell disorder or a reacquisition of stem cell characteristics? Proc. Natl. Acad. Sci. *100*, 11842 LP – 11849.
Patel, M.S., and Korotchkina, L.G. (2001). Regulation of mammalian pyruvate dehydrogenase complex by phosphorylation: complexity of multiple phosphorylation sites and kinases. Exp. Mol. Med. *33*, 191–197.
Patti, G.J., Yanes, O., and Siuzdak, G. (2012). Metabolomics: the apogee of the omics trilogy. Nat. Rev. Mol. Cell Biol. *13*, 263–269.
Percival, B.C., Grootveld, M., Gibson, M., Osman, Y., Molinari, M., Jafari, F., Sahota, T., Martin, M., Casanova, F., Mather, M.L., et al. (2018). Low-Field, Benchtop NMR Spectroscopy as a Potential Tool for Point-of-Care Diagnostics of Metabolic Conditions: Validation, Protocols and Computational Models. High-Throughput *8*, 2.
Perl, A.E., Altman, J.K., Cortes, J., Smith, C., Litzow, M., Baer, M.R., Claxton, D., Erba, H.P., Gill, S., Goldberg, S., et al. (2017). Selective inhibition of FLT3 by gilteritinib in relapsed or refractory acute myeloid leukaemia: a multicentre, first-in-human, open-label, phase 1–2 study. Lancet Oncol. *18*, 1061–1075.
Pikman, Y., Puissant, A., Alexe, G., Furman, A., Chen, L.M., Frumm, S.M., Ross, L., Fenouille,

N., Bassil, C.F., Lewis, C.A., et al. (2016). Targeting MTHFD2 in acute myeloid leukemia. J. Exp. Med. *213*, 1285–1306.
Piloto, O., Wright, M., Brown, P., Kim, K.-T., Levis, M., and Small, D. (2006). Prolonged exposure to FLT3 inhibitors leads to resistance via activation of parallel signaling pathways. Blood *109*, 1643–1652.
Pollyea, D.A., Stevens, B.M., Jones, C.L., Winters, A., Pei, S., Minhajuddin, M., D'Alessandro, A., Culp-Hill, R., Riemondy, K.A., Gillen, A.E., et al. (2018). Venetoclax with azacitidine disrupts energy metabolism and targets leukemia stem cells in patients with acute myeloid leukemia. Nat. Med. 1.
Purcell, E.M., Torrey, H.C., and Pound, R. V (1946). Resonance Absorption by Nuclear Magnetic Moments in a Solid. Phys. Rev. *69*, 37–38.
Raffel, S., Falcone, M., Kneisel, N., Hansson, J., Wang, W., Lutz, C., Bullinger, L., Poschet, G., Nonnenmacher, Y., Barnert, A., et al. (2017). BCAT1 restricts αKG levels in AML stem cells leading to IDHmut-like DNA hypermethylation. Nature *551*, 384–388.
Randhawa, J.K., Kantarjian, H.M., Borthakur, G., Thompson, P.A., Konopleva, M., Daver, N., Pemmaraju, N., Jabbour, E., Kadia, T.M., Estrov, Z., et al. (2014). Results of a Phase II Study of Crenolanib in Relapsed/Refractory Acute Myeloid Leukemia Patients (Pts) with Activating FLT3 Mutations. Blood *124*, 389.
Reckzeh, K., Bereshchenko, O., Mead, A., Rehn, M., Kharazi, S., Jacobsen, S.-E., Nerlov, C., and Cammenga, J. (2012). Molecular and cellular effects of oncogene cooperation in a genetically accurate AML mouse model. Leukemia *26*, 1527–1536.
Reed, G.A., Schiller, G.J., Kambhampati, S., Tallman, M.S., Douer, D., Minden, M.D., Yee, K.W., Gupta, V., Brandwein, J., Jitkova, Y., et al. (2016). A Phase 1 study of intravenous infusions of tigecycline in patients with acute myeloid leukemia. Cancer Med. *5*, 3031–3040.
Reed, M.A.C., Roberts, J., Gierth, P., Kupče, Ē., and Günther, U.L. (2019). Quantitative Isotopomer Rates in Real-Time Metabolism of Cells Determined by NMR Methods. ChemBioChem *20*, 2207–2211.
Roca-Portoles, A., Rodriguez-Blanco, G., Sumpton, D., Cloix, C., Mullin, M., Mackay, G.M., O'Neill, K., Lemgruber, L., Luo, X., and Tait, S.W.G. (2020). Venetoclax causes metabolic reprogramming independent of BCL-2 inhibition. Cell Death Dis. *11*, 616.
Roche, T.E., Baker, J.C., Yan, X., Hiromasa, Y., Gong, X., Peng, T., Dong, J., Turkan, A., and Kasten, S.A. (2001). Distinct regulatory properties of pyruvate dehydrogenase kinase and phosphatase isoforms. Prog. Nucleic Acid Res. Mol. Biol. *70*, 33–75.
Rocnik, J.L., Okabe, R., Yu, J.-C., Lee, B.H., Giese, N., Schenkein, D.P., and Gilliland, D.G. (2006). Roles of tyrosine 589 and 591 in STAT5 activation and transformation mediated by FLT3-ITD. Blood *108*, 1339–1345.
Rosnet, O., Matteï, M.-G., Marchetto, S., and Birnbaum, D. (1991). Isolation and chromosomal localization of a novel FMS-like tyrosine kinase gene. Genomics *9*, 380–385.
Rytelewski, M., Harutyunyan, K., Baran, N., Mallampati, S., Zal, M.A., Cavazos, A., Butler, J.M., Konoplev, S., El Khatib, M., Plunkett, S., et al. (2020). Inhibition of oxidative phosphorylation reverses bone marrow hypoxia visualized in imageable syngeneic B-ALL mouse model. Front. Oncol. *10*, 991.
Saborano, R., Eraslan, Z., Roberts, J., Khanim, F.L., Lalor, P.F., Reed, M.A.C., and Günther, U.L. (2019). A framework for tracer-based metabolism in mammalian cells by NMR. Sci. Rep. *9*, 2520.
Sakai, T., Tochio, H., Tenno, T., Ito, Y., Kokubo, T., Hiroaki, H., and Shirakawa, M. (2006). In-cell NMR spectroscopy of proteins inside Xenopus laevis oocytes. J. Biomol. NMR *36*, 179–188.
Sakakibara, D., Sasaki, A., Ikeya, T., Hamatsu, J., Hanashima, T., Mishima, M., Yoshimasu, M., Hayashi, N., Mikawa, T., Wälchli, M., et al. (2009). Protein structure determination in living cells by in-cell NMR spectroscopy. Nature *458*, 102–105.
Sarma, N.J., Takeda, A., and Yaseen, N.R. (2010). Colony forming cell (CFC) assay for human hematopoietic cells. JoVE e2195.
Schlenk, R.F. (2014). Post-remission therapy for acute myeloid leukemia. Haematologica *99*, 1663 LP – 1670.

Schlenk, R., Döhner, K., Salih, H., Kündgen, A., Fiedler, W., Salwender, H.-J., Westermann, J., Götze, K.S., Horst, H.-A., Wulf, G., et al. (2015). Midostaurin in Combination with Intensive Induction and As Single Agent Maintenance Therapy after Consolidation Therapy with Allogeneic Hematopoietic Stem Cell Transplantation or High-Dose Cytarabine (NCT01477606). Blood *126*, 322.
Schnittger, S., Schoch, C., Dugas, M., Kern, W., Staib, P., Wuchter, C., Löffler, H., Sauerland, C.M., Serve, H., Büchner, T., et al. (2002). Analysis of FLT3 length mutations in 1003 patients with acute myeloid leukemia: correlation to cytogenetics, FAB subtype, and prognosis in the AMLCG study and usefulness as a marker for the detection of minimal residual disease: Presented in part at the 4. Blood *100*, 59–66.
Serber, Z., Keatinge-Clay, A.T., Ledwidge, R., Kelly, A.E., Miller, S.M., and Dötsch, V. (2001). High-Resolution Macromolecular NMR Spectroscopy Inside Living Cells. J. Am. Chem. Soc. *123*, 2446–2447.
Sexauer, A., Perl, A., Yang, X., Borowitz, M., Gocke, C., Rajkhowa, T., Thiede, C., Frattini, M., Nybakken, G.E., Pratz, K., et al. (2012). Terminal myeloid differentiation in vivo is induced by FLT3 inhibition in FLT3/ITD AML. Blood *120*, 4205–4214.
Shan, C., Kang, H.-B., Elf, S., Xie, J., Gu, T.-L., Aguiar, M., Lonning, S., Hitosugi, T., Chung, T.-W., Arellano, M., et al. (2014). Tyr-94 phosphorylation inhibits pyruvate dehydrogenase phosphatase 1 and promotes tumor growth. J. Biol. Chem. *289*, 21413–21422.
Shen, B., Huang, T., Sun, Y., Jin, Z., and Li, X.-F. (2017). Revisit 18F-fluorodeoxyglucose oncology positron emission tomography: “systems molecular imaging” of glucose metabolism. Oncotarget *8*, 43536–43542.
Shestov, A.A., Liu, X., Ser, Z., Cluntun, A.A., Hung, Y.P., Huang, L., Kim, D., Le, A., Yellen, G., Albeck, J.G., et al. (2014). Quantitative determinants of aerobic glycolysis identify flux through the enzyme GAPDH as a limiting step. Elife *3*, e03342.
Shih, A.H., Abdel-Wahab, O., Patel, J.P., and Levine, R.L. (2012). The role of mutations in epigenetic regulators in myeloid malignancies. Nat. Rev. Cancer *12*, 599–612.
Shiraki, N., Shiraki, Y., Tsuyama, T., Obata, F., Miura, M., Nagae, G., Aburatani, H., Kume, K., Endo, F., and Kume, S. (2014). Methionine metabolism regulates maintenance and differentiation of human pluripotent stem cells. Cell Metab. *19*, 780–794.
Shulman, R.G., Brown, T.R., Ugurbil, K., Ogawa, S., Cohen, S.M., and den Hollander, J.A. (1979). Cellular applications of 31P and 13C nuclear magnetic resonance. Science (80-.). *205*, 160 LP – 166.
Shyh-Chang, N., Locasale, J.W., Lyssiotis, C.A., Zheng, Y., Teo, R.Y., Ratanasirintrawoot, S., Zhang, J., Onder, T., Unternaehrer, J.J., Zhu, H., et al. (2013). Influence of threonine metabolism on S-adenosylmethionine and histone methylation. Science *339*, 222–226.
Singh, V., Khatana, S., and Gupta, P. (2013). Blood gas analysis for bedside diagnosis. Natl. J. Maxillofac. Surg. *4*, 136–141.
Skoda, J., Borankova, K., Jansson, P.J., Huang, M.L.H., Veselska, R., and Richardson, D.R. (2019). Pharmacological targeting of mitochondria in cancer stem cells: An ancient organelle at the crossroad of novel anti-cancer therapies. Pharmacol. Res. *139*, 298–313.
Skrtic, M., Sriskanthadevan, S., Jhas, B., Gebbia, M., Wang, X., Wang, Z., Hurren, R., Jitkova, Y., Gronda, M., Maclean, N., et al. (2011). Inhibition of mitochondrial translation as a therapeutic strategy for human acute myeloid leukemia. Cancer Cell *20*, 674–688.
Škrtić, M., Sriskanthadevan, S., Jhas, B., Gebbia, M., Wang, X., Wang, Z., Hurren, R., Jitkova, Y., Gronda, M., Maclean, N., et al. (2011). Inhibition of Mitochondrial Translation as a Therapeutic Strategy for Human Acute Myeloid Leukemia. Cancer Cell.
Small, D., Levenstein, M., Kim, E., Carow, C., Amin, S., Rockwell, P., Witte, L., Burrow, C., Ratajczak, M.Z., and Gewirtz, A.M. (1994). STK-1, the human homolog of Flk-2/Flt-3, is selectively expressed in CD34+ human bone marrow cells and is involved in the proliferation of early progenitor/stem cells. Proc. Natl. Acad. Sci. *91*, 459 LP – 463.
Song, K., Li, M., Xu, X.-J., Xuan, L., Huang, G.-N., Song, X.-L., and Liu, Q.-F. (2014). HIF-1α and GLUT1 gene expression is associated with chemoresistance of acute myeloid leukemia. Asian Pacific J. Cancer Prev. *15*, 1823–1829.
Song, K., Li, M., Xu, X., Xuan, L., Huang, G., and Liu, Q. (2016). Resistance to chemotherapy

is associated with altered glucose metabolism in acute myeloid leukemia. Oncol. Lett. *12*, 334–342.
Sontakke, P., Koczula, K.M., Jaques, J., Wierenga, A.T.J., Brouwers-Vos, A.Z., Pruis, M., Günther, U.L., Vellenga, E., and Schuringa, J.J. (2016). Hypoxia-like signatures induced by BCR-ABL potentially alter the glutamine uptake for maintaining oxidative phosphorylation. PLoS One *11*, e0153226.
Souers, A.J., Leverson, J.D., Boghaert, E.R., Ackler, S.L., Catron, N.D., Chen, J., Dayton, B.D., Ding, H., Enschede, S.H., Fairbrother, W.J., et al. (2013). ABT-199, a potent and selective BCL-2 inhibitor, achieves antitumor activity while sparing platelets. Nat. Med. *19*, 202–208.
Spencer, J.A., Ferraro, F., Roussakis, E., Klein, A., Wu, J., Runnels, J.M., Zaher, W., Mortensen, L.J., Alt, C., Turcotte, R., et al. (2014). Direct measurement of local oxygen concentration in the bone marrow of live animals. Nature *508*, 269–273.
Sriskanthadevan, S., Jeyaraju, D. V., Chung, T.E., Prabha, S., Xu, W., Skrtic, M., Jhas, B., Hurren, R., Gronda, M., Wang, X., et al. (2015). AML cells have low spare reserve capacity in their respiratory chain that renders them susceptible to oxidative metabolic stress. Blood *125*, 2120–2130.
Stark, C., Breitkreutz, B.-J., Reguly, T., Boucher, L., Breitkreutz, A., and Tyers, M. (2006). BioGRID: a general repository for interaction datasets. Nucleic Acids Res. *34*, D535–D539.
Stein, E.M., DiNardo, C.D., Pollyea, D.A., Fathi, A.T., Roboz, G.J., Altman, J.K., Stone, R.M., DeAngelo, D.J., Levine, R.L., Flinn, I.W., et al. (2017). Enasidenib in mutant IDH2 relapsed or refractory acute myeloid leukemia. Blood *130*, 722–731.
Stephens, N.S., Siffledeen, J., Su, X., Murdoch, T.B., Fedorak, R.N., and Slupsky, C.M. (2013). Urinary NMR metabolomic profiles discriminate inflammatory bowel disease from healthy. J. Crohn's Colitis *7*, e42–e48.
Stirewalt, D.L., Kopecky, K.J., Meshinchi, S., Engel, J.H., Pogosova-Agadjanyan, E.L., Linsley, J., Slovak, M.L., Willman, C.L., and Radich, J.P. (2006). Size of FLT3 internal tandem duplication has prognostic significance in patients with acute myeloid leukemia. Blood *107*, 3724–3726.
Stone, R.M., DeAngelo, D.J., Klimek, V., Galinsky, I., Estey, E., Nimer, S.D., Grandin, W., Lebwohl, D., Wang, Y., Cohen, P., et al. (2005). Patients with acute myeloid leukemia and an activating mutation in FLT3 respond to a small-molecule FLT3 tyrosine kinase inhibitor, PKC412. Blood *105*, 54–60.
Stone, R.M., Mandrekar, S.J., Sanford, B.L., Laumann, K., Geyer, S., Bloomfield, C.D., Thiede, C., Prior, T.W., Döhner, K., Marcucci, G., et al. (2017). Midostaurin plus Chemotherapy for Acute Myeloid Leukemia with a FLT3 Mutation. N. Engl. J. Med. *377*, 454–464.
Stuani, L., Sabatier, M., and Sarry, J.-E. (2019). Exploiting metabolic vulnerabilities for personalized therapy in acute myeloid leukemia. BMC Biol. *17*, 57.
Stubbs, M.C., Kim, Y.M., Krivtsov, A. V, Wright, R.D., Feng, Z., Agarwal, J., Kung, A.L., and Armstrong, S.A. (2008). MLL-AF9 and FLT3 cooperation in acute myelogenous leukemia: development of a model for rapid therapeutic assessment. Leukemia *22*, 66–77.
Sugimura, T., Birnbaum, S.M., Winitz, M., and Greenstein, J.P. (1959). Quantitative nutritional studies with water-soluble, chemically defined diets. VIII. The forced feeding of diets each lacking in one essential amino acid. Arch. Biochem. Biophys. *81*, 448–455.
Sullivan, L.B., Gui, D.Y., Hosios, A.M., Bush, L.N., Freinkman, E., and Vander Heiden, M.G. (2015). Supporting aspartate biosynthesis is an essential function of respiration in proliferating cells. Cell *162*, 552–563.
Szyperski, T. (1995). Biosynthetically directed fractional 13C-labeling of proteinogenic amino acids. Eur. J. Biochem. *232*, 433–448.
Szyperski, T., Bailey, J.E., and Wüthrich, K. (1996). Detecting and dissecting metabolic fluxes using biosynthetic fractional 13C labeling and two-dimensional NMR spectroscopy. Trends Biotechnol. *14*, 453–459.
Szyperski, T., Glaser, R.W., Hochuli, M., Fiaux, J., Sauer, U., Bailey, J.E., and Wüthrich, K. (1999). Bioreaction Network Topology and Metabolic Flux Ratio Analysis by Biosynthetic

Fractional 13C Labeling and Two-Dimensional NMR Spectroscopy. Metab. Eng. *1*, 189–197.
Takis, P.G., Ghini, V., Tenori, L., Turano, P., and Luchinat, C. (2019). Uniqueness of the NMR approach to metabolomics. TrAC Trends Anal. Chem. *120*, 115300.
Teng, C.-L., Young, J.-H., Hsu, S.-L., Chou, G., Kuo, I.-T., Yu, C.-Y., and Hwang, G.-Y. (2006). Lactate dehydrogenase, not vascular endothelial growth factor or basic fibroblast growth factor, positively correlates to bone marrow vascularity in acute myeloid leukemia. J. Chinese Med. Assoc. *69*, 534–537.
Terunuma, A., Putluri, N., Mishra, P., Mathé, E.A., Dorsey, T.H., Yi, M., Wallace, T.A., Issaq, H.J., Zhou, M., Killian, J.K., et al. (2014). MYC-driven accumulation of 2-hydroxyglutarate is associated with breast cancer prognosis. J. Clin. Invest. *124*, 398–412.
Thiede, C., Steudel, C., Mohr, B., Schaich, M., Schäkel, U., Platzbecker, U., Wermke, M., Bornhäuser, M., Ritter, M., Neubauer, A., et al. (2002). Analysis of FLT3-activating mutations in 979 patients with acute myelogenous leukemia: association with FAB subtypes and identification of subgroups with poor prognosis. Blood *99*, 4326–4335.
Thomlinson, R.H., and Gray, L.H. (1955). The histological structure of some human lung cancers and the possible implications for radiotherapy. Br. J. Cancer *9*, 539–549.
Tohyama, S., Fujita, J., Hishiki, T., Matsuura, T., Hattori, F., Ohno, R., Kanazawa, H., Seki, T., Nakajima, K., Kishino, Y., et al. (2016). Glutamine Oxidation Is Indispensable for Survival of Human Pluripotent Stem Cells. Cell Metab. *23*, 663–674.
Tse, K.-F., Mukherjee, G., and Small, D. (2000). Constitutive activation of FLT3 stimulates multiple intracellular signal transducers and results in transformation. Leukemia *14*, 1766–1776.
Tzelepis, K., De Braekeleer, E., Aspris, D., Barbieri, I., Vijayabaskar, M.S., Liu, W.-H., Gozdecka, M., Metzakopian, E., Toop, H.D., Dudek, M., et al. (2018). SRPK1 maintains acute myeloid leukemia through effects on isoform usage of epigenetic regulators including BRD4. Nat. Commun. *9*, 5378.
Ugurbil, K., Brown, T.R., den Hollander, J.A., Glynn, P., and Shulman, R.G. (1978a). High-resolution 13C nuclear magnetic resonance studies of glucose metabolism in Escherichia coli. Proc. Natl. Acad. Sci. U. S. A. *75*, 3742–3746.
Ugurbil, K., Rottenberg, H., Glynn, P., and Shulman, R.G. (1978b). 31P nuclear magnetic resonance studies of bioenergetics and glycolysis in anaerobic Escherichia coli cells. Proc. Natl. Acad. Sci. U. S. A. *75*, 2244–2248.
Ulanovskaya, O.A., Zuhl, A.M., and Cravatt, B.F. (2013). NNMT promotes epigenetic remodeling in cancer by creating a metabolic methylation sink. Nat. Chem. Biol. *9*, 300–306.
USA's Food and Drug Administration (2017). Pescribing Information of Midostaurin (Rydapt) capsules, for oral use.
Vansteenkiste, J.F., and Stroobants, S.G. (2001). The role of positron emission tomography with 18F-fluoro-2-deoxy-D-glucose in respiratory oncology. Eur. Respir. J. *17*, 802 LP – 820.
Vaupel, P., Schlenger, K., Knoop, C., and Höckel, M. (1991). Oxygenation of human tumors: evaluation of tissue oxygen distribution in breast cancers by computerized O2 tension measurements. Cancer Res. *51*, 3316 LP – 3322.
Verhaak, R.G.W., Wouters, B.J., Erpelinck, C.A.J., Abbas, S., Beverloo, H.B., Lugthart, S., Löwenberg, B., Delwel, R., and Valk, P.J.M. (2009). Prediction of molecular subtypes in acute myeloid leukemia based on gene expression profiling. Haematologica *94*, 131 LP – 134.
Viale, A., Pettazzoni, P., Lyssiotis, C.A., Ying, H., Sánchez, N., Marchesini, M., Carugo, A., Green, T., Seth, S., Giuliani, V., et al. (2014). Oncogene ablation-resistant pancreatic cancer cells depend on mitochondrial function. Nature *514*, 628–632.
Vignoli, A., Ghini, V., Meoni, G., Licari, C., Takis, P.G., Tenori, L., Turano, P., and Luchinat, C. (2019). High-Throughput Metabolomics by 1D NMR. Angew. Chemie Int. Ed. *58*, 968–994.
Wang, Y.-H., Israelsen, W.J., Lee, D., Yu, V.W.C., Jeanson, N.T., Clish, C.B., Cantley, L.C., Vander Heiden, M.G., and Scadden, D.T. (2014). Cell-state-specific metabolic dependency in hematopoiesis and leukemogenesis. Cell *158*, 1309–1323.
Wang, Y., Zhang, L., Chen, W.-L., Wang, J.-H., Li, N., Li, J.-M., Mi, J.-Q., Zhang, W.-N., Li, Y., Wu, S.-F., et al. (2013). Rapid diagnosis and prognosis of de novo acute myeloid leukemia by serum metabonomic analysis. J. Proteome Res. *12*, 4393–4401.

Wang, Z., Yip, L.Y., Lee, J.H.J., Wu, Z., Chew, H.Y., Chong, P.K.W., Teo, C.C., Ang, H.Y.-K., Peh, K.L.E., Yuan, J., et al. (2019). Methionine is a metabolic dependency of tumor-initiating cells. Nat. Med. *25*, 825–837.
Warburg, O. (1956). On the origin of cancer cells. Science (80-.). *123*, 309–314.
Warburg, O., Wind, F., and Negelein, E. (1927). The metabolism of tumors in the body. J. Gen. Physiol. *8*, 519–530.
Weinberg, S.E., and Chandel, N.S. (2015). Targeting mitochondria metabolism for cancer therapy. Nat. Chem. Biol. *11*, 9–15.
Whitman, S.P., Archer, K.J., Feng, L., Baldus, C., Becknell, B., Carlson, B.D., Carroll, A.J., Mrózek, K., Vardiman, J.W., George, S.L., et al. (2001). Absence of the wild-type allele predicts poor prognosis in adult de novo acute myeloid leukemia with normal cytogenetics and the internal tandem duplication of FLT3: A cancer and leukemia group B study. Cancer Res. *61*, 7233 LP – 7239.
Whitman, S.P., Maharry, K., Radmacher, M.D., Becker, H., Mrózek, K., Margeson, D., Holland, K.B., Wu, Y.-Z., Schwind, S., Metzeler, K.H., et al. (2010). FLT3 internal tandem duplication associates with adverse outcome and gene- and microRNA-expression signatures in patients 60 years of age or older with primary cytogenetically normal acute myeloid leukemia: a Cancer and Leukemia Group B study. Blood *116*, 3622–3626.
Wierenga, A.T.J., Schepers, H., Moore, M.A.S., Vellenga, E., and Schuringa, J.J. (2006). STAT5-induced self-renewal and impaired myelopoiesis of human hematopoietic stem/progenitor cells involves down-modulation of C/EBPα. Blood *107*, 4326–4333.
Willems, L., Jacque, N., Jacquel, A., Neveux, N., Maciel, T.T., Lambert, M., Schmitt, A., Poulain, L., Green, A.S., Uzunov, M., et al. (2013). Inhibiting glutamine uptake represents an attractive new strategy for treating acute myeloid leukemia. Blood *122*, 3521–3532.
Wishart, D.S. (2016). Emerging applications of metabolomics in drug discovery and precision medicine. Nat. Rev. Drug Discov. *15*, 473–484.
Wishart, D.S. (2019). NMR metabolomics: A look ahead. J. Magn. Reson. *306*, 155–161.
Wishart, D.S., Tzur, D., Knox, C., Eisner, R., Guo, A.C., Young, N., Cheng, D., Jewell, K., Arndt, D., Sawhney, S., et al. (2007). HMDB: the Human Metabolome Database. Nucleic Acids Res. *35*, D521-6.
Xiao, M., Yang, H., Xu, W., Ma, S., Lin, H., Zhu, H., Liu, L., Liu, Y., Yang, C., Xu, Y., et al. (2012). Inhibition of α-KG-dependent histone and DNA demethylases by fumarate and succinate that are accumulated in mutations of FH and SDH tumor suppressors. Genes Dev. *26*, 1326–1338.
Yang, L., Venneti, S., and Nagrath, D. (2017). Glutaminolysis: A Hallmark of Cancer Metabolism. Annu. Rev. Biomed. Eng *19*, 163–194.
Yang, M., Soga, T., and Pollard, P.J. (2013). Oncometabolites: linking altered metabolism with cancer. J. Clin. Invest. *123*, 3652–3658.
Yang, X., Sexauer, A., and Levis, M. (2014). Bone marrow stroma-mediated resistance to FLT3 inhibitors in FLT3-ITD AML is mediated by persistent activation of extracellular regulated kinase. Br. J. Haematol. *164*, 61–72.
Ye, H., Adane, B., Khan, N., Alexeev, E., Nusbacher, N., Minhajuddin, M., Stevens, B.M., Winters, A.C., Lin, X., Ashton, J.M., et al. (2018). Subversion of systemic glucose metabolism as a mechanism to support the growth of leukemia cells. Cancer Cell *34*, 659-673.e6.
Yépez, V.A., Kremer, L.S., Iuso, A., Gusic, M., Kopajtich, R., Koňaříková, E., Nadel, A., Wachutka, L., Prokisch, H., and Gagneur, J. (2018). OCR-Stats: Robust estimation and statistical testing of mitochondrial respiration activities using Seahorse XF Analyzer. PLoS One *13*, e0199938.
Yu, W.M., Liu, X., Shen, J., Jovanovic, O., Pohl, E.E., Gerson, S.L., Finkel, T., Broxmeyer, H.E., and Qu, C.K. (2013). Metabolic regulation by the mitochondrial phosphatase PTPMT1 is required for hematopoietic stem cell differentiation. Cell Stem Cell *12*, 62–74.
Zacharias, N.M., Chan, H.R., Sailasuta, N., Ross, B.D., and Bhattacharya, P. (2012). Real-time molecular imaging of tricarboxylic acid cycle metabolism in vivo by hyperpolarized 1-13C diethyl succinate. J. Am. Chem. Soc. *134*, 934–943.
Zambrello, M.A., Schuyler, A.D., Maciejewski, M.W., Delaglio, F., Bezsonova, I., and Hoch,

J.C. (2018). Nonuniform sampling in multidimensional NMR for improving spectral sensitivity. Methods *138–139*, 62–68.
Zarrinkar, P.P., Gunawardane, R.N., Cramer, M.D., Gardner, M.F., Brigham, D., Belli, B., Karaman, M.W., Pratz, K.W., Pallares, G., Chao, Q., et al. (2009). AC220 is a uniquely potent and selective inhibitor of FLT3 for the treatment of acute myeloid leukemia (AML). Blood *114*, 2984–2992.
Zhang, A., Sun, H., Qiu, S., and Wang, X. (2013). NMR-based metabolomics coupled with pattern recognition methods in biomarker discovery and disease diagnosis. Magn. Reson. Chem. *51*, 549–556.
Zhang, J., Pavlova, N.N., and Thompson, C.B. (2017). Cancer cell metabolism: the essential role of the nonessential amino acid, glutamine. EMBO J. *36*, 1302–1315.
Zhang, W., Gao, C., Konopleva, M., Chen, Y., Jacamo, R.O., Borthakur, G., Cortes, J.E., Ravandi, F., Ramachandran, A., and Andreeff, M. (2014). Reversal of acquired drug resistance in FLT3-mutated acute myeloid leukemia cells via distinct drug combination strategies. Clin. Cancer Res. *20*, 2363–2374.
Zhang, Y., Morar, M., and Ealick, S.E. (2008). Structural biology of the purine biosynthetic pathway. Cell. Mol. Life Sci. *65*, 3699–3724.
Zhao, Y., Butler, E.B., and Tan, M. (2013). Targeting cellular metabolism to improve cancer therapeutics. Cell Death Dis. *4*, e532–e532.
Zheng, R., Friedman, A.D., and Small, D. (2002). Targeted inhibition of FLT3 overcomes the block to myeloid differentiation in 32Dcl3 cells caused by expression of FLT3/ITD mutations. Blood *100*, 4154–4161.
Zhou, F.-L., Zhang, W.-G., Wei, Y.-C., Meng, S., Bai, G.-G., Wang, B.-Y., Yang, H.-Y., Tian, W., Meng, X., Zhang, H., et al. (2010). Involvement of oxidative stress in the relapse of acute myeloid leukemia. J. Biol. Chem. *285*, 15010–15015.

Appendices

Appendix 1: Patients details

Appendix Table A1: patient details of primary AML blasts. Age, % bone marrow (BM) blasts and white blood cell (WBC) count are indicated at the time of diagnosis. Sex; M: male, F: female. For Patient 4, cells with both karyotype (46 XX and 47 XX) were present. +22 indicates a translocation trisomy.

Number	Sex	Age	% BM blasts	WBC	FAB subtype	Karyotype	Molecular genetics
1	F	50	38	18.51	M2	n.a.	IDH2, ASXL1, DNMT3A
2	M	53	66	53	M1	46,XY	NPM1, FLT3-ITD
3	M	83	34	27.22	M4	46,XY	CEBPA
4	F	41	52	3.01	M4eo	46 XX, Inv(16)(p13q22), 47 XX, Inv(16)(p13q22)+22	CBFB-MYH11
5	M	55	58	12.55	M2	46,XY	NPM1
6	F	73	81	81	M4	46,XX	NPM1, FLT3-ITD
7	M	73	>80	80	M1/2	46,XY	NPM1, FLT3-ITD
8	M	77	>90	90	M4	46,XY	NPM1, FLT3-ITD, CEBPA
9	F	46	90	90	n.a.	46,XX	NPM1, FLT3-ITD
10	M	46	60	207.74	M4	46,XY	NPM1, FLT3-ITD (VAF 0.6) (AC220-resistant)

Appendix 2: Media formulation

Appendix Table A2: LB Agar composition. LB agar media composition of Carl Roth (Article number: X968.2).

Components	Amount (g/l)
Tryptone	10
Yeast extract	5
Sodium chloride (NaCl)	10
Agar Agar	15
pH	7.0 ± 0.2

Appendix Table A3: LB medium composition. LB agar media composition of Carl Roth (Article number: X964.2).

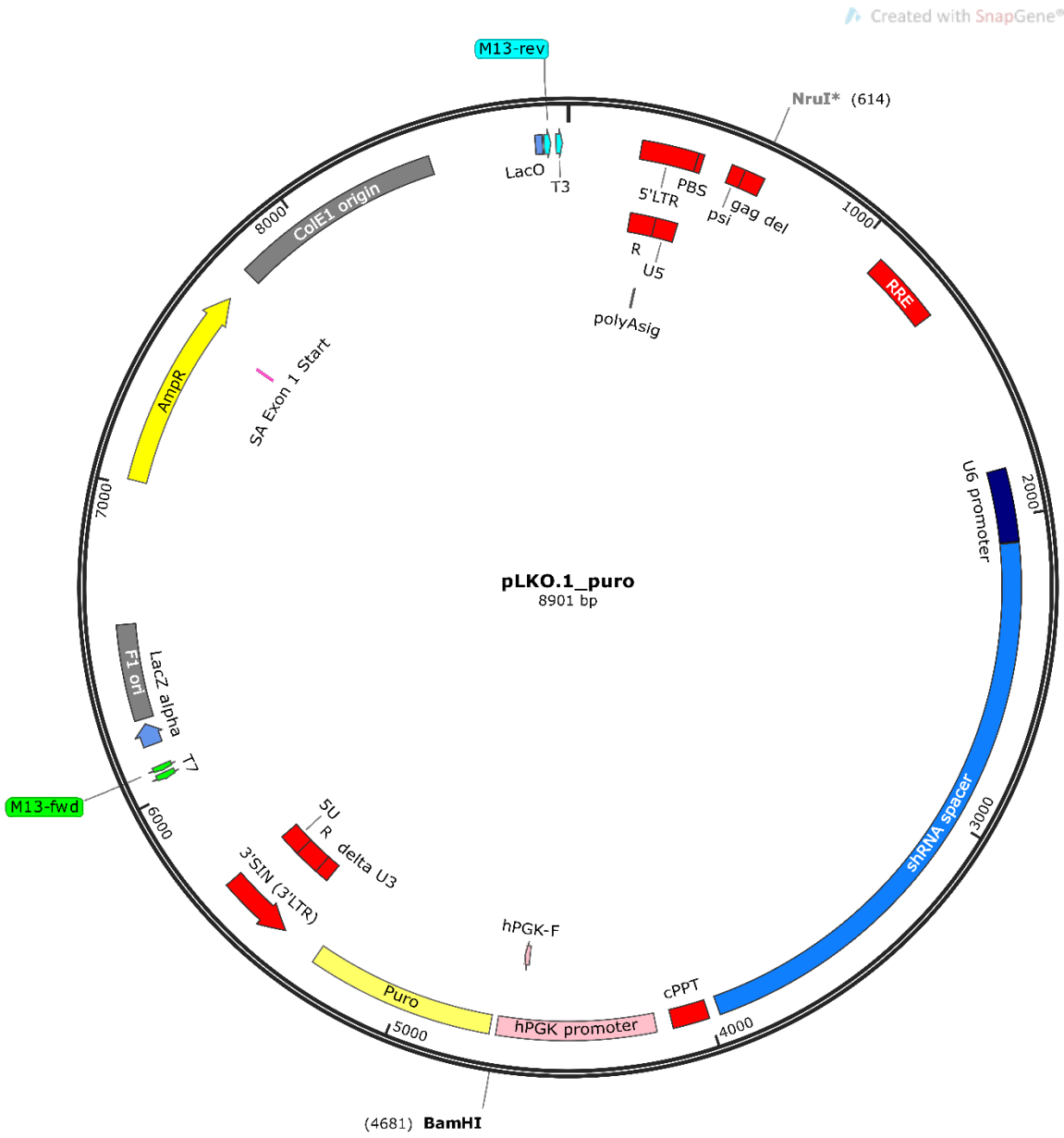
Components	Amount (g/l)
Tryptone	10
Yeast extract	5
Sodium chloride (NaCl)	5
pH	7.0 ± 0.2

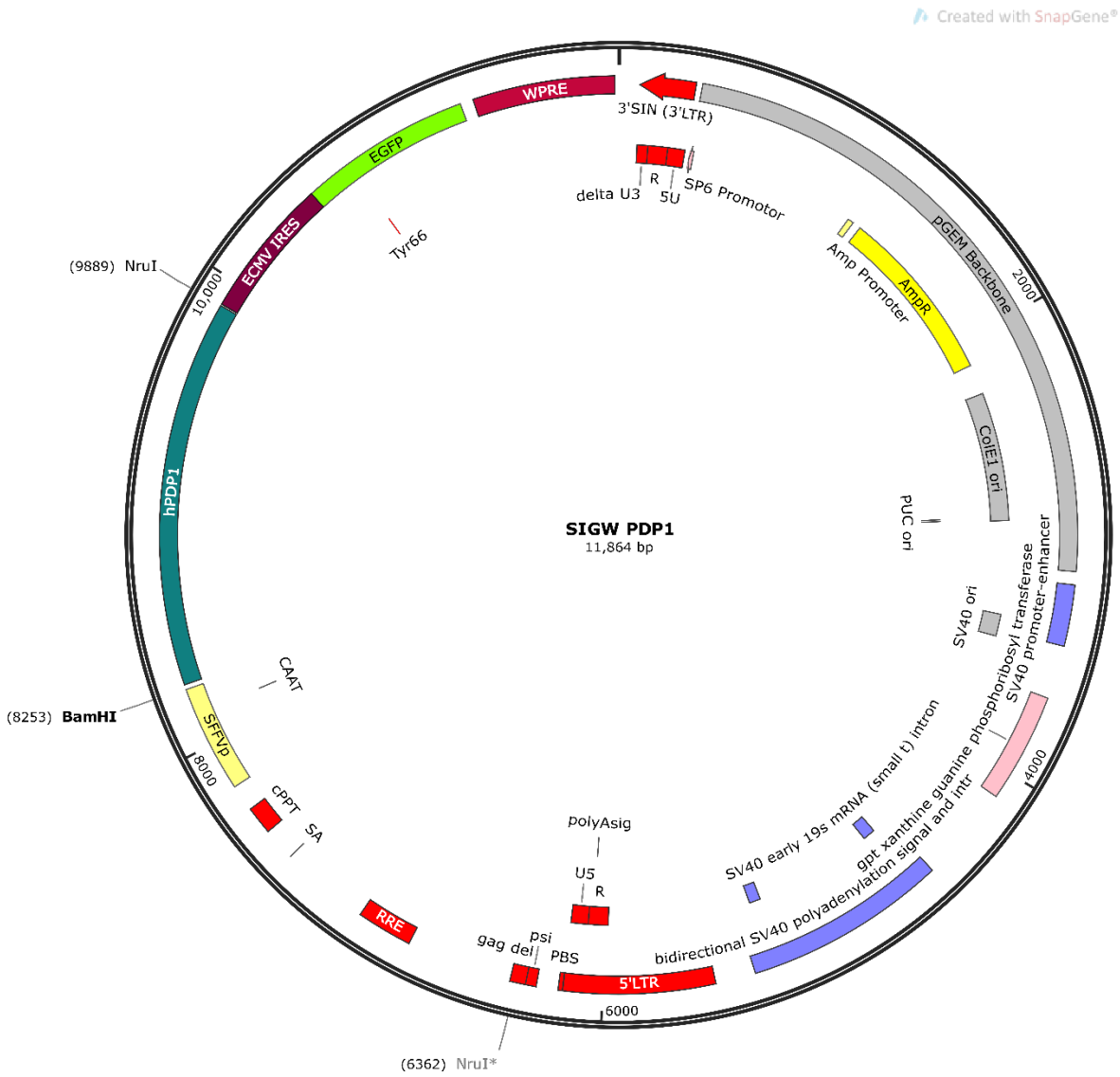
Appendix Table A4: Homemade RPMI media composition. RPMI media composition of ThermoFisher (Catalog number: 11875 - RPMI 1640) followed for the composition of the homemade media.

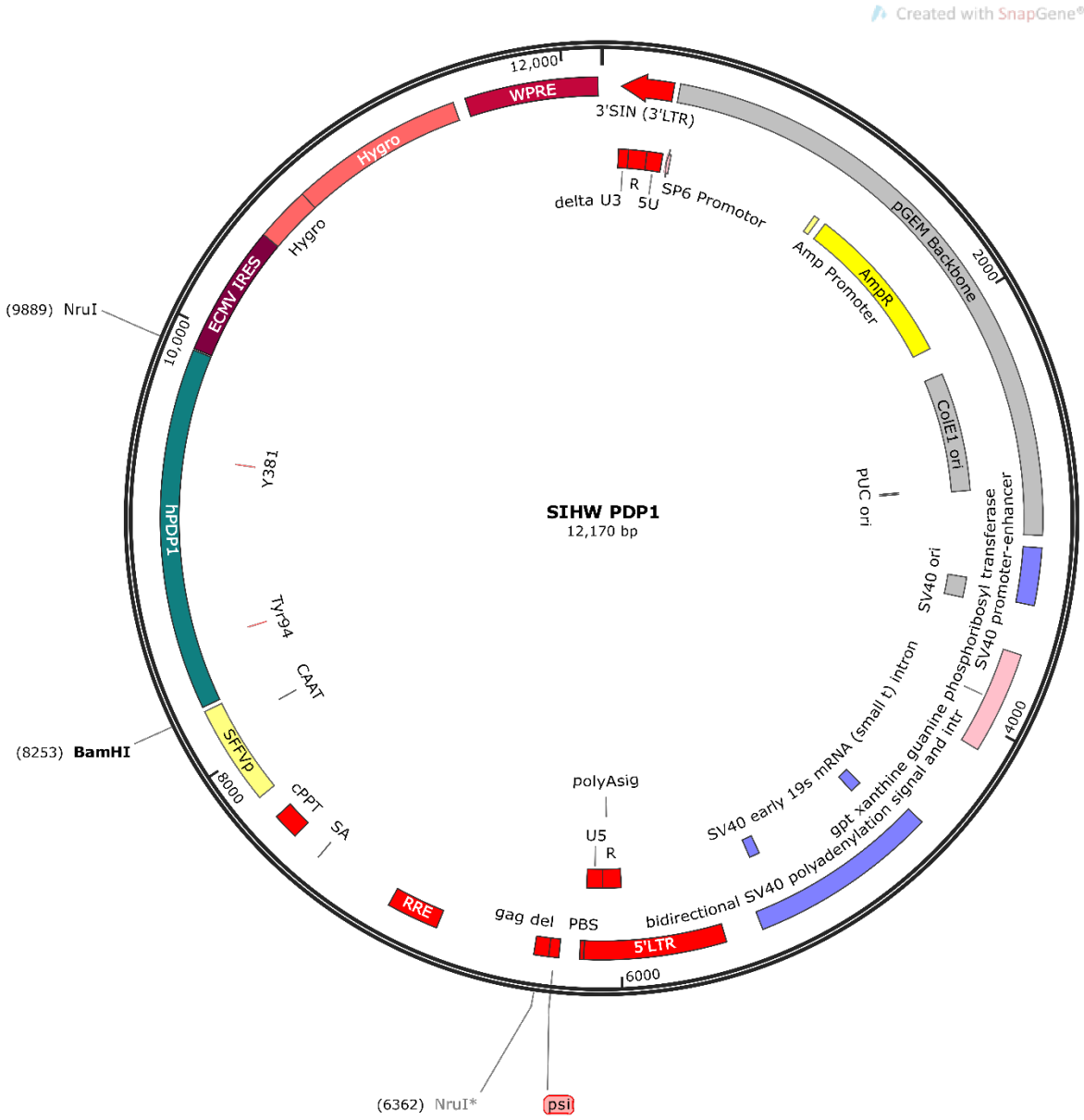
Components	Molecular Weight	Amount (mg/l)	Concentration (mM)
Amino Acids			
Glycine	75	10	0.13333334
L-Arginine	174	200	1.1494253
L-Asparagine	132	50	0.37878788
L-Aspartic acid	133	20	0.15037593
L-Cystine 2HCl	313	65	0.20766774
L-Glutamic Acid	147	20	0.13605443
L-Glutamine	146	300	2.0547945
L-Histidine	155	15	0.09677419
L-Hydroxyproline	131	20	0.15267175
L-Isoleucine	131	50	0.3816794
L-Leucine	131	50	0.3816794
L-Lysine hydrochloride	183	40	0.21857923
L-Methionine	149	15	0.10067114
L-Phenylalanine	165	15	0.09090909
L-Proline	115	20	0.17391305
L-Serine	105	30	0.2857143
L-Threonine	119	20	0.16806723
L-Tryptophan	204	5	0.024509804
L-Tyrosine disodium salt dihydrate	261	29	0.11111111
L-Valine	117	20	0.17094018
Vitamins			

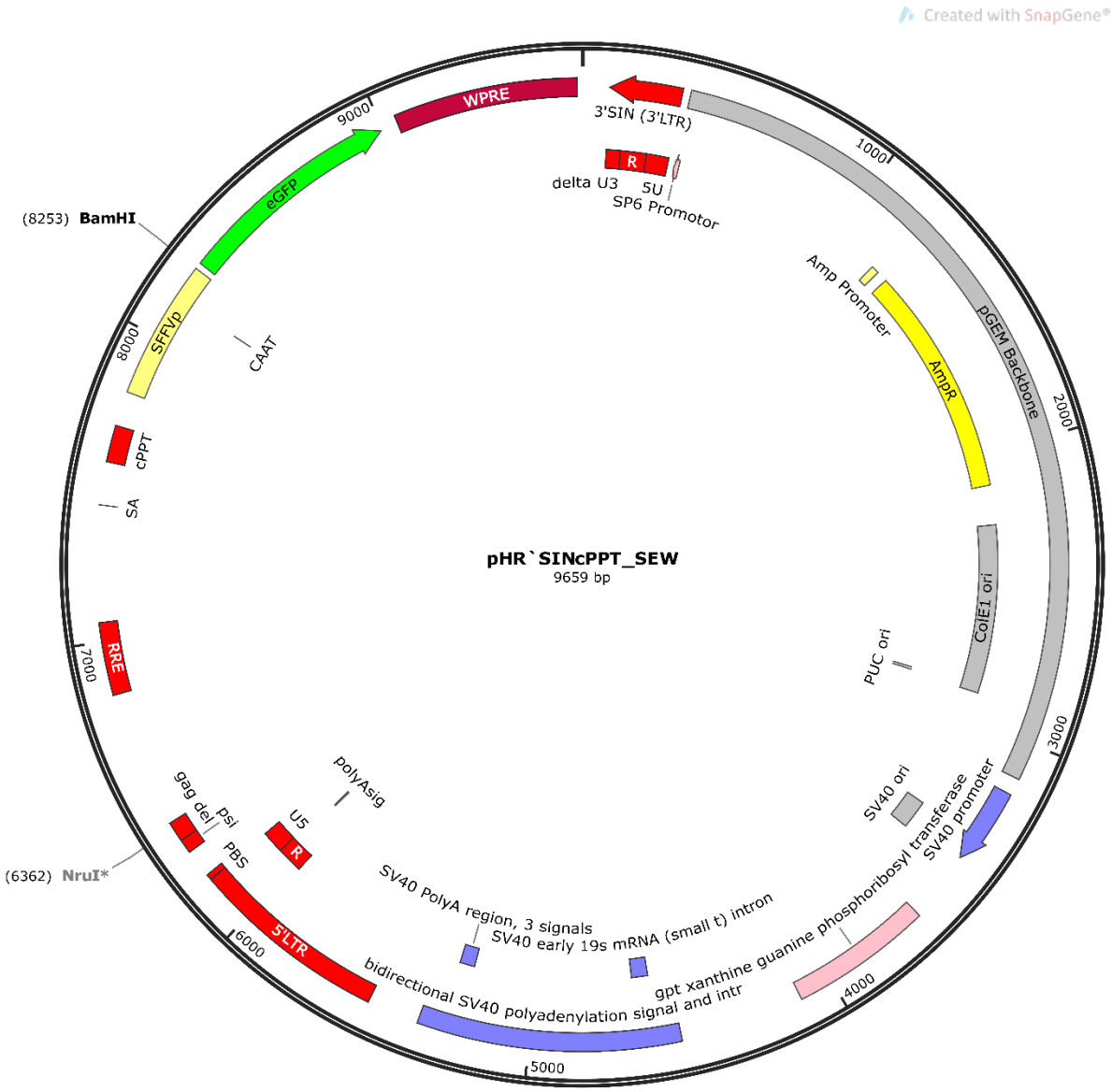
Biotin	244	0.2	8.20E-04
Choline chloride	140	3	0.021428572
D-Calcium pantothenate	477	0.25	5.24E-04
Folic Acid	441	1	0.002267574
Niacinamide	122	1	0.008196721
Para-Aminobenzoic Acid	137	1	0.00729927
Pyridoxine hydrochloride	206	1	0.004854369
Riboflavin	376	0.2	5.32E-04
Thiamine hydrochloride	337	1	0.002967359
Vitamin B12	1355	0.005	3.69E-06
i-Inositol	180	35	0.19444445
Inorganic Salts			
Calcium nitrate (Ca(NO3)2 4H2O)	236	100	0.42372882
Magnesium Sulfate (MgSO4) (anhyd.)	120	48.84	0.407
Potassium Chloride (KCl)	75	400	5.3333335
Sodium Bicarbonate (NaHCO3)	84	2000	23.809525
Sodium Chloride (NaCl)	58	6000	103.44827
Sodium Phosphate dibasic (Na2HPO4) anhydrous	142	800	5.633803
Other Components			
D-Glucose (Dextrose)	180	2000	11.111111
Glutathione (reduced)	307	1	0.003257329
Phenol Red	376.4	5	0.013283741

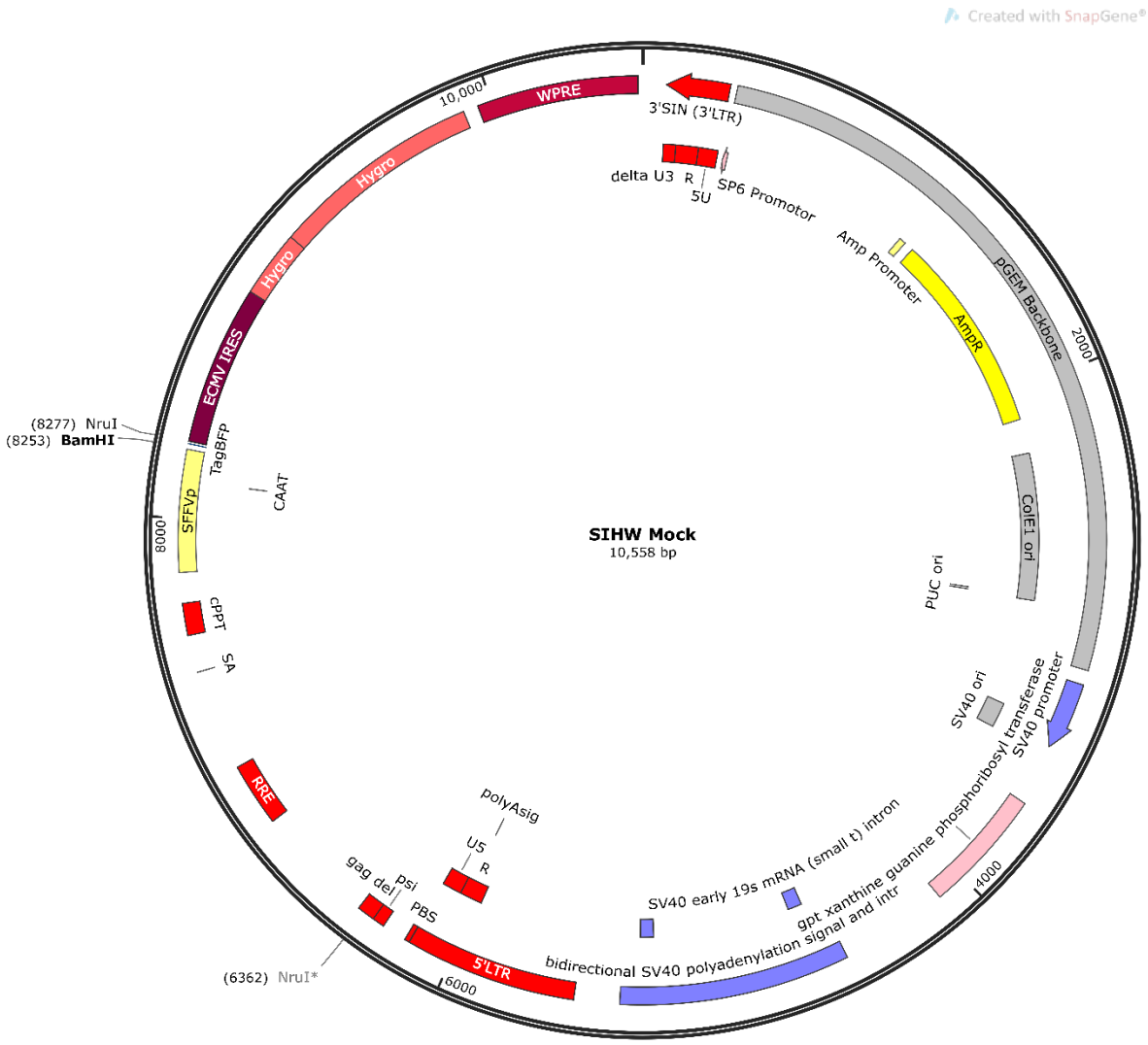
Appendix 3: Vectors maps

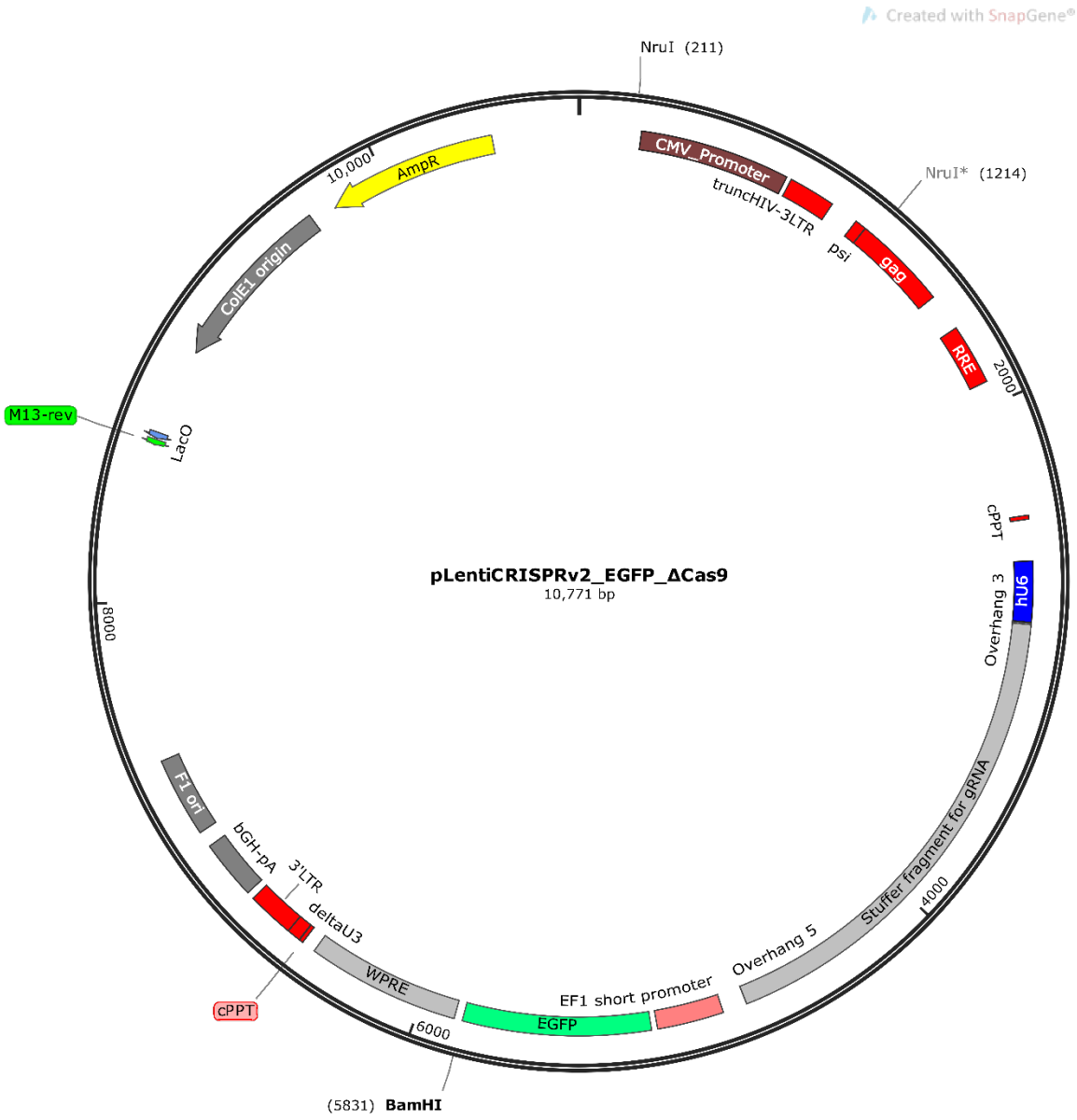


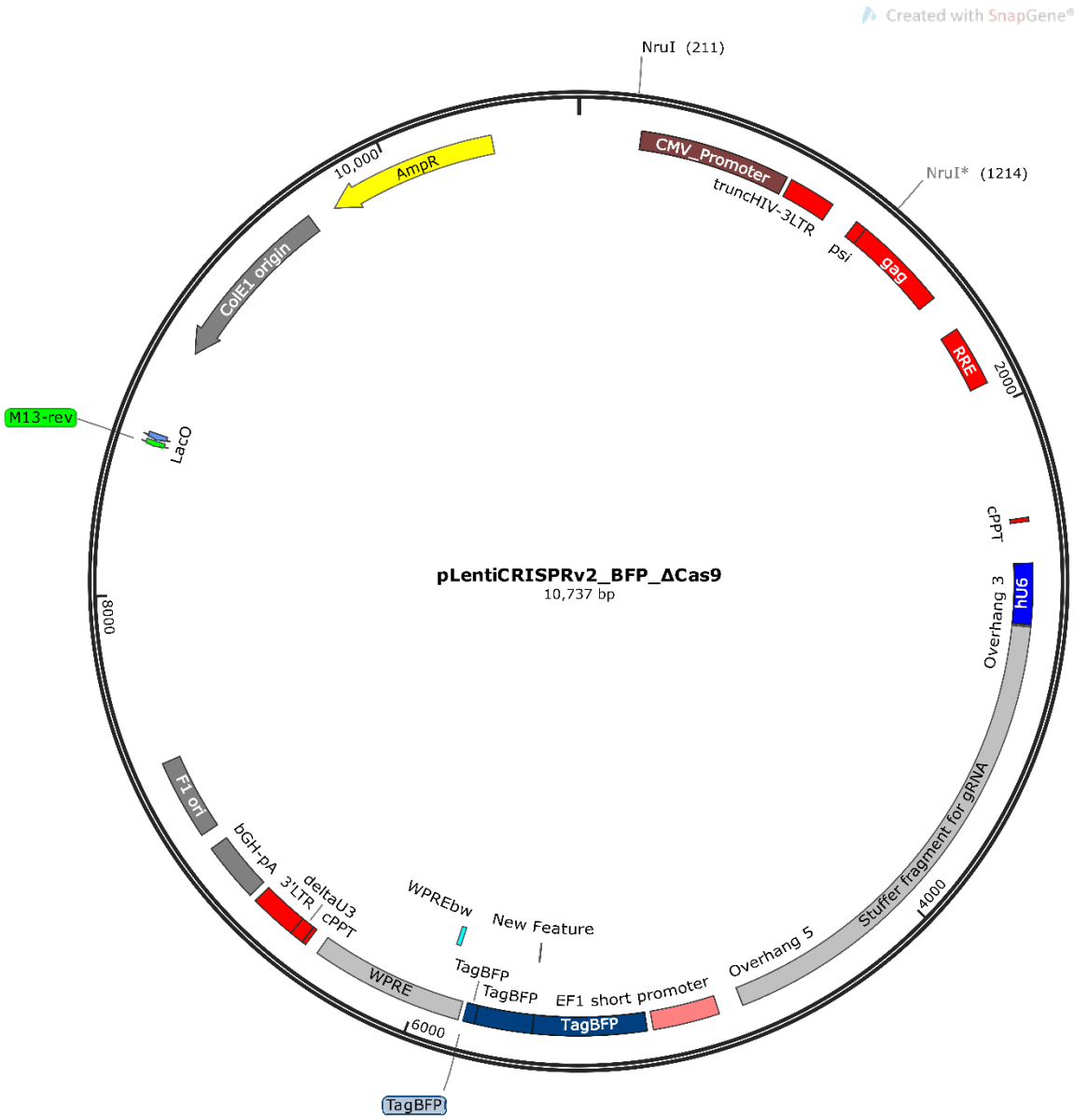

Created with SnapGene®
WPRE
3'SIN (3'LTR)
EGFP
R
delta U3
5U
SP6 Promotor
ECMV IRES
Tyr66
(9889) NruI
10,000
Amp Promoter
AmpR
pGEM Backbone
2000
hPDP1
ColE1 ori
PUC ori
SIGW PDP1
11,864 bp
SV40 ori
SV40 promoter-enhancer
CAAT
(8253) BamHI
SFFVp
8000
cPPT
SA
polyAsig
SV40 early 19s mRNA (small t) intron
gpt xanthine guanine phosphoribosyl transferase
U5
R
RRE
gag del
psi
PBS
bidirectional SV40 polyadenylation signal and intr
5'LTR
4000
6000
(6362) NruI*


Created with SnapGene®
SIHW PDP1
12,170 bp
12,000
WPRE
3'SIN (3'LTR)
R
delta U3
5U
SP6 Promotor
pGEM Backbone
2000
Amp Promotor
AmpR
ColE1 ori
PUC ori
SV40 ori
SV40 promoter-enhancer
4000
SV40 early 19s mRNA (small t) intron
gpt xanthine guanine phosphoribosyl transferase
bidirectional SV40 polyadenylation signal and intr
5'LTR
6000
PBS
gag del
psi
(6362) NruI*
RRE
U5
R
polyAsig
cPPT
SA
8000
SFFVp
(8253) BamHI
hPDP1
CAAT
Tyr94
Y381
10,000
ECMV IRES
Hygro
Hygro
(9889) NruI


Created with SnapGene®
pHR`SINcPPT_SEW
9659 bp
WPRE
3'SIN (3'LTR)
R
delta U3
5U
SP6 Promotor
Amp Promoter
AmpR
pGEM Backbone
ColE1 ori
PUC ori
SV40 ori
SV40 promoter
gpt xanthine guanine phosphoribosyl transferase
SV40 early 19s mRNA (small t) intron
SV40 PolyA region, 3 signals
bidirectional SV40 polyadenylation signal and intr
5'LTR
PBS
gag del
psi
U5
R
polyAsig
RRE
SA
cPPT
SFFVp
CAAT
eGFP
(8253) BamHI
(6362) NruI*
1000
2000
3000
4000
5000
6000
7000
8000
9000


Created with SnapGene®
SIHW Mock
10,558 bp
10,000
WPRE
3'SIN (3'LTR)
delta U3
R
5U
SP6 Promotor
Amp Promoter
AmpR
pGEM Backbone
2000
ColE1 ori
PUC ori
SV40 ori
SV40 promoter
Hygro
Hygro
ECMV IRES
(8277) NruI
(8253) BamHI
TagBFp
CAAT
SFFVp
8000
cPPT
SA
RRE
polyAsig
U5
R
gag del
Psi
PBS
5'LTR
(6362) NruI*
6000
SV40 early 19s mRNA (small t) intron
gpt xanthine guanine phosphoribosyl transferase
bidirectional SV40 polyadenylation signal and intr
4000


Created with SnapGene®
NruI (211)
NruI* (1214)
10,000
AmpR
ColE1 origin
M13-rev
LacO
CMV_Promoter
truncHIV-3LTR
psi
gag
RRE
20000
cPPT
hU6
Overhang 3
Stuffer fragment for gRNA
Overhang 5
EF1 short promoter
EGFP
WPRE
deltaU3
3'LTR
bGH-pA
F1 ori
cPPT
8000
6000
4000
(5831) BamHI
pLentiCRISPRv2_EGFP_ΔCas9
10,771 bp

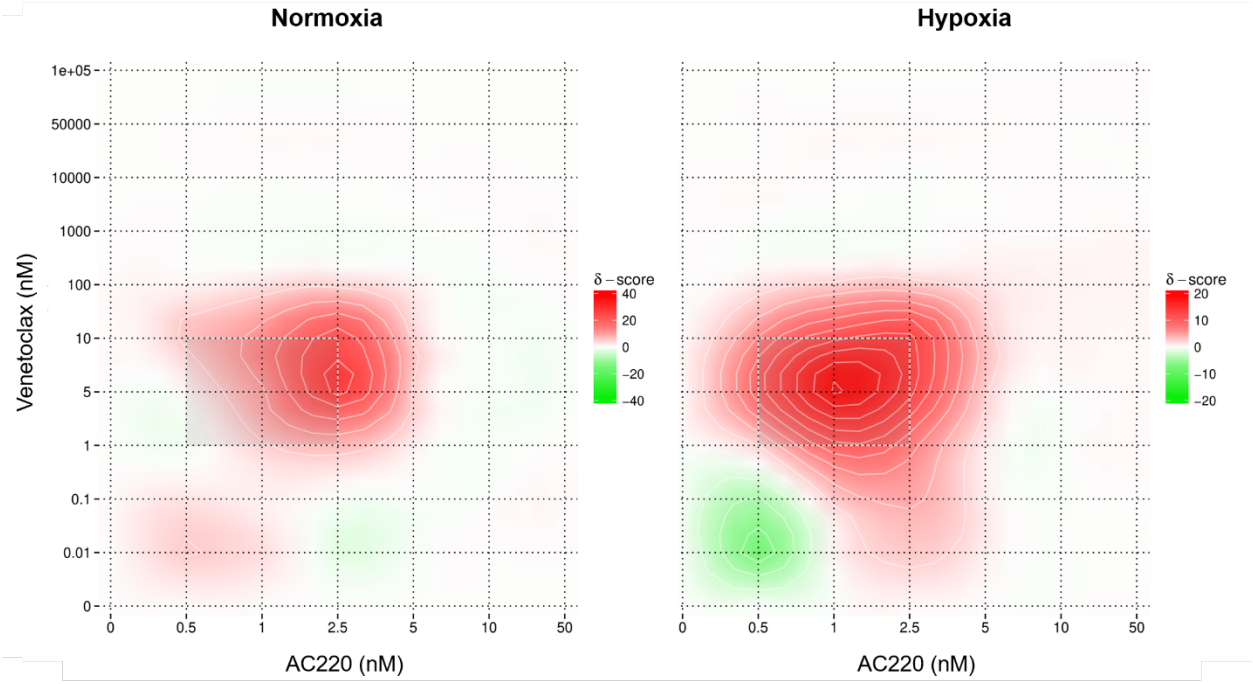

Created with SnapGene®
NruI (211)
NruI* (1214)
CMV_Promoter
truncHIV-3LTR
psi
gag
RRE
2000
cPPT
hU6
Overhang 3
Stuffer fragment for gRNA
4000
Overhang 5
EF1 short promoter
TagBFP
TagBFP
TagBFP
New Feature
WPREbw
WPRE
6000
TagBFP
deltaU3
3'LTR
cPPT
bGH-pA
F1 ori
8000
M13-rev
LacO
ColE1 origin
AmpR
10,000
pLentiCRISPRv2_BFP_ΔCas9
10,737 bp

Appendix 4: NMR metabolites assignment

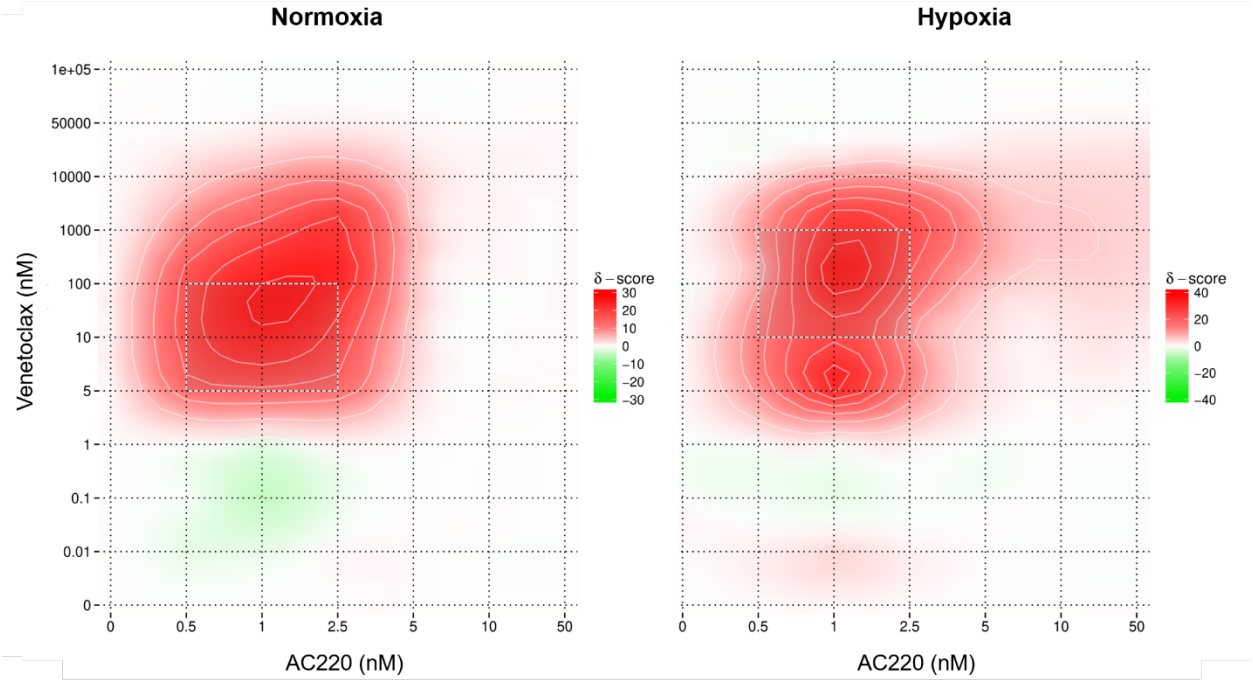
Appendix Table A5: Metabolites chemical shifts assignment (peak list).

Metabolite	ppm
Leucine	0.95
Isoleucine	1
Valine	1.03
Lactate	1.33
Alanine	1.48
Acetate	1.92
Glutamate	2.36
Succinate	2.41
Glutamine	2.44
Glutathione	2.54
Aspartate	2.8
Asparagine	2.88
lysine	3.02
Creatine	3.025
Phosphocreatine	3.04
Choline	3.18
phosphocholine	3.21
Taurine	3.42
glycine	3.55
Glucose	5.22
Fumarate	6.52
Histidine	7.1
Tyrosine	7.19
Phenylalanine	7.42
Tryptophan	7.73
Formate	8.44

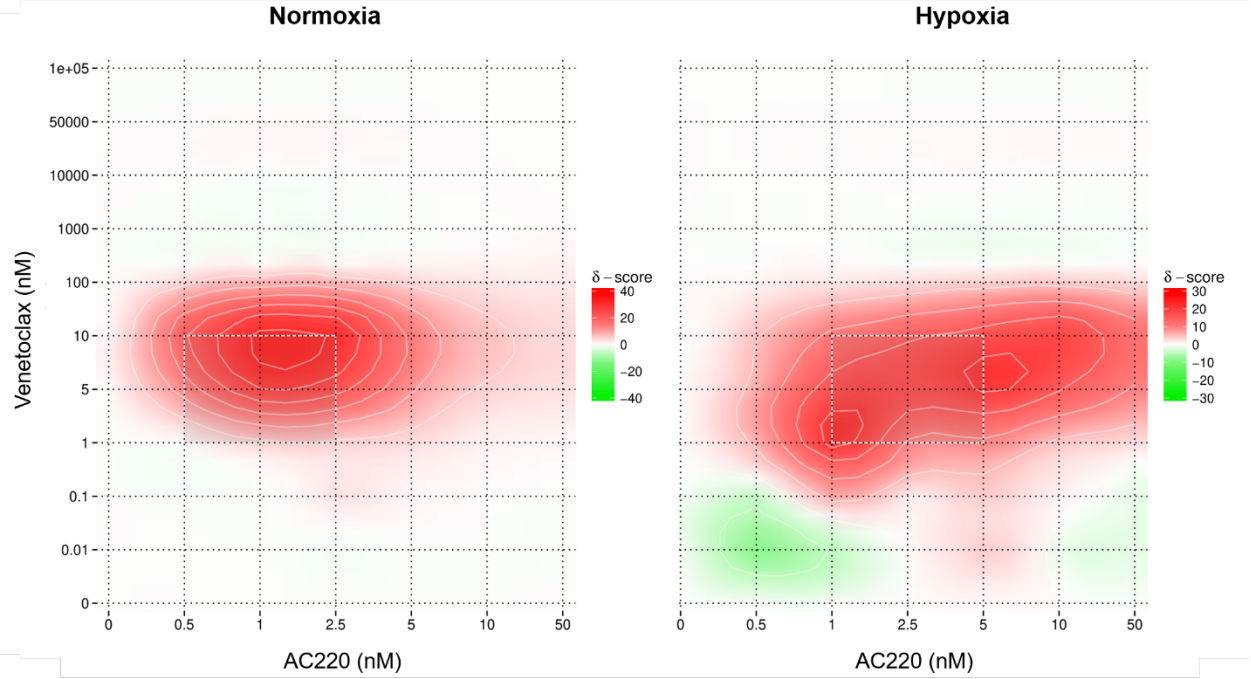
Appendix 5: Synergism between venetoclax and AC220



Appendix Figure A1: Venetoclax and AC220 synergy in Molm13. Synergy score is 1.79 for normoxia and 1.67 for hypoxia.

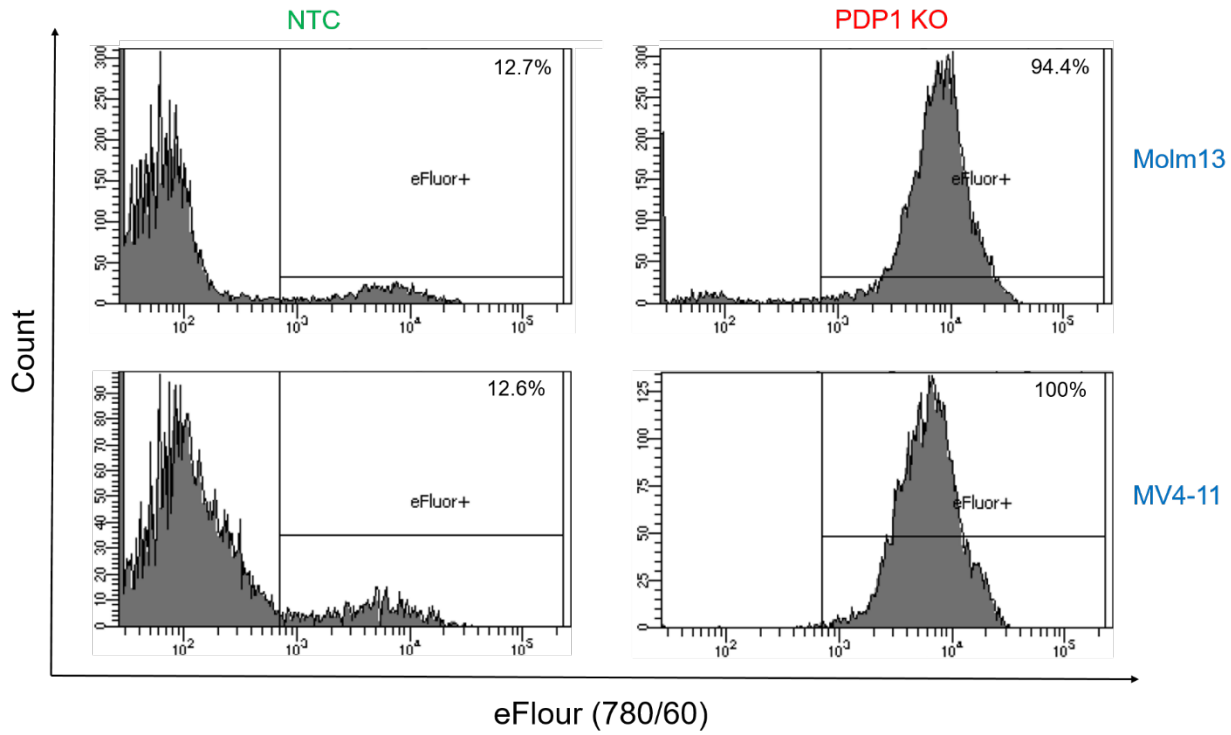


Appendix Figure A2: Venetoclax and AC220 synergy in Molm14. Synergy score is 3.96 for normoxia and 4.9 for hypoxia.



Appendix Figure A3: Venetoclax and AC220 synergy in MV4-11. Synergy score is 3.55 for normoxia and 3.9 for hypoxia[11].

Appendix 6: PDP1 knockout leads to cell death in FLT3-ITD cells



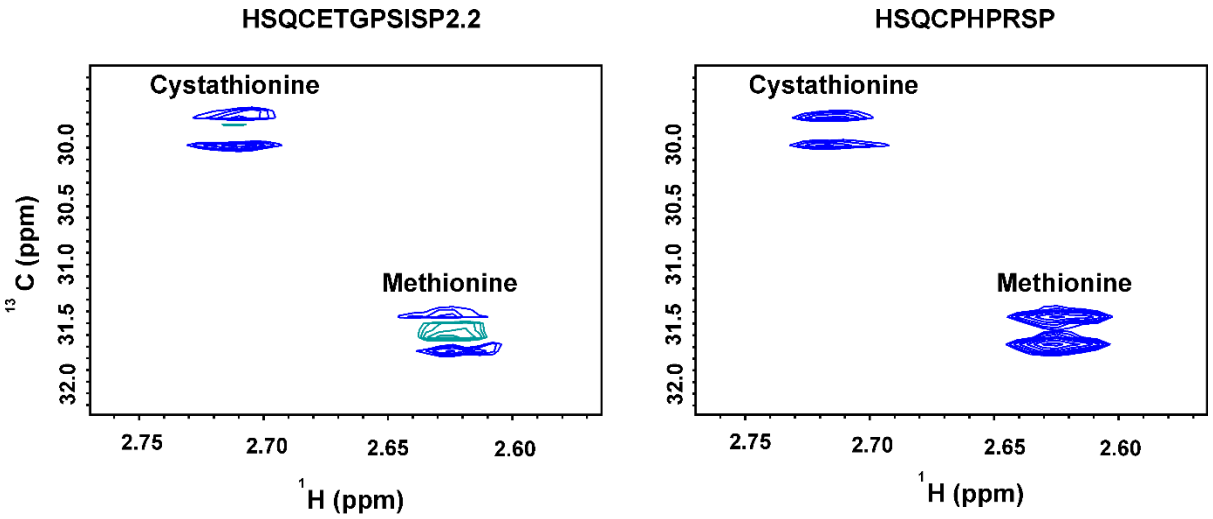
Appendix Figure A4: PDP1 knockout induces cell death in FLT3-ITD cells. eFlour staining of dead cells after PDP1 knockout in Molm13 and MV4-11 cells.

[11] Appendix figures 1-3 and their experiments were performed by Philipp Makowka.

Appendix 6: PDP1 knockout leads to cell death in FLT3-ITD cells

Some parts of the methionine tracing spectra were originally recorded with the HSQCETGPSISP2.2. pulse program. The peaks however, showed phase error (Figure A5) which affects the accuracy of label quantification. These samples could not be preserved after the measurements. Thus, three new different samples were measured again with the HSQCETGPSISP2.2. pulse program and then repeated with HSQCPHPRSP.UG4 pulse program. In each of the spectra, the ratio of ^{13}C label between C_4 of methionine and cystathionine was calculated (integral). An average error factor of 1.7 was found in spectra measured with HSQCETGPSISP2.2. pulse program. Thus, previous samples measured with this pulse program were corrected with a 1.7 factor when assessing cystathionine/ methionine ratio.

Similarly, when calculating the ratio between C_4/C_5 of methionine, a correction factor of 1.13 was applied.



Appendix Figure A5: Phase error correction. ^{1}H-^{13}C NMR spectra of cellular extracts with prior ^{13}C methionine labelling, recorded at 25°C on a 600MHz spectrometer using either HSQCETGPSISP2.2. or HSQCPHPRSP.UG4 pulse programs.

Declaration for collaboration work

Unless noted otherwise by referencing or acknowledgement, the work presented in this thesis was generated by myself during my doctoral studies. All contributions from colleagues are explicitly referenced in the thesis.

Chapter III (PDP1 is a key metabolic gatekeeper in FLT3-ITD-positive AML) is under revision in Leukemia:

Alshamleh I, Kurrle N, Makowka P, Kumar R, Ludig D, Wolf S, Koschade S, Stoschek K, Kreitz J, Fuhrman D, Toenges R, Berg T, Bruene B, Krause D, Oellerich T, Schnuetgen F*, Schwalbe H*, Serve H*. 2021. PDP1 is a key metabolic gatekeeper and modulator of drug resistance in FLT3-ITD-positive acute myeloid leukemia (under revision in Leukemia).

Chapter V (Real time NMR for studying metabolism) has been already published:

Alshamleh, I., Krause, N., Richter, C., Kurrle, N., Serve, H., Günther, U.L., and Schwalbe, H. 2020. Real-Time NMR Spectroscopy for Studying Metabolism. Angew. Chemie Int. Ed. 59, 2304–2308.

The material listed below was obtained in the context of collaborative research:

Figures 38, 40 and 43 were kindly provided by Alan Cunningham, group of Prof. JJ Schuringa, University of Groningen, Netherlands.

Acknowledgments

I cannot but to express my gratitude to the following humans:

To **Prof. Harald Schwalbe** for the uncountable deeds, starting by the job opportunity, the close supervision, supporting opportunities to travel and interact with scientific communities, openings horizons for collaborations, helping with personal matters, advice for future plans and finally, for bringing me closer to the 'Prof-to-be Alshamleh'.

To **Prof. Hubert Serve** for the opportunity to perform parts of my research in his lab, for the entertaining weekend research chats, the 'cool' research perspective and importantly, for opening my eyes to how much FUN research could be.

To **Prof. Ulrich Günther** for being my second supervisor on this Marie Curie opportunity in Birmingham. Special thanks to all of the research team in Birmingham.

To my scientific collaborators: **Prof. Daniella Krause** and **Dr. Rahul Kumar** for performing the in vivo experiment, **Prof. Thomas Oellerich** and **Dr. Sebastian Wolf** for the proteomics data, **Prof. Bernhard Brüne** and **Dr. Dominik Fuhrmann** for the opportunity to perform the seahorse experiments in their lab.

To **Prof. JJ Schuringa** and **Alan Cunningham** for the wonderful and fruitful collaboration.

To **Dr. Erhan Cetiner, Dr. Nina Kurrle, Dr. Nina Kubatova, Dr. Frank Schnuetgen, Dr. Swen Warhaut, Jasleen Bains, Dr. Christian Richter, Betül Ceylan, Johanna Kreitz** and **Alan Cunningham** for reading and correcting my thesis.

To **Dr. Christian Richter** and **Dr. Sridhar Sreeramulu, Robbin Schnieders and Nusrat Qureshi** for their help with my 'very basic' NMR questions.

To the new Junior PhD students **Daniel Hymon** and **Christina 'Küken' Muhs** with whom I worked side by side to drive the metabolomics projects further.

To my then-bachelor student '**Ala'Nina Krause** and my intern **Damian Ludig** for their dedication, discipline and substantial contribution to the real-time NMR and PDP1 projects. Without you, this work would not have been accomplished. A BIG thank you.

To the fellow PhD students and friends in Riedberg, **Erhan Cetiner, Jasleen Bains, Bozana Knezic, Nina Kubatova, Sara Kheyani, Swen Warhaut, Kerstin Dathe, Gerd Hanspach, Kathi Hohmann, Tassilo Grun, Robbin Schnieders, Feli Kutz** and **Nusrat Qureshi,** who tremendously helped me integrating and learning German language. Thanks to all of the other 40+ 'PhD army' in Riedberg. My apologies to those whom I might have forgotten.

To **Dr. Nina Kurrle** and **Dr. Frank Schnuetgen** for their close scientific support, advancing my research and for the nice working environment.

To the medical fellows in Prof. Serve's lab **Dr**. **Tobias Berg, Dr**. **Philipp Makowka** and Dr. **Sarah Weber** for their support with clinical matters.

To the fellow PhD students in Niederrad, **Johanna Kreitz, Christine Schoenfeld, Marcel Seibert** and **Verena Stolp** for the fantastic scientific and social atmosphere and of course, for The One and Only WeinMittwoch.

To **Marie Skłodowska-Curie Actions** funded by the **EU commission,** without which, this thesis would never have seen the light.

My family, I know you're curiously skimming through to read this part…

My father who got consumed to bring me to where I am right now, **my mother** who always cared for me and supported me unconditionally, **my sister Aseel and my brothers Osaid and Osama** who -effortlessly- saved me from growing up as a lonely child. Thanks for being proud of me. Love you all.

My 'surrogate family' in Germany '**Stefan Weckesser** and **Isabelle Maffre'** who adopted me and cared for me like my biological parents …. Vielen Dank & Merci beaucoup.

To my late uncle, teacher and friend **Zuhair Shamleh** … As you always taught me 'aim high …the limit is the sky'…. Your energy kept me going.

Finally,

To all of those who inspired me, even if you don't read this… Thank you.

Curriculum vitae



Personal **Islam Alshamleh**

Born on

Nationality

Address

Mobile

E-mail

LinkedIn

Education and Research

2016-2021 **Joint PhD degree** (Goethe University, Germany & Birmingham University, UK)

Marie Curie fellowship

Thesis title: Investigating metabolic vulnerabilities in acute myeloid leukaemia

Thesis advisor: Prof. Harald Schwalbe

2015-2016 **Master degree (MRes)** (Newcastle University, UK)

Stem Cells & Regenerative Medicine

Induced pluripotent stem cell technology in disease modelling

Thesis advisor: Prof. Majlinda Lako

2011-2014 **Bachelor degree (BSc)** (An-Najah University, Palestine)

Medical Laboratory Sciences

Work and training experience

2014-2015 Practical training and internships in the following laboratories (Palestine):

An-Najah hospital (Blood bank department)

Public Health Central Laboratory (molecular genetics department)

Rafedia general hospital (routine department)

Medicare laboratory (routine and hormonal analysis department)

2016	Two months research secondment on NMR metabolomics. Group Prof. Ulrich Guenther (Birmingham University, UK)
2017-2018	Two months conducting NMR metabolomics experiments Group Prof. Ulrich Guenther (Birmingham University, UK)

Workshops and training

Jan, 2017	First HaemMetabolome meeting and workshop (Barcelona, Spain)
Sep, 2017	Second HaemMetabolome meeting and workshop (Brussels, Belgium)
Sep, 2017	Third G-NMR school, small molecules and biological NMR (Berlin, Germany)
Feb, 2018	Marie Curie Association annual meeting (career development workshop) (Leuven, Belgium). Meeting travel grant award.
Mar, 2018	Introduction to Metabolomics workshop at the EMBL (Cambridge, UK)
Jul, 2018	HaemMetabolome metabolomics workshop (Groningen, Netherlands)
May, 2019	HaemMetabolome metabolomics workshop (Barcelona, Spain)

Selected conferences

Oct, 2017	Fourth ESH International Conference on Acute Myeloid Leukaemia (Estoril, Portugal)
Jun, 2018	XXII. Wilsede Meeting (modern trends in human leukaemia & cancer) (Hamburg, Germany)
May, 2019	Acute leukaemia retreat (Bad Kreuznach, Germany)
Jun, 2019	Fingerprinting in metabolomics by NMR (Florence, Italy)
Oct, 2019	Fifth ESH International Conference on Acute Myeloid Leukaemia (Estoril, Portugal). Conference travel grant award.
Dec, 2019	61th American Society of Haematology International Conference (Orlando, USA)
Oct, 2020	Rhein-Main Cancer retreat (Speaker) (Frankfurt, Germany)

Research and publication list

First authorship papers:

Alshamleh I, Kurrle N, Makowka P, Kumar R, Ludig D, Wolf S, Koschade S, Stoschek K, Kreitz J, Fuhrman D, Toenges R, Berg T, Bruene B, Krause D, Oellerich T, Schnuetgen F*, Schwalbe H*, Serve H*. 2021. PDP1 is a key metabolic gatekeeper and modulator of drug resistance in FLT3-ITD-positive acute myeloid leukemia (Under revision in Leukemia).

Alshamleh, I., Krause, N, Richter, C, Kurrle, N, Serve, H, Günther, U.L, and Schwalbe, H. 2020. Real-Time NMR Spectroscopy for Studying Metabolism. Angew. Chemie Int. Ed. 59, 2304–2308.

Kreitz J*, Schoenfeld C*, Seibert M*, Stolp V*, **Alshamleh I***, Oellerich T, Steffen B, Schwalbe H, Schnuetgen F, Kurrle N, Serve H. 2019. Metabolic plasticity of Acute Myeloid Leukemia. Cells 8, 805.

* Authors contributed equally to the work.

Co-authorship contribution:

Mostazo M, Kurrle N, Casado M, Fuhrmann D, **Alshamleh I**, Häupl B, Martín-Sanz P, Bruene B, Serve H, Schwalbe H, Schnuetgen F, Marin S, Cascante M. 2020. Metabolic plasticity is an essential requirement of acquired tyrosine kinase inhibitor resistance in Chronic Myeloid Leukemia. Cancers 12, 3443.

Nimbarte V, Wirmer-Bartoschek J, Gande S, **Alshamleh I**, Nasiri H, Schnuetgen F, Serve H, Schwalbe H. 2021. Synthesis and in vitro evaluation of novel 5-nitroIndole derivatives as c-Myc G-quadruplex binders with anticancer activities. ChemMedChem (ahead of print).

Altincekic N, Korn S, Qureshi N, Dujardin M, Pedrosa M, Abele R, Saad M, Alfano C, Almeida F, **Alshamleh I,** … 2021. Large-scale recombinant production of the SARS-CoV-2 proteome for high-throughput and structural biology applications. Frontiers in Molecular Biosciences (accepted for publication).

Cunningham A, **Alshamleh I**, Erdem A, Huls G, Schwalbe H, Schuringa JJ. 2021. Exploiting amino dependency in acute myeloid leukaemia unravels impaired methionine recycling as a targetable vulnerability (to be submitted).

Contribution to other collaboration projects (metabolomic analysis by NMR):

1. Hypoxia regulation as a key determinant of leukaemia microenvironment (Prof. Hubert Serve).
2. GATOR signalling and its role as a regulator of amino acids sensing (Dr. Nina Kurrle).
3. IRPII as a vulnerability in acute myeloid leukaemia and its role in regulating cellular metabolism (Dr. Sara Weber).
4. Metabolic reprogramming in colorectal cancer as a potential strategy for tumour metastasis (Prof. Florian Greten).
5. Influence of intestinal microflora on the development of colorectal cancer (Dr. Malak Canan Arkan).
6. Metabolic rewiring induced by LSD1 targeting in acute myeloid leukaemia (Dr. Tobias Berg).